Dissertation zur Erlangung des Doktorgrades
der Fakultät für Chemie und Pharmazie
der Ludwig-Maximilians-Universität München

Developing Photoswitchable Ligands for Transmembrane Receptors

Matthias Schönberger

aus

Trier, Deutschland

2014

Erklärung

Diese Dissertation wurde im Sinne von § 7 der Promotionsordnung vom 28. November 2011 von Herrn Prof. Dr. Dirk Trauner betreut.

Eidesstattliche Versicherung

Diese Dissertation wurde eigenständig und ohne unerlaubte Hilfe erarbeitet.

München, ...

.....

Dissertation eingereicht am .....

1. Gutachter: Prof. Dr. Dirk Trauner

2. Gutachter: Prof. Dr. Wolfgang Clauss

Mündliche Prüfung am ....16.04.2014.....

Developing Photoswitchable Ligands for Transmembrane Receptors

Content

Parts of this doctoral thesis have been published in scientific journals, or are considered for publication, respectively:

Fehrentz, T., **Schoenberger, M**. & Trauner, D. Optochemical genetics. *Angew Chem Int Ed Engl* **50**, 12156-82 (2011).

Schoenberger, M. & Althaus, M. Novel small molecule epithelial sodium channel inhibitors as potential therapeutics in cystic fibrosis - a patent evaluation. *Expert Opinion on Therapeutic Patents* **23**, 1383-1389 (2013).

Schoenberger, M., Althaus, M., Fronius, M., Clauss, W. & Trauner, D. Controlling Epithelial Sodium Channels with Light Using Photoswitchable Amiloride. *Nat. Chem.* (in revision).

Schoenberger, M., Damijonaitis, A., Zhang, Z., Nagel, D. & Trauner, D. Fotocaine – a new type of Photochromic Ion Channel Blocker. *ACS Chem. Neurosci.* (submitted).

Schoenberger, M. & Trauner, D. A Photochromic Agonist for μOpioid Receptors. *Angew Chem Int Ed Engl* (2014), in press.

I

Optochemical Genetics

Timm Fehrentz, Matthias Schönberger, and Dirk Trauner

Department of Chemistry, Ludwig-Maximilians-Universität, and Center for Integrated Protein Science, 81377 Munich, Germany.

Transmembrane receptors allow a cell to communicate with its environment in response to a variety of input signals. These can be changes in the concentration of ligands (e.g. hormones or neurotransmitters), temperature, pressure (e.g. via acoustic waves or touch), transmembrane potential, or light intensity. Many important receptors have now been characterized in atomic detail and our understanding of their functional properties has markedly increased in recent years. As a consequence, these sophisticated molecular machines can be reprogrammed to respond to unnatural input signals. In this review, we will show how voltage-gated and ligand-gated ion channels can be endowed with synthetic photoswitches. The resulting artificial photoreceptors can be used to optically control neurons with exceptional temporal and spatial precision. They work well in animals and might find applications in the restoration of vision and the optical control of other sensations. The combination of synthetic photoswitches and receptor proteins contributes to the field of optogenetics and adds a new functional dimension to chemical genetics. As such, we propose to call it "optochemical genetics".

Contents

"The trick then is not to use the clumsy and inefficient techniques of classical organic chemistry by themselves but to make use of Nature's tools."

Sir Francis Crick, 1999[1]

1. Introduction

Nature's molecular devices are unsurpassed in their beauty, efficiency and ability to integrate into complex systems. This is not entirely surprising, given that they have evolved over billions of years. Organic chemistry, by contrast, is about two hundred years old. The synthesis of complex molecules is barely a third of that age and far from being a mature and efficient technique. Nevertheless, synthetic chemistry has made remarkable progress over the last decades and many molecules have been created that have no structural or functional counterpart in Nature.

Still, what we can make today comes nowhere near to what Nature can achieve. The drugs we synthesize are comparatively simple molecules and the switches, motors, and machines we forge are conceptually beautiful but pale in comparison with Nature's devices.[2] These have been studied in great detail with various biophysical methods and our understanding of how they work has dramatically increased in recent years. Some famous examples of molecular machines that have now been elucidated in atomic detail include ATP synthase,[3] the ribosome,[4] RNA polymerase,[5] various molecular motors,[6] or ion channels that control nervous activity.[7] Although they operate on a scale where the peculiarities of quantum mechanics apply, they can be often described in terms of relatively simple and intuitive mechanical models.

This much-improved understanding of Nature's molecular machines opens the door for their functional manipulation using synthetic chemistry. Just as macroscopic engines can be taken apart, "souped up", and fitted with an ignition key, nanomachines can be manipulated and endowed with additional features and control elements. This can be done to a certain extent at a genetic level, *i.e.* through classical protein engineering, but also by adding and attaching synthetic molecules. The trick is then not to use the traditional techniques of synthetic organic chemistry

by themselves, but to make use of them *in combination* with Nature's tools. This approach creates hybrid devices that can be controlled with unnatural input signals and can be easily integrated into highly complex biological systems. As such, they not only function *in vitro* or in single cells but also in complex cellular networks, even in neural tissues and in behaving animals.

In this review, we will show how the paradigm - that Nature's molecular machines can be harnessed with synthetic chemistry - can be applied to a set of transmembrane proteins that play key roles in neurophysiology. To this end, we will first review some of the elementary machinery that is involved in sensory perception, synaptic transmission, and the generation of action potentials. We will then discuss in general terms how it can be reprogrammed to become sensitive to a very useful stimulus - light - and how the resulting artificial photoreceptors can be used to control and study neural networks. This is also the goal of "optogenetics", a new field of neuroscience that is currently undergoing rapid expansion.[8] We will show how the addition of a chemical component complements and extends optogenetics and how "optochemical genetics" contributes to the dissection and functional enhancement of nervous systems in new and exciting ways.[9]

2. Transmembrane receptors and their role in neurobiology

Transmembrane receptors underlie cellular communication, including the electrical and chemical communication within and in-between neurons. For the purposes of this review, we define these receptors as transmembrane proteins that respond to changes in an input signal, be it light-intensity, pressure, voltage, temperature or the concentration of a small ligand. These include ion channels (ionotropic receptors), G-protein coupled receptors (metabotropic receptors) and receptor-linked enzymes. For many years, these proteins were considered to be very difficult to study with structural methods, particularly with X-ray crystallography. This perception changed in 1998, when MacKinnon disclosed the X-ray structure of KcsA, a potassium selective ion channel sensitive to changes in pH.[10] Since this groundbreaking work,

representatives of several fundamental receptor classes have been characterized in atomic detail, including G-protein coupled receptors (GPCRs),[11] ionotropic glutamate receptors (iGluRs),[12] trimeric ATP receptors (P2X),[13] voltage-gated ion channels,[14] and pentameric ligand-gated ion channels (pLGICs).[15] For convenience, these receptors are grouped according to their symmetry in Fig. 1. Note that these receptors can exist as homomultimers, but often assemble as heteromultimers composed of several similar, but not identical, subunits.

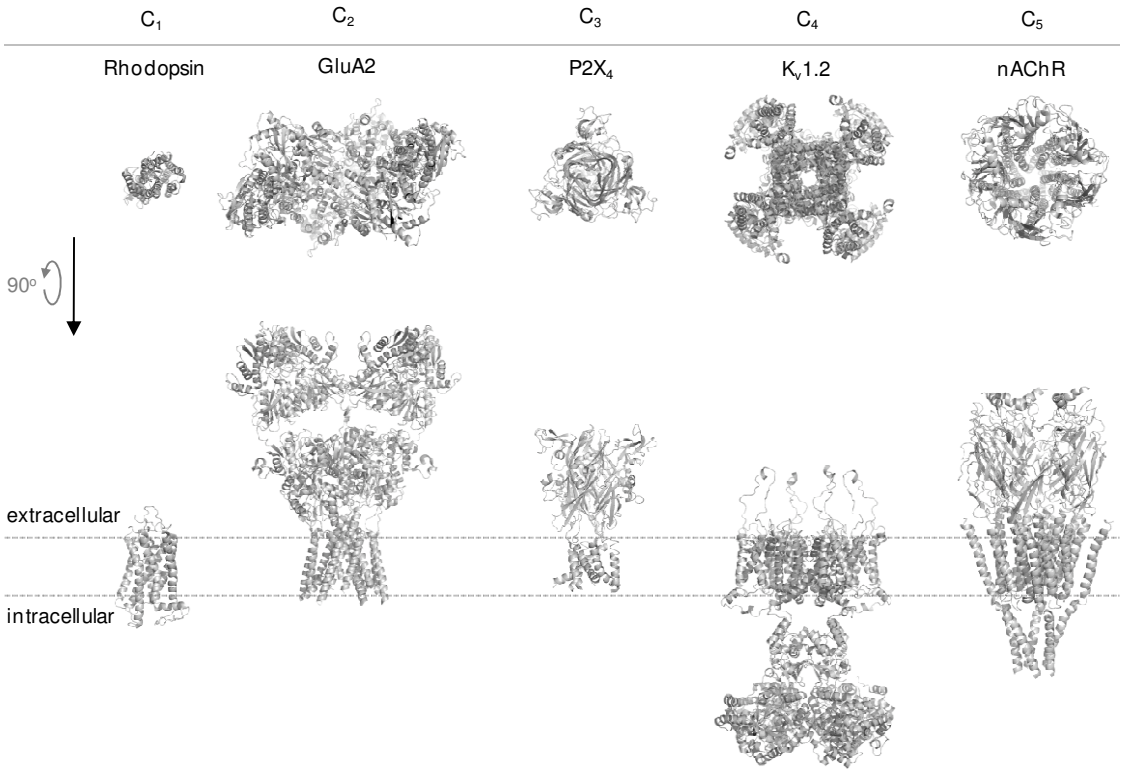

Figure 1. **Selected transmembrane receptors of different symmetry characterized by X-ray crystallography and electron microscopy**. Each receptor is shown in side- and top-view (from the extracellular side) and fitted to the same scale. Left to right: Rhodopsin, a G-protein coupled receptor responsible for vision (pdb 1U19). GluA2, a glutamate-gated ion channel involved in excitatory neurotransmission (pdb 2KG2). $P2X_4$, an ATP-gated cation channel that mediates pain sensation (pdb 3H9V). $K_v1.2$, a voltage-gated potassium channel involved in controlling cellular excitability (pdb 2A79). nAChR, a nicotinic acetylcholine receptor that mediates the communication between nerves and muscles (pdb 2BG9).

With the exception of rhodopsin,[11b] none of the receptors shown in Fig. 1 are inherently light-sensitive. Three of them, GluA2,[12] $P2X_4$,[13] and the nicotinic acetylcholine receptor,[15a] are ligand-gated ion channels that respond to changes in the concentration of neurotransmitters or extracellular metabolites. Voltage-gated ion channels, such as $Kv_{1.2}$,[16] are opened and closed by changes in transmembrane potential. They can be also influenced by ligands, however, such as channel blockers. As a consequence, all of the receptors shown in Fig. 1 can be regulated in one form or another by a small molecule. Provided this small molecule can be persuaded to change its activity in response to light, the whole receptor-ligand assembly could be transformed into a photoreceptor.

Before we address this topic, however, it may be worthwhile to briefly review how some of these receptors are involved in neurotransmission and the all-important generation of action potentials (APs).[17] These can be studied with electrophysiology, a very powerful technique that allows for microsecond to millisecond resolution. The generalized shape of an AP and a schematic view of a typical neuron are shown in Fig. 2. Ligand-gated cationic ion channels, such as ionotropic glutamate receptors (in the human central nervous system) or nicotinic acetylcholine receptors (in the periphery) are responsible for the initial depolarization of the postsynaptic membrane. Binding of the neurotransmitter to its respective channel leads to pore opening, allowing sodium and potassium ions to pass. Given the resting potential of the neuron and the tightly controlled relative concentration of sodium and potassium on either side of the membrane, this will lead to a net influx of positive charge, which changes the membrane potential (see Fig. 2). Once a certain value has been reached (typically around – 40 mV), voltage-gated sodium channels begin to open. As sodium rushes in, the membrane is further depolarized and the transmembrane potential inverts its sign (up to + 50 mV). The neuron is quickly repolarized, however, as the voltage-gated sodium channels inactivate and voltage-sensitive potassium channels begin to open after a brief delay. Once those are inactivated, the cell regains its resting potentials through the action of transporters and pumps, such as Na/K-ATPase.

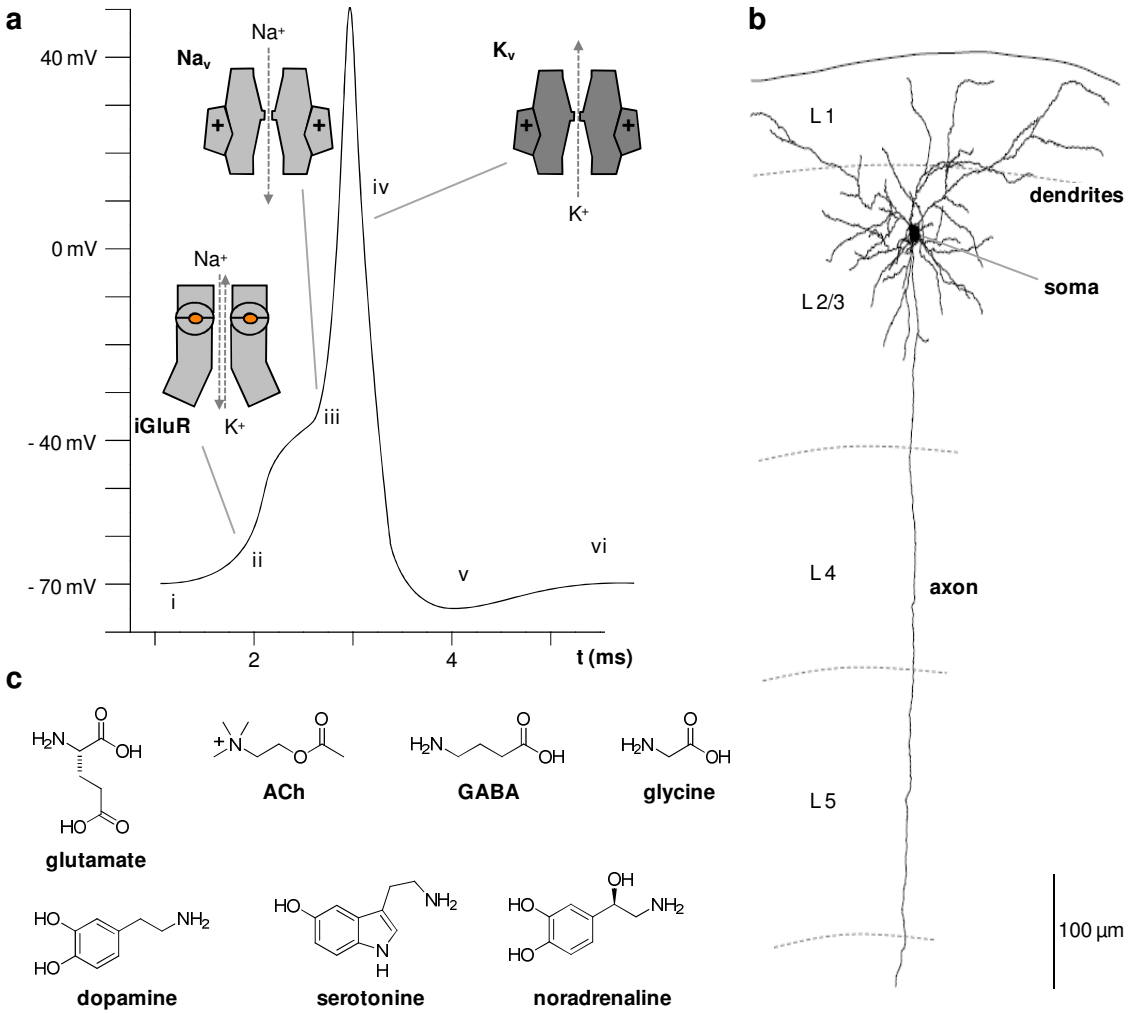

Figure 2. Neurotransmission in a nutshell. a) The action potential: i) the transmembrane potential of a neuron at rest; ii) a neurotransmitter binds to a ligand-gated ion channel, e.g. a glutamate receptor (iGluR), and evokes an excitatory postsynaptic potential; iii) voltage-gated sodium channels (Na_V) respond and further depolarize the membrane, but quickly inactivate; iv) voltage-gated potassium channels (K_V) follow suit and repolarize the membrane, even beyond its resting potential (v); vi) the undershoot is removed through the concerted action of channels that are open at the resting potential and ATP-driven ion pumps. b) A representative neuron from the visual cortex. The dendrites, the soma and the axon are clearly visible. The soma resides in layer 2/3 (L2/3) and is much less extended than the axon, which spans several layers of the cortex. c) The most important neurotransmitters and neuromodulators.

Ion channels can have both excitatory and inhibitory effects on neurons, depending on whether they make the transmembrane potential less or more negative when opened. This is not only dependent on the charge of the ions they conduct but also on relative concentration of ions on either side of the membrane. Consequently, at

physiological conditions, non-selective cation channels and sodium channels will depolarize, whereas potassium channels hyper- or repolarize cells when opened. Chloride channels, such as $GABA_A$ or glycine receptors are generally inhibitory on AP firing.[17a]

In addition to these primary ion channels, there are receptors that perform a more modulatory role and influence the shape, duration and frequency of action potentials. These receptors can also be ion channels (such as KCNQ channels)[18] or, more often, G-protein coupled receptors (GPCRs).[17a, 19] In comparison to ion channels, GPCRs are "slow acting", since their effect is mediated by heterotrimeric G-proteins, enzymes, second messengers, and transcription factors. Notably, the same neurotransmitter, e.g. glutamate, acetylcholine or GABA, can act on both ionotropic receptors and metabotropic receptors. Even neuromodulators that primarily target metabotropic receptors, such as serotonin, have an occasional ion channel target.[20]

3. Lighting up the brain

Amongst different input signals that can actuate a receptor, light stands out for a variety of reasons: light can be modulated in its intensity within femtoseconds, can be focused onto very small areas (on the order of its wavelength) and can carry enough energy to trigger molecular motions. As such, it is unsurpassed in its temporal and spatial precision and in its ability to remote-control molecular devices and systems, including neural systems.

Light has been used for ages to glean information *from* the environment. Visual systems have emerged at almost all levels in evolution and have been greatly enhanced by human technology, such as microscopy. This is still a highly active area of research as new imaging technologies continue to be developed. Recent examples include superresolution microscopy[21] and two-photon imaging.[22] As a consequence of these technical advances, neurons can now be described in incredible detail, action potentials can be visualized with fluorescent calcium sensors, and the activity of many neurons in a network can be monitored simultaneously in live, behaving animals. [23]

Light, however, can also be used to put information *into* systems - provided suitable photoreceptors are present. As in imaging, this can be done with exquisite temporal and spatial precision and the optical setups needed are largely the same. If the light intensities are not too high and the wavelengths are not too short, it can be done with little tissue damage, especially when compared with the invasiveness of multiple electrodes. The usefulness of light as an input signal for neuroscience was realized by none other than Sir Francis Crick, who stated in 1999: "The ideal signal [to study and control a brain] would be light, probably at an infrared wavelength to allow the light to penetrate far enough. This seems rather far-fetched but it is conceivable that molecular biologists could engineer a particular cell type to be sensitive to light in this way." [1]

It did not take long for molecular biologists to take up this challenge, which gave rise to a new field called "optogenetics" (Fig. 3).[8a, 8b] In essence, optogenetics is an effort to control neurons, or other cells of interest, with genetically targeted photoreceptors. Due to this genetic component, the sensitivity to a stimulus and not the stimulus itself can be precisely located. Therefore, the light beam itself does not need to be spatially controlled with very high resolution and light scattering is less of an issue than it is in imaging.

The targeting of innately "blind" neurons with genetically encoded photoreceptors has been achieved in several ways. Historically, the first system used was "ChARGe", which essentially consists of the primary components of the *Drosophila* visual cascade (rhodopsin, the associated heterotrimeric G-protein, and arrestin).[24] This multicomponent system was shown to trigger APs when heterologously expressed in dissociated hippocampal neurons. This was quickly followed by early optochemical systems, which will be discussed in much more detail below. In 2004, a natural photoreceptor called channelrhodopsin-2 (ChR2) was introduced, which has since established itself as the most practical and popular tool.[25] ChR2 is an excitatory cation channel isolated from the alga *Chlamydomonas reinhardtii*.[25a] It can be activated with blue light and is rapidly deactivated once the light is gone, which allows for the control of AP firing with high precision.[26] Like the rhodopsins, it uses retinal as a

photoswitch, but unlike the mammalian visual pigments, the retinal is not excised after photoswitching. Therefore, ChR2 can be repeatedly used to trigger action potentials. As an added advantage, retinal is endogenously produced in many tissues and does not need to be added externally.[25b]

Shortly after the excitatory photoreceptor channel ChR2, an inhibitory counterpart, namely a light-driven chloride pump called *Natromonas pharaonis* halorhodopsin (NpHR) was introduced.[27] NpHR can be stimulated with bright yellow light and is capable of silencing neurons, also with millisecond resolution. Importantly, due to little spectral overlap, ChR2 and NpHR can be expressed and used in the same neuron simultaneously.[8b, 27] Variants of ChR2 and NpHR with modified spectral and kinetic features continue to be developed,[28] and other systems, such as light-driven proton pumps, have been recently discovered that can control neuronal activity with light.[29]

Since its inception at the beginning of the new millennium, optogenetics has found many applications in dissecting neuronal circuitries and has helped to answer fundamental questions in neuroscience. As a testament to its enthusiastic reception by the scientific community, it was deemed "Method of the Year" in 2010.[8a, 8c] In addition to its important role in basic neuroscience, optogenetics has, within a few years, also found its first applications in clinical research. For example, ChR2 and NpHR have been used to investigate the mechanism of deep brain stimulation, which ameliorates the symptoms of Parkinson disease.[30] A second study was aimed at *Retinitis pigmentosa*, which involves the loss of photoreceptor cells. Here, the light sensitivity of the retina could be restored by expressing NpHR, which resulted in visually guided behavior in previously blind mice.[31] In another application of ChR2 and NpHR, cardiac pacemaker cells of zebrafish could be optically stimulated or inhibited, enabling the control of heart beat patterns.[32]

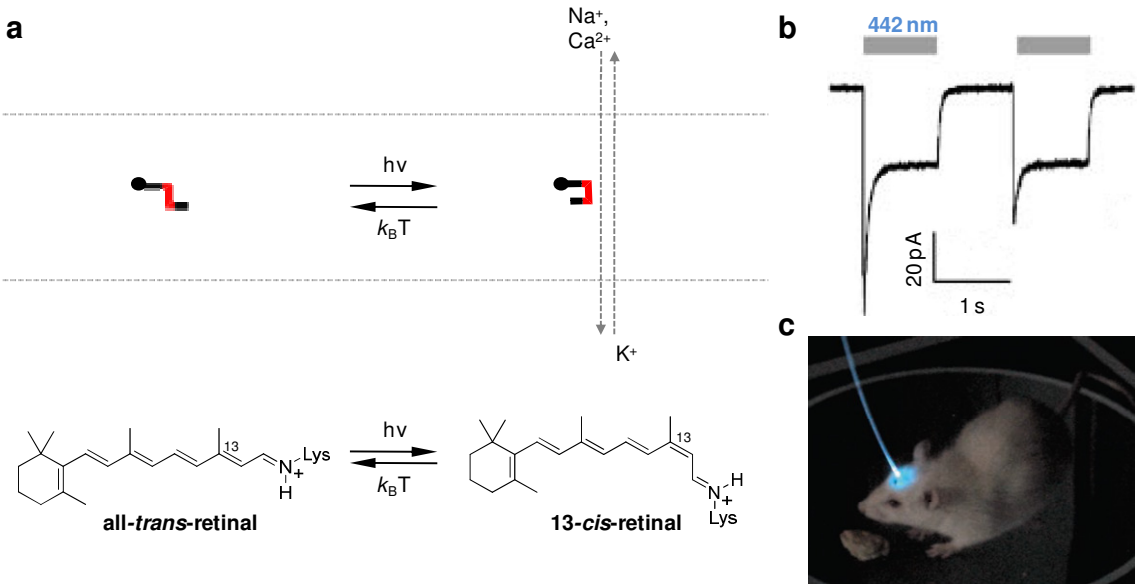

Figure 3. Optogenetics. Schematic drawing of ChR2, a light-gated ion channel. The chromophore 13-*trans*-retinal (shown here conjugated as a Schiff base) undergoes isomerization with blue light and thermal relaxation, gating the channel. b) Shining blue light on ChR2 triggers inward currents of ChR2. c) Mouse behavior controlled with blue light. Note the glass fiber cable that delivers light deep into the brain.[8b]

4. Optochemical genetics

Given that the molecular tools used in optogenetics are mostly derived from bacteria and protozoa, they work amazingly well in the neurons of worms, flies and furry animals. These neurons, however, express numerous receptors on their own that are easily accessible on their extracellular side but not inherently photosensitive. The challenge then is to persuade endogenous receptors to become sensitive toward light.

Three general strategies have emerged to do just that using small synthetic molecules (Fig. 4). The simplest and oldest approach employs caged-ligands (**CL** approach).[33] Here, a ligand is endowed with a protecting group that renders it ineffective. This protecting group is rarely a true molecular cage (in the sense a chemist would use this term) but typically a photolabile moiety that masks a functional group crucial to the ligand-receptor interaction. Photochemical cleavage of the protecting group then sets the active ligand free and triggers the desired biological effect.

Caged ligands have indeed been applied to great effect in neuroscience. Caged glutamate, for instance, has been very useful for unraveling neural systems and two-photon cages have enabled the stimulation of single synapses due to the spatial

precision that can be achieved with two-photon techniques.[34] The photosensitization of $P2X_2$ receptors and TRPV1 channels with caged ATP and capsaicin, respectively, was the first approach shown to work in living animals (in this case decapitated fruit flies, to ensure that the visual system was inactivated).[35]

There are, however, certain functional disadvantages associated with caged ligands. Uncaging is a unidirectional process and it is difficult, if not impossible, to "stuff the beast back into the cage". Unless one is interested in tonic effects, one can only hope that the ligand leaves the active zone as quickly as possible or is cleared by either a reuptake pump or a deactivating enzyme. The former exists for glutamate itself but not for more selective synthetic agonist and antagonists. In addition, uncaging produces byproducts, *i.e.* the remnants of the protecting group, which can be toxic. The background release of the neurotransmitter, *e.g.* through thermal hydrolysis, can also be a problem, as can be the fact that some caged compounds have off-target effects, for example as antagonists on other receptors.

Some of these shortcomings can be overcome with a second approach that we call the photochromic ligand (**PCL**) approach. Here, the ligand carries a photoswitchable side-chain that can be switched between two configurations. As the photoswitch toggles between these states, the efficacy of the ligand changes, triggering the desired biological effect in a reversible fashion. The ligand can change its efficacy upon photoswitching and could even be an agonist in one form and an antagonist in the other.

PCLs have all the advantages of small-molecule drugs, including their ease of application and fast tissue distribution. As with drugs, selectivity between receptor subtypes can be a challenge, but this can often be overcome through systematic variation of the molecule. In addition, one could be concerned that their photoisomers show relatively small differences in efficacy. However, in our experience PCLs work remarkably well in complex systems that have nonlinear responses, particularly in neural networks. Here, it is often the case that small changes in the activity of a modulator have dramatic effects on the output. Since the AP is an "all or nothing" response that is triggered only when a certain threshold is

reached after a complex cellular integration, compounds that subtly influence this integration can have pronounced effects.

Of course, there are situations where receptor-subtype selectivity and cellular targeting is highly desirable. In this case, a third approach, which we call the photoswitched tethered ligand approach (**PTL** approach), can be employed. Here, the ligand is *covalently* attached to its receptor through a tether that contains a photoswitch. As the photoswitch toggles between long and short forms, the local concentration and/or efficacy of the ligand changes, triggering a biological response in a reversible fashion. Importantly, PTLs can be genetically encoded, since the point of attachment is an engineered cysteine residue or any other encodable chemical motif that allows for specific bioconjugation. Since the PTL is covalently tethered, its local concentration at the site of attachment is very high in the active form of the photoswitch, which means that the affinity of the ligand is not a major concern. In fact, low-affinity ligands are usually preferred to ensure that photoswitching removes the ligand from the binding site.

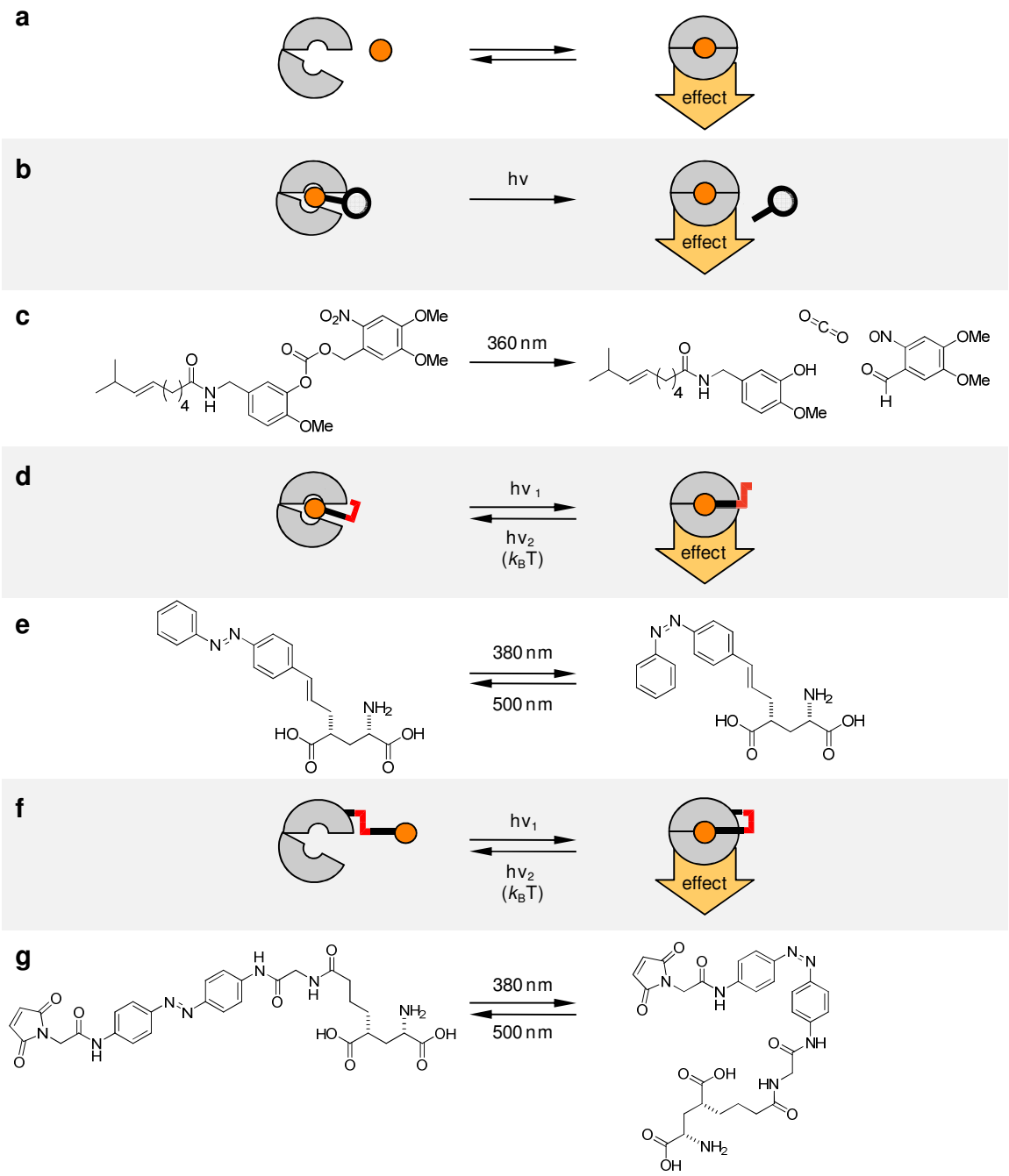

Figure 4. Three strategies used in optochemical genetics. a) A ligand binds to a generic receptor (not necessarily the clamshell-like receptor domain shown here), triggering a biological response. b) A caged ligand (CL) is broken apart with light, thus releasing its active form. c) Caged capsaicin, used to stimulate TRPV1 channels. d) A photochromic ligand (PCL) reversibly acts on a receptor. e) 4-GluAzo, a PCL that functions as "reversibly caged glutamate". f) A covalently attached photoswitched tethered ligand (PTL) can optically regulate a receptor. g) **MAG-1**, a typical PTL in its unconjugated form.

The PTL approach is essentially a variant of optogenetics, since it combines a genetically encodable receptor with light to precisely control neural activity. As

opposed to “classical” optogenetics, a synthetic component, *i.e.* a reactive chemical, is needed, which is not endogenously produced, but needs to be synthesized and supplied by a chemist. The PCL and the CL strategies, on the other hand, are more akin to “chemical genetics”.[36] Chemical genetics attempts to address every protein target with a selective small molecule ligand. Although such pharmacological control has a rapid onset, it still not fast enough for many applications in neuroscience, where millisecond precision is required. This limitation can be overcome by optically controlling the small molecules that function as ligands.

Taken together, the CL, PCL and PTL approaches provide the basis for what we call “optochemical genetics”. It is an effort to control neural activity (or any network activity) with light and light-responsive synthetic molecules, with or without a genetically determined component. It shares with chemical genetics a certain desire to overcome the limitations of conventional genetic manipulation, but it also acknowledges that the targeted expression of proteins can be very powerful.

The variant used depends on the exact application one has in mind. For therapeutic applications, where a certain lack of selectivity can be tolerated or is even desirable,[37] the PCL approach may be more suitable. On the other hand, in the analysis of functional pathways, e.g. in neural circuitry mapping, the genetically targeted transfection of a specific cell is clearly advantageous. In addition, PTLs could be extremely useful in the functional dissection of closely related receptor subtypes, since selectivity can be achieved through covalent attachment to genetically engineered isoforms (Fig. 5). Following conjugation, tonic activation or inhibition of the receptor can be prevented through action of the photoswitch. Overall, this PTL approach to selective pharmacology bears a certain resemblance to the “bump-hole” technique, which has been used so successfully in dissecting the human kinome.[38] In both cases, engineered proteins and unnatural ligands are needed. The PTL approach, however, not only provides a precise answer to the question “who”, but also to “when” and “where”.

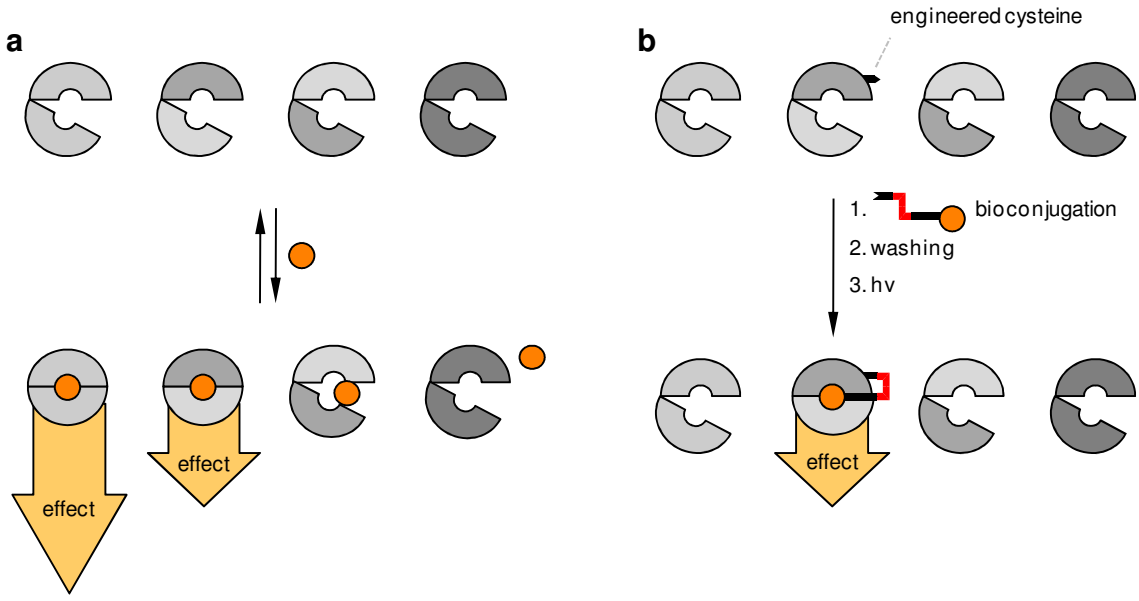

Figure 5. **The PTL approach to selective pharmacology**. a) Chemical genetics and pharmacology generally aim at individually targeting receptors and receptor isoforms. This requires ligands that bind with high affinity and selectivity. b) In optochemical genetics, selectivity can be achieved through genetic engineering of a bioconjugation site. In addition, the photoactivatable ligand can have low affinity to the receptor subtype.

Caged ligands have been mostly developed by other groups and have been extensively reviewed elsewhere,[33] which is why our discussion here will focus on synthetic photoswitches, i.e. on PTLs and PCLs. Among different photoswitch architectures, azobenzenes have so far proven to be the most versatile and reliable ones.[39] This is due to several functional features that distinguish them (Fig. 6). For instance, their geometries in their *cis* and *trans* states are well defined and the conformational space that can be mapped by both isomers has relatively little overlap. Substituents in the 4 and 4' positions are substantially closer in their *cis* form than in their *trans* form, an effect that can be amplified further by appropriate substitution. Although azobenzenes are axially chiral in their *cis* -form, which is not planar, they are typically not optically active due to facile racemization and they do not generate stereocenters upon switching between a long and short form. They often display high extinction coefficients and quantum yields, meaning that light of relatively low intensity can be used for photoisomerization. In addition, azobenzenes undergo photoswitching at very fast rates, which prevents intersystem crossing and

formation of triplet diradicals. These would react with triplet oxygen to generate singlet oxygen, a highly reactive and cytotoxic species, which is also damaging to the chromophore itself. Consequently, azobenzenes are relatively photostable and can be switched over many cycles. Their spectral tuning through substitution is straightforward and follows well-established rules. While most azobenzenes used to date are isomerized to their *cis* form with UV-A or deeply violet light (315-380 nm), red-shifted versions that are less harmful upon prolonged tissue application are also known (see below). Finally, azobenzenes are relatively easy to synthesize and modify, as several synthetic strategies are available, including diazonium coupling, Mills reactions, and transition metal catalyzed cross-coupling strategies.[40] One potential disadvantage is their comparatively low solubility, but this can be usually overcome with appropriate functional group, in particular with charged substituents.

Notably, azobenzene photoswitches are marked by photostationary states that are a function of the wavelength. While they can exist 100% in the thermodynamically more stable *trans* form (also the dark-adapted form) and their photostationary *cis*:*trans* ratios can exceed 9:1 at short wavelengths (Fig. 6), it is practically impossible to push them fully into the *cis* state through irradiation. Therefore, the background activity of the remaining *trans* isomer is a concern, but for the reasons stated above this is often not a problem in neural networks. In fact, the dependence of the photostationary ratio on the wavelength also offers an opportunity to tune the response by gradually tuning the color. The thermal bistability of photoswitches can be further influenced through appropriate substitution. PTLs wherein one end of the *cis* azobenzene interacts with the protein covalently and the other non-covalently show slow thermal relaxation, at least on a neurobiological time scale. On the other hand, certain red-shifted azobenzene PCLs can revert to their dark-adapted state within milliseconds.[41]

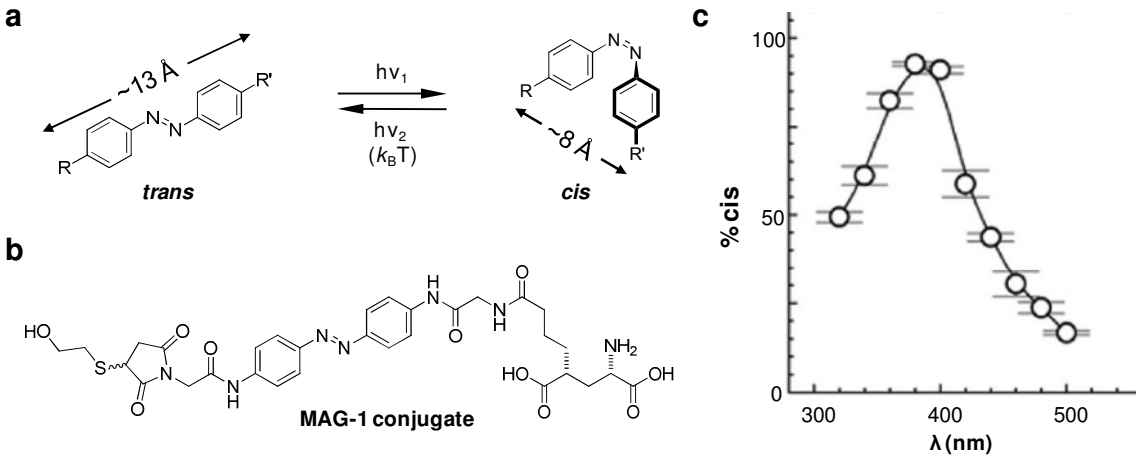

Fig. 6. The logic of azobenzene photoswitches. a) Azobenzenes change their configuration and length upon irradiation with different wavelengths. They revert thermally or photochemically to their thermodynamically more stable state, which is usually the *trans*-state. b) The mercaptoethanol conjugate of **MAG-1**, a model for the tethered PTL. c) The photostationary *cis*:*trans* ratio of the **MAG-1** conjugate, as a function of wavelength.

Once a photoswitch has been chosen, the design of PTLs and PCLs is straightforward, provided both structural coordinates for the receptor and extensive structure-activity relationship data for the ligands are available. The latter is often the case, since neuropharmacology is a well developed field. Today, one cannot complain about a lack of the former either, since relevant structures appear in the literature almost every week.

The design of PCLs and PTLs is closely intertwined. It typically starts out with a structure of a ligand, gleaned from the crystal structure or from the pharmacology literature. From this, it is often immediately clear where and how to attach the photoswitch to the ligand and which stereochemistry to choose at the point of attachment. In an intermediate stage, we sometimes synthesize a so-called "tether model", which retains one phenyl ring of an azobenzene. This is then extended to a full-blown PCL that contains the entire chromophore and, finally, after addition of an electrophilic functional group, to the corresponding PTL. In general, extensive structure-activity data are sufficient to design a PCL with a reasonable chance of success, whereas X-ray structures are normally needed for a PTL. The latter requires cysteine sites for covalent attachment, and choosing those can be difficult without

structural coordinates. Increasingly, sophisticated computational tools are used for that purpose.

Since most PTLs used to date are cysteine-reactive compounds, unspecific labeling of the cell-surface might be a concern. However, one has to bear in mind that reduced, accessible cysteines are rare on the surface of cells and the bioconjugation typically proceeds *via* affinity labeling. This means that the non-covalent interaction of the PTL with its ligand-binding site precedes covalent bond formation, enhancing the rate and selectivity of labeling, which will also depend on the state of the photoswitch. In addition, cells seem to be remarkably tolerant toward molecules attached to their surface, as long as they do not interfere with vital cell/cell interactions.[42]

The design of suitable PTLs and PCLs also goes hand in hand with their syntheses. These can present considerable challenges since the chemistry of photoswitches needs to interface with the chemistry of polar and charged ligands, which requires intricate protecting group operations. In the case of PTLs, this is acerbated by the presence of an electrophile, which should be introduced into the molecule as late as possible. The syntheses have to be practical and efficient enough to support a sustained biology program that includes *in vivo* investigations and, eventually, behavioral studies in animals.

In the following paragraphs, we will show how optochemical genetics can be applied to some of the most basic molecular machines involved in synaptic transmission: voltage-gated potassium channels and ionotropic glutamate receptors. To this end, we will first discuss their innate functions and systemic roles in some detail and then show how they can be converted into hybrid photoreceptors through covalent or non-covalent attachment of azobenzene photoswitches. Afterward, we will address other targets, such as the nicotinic acetylcholine receptor (nAChR) or the $P2X_4$ receptor, where this has been previously done to a limited extent. Finally, we will address a few receptors that have not yet been converted into photoreceptors, but which are "sitting ducks" for the optochemical approach.

5. Voltage-gated potassium channels

Together with voltage-gated sodium channels (Na_v), voltage-gated potassium channels (K_v) modulate cellular excitability and play a key role in the generation of action potentials.[17c] K_v channels are transmembrane proteins that assemble as tetramers from four single polypeptide chains that are known as α-subunits.[43] In humans, 40 genes encode 12 α-subunit families (K_v1 to K_v12).[44] Within each subfamily, different genes exist as indicated by an additional number, e.g. $K_v1.2$. This diversity is further increased by heterotetrameric α-subunit assembly, which results in a very large number of potential combinations. K_v1 channels additionally interact with intracellular tetrameric β-subunits that alter gating behavior.[44]

To date, several potassium channels have been elucidated in atomic detail with X-ray crystallography. The first structure to be reported was KcsA, a simple bacterial channel from *Streptomyces lividans*. Its disclosure in 1998 stands as a milestone in biophysics.[10] Subsequently, the structures of a calcium-gated potassium channel (MthK),[45] several inward-rectifier potassium channels (e.g. $K_{ir}3.1$),[46] a sodium and potassium-conducting channel (NaK),[47] and several prokaryotic and eukaryotic voltage-gated potassium channels have been reported.[14b, 16] The structure of $K_v1.2$, a mammalian voltage-gated ion channel that modulates the electric excitability of neurons, in its open form is shown in Fig. 7.[14b] In this representative structure, the voltage-sensors, the pore, and both the inner and outer vestibule of the channel are clearly visible (the β-subunit is removed here but present in Fig.1). Each single subunit contains an intracellular tetramerization domain, a voltage sensor domain (with helices S1-S4), and a pore domain (containing helix S5, a short pore helix, a pore loop and the C-terminal helix S6).[43] Both the N- and the C-termini are located in the cytosol but the N-terminal domain is not resolved in the structure.

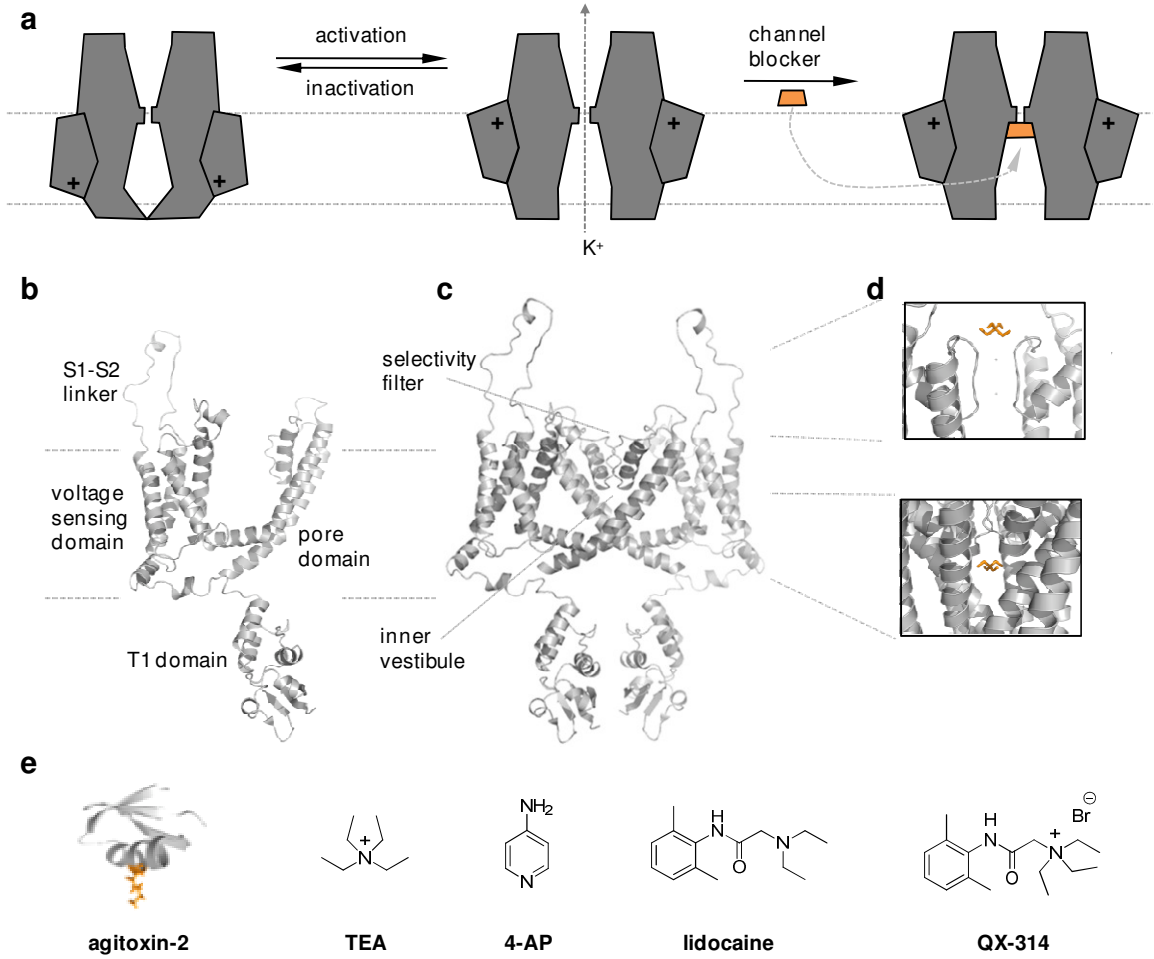

Figure 7. Structure and function of voltage-gated potassium channels. a) A highly schematic drawing of K_v channels illustrates their functional cycle and channel block. b) A single $K_v1.2$ subunit showing the extracellular S1-S2 linker, the voltage-sensing domain, the pore domain embedded in the membrane, and the intracellular T1-domain (pdb 3LUT). The β-subunit has been removed and the ball-peptide is not resolved in this structure. c) Two of the four subunits, indicating the architecture of the selectivity filter and the inner vestibule. d) Expanded view of the **TEA** binding sites in the inner and outer vestibule (pdb 2BOB and 2BOC). e) Chemical structures of extracellular and intracellular potassium channel blockers.

Like most ion channels, K_v channels have three elementary functions that are physically represented by protein domains and their movements: first, an "activation gate" that interacts with the input signal (i.e. voltage) and opens the channel, second, a "selectivity filter", which determines which ions can pass through the channel and third, an "inactivation gate", which is responsible for their desensitization. Activation is initiated by the voltage sensor once the membrane potential reaches –40 mV. The S4 helix of the voltage sensor domain in each subunit contains several

positively charged residues, usually arginines, that move across the membrane as the cell depolarizes. This movement is mechanically coupled with a hinged motion of the inner helix bundle (S6) of the pore-domain, which opens a gate through which the ions can pass.[7, 43-44] Driven by the electrochemical gradient, the ions then permeate the selectivity filter generating a current that is specific for K_v channels. The selectivity filter is essentially a stack of backbone carbonyls that compensate for the hydration sphere of the cation as it passes through. This compensation is energetically more favorable for potassium ions than sodium ions.[7]

There are two native mechanisms of inactivation of K_v channels called N-type- and C-type-inactivation. N-type inactivation is mediated by the positively charged intracellular N-terminus, which functions like a "ball" (or plug) on a chain. Once the voltage gate is opened, the N-terminus follows the outward K^+ current. This pushes the "ball" into the inner vestibule of the channel and blocks further ion conduction.[48] In comparison, slow or C-type inactivation depends on permeant ions and blockers and is believed to occur through a conformational change near the extracellular pore region.[48a, 49] In a physiological context, fast sodium channel inactivation and K_v channel currents repolarize neurons after an AP and determine the duration and frequency of APs.[50]

K_v channels can be blocked by Cs^+, small organic cations, and venom peptides. Venom peptides, such as agitoxin-2, are produced by some of the most dangerous animals known, e.g. the death-stalker scorpion, certain sea anemones, or the green mamba.[44, 51] These peptides bind to the outer vestibule of the channel and literally plug its pore from the extracellular side, usually with a protonated lysine side chain. Typical small organic K_v channel blockers are quaternary ammonium ions, such as tetraethylammonium (TEA) and 4-aminopyridine (4-AP) (Fig. 7).[17c, 52]

Interestingly, K_v channels feature both an internal and external binding site for quaternary ammonium ions.[53] External TEA mimics the protonated lysine side chain that functions as the plug in agitoxin-2, whereas internally applied TEA acts similar

to the positively charged ball peptide involved in N-type inactivation. This blockade requires opening of the activation gate. Therefore, charged blockers that act from the internal side are called "open channel blockers" or "use-dependent blockers."[17c] The KcsA structure was also solved in the presence of analogues of TEA, which helped to exactly locate its intracellular and extracellular binding sites.[53]

6. Photosensitizing voltage-gated ion channels

With their structures elucidated and their functions reasonably well understood, voltage-gated potassium channels have become prime targets for optochemical genetics. The first system to emerge was the "photoisomerizable azobenzene-regulated K^+ channel" (SPARK), which is an example of the PTL approach (Fig. 8).[54] Due to its hyperpolarizing effect, it was later renamed H-SPARK. H-SPARK consists of the channel blocker **MAQ** (maleimide-azobenzene-quaternary-ammonium) covalently attached to a genetically introduced cysteine on an extracellular loop of a K_V1-type channel. The location of this cysteine (E422C) could be determined based on existing X-ray structures and previous experiments with "molecular tape measures."[55] Once attached, **MAQ** essentially functions as **TEA** on a leash that can be lengthened or shortened with light. **MAQ** was designed to block the channel in its elongated *trans*-state, i.e. at 500 nm or in the dark, whereas the block would be lifted in the *cis*-state of the photoswitch, i.e. at 380 nm. To make H-SPARK an effective modulator of membrane potential, slow and fast inactivation of the channel had to be deleted using genetic engineering. The activation voltage was shifted from -35 mV to -70 mV through another point mutation (L366A), leading to a constantly open channel before conjugation of *trans*-**MAQ**. As a result, in the dark or under 500 nm light, the potassium channel is blocked. Illumination with 380 nm unblocks the pore and the resulting outward current leads to re- or hyperpolarization of the membrane. To our amazement, SPARK not only worked in excised patches from *Xenopus oocytes* but also in excitable cells, such as dissociated hippocampal neurons.[54] Indeed, when SPARK was introduced in 2004, it was the first system that allowed for optical silencing of neuronal activity.

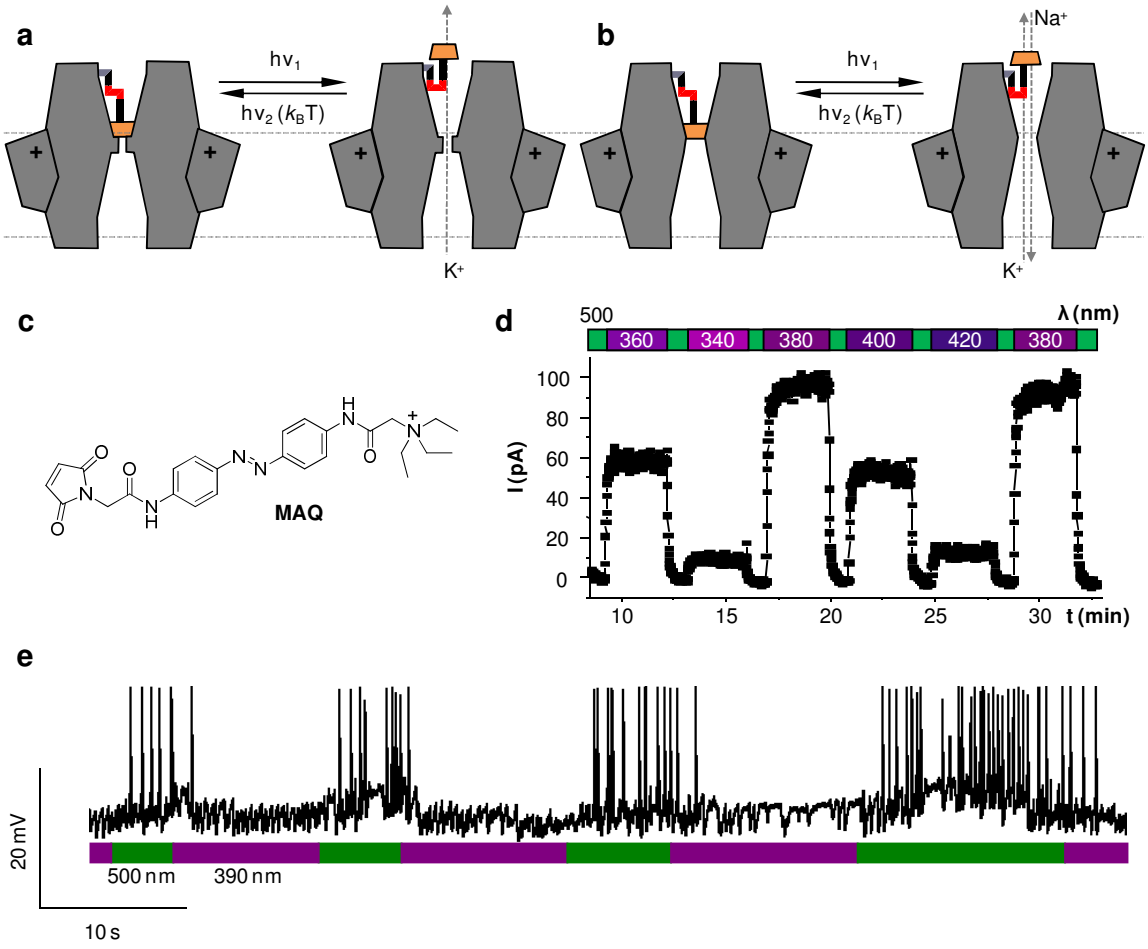

Figure 8. **SPARK, the light-sensitive potassium channel**. a) A highly schematic view of H-SPARK, the hyperpolarizing channel. b) A schematic view of D-SPARK the depolarizing variant. c) The chemical structure of **MAQ**, the PTL used for SPARK. d) Reversible light control of potassium currents by H-SPARK. Irradiation in the UV range unblocks channels while 500 nm light induces block. By convention, outward currents are plotted upwards. e) Light depending induction of AP firing, by H-SPARK expressed in neurons. This is the original recording of the first experiment where neuronal activity was controlled reversibly by a **PTL**.

As a complement to the silencing H-SPARK, we also engineered a depolarizing version, termed D-SPARK.[56] A single additional mutation (V443Q) was sufficient to convert the potassium selective H-SPARK into a nonselective cation channel. With this mutation in the selectivity filter, the permeability ratio of K^+/ Na^+ ions changes to 0.7 and Na^+ influx into the cell dominates the net effect on the membrane potential. After attachment of **MAQ**, the channel depolarizes the membrane upon UV illumination instead of hyperpolarizing it, thus allowing for AP-firing rather than

silencing. This is a nice case of "sign inversion," which is often encountered in neuroscience.

The diversity of K^+ channels, the lack of selective pharmacology, and the success of H/D-SPARK provided the motivation to extend the PTL strategy to other members of the family.[57] K_v1.3, which is involved in membrane repolarization after AP firing of neurons and has immunosuppressive effects when blocked, became the next channel to be rendered light sensitive by attachment of **MAQ**. Its very low affinity for **TEA** could be overcome by introducing a point mutation (H401Y). Both K_v3.1 and K_v7.1 could be converted into photoreceptors in a similar fashion. Based on their fast deactivation, K_v3.1 channels play an important role in generating high frequency APs, which occurs in neurons of the auditory brainstem and the cerebellum. Finally, the **PTL** concept could be applied to the small conductance Ca^{2+}-activated K^+ channel 2 (SK2), a channel that is naturally sensitive to voltage and an intracellular ligand.[57] Taken together, these studies provide a first example for the PTL-driven selective pharmacology discussed in Fig. 5.

As an alternative to PTLs, PCLs offer a way to control *native* K_v channels and neuronal activity with light. For this purpose, the cysteine-reactive maleimide group of **MAQ** was replaced with various moieties. This yielded a series of photochromic blockers, termed **XAQs**, which display different pharmacological and photophysical properties.[58] These compounds include the benzoate **BzAQ**, the propyl derivative **PrAQ** and the acrylamide **AAQ** (Fig. 9). Detailed investigations showed that the **XAQ**s act as use-dependent, photochromic open channel blockers. This also applies to **AAQ**, which does not react with the extracellular surface of native channels, as initially hypothesized. To reach the inner vestibule, the amphiphilic **XAQ**s have to cross the membrane or they can be added to the cytosol through a patch pipette. External application of **AAQ** and **BzAQ** to cells or tissues blocks K_v channels in the *trans*-state of the photoswitch, i.e. in the dark or under 500 nm irradiation, while 380 nm light relieves the block. Interestingly, **PrAQ** preferentially blocks in its *cis*-state (i.e. at 380 nm), which is another instance of sign-inversion.

Structurally as well as functionally, **XAQ**s resemble the well-known analgesic lidocaine or its permanently charged derivative **QX-314**, with the important difference that their efficacy is light dependent. Like lidocaine, **XAQ**s can be simply added to nervous tissues, which makes them very attractive for therapeutic applications. After a brief waiting period, they reliably control action potential firing (Fig. 9). When added to cerebellar slices, **AAQ** controls the activity of Purkinje neurons, mostly through its effect on inhibitory interneurons known as basket neurons.[58b] **AAQ** also has effects on the heartbeat of the medicinal leech *Hirudo medicinalis*.[58b] In this animal, central pattern generator interneurons (co-called HN cells) control the frequency of heart contractions. Earlier studies indicated that K^+ channels play a crucial role in HN cell burst firing. After applying **AAQ**, the activity of HN neurons could be modulated with light. Interestingly, burst periods decreased under 380 nm light illumination, whereas 500 nm light extended the period.

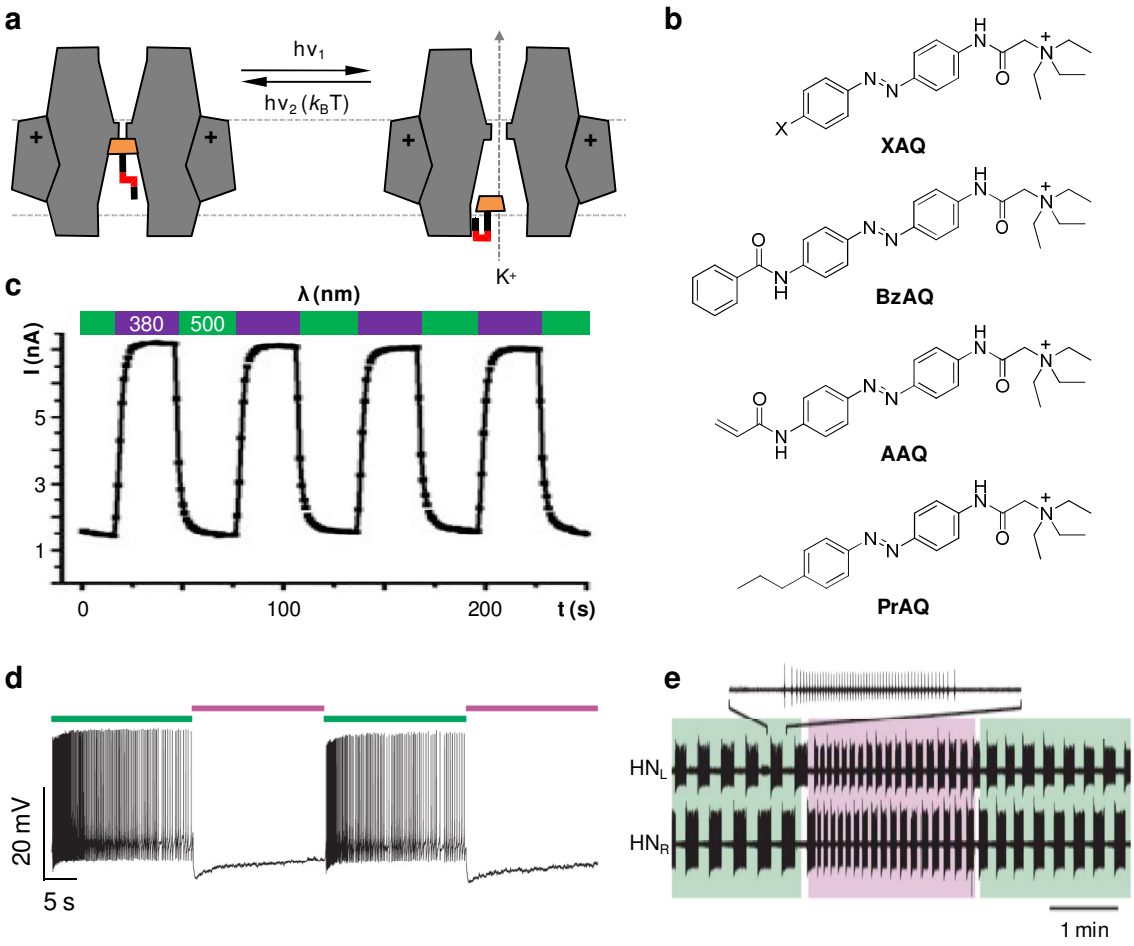

Figure 9. PCLs for voltage-gated ion channels. a) A schematic depiction of a **XAQ** that functions as a photochromic open-channel blocker on K_v channels. b) The chemical structures of **BzAQ**, **AAQ** and **PrAQ**, three typical **XAQ** PCLs for potassium channels. c) **AAQ** reversibly blocks potassium currents of a Kv1 family channel. d) AP firing of hippocampal neurons controlled by **AAQ**. e) Controlling the heart beat of a leech with **AAQ**.

A major goal of our program is to shift the absorption and action spectra of PTLs and PCLs toward the red, which would allow for deeper tissue penetration and would diminish phototoxicity. This can be easily done through chemical derivatization of the azobenzene chromophore. For instance, introduction of an electron-donating substituent yielded **XAQ**s that can be isomerized to their *cis*-isomers with blue light. As an added advantage, these compounds revert to their *trans*-form in the dark within milliseconds, effectively turning themselves off (Fig. 10). Therefore, it is not necessary to toggle between two different wavelengths. An example for this type of compound is **DENAQ**, whose action spectrum peaks at 480 nm. Interestingly, its

analog **PhENAQ** does not act as a blocker in the *trans*-state but rather in the *cis*-state (another case of sign inversion). It can also be switched to the blocking state with blue light and reverts to the inactive state automatically. Therefore, neuronal firing could be triggered with irradiation and quickly silenced by turning the light off.[41]

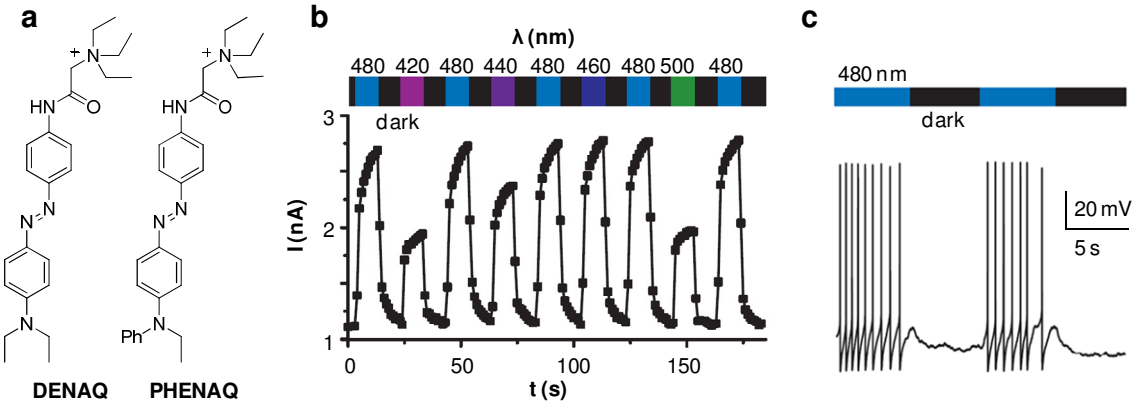

Figure 10. **Red-shifted photochromic blockers**. a) The chemical structures of **DENAQ** and **PhENAQ**, two red-shifted **XAQ**s. b) Action spectrum of **DENAQ**. c) Controlling neuronal firing with **PhENAQ**.

7. Ionotropic glutamate receptors

Ionotropic glutamate receptors (iGluRs) play a central role in synaptic transmission.[17a, 50, 59] Located primarily in postsynaptic membranes, these ligand-gated ion channels respond to the neurotransmitter glutamate released from vesicles on the presynaptic side. Upon glutamate binding, iGluRs generate a depolarizing current, which results in an excitatory postsynaptic potential (EPSP). With their fundamental involvement in neuronal communication, iGluRs are associated with a wide variety of neurological diseases, including Alzheimer's disease, epilepsy and neuronal damage from stroke, and have therefore been very important neuropharmacological targets.[60]

All ionotropic glutamate receptors in higher animals assemble as tetramers and allow permeation of monovalent cations with little selectivity (Fig. 11). Some are also permeable to calcium. Based on functional differences and their response to synthetic ligands, they can be classified into N-methyl-D-aspartate (NMDA) receptors and

non-NMDA receptors. The latter can be divided into three subgroups, namely so-called AMPA, kainate- and δ-receptors.[50, 61]

AMPA receptors, named after a selective agonist, form homo- and heteromeric channels composed of GluA1-GluA4 subunits.[50, 61] AMPA receptors exhibit fast activation and deactivation kinetics - events occur within milliseconds - and initiate depolarization as a first response to synaptic glutamate release close to a postsynaptic site within the dendritic tree. This feature makes them the principle molecular component of fast excitatory synaptic transmission.[50, 61]

By contrast, kainate receptors play a role in the modulation of neuronal excitability rather than in fast excitatory transmission.[61-62] Their mode of action, however, is not as well understood as in the case of AMPA receptors. Homo- and heteromeric channels assemble from so-called GluK1-GluK5 subunits. Delta receptors assemble as homomeric receptors of GluD1 or GluD2 subunits. The function of these receptors, however, remains largely unknown.[61]

NMDA receptors assemble as obligate heterotetramers from a pool of seven subunits. Activation requires not only simultaneous binding of glutamate and glycine (or D-serine), but also an elevated membrane potential of greater than –30 mV. This renders NMDA receptors coincidence detectors, since they are sensitive both to the release of ligands by the presynaptic neuron (and from glial cells) [50, 61] and changes in voltage on the postsynaptic side. In addition, NMDA receptors are not only permeable for Na^+ and K^+, but also for Ca^{2+} ions. These activate various intracellular targets, such as the Ca^{2+}/calmoduline-dependent protein kinase II (CamKII). As such, NMDA receptors are involved in the strengthening of synapses, which is believed to underlie learning and memory.[63]

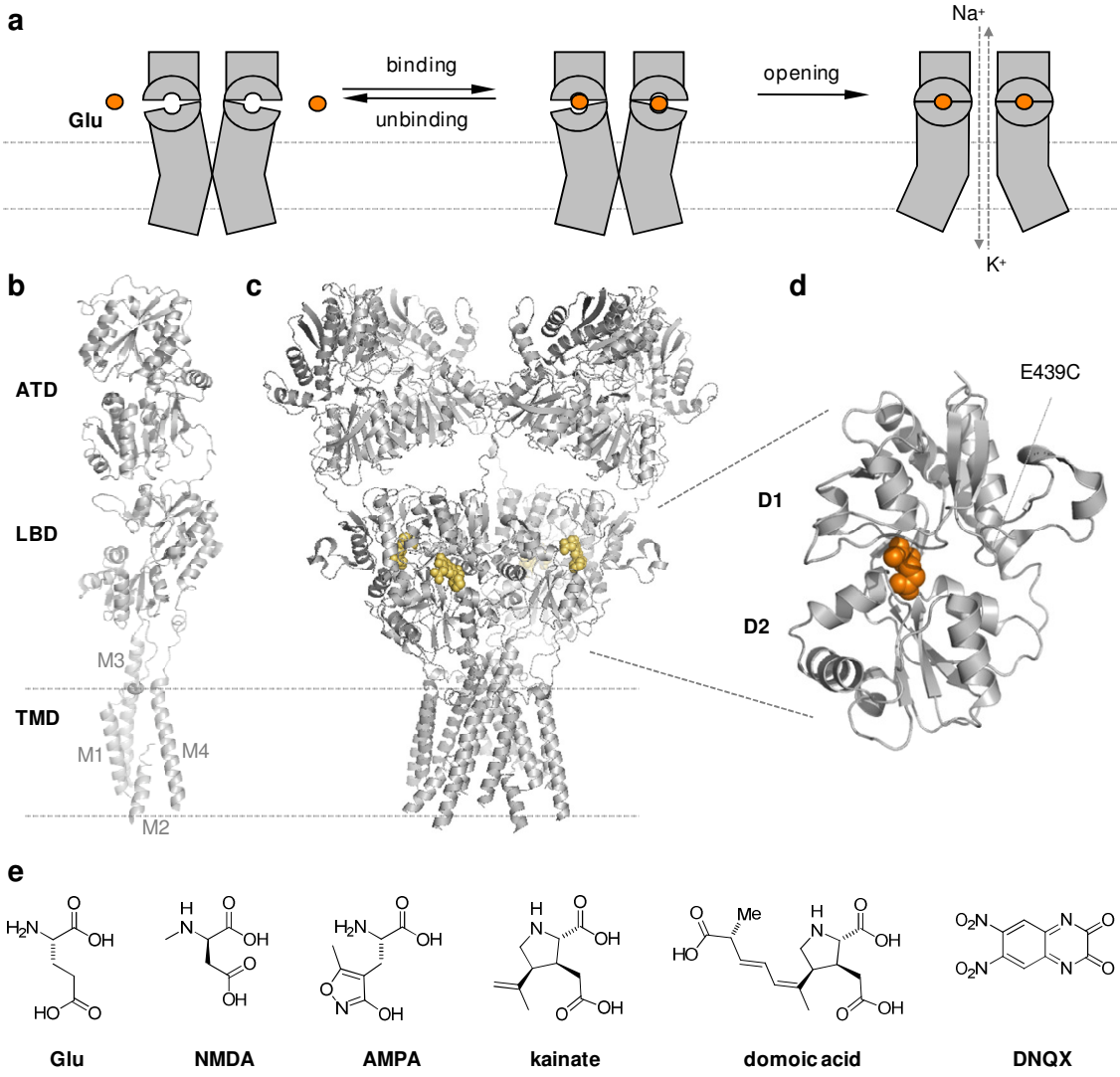

Figure 11. **Ionotropic glutamate receptors**. a) A highly schematic illustration of glutamate receptor gating. b) X-ray structure of single GluA2 subunit indicating the TMD including M1-4, and the extracellular LBD and TMD. c) The fully functional tetrameric GluA2 channel co-crystallized with an antagonist (yellow) (pdb 3KG2). d) Expanded view of a GluA2 LBD co-crystallized with glutamate emphasizing the clamshell (pdb 1FTJ). e) The chemical structures of various agonists and antagonists for iGluRs.

A single iGluR subunit contains an extracellular amino-terminal domain (NTD), a ligand-binding domain (LBD), a transmembrane domain (TMD), and an intracellular carboxyl-terminal domain (CTD). The NTD is involved in subtype-specific assembly and modulation of the receptor. The LBD provides a binding site for agonists (and antagonists). Two subdomains called D1 and D2 form the LBD in a clamshell-like arrangement. The TMD is composed of three transmembrane helices, M1, M3, M4

and a pore helix M2. The CTD plays a role in channel localization, stabilization and targeting for degradation. [50, 61]

X-ray crystallographic studies on GluRs began with soluble versions of LBD clamshells carved out of the full-length receptors through clever protein engineering.[64] These structures were obtained in conjunction with various ligands and proved to be remarkably insightful, since they could explain the activity of agonists, antagonists and modifiers that affect desensitization. [61] For instance, they showed that the binding mode of glutamate to the LBD clamshell is highly conserved in glutamate receptors and that degree of clamshell closure is roughly correlated with the activity of a partial or full agonist. [61] In line with this logic, antagonists, such as DNQX, bind to the clamshell but do but allow it to close tight enough to trigger the biological effect. [61] This "foot-in-the-door" mechanism of antagonism also explains why relatively small changes in the molecular structure can turn an agonist into an antagonist.

In a recent breakthrough in structural biology, the first crystal structure of a full-length homomeric GluA2 receptor was determined at 3.6 Å resolution (Fig. 11b).[12] This AMPA receptor was co-crystallized with a strong competitive antagonist, resulting in a closed, non-conducting state of the receptor. The structure confirmed that the subunits arrange as a dimer of dimers with an overall C_2-symmetry. The TMD architecture resembles an "inverted" K^+ channel", which is linked to a ligand-sensor (the LBDs) instead of a voltage-sensor.

The activation cycle of glutamate receptors can be divided into an inactive resting state, an active non-desensitized state and an inactive desensitized state. The LBDs of the four subunits are arranged in such a way that two clamshells on either side of the C_2-axis are sitting back to back. Glutamate binding to the LBD of the inactive receptor initiates closure of the clamshell cleft. The movement of the lower lobe of the clamshell (D2) during this event rearranges the connector between the LBD and the TMD, which exerts a mechanical force that opens the channel. However, this active non-desensitized state creates tension at the LBD interface. This tension can be

lifted by dissociation of the agonist or by rearrangement at the LBD dimer interface that leads to a closed, desensitized state.[61]

8. Sensitizing ionotropic glutamate receptors toward light

Just as the outer vestibule of K_v channels had provided a suitable platform for the attachment of **MAQ**, the structurally well-characterized extracellular clamshell of glutamate receptors presented an opportunity to explore tethered ligands. In this case, we opted for an agonist, instead of a blocker or antagonist. This approach yielded LiGluR, the "light-gated ionotropic glutamate receptor," which combines a genetically engineered kainate receptor (GluK2) with a PTL called **MAG-1** (Fig. 12).[65] **MAG-1** consists of a maleimide for covalent attachment, an azobenzene photoswitch and a substituted glutamate as the ligand. Once **MAG-1** is attached to a cysteine at the LBD of GluK2 (L439C), light-induced *cis*- and *trans*-isomerization of the azobenzene moiety results in reversible binding of the tethered agonist and translates into opening and closing of the channel.

The design of LiGluR was based on the crystal structure of a closed GluK2-LBD containing the agonist (2*S*,4*R*)-4-methyl glutamate (pdb 1SD3).[62] This structure suggested the existence of a small "exit tunnel" from the bound ligand to the surface of the closed clamshell. It was therefore hypothesized that a tethered glutamate with this stereochemistry could bind to the LBD and still activate the receptor as an agonist or at least a partial agonist. To support this hypothesis, a so-called tether model (**T-Mod**) was synthesized. Using calcium imaging in HEK293 cells, we showed that the tether model, and later MAG-1, indeed act as agonists.[65] Other crystal structures, such as the one of the partial agonist domoic acid bound to GluK2 (pdb 1YAE) also facilitated the design of suitable PTLs.[66]

Once the tether model was found to work, the molecule was extended to **MAG-1** by installing the azobenzene photoswitch and adding a maleimide as an electrophile for cysteine conjugation. In order to find a suitable attachment site for this maleimide, several cysteine mutants of GluK2 were generated by site-directed mutagenesis. After screening about a dozen mutants, L439C turned out to be the best position for **MAG-1** attachment and light-dependent channel activation.[65]

Since it was not clear whether and how the attachment of the PTL to the protein would affect its azobenzene photophysics, the optimal wavelength for activation and inactivation was determined experimentally (Fig. 12). It was found that 380 nm light gave the maximum current, whereas 500 nm led to the fastest channel closure. Interestingly, this observation corresponds very well to the photostationary states of **MAG-1** in solution (Fig. 11). In addition, the thermal relaxation of *cis*-**MAG-1** bound to the channel was found to be much slower than in solution, probably due to the non-covalent interaction of the glutamate ligand with the clamshell, which stabilizes the *cis*-configuration.

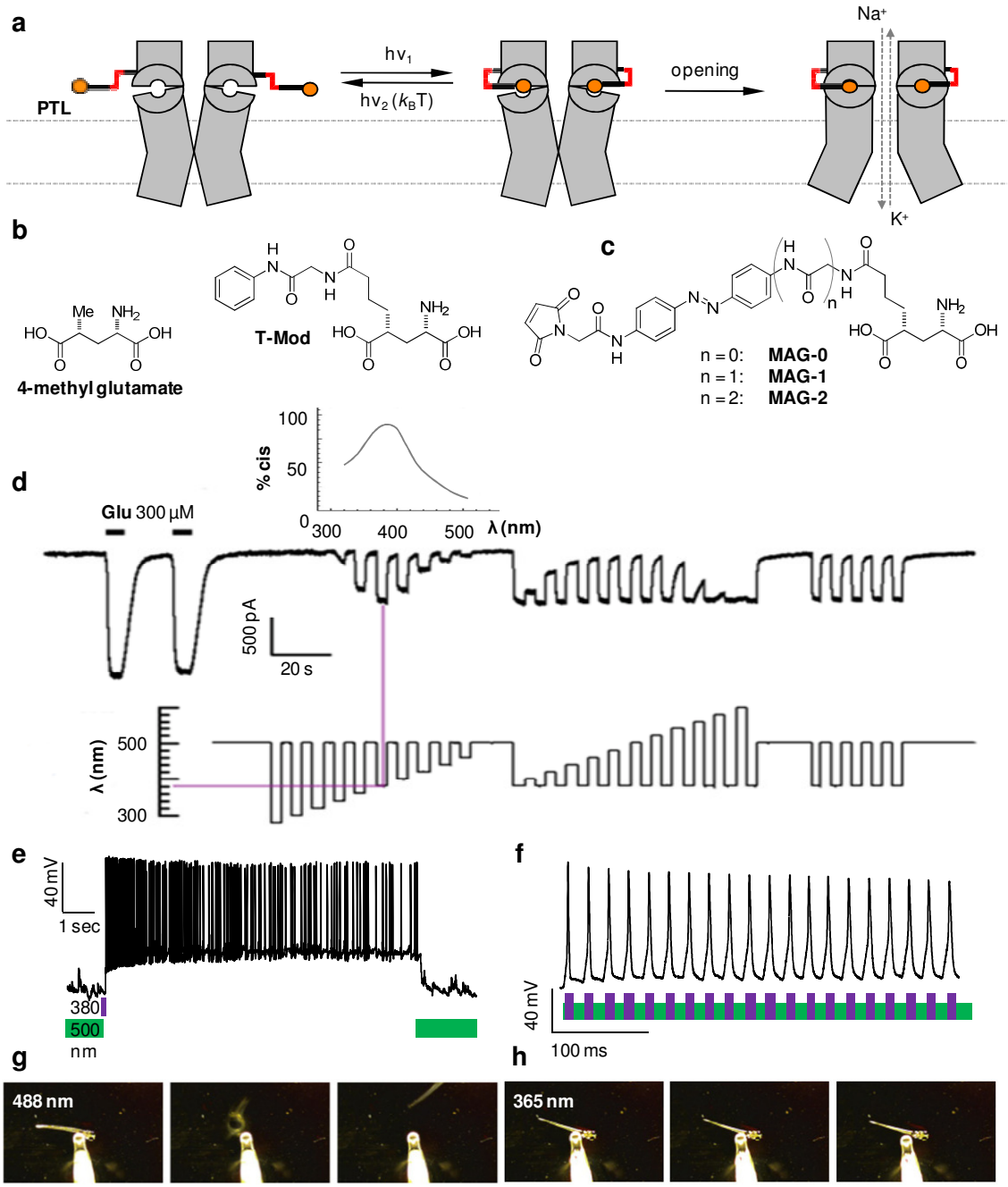

Figure 12. **The light-gated glutamate receptor, LiGluR**. a) A highly schematic illustration of LiGluR. b) The chemical structure of 4-methyl glutamate and the "tether model" (**T-Mod**), two important milestones on the way to LiGuR. c) The chemical structure of **MAG-0**, **MAG-1** and **MAG-2**, three PTLs used. e) The action spectrum of LiGluR. By convention, inward currents are plotted downwards. The phototunability of the system is apparent. f) LiGluR controls AP firing with millisecond precision. A very brief UV–flash induces a train of APs, demonstrating the *cis* stability of the system. f) LiGluR enables AP firing with up to 50 Hz. g) Controlling the escape reflex in zebrafish.

When expressed in neurons, which contain the full machinery to generate APs, LiGluR allows for the optical control of neuronal firing with millisecond resolution.[67] At a given intensity, brief light pulses (1-5 ms) alternating between 380 nm and 500 nm are sufficient to generate reproducible patterns of APs. In dissociated hippocampal neurons, APs can be induced with a frequency up to 50 Hz without missing a beat (Fig. 12).[67] Based on the *cis*-stability of MAG, it is possible to induce constant AP firing for seconds following a single 380 nm light flash that lasts only a few milliseconds. Thus, long illumination periods leading to toxic side effects can be avoided.[67-68]

Compared with SPARK, LiGluR shows some fundamental functional differences. Both irradiation and depolarization are needed to open the SPARK channel (corresponding to a logic AND gate). By contrast, in LiGluR, either soluble glutamate or light is sufficient to allow ions to flow along their electrochemical gradient (corresponding to a logic OR gate). LiGluR is a light-powered molecular machine, since the energy of the photoisomerization translates into the free energy released upon ligand binding, triggering clamshell-closure and channel opening. It can be reset through slow thermal isomerization or active photoswitching with a longer wavelength. SPARK, on the other hand, is a more passive system, since the tethered blocker functions as an extracellular gatekeeper but does not trigger large molecular motions *per se*. These need to be generated by membrane depolarization, which moves the voltage sensor and opens the voltage gate.

One of the hallmarks of our systems in general and LiGluR in particular is their remarkable flexibility and tunability. This is evident at the level of the photoswitches and also at the level of the protein. In addition to **MAG-1**, further derivatives called **MAG-0** and **MAG-2** with different length and flexibility were synthesized and additional attachment sites were generated by site-directed mutagenesis. This "mix and match" approach led to some interesting results. For instance, **MAG-0** anchored at L439C provided the biggest change in effective concentration in competition with the antagonist DNQX. By comparison, **MAG-1**, our original PTL, and **MAG-2** are less effective.[69]

In another case of "sign inversion," we found that the point of attachment can determine whether a PTL activates the channel in the *cis*- or in the *trans* form of the photoswitch (Fig. 13).[69] **MAG-0** bound to L439C, our original attachment site, acts as a *cis*-agonist but becomes a *trans*-agonist when attached to L486C. This is somewhat surprising given that these two sites are only a few Ångstroms apart in the X-ray structures of GluK2. As a consequence of this inverted wavelength sensitivity, transfection of neurons with L486C, followed by **MAG-0** attachment, triggers AP firing at 500 nm and not at 380 nm, as previously observed.

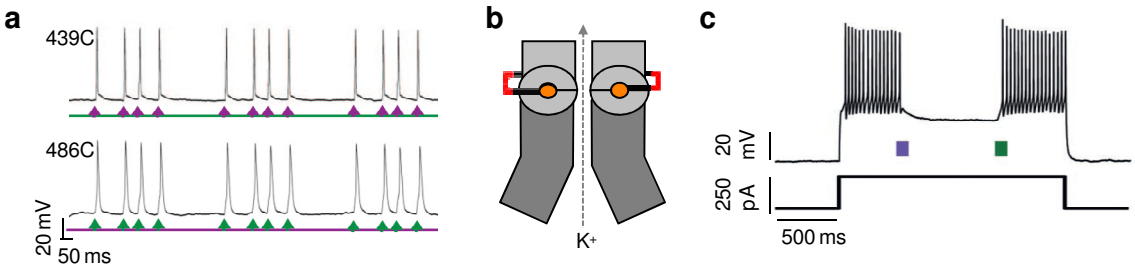

Figure 13. **Sign-inversion through variation of LiGluR**. a) **MAG-0** attached to 439C activates with 380 nm, whereas **MAG-0** attached to 486C induces neuronal firing at 500 nm. b) Schematic drawing of HyLighter, a hyperpolarizing light-gated glutamate receptor. c) HyLighter can be used to silence neurons. Evoked AP firing can be stopped and re-induced by 380 nm and 500 nm light pulses, respectively, demonstrating the bistability of the system.

Just as H-SPARK could be converted into D-SPARK, LiGluR, a light-gated depolarizing ion channel, could be converted into a hyperpolarizing ion channel, which we call HyLighter.[70] As before, this could be achieved by changing the ion-selectivity of the transmembrane domain through genetic manipulation. However, in the case of HyLighter, not a single point mutation, but the exchange of a whole protein domain was necessary. HyLighter combines the GluK2-derived photosensitive LBD of LiGluR with the potassium-selective TMD of a prokaryotic glutamate receptor, SGluR0, which contains the signature GYG motif of K^+ channels.[71] Expression of HyLighter in hippocampal neurons showed that inhibition of neuronal firing can be reversibly turned on and off by irradiation with 380 nm and

500 nm light, respectively. The main advantage of HyLighter in comparison to fully genetically encoded hyperpolarizing systems is the thermal stability of *cis*-**MAG-1** bound to the LBD. Therefore, in analogy to LiGluR, a single 380 nm light flash of a few milliseconds is sufficient to prevent neurons from firing for second to minutes.

One of the big surprises in the development of optochemical systems was how quickly they could be transferred to animals and could be used to dissect behavior.[70] The first *in vivo* experiments with LiGluR were performed in zebrafish larvae. Zebrafish at this stage of development are fully transparent, which is a necessary requirement for reaching neuronal circuits with light. To implement LiGluR, iGluK2-L439C was genetically encoded in small subsets of neurons, which are involved in touch sensation and located at the head and trunk of the animals. For the delivery of the photoswitch to the tissue of interest, it was enough to bath the larvae a solution containing **MAG-1**. Following this treatment, an escape reflex initiated by touching the trunk with a pipette tip could be controlled by optical activation of LiGluR. This reflex could be suppressed by brief illumination with 365 nm light and restored with 488 nm light. HyLighter could be applied to zebrafish larvae in a similar way.[67] In more sophisticated subsequent studies, LiGluR was genetically targeted to a single type of cell and used to elucidate the functional role of so-called Kolmer–Agduhr neurons - a mystery unsolved for 75 years. They turned out to be the central pattern generators of locomotion in the early development of vertebrates.[72]

In addition to PTLs, PCLs turned out to be applicable to glutamate receptors as well (Fig. 14). Their design was based on the extensive pharmacology of iGluR agonists, antagonists and blockers, but was also supported by the LBD X-ray structures. Replacement of the naphthyl moiety of LY339434, a know agonist of GluK1 and GluK2, with an azobenzene gave a molecule that we call **4-GluAzo**. This compound turned out to be a highly effective photochromic agonist of certain kainate receptors.[73] Application to GluK1 and GluK2 channels expressed in HEK293 cells demonstrated the reversible control of inward currents in a light dependent manner. In this case, the *trans*-state of the azobenzene preferentially activates the receptors and **4-GluAzo** showed a slightly higher selectivity for GluK1 than for GluK2. When

applied to dissociated rat hippocampal neurons, **4-GluAzo** functioned as "reversibly caged" glutamate.[73] AP-firing could be triggered by changing from 380 to 500 nm light and stopped by switching back to the lower wavelength. In subsequent work, the burst-firing of cerebellar Purkinje neurons could be effectively controlled with **4-GluAzo**.[74]

Detailed biophysical studies will be needed to understand how **4-GluAzo** and other PCLs work. In particular, it would be interesting to know whether the photoisomerization can take place while they are attached to their binding sites or whether have to dissociate before switching can occur. X-ray crystallographic studies could also provide important insights into the binding modes of PCLs (and PTLs) and guide their further development.

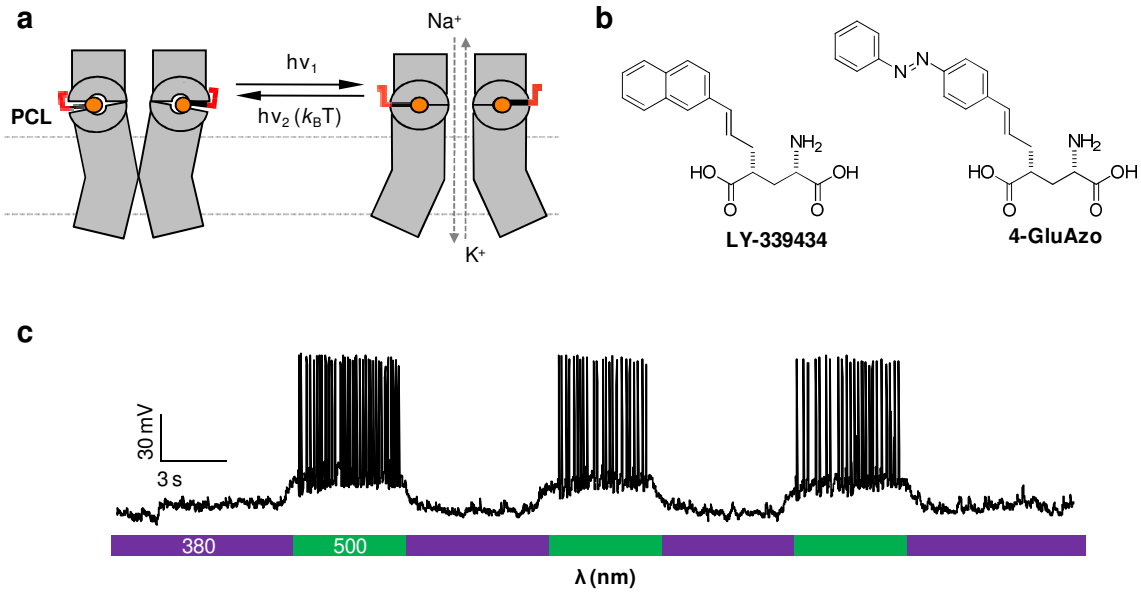

Figure 14. **The PCL logic applied to ionotropic glutamate receptors**. a) Schematic view of a PCL operating on LiGluR. b) The structures of **LY-339434** and its derivative **4-GluAzo**, a PCL that targets kainate receptors. c) Controlling AP firing of hippocampal neurons with **4-GluAzo**.

9. Pentameric ligand-gated ion channels

Pentameric ligand gated ion channels (pLGICs) also play important roles in synaptic transmission.[50] As opposed to mammalian glutamate receptors, they can have both excitatory and inhibitory effects on the postsynaptic cell, which can be a neuron or a muscle cell. The superfamily of pLGICs includes nicotinic acetylcholine receptors (nAChR), γ-aminobutyric acid receptors ($GABA_A$ and $GABA_C$), 5-hydroxytryptamine receptors ($5\text{-}HT_3$) and glycine receptors (GlyRs).[75] Due to the fact that all pLGICs subunits feature an extracellular disulfide bond in a conserved region, they are sometimes also called Cys–loop receptors. $GABA_A$ and $GABA_C$ are chloride-selective ion channels that mediate fast inhibition of neuronal activity in the brain and the retina.[76] $5\text{-}HT_3$, a serotonin receptor, is an excitatory cation channel that modulates neurotransmitter release. Like $GABA_A$ receptors, GlyRs have an inhibitory effect on neuronal communication. They are ligand-gated chloride channels that are mostly expressed in the spinal cord and the brain stem (Fig. 15).[77]

Nicotinic acetylcholine receptors are excitatory cation channels that are expressed throughout the mammalian nervous system and at the neuromuscular junction. [78] Five classes of subunits exist for the muscle-type receptor, called α_1, β_1, γ, ε and δ.[50, 78b] Together, they form a cation-selective pentameric ion channel with $(\alpha_1)_2\beta_1\gamma\delta$ stoichiometry. In contrast, the neuronal types are composed of α_2-α_{10} and β_2-β_4 subunits and can form both heteromeric (e.g. $(\alpha_4)_2(\beta_2)_3$) and homomeric (e. $(\alpha_7)_5$) pentamers. Notably, only α_7, α_8 and α_9 form homomers when expressed heterologously.[78b, 79]

Each subunit of the nAChR is divided into an extracellular, N-terminal ligand-binding domain, a transmembrane region with four transmembrane spanning helices and an intracellular region (Fig. 15). Both the N- and C-terminus are located in the extracellular space. The transmembrane helices of five single subunits line up to form the pore of the ion channel. The $(\alpha_1)_2\beta_1\gamma\delta$ receptor at the neuromuscular end-plate has two ligand bindings sites located between α-γ and α-δ subunits, which have distinct affinities for the neurotransmitter acetylcholine (Ach). Both binding sites must be occupied to open the channel pore.[50, 78b]

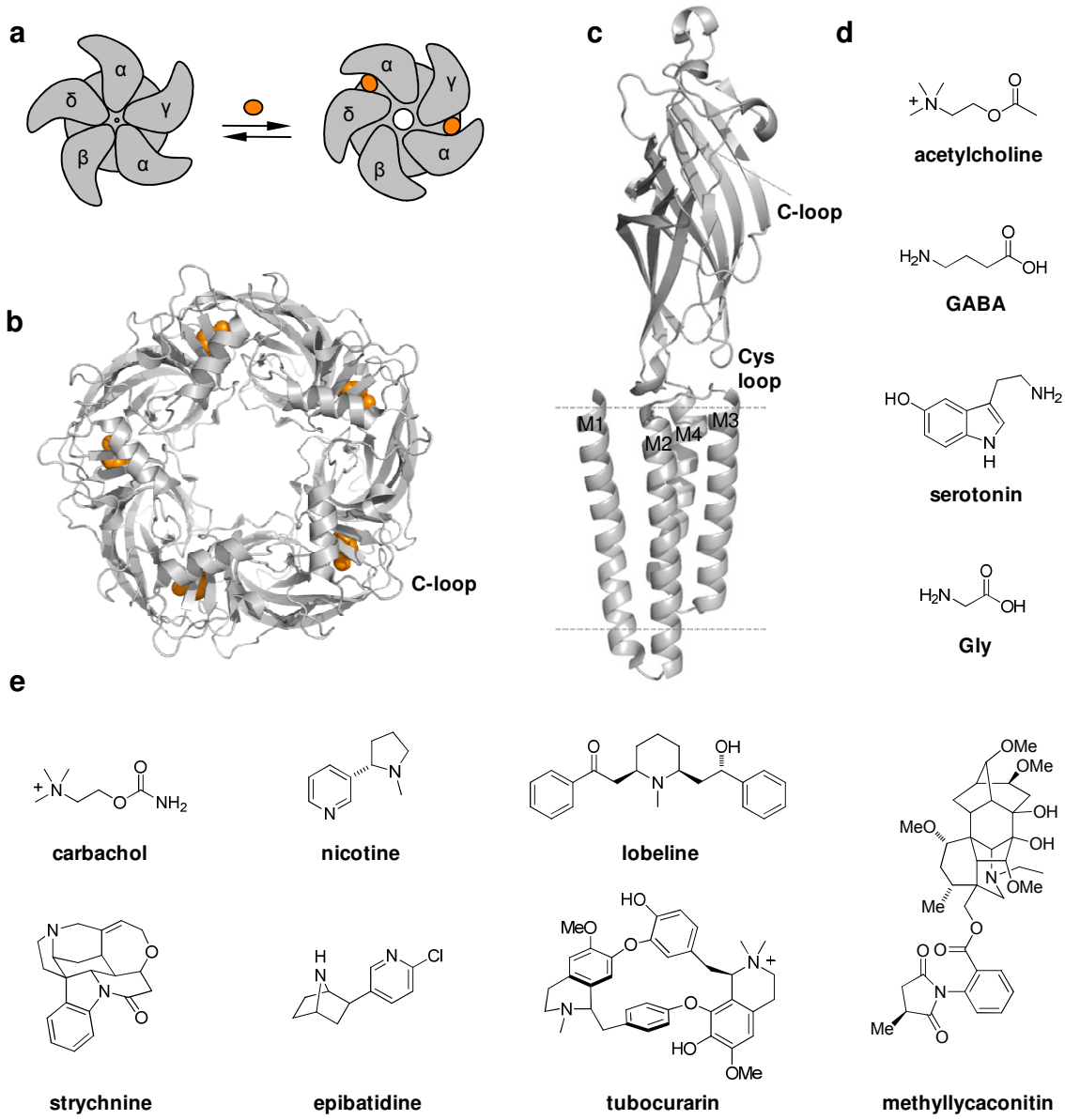

Figure 15. Pentameric ligand-gated ion channels (pLGICs). a) A highly schematic view of nAChR-gating. b) Crystal structure of the acetylcholine-binding protein (AChBP) co-crystallized with nicotine (pdb 1UW6). c) A single subunit of a pLGIC, showing the transmembrane domain, the extracellular ligand-binding domain and the Cys-loop (pdb 3P4W). d) Endogenous ligands that gate pLGICs. e) Other well-known ligands of pentameric ligand-gated ion channel that have been co-crystallized with the AChBP.

The structural biology of the nAChR has a long history, since it was accessible from the electric organ of the ray *Torpedo californica* well before the advent of molecular cloning and heterologous expression.[17c, 50] Using electron microscopy, a structural model of the *Torpedo* nAChR could be gradually built and ultimately refined to 4 Å

resolution.[15a, 80] More recently, X-ray structures of two bacterial homologues, GLIC and ELIC, were solved in their closed and open states, respectively, which provided a detailed view of the pentameric assembly and shed some light on channel gating.[15b, 15c] Unfortunately, none of the abovementioned receptors were crystallized and elucidated in conjunction with agonists or antagonists.

The X-ray structure of two acetylcholine binding proteins, isolated from the sea snails *Limnia stagnalis* (L-AChBP) and *Aplysia californica* (A-AChBP) provided more insight into the interaction of pLGICs with their ligands.[81] These soluble proteins are homologous to the extracellular ligand-binding domain of pLGICs, but lack their transmembrane domain. Sequence alignment of L-AChBP with various pLGICs gave a 20-24% match with nAChR subunits and a 15-18% match to the 5-HT_3, $GABA_A$, $GABA_C$ and glycine receptor subunits.[81b] The X-ray structures of L-AChBP co-crystallized with the agonists nicotine and carbachol showed that the cationic ligands binds at the interface between two subunits in an "aromatic box" made up mostly of tyrosine and tryptophan side chains. This confirmed the importance of cation-pi interactions that had been previously proposed based on intricate biophysical studies with labeled amino acids.[81c] One side of the binding site is covered by the so-called C-loop, which closes like a flap upon agonist binding. This flexible C-loop also carries a cystine disulfide at its tip but is not to be confused with the Cys-loop, which is located closer to the membrane.

Subsequently, other ligands for pLGICs, such epibatidine (an agonist for nAChR),[81d] lobeline (a mixed agonist/antagonist for nAChR),[81d] methyl-lycaconitine (an antagonist for nAChR),[81d] as well as strychnine (an antagonist for GlyR), [82] were co-crystallized with the A-AChBP. These structures showed that the C-loop indeed acts as an induced-fit sensor for ligands, and that the degree of C-loop closure correlates with agonist vs. antagonist activity. How this movement is mechanically linked with the opening of the channel is still matter of debate.

10. Photosensitizing pentameric ligand-gated ion channels

The nicotinic acetylcholine receptor has been studied for many decades, since it was the first ligand-gated ion channels to be isolated and characterized as a protein.[17c] It occurs in high concentrations in the electric organs of certain fish, such as the ray *Torpedo electroplax* or the eel *Electrophorus electricus*, which is why it could be investigated with biophysical methods that were not applicable to other types of receptors at the time. This may be the reason why the nAChR was also the first receptor to be photosensitized, both with a PCL and a PTL.[83] Amazingly, this was done in the early 1970s, well before the advent of molecular cloning, heterologous expression, modern structural biology, and patch-clamp electrophysiology. It took more than three decades to repeat this achievement with other types of receptors!

The PCL used in this case was an azobenzene called **Bis-Q**, which bears a quaternary ammonium ion (Q) on either side of the chromophore. This simple, symmetric molecule functions as a photoswitchable version of the natural agonist acetylcholine.[83] *Trans*-**Bis-Q** activated nAChRs in *Electrophorus electricus*, whereas the corresponding *cis*-isomer was found to be less active. The activity of the two isomers was assayed by measuring the transmembrane potential of *Electrophorus* electroplaques, which are specialized cells from its electric organ. The system was later used to determine the opening and closing rates of nAChRs.[84]

The corresponding PTL system was based on careful reasoning and a bit of luck, because the native receptor could be used without genetic manipulation. It turns out that nAChRs possess a disulfide bond on the tip of their C-loops in the ⊚-subunits, in close proximity to the ligand-binding site (Fig. 16). This disulfide could be reduced without greatly affecting the function of the receptor, providing a reactive thiol for covalent of attachment of a PTL.[83] The PTL was a benzylic bromide, called **QBr**, which also carried the requisite quaternary ammonium ion for receptor activation. Conveniently, **QBr** could be obtained through a slight modification of the synthetic protocol used to make **Bis-Q**. Once attached to nAChRs, **QBr** could be used to reversibly stimulate *Electrophorus* electroplaques, frog-muscles and rat myoballs with light.[85]

Of course, in the 1970s and 80s the light-activated nAChR could not be heterologously expressed and genetically targeted, and it was therefore never used to control AP-firing. Similarly, **Bis-Q** was mostly seen as a tool to study the innate function of nAChRs and not as a practical way to optically control nervous systems or animal behavior. However, with detailed structures and the modern tools of molecular biology now available, it is highly likely that light-gated nAChRs will soon resurface and be used in optochemical genetics. In addition, PCLs and PTLs for other pLGICs are bound to be developed.

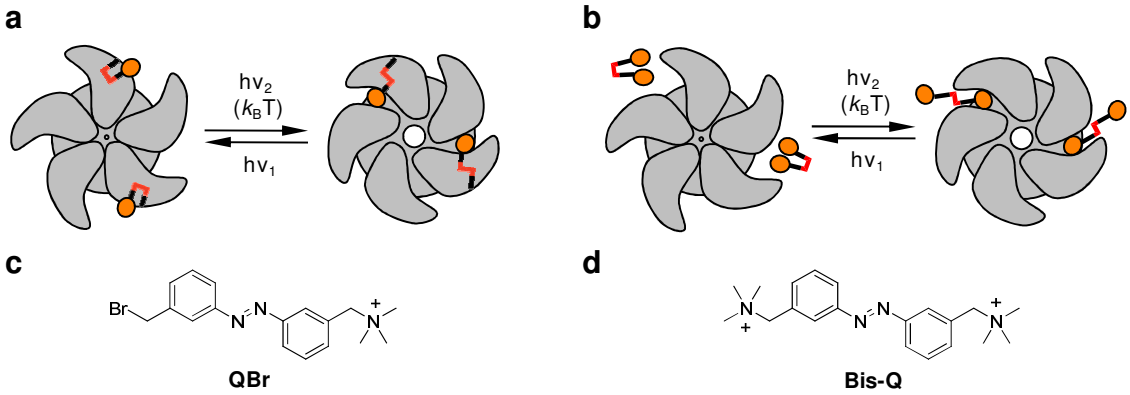

Figure 16. **Photosensitizing the nicotinic acetylcholine receptor**. A highly schematic depiction of a) a PTL reversibly acting on a nAChR, and b) a PCL controlling a nAChRs. c) The structure of **BisQ**, a PCL, and d) **QBr**, a PTL.

11. An abundance of targets

From the preceding paragraphs it is clear that a wide variety of receptors from different structural classes can be rendered photosensitive using synthetic PTLs and PCLs. Still, the vast majority of potential candidates with sufficient structural and pharmacological data have not yet been investigated and opportunities abound to explore the optochemical genetics of these targets. For instance, given the many structural and functional similarities between voltage gated potassium (K_v), sodium (Na_v) and calcium channels (Ca_v), the photochromic open-channel blockers discussed above could be applied to the latter as well. In addition, Na_v and Ca_v channels have extensive pharmacology of their own, which could be exploited to design more

selective PCLs. The long-awaited X-ray structure of a Na_v channel has just been reported and could greatly facilitate the design of corresponding PTLs.[86]

Even if one were confined to clamshell-bearing receptors, there would be a large number of interesting targets to work on. Clamshell-like ligand binding domains have appeared early in evolution and are a prime example for how a successful structural motif has been used again and again in different functional contexts.[87] Originally evolved as bacterial periplasmic binding proteins (such as the well-known maltose binding protein or amino-acid binding proteins), clamshells have been subsequently integrated as functional and structural domains into prokaryotic and eukaryotic transmembrane proteins. Apparently, they were first captured by bacterial ABC-transporters that initially interacted with soluble periplasmic binding proteins in a non-covalent fashion. At some point, they made their way into ion channels, such as ionotropic glutamate receptors. These include several prokaryotic glutamate-gated channels,[71] a plant receptor,[88] and one that was recently found in a comparatively simple eukaryotic rotifer.[89] As discussed above, glutamate-gated ion channels have then assumed a major role in the fast synaptic transmission of higher animals. However, glutamate-binding clamshells can also be found in metabotropic glutamate receptors (mGluRs), which are Family C GPCRs.[90] This large and important class also includes $GABA_B$ receptors [91] and T1R taste receptors[92] and are found in many places in neurophysiology. The clamshell of several of these mGluRs has been characterized by X-ray crystallography in atomic detail and their pharmacology is very well developed (Fig. 17).[93] Therefore, they are logical next targets for manipulation with PTLs or PCLs. Finally, clamshell-like ligand binding domains have been found in certain receptor-linked enzymes, which represent the third major class of receptors involved in signal transduction, aside from ion channels and GPCRs. An example is the ANP receptor, the clamshell-dimer of which has been crystallized bound to the atrial natriuretic peptide (Fig. 17).[94] Clamshell-containing receptor tyrosine kinases have also been recently described.[95]

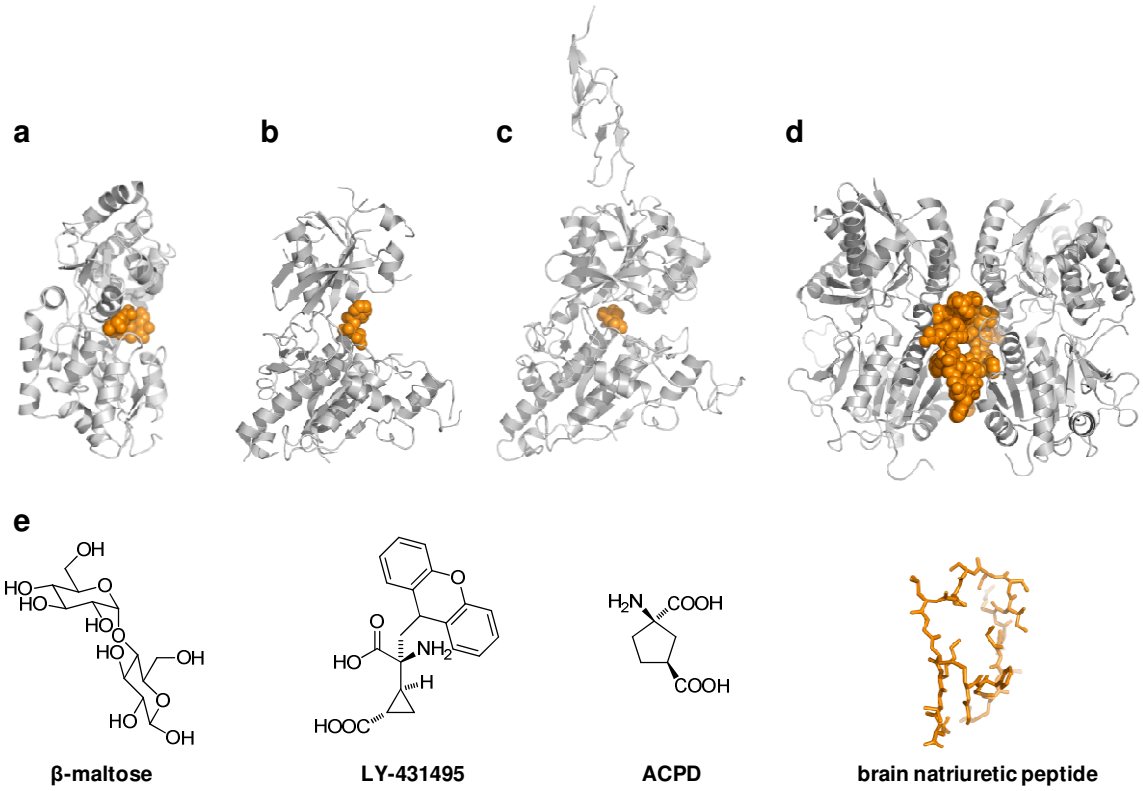

Figure 17. **Clamshell-like LBDs as potential targets for optochemical genetics**. a) The clamshell of the maltose-binding protein, a typical periplasmic binding protein (pdb 1ANF). b) The extracellular clamshell of mGluR3 with an agonist (pdb 2E4X). c) The extracellular clamshell of mGluR1 with an antagonist (pdb 3KS9). The clamshell-dimer of the ANP receptor, a receptor-linked enzyme (pdb 1YK0). d) The chemical structures of ligands for clamshell-containing receptors.

The X-ray structure of a full-length family B GPCR that includes the transmembrane domain has not yet been reported. In contrast, several GPCRs belonging to family A have been recently elucidated with X-ray crystallography (Fig. 18). These receptors comprise the largest class of GPCRs and have a ligand-binding site that is embedded more or less deeply within the membrane. They include such important pharmacological targets as adrenergic receptors (e.g. ◎2A),[96] adenosine receptors (e.g. A_{2A}, which is a target of the antagonist caffeine),[11c] and dopamine receptors (e.g. D3).[11d] Rhodopsin, the photoreceptor used in animal vision, also belongs to this category.[11b] In this case, however, the photoswitch retinal is covalently bound in an inactive form (11-*cis*) and undergoes photoisomerization to the active form (all-*trans*), followed by hydrolysis and recycling, instead of reversible binding. As such, it resembles a PTL to a certain extent**.** Given this analogy, it is entirely conceivable that

well-characterized ligands for other class A GPCRs could be replaced with PTLs and PCLs, turning them into photoreceptors.

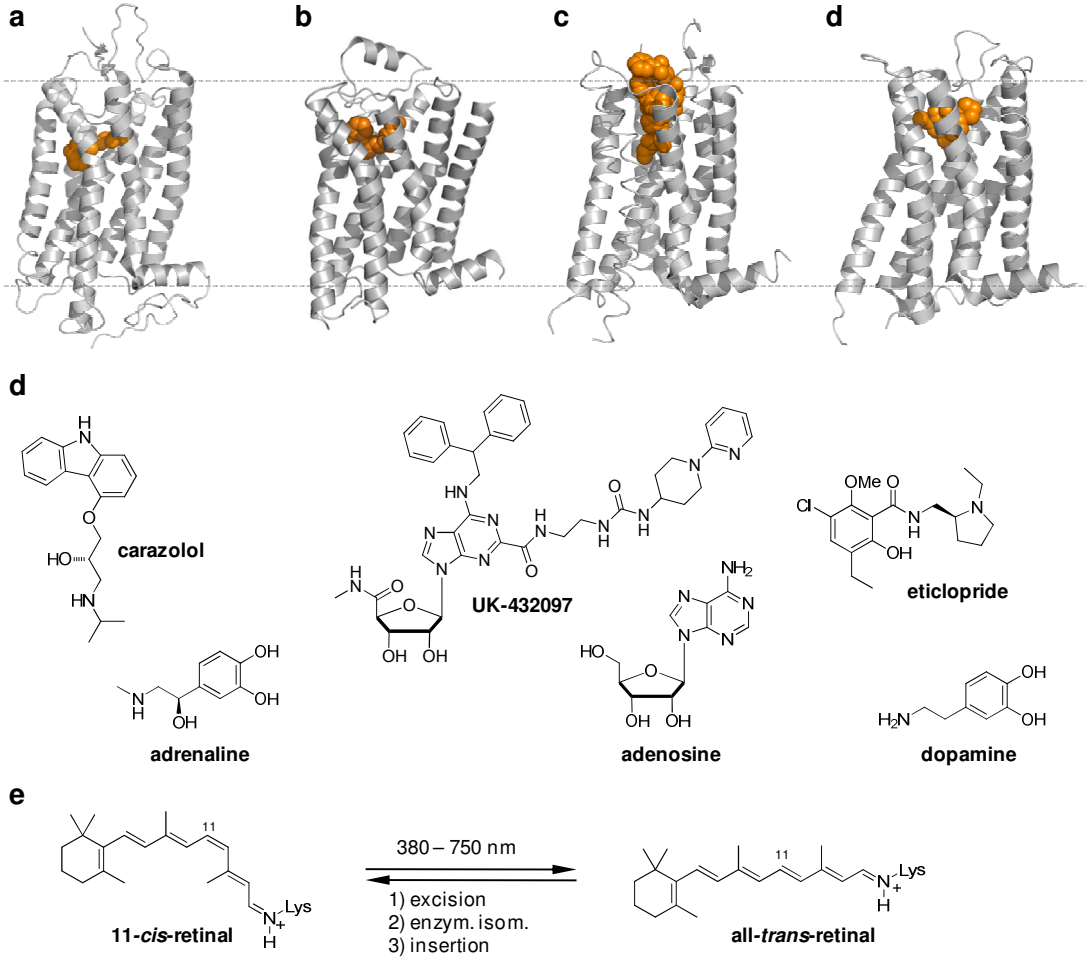

Figure 18. **Family A GPCRs as potential targets of optochemical genetics**. a) Rhodopsin, a natural photoreceptor with a covalently attached photoswitch (pdb 1U19). b) The □2 adrenergic receptor bound to the inverse agonist **carazolol** (pdb 2RH1). b) The A_{2A} adenosine receptor bound to the agonist **UK-432097** (pdb 3QAK). c) The D3 dopamine receptor bound to the antagonist **eticlopride** (pdb 3PBL). Protein domains used to facilitate the crystallization have been cut off. d) Chemical structures of the co-crystallized and endogenous ligands for the receptors depicted above. e) Isomerization of **11-*cis* retinal** to **all-*trans* retinal** in rhodopsin.

Trimeric ion channels are also interesting targets, since they have recently been structurally characterized in atomic detail and have good pharmacology (Fig. 19).

They include purinergic receptors (P2X receptors), acid–sensing ion channels (ASICs) and epithelial sodium channels (ENaCs). The ionotropic P2X receptors are non-selective cation channels that are activated by extracellular adenosine 5'-triphosphate (ATP). They are widely expressed in the nervous and immune system and are involved in numerous neurological functions, such as pain sensation.[97]

The first X-ray crystal structure of a P2X receptor, the zebrafish $P2X_4$ receptor, was solved in its closed state at 3.1 Å resolution.[13] The structure confirmed the trimeric channel architecture and provided important insights into the ion-conducting pore. The position of the ATP binding site was proposed to be located between each subunit at the outer extracellular surface of the receptor. However, the $P2X_4$ structure was solved without ATP or an antagonist bound (e.g. the aza-azobenzene PPADS), leaving the exact binding mode of ligands undefined.

One particular P2X-receptor, $P2X_2$, holds a special place in the development of optochemical genetics. After heterologous expression, this cationic channel could be optically stimulated with caged ATP. Published in 2003, this was one of the first systems shown to work in neurons. Since ATP is hydrolyzed rapidly, even in the extracellular space, photostimulation could be carried out repeatedly and with relatively good temporal resolution. Incidentally, caged ATP is also one of the first, if not the first caged ligand.[35]

ASIC channels belong to the epithelial sodium channel/degenerin (ENaC/DEG) family. They are ligand-gated trimeric cation channels that are activated by extracellular protons and favor Na^+ over K^+ by a factor of ten. Isoforms of ASICs are distributed throughout the mammalian central and peripheral nervous system. They play important physiological roles, e.g. in the detection of tissue acidosis during ischemia.[98] Two crystal structures of homotrimeric ASIC channels have been recently reported.[99] Unfortunately, this is not yet the case for ENaC, a heterotrimeric channel that is constitutively open and is extremely selective for sodium. It plays a key role in sodium reabsorption and salt taste perception and is the target of widely used diuretics, such as amiloride.[100]

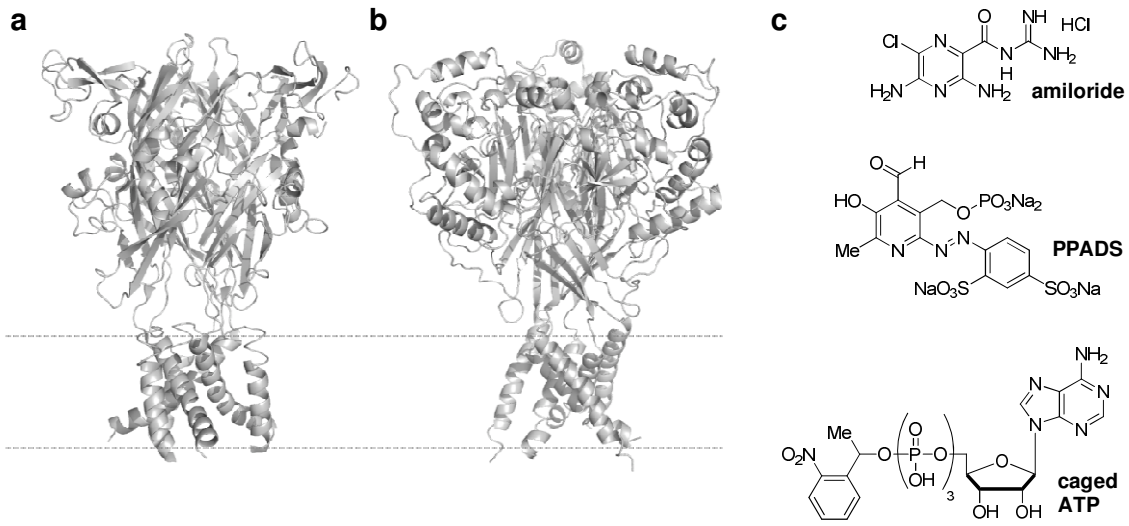

Figure 19. **Trimeric ion channels as potential targets for optochemical genetics**. a) The ASIC1 channel (pdb 3HGC). b) The $P2X_4$ receptor (pdb 3H9V). c) Chemicals acting on trimeric ion channels. **Amiloride**: a blocker for ASIC and ENaC channels. **PPADS**: an antagonist of purinergic receptors. **Caged ATP**: a CL for $P2X_2$ receptors.

Transient-receptor potential channels (TRP channels) have been identified as major molecular players in sensory perception.[101] They are tetrameric cation channels that are polymodal and sensitive to a wide variety of input signals, including temperature, small molecules and ligands. One famous member of this large superfamily is TRPV1, which is activated upon heating but also responds to capsaicin, the active component of chili peppers,[102] Therefore, on a molecular level, "hot" as in "hotplate" and "Red Hot Chili Peppers" are really the same thing. In one of the first applications of optochemical genetics, TRPV1 was heterologously expressed in neurons and stimulated with caged capsaicin and light (see Fig. 4b/c).[35]

TRP channels are not only responsible for sensing heat and coldness but may play a role in sensing pressure as well.[101] As such, they could have physiological roles in mechanoreception (touch), balance, pain, the regulation of blood flow, and hearing.[103] The regulation of pressure-sensors with light would indeed be a very interesting exercise. This has not yet been done with a TRP channel, but proof of

principle has been given with a comparatively simple bacterial mechanoreceptor isolated from *Myxobacterium tuberculosis* (Fig. 20).[104] This homopentameric channel, called MscL, was crystallized in its closed form and its structure was elucidated by X-ray crystallography.[105] If the tension of the membrane in which it is embedded exceeds a certain value, it opens to form a very large pore, thus functioning like a valve that relieves osmotic pressure in the bacterium. The closed gate of the channel is formed by a ring of five hydrophobic residues that prevent ions and other solutes from passing through. Detailed biophysical investigations had shown that replacement of these hydrophobic residues with charged amino acids leads to a constitutively open channel, presumably due to electrostatic repulsion.[106] In a first approach toward photosensitization of MscL, a caged carboxylic acid was covalently attached to a cysteine replacing the hydrophobic residues at the gate. Upon irradiation with UV light, the cages were cleaved and the resulting negative charges triggered the opening of the channel. In a second stage of development, the caged acids were replaced with a covalently attached spiropyran/merocyanine (SPMC) photoswitch. Switching from the comparatively non-polar SP state to the highly polar MC state resulted in opening of the valve. This process was reversible over a few cycles.[104] Although this system was developed as a "nanovalve" for drug delivery and may never find its way into neurobiology, it is nevertheless a very nice example for the optical control of channel activity and it involves both cages and photoswitches. Interestingly, photoswitchable lipids have also been used to change the membrane tension with light and reversibly activate MsCl.[107][100] Indeed, photoswitchable lipids may provide yet another general way to influence the function of transmembrane proteins and cells with light.

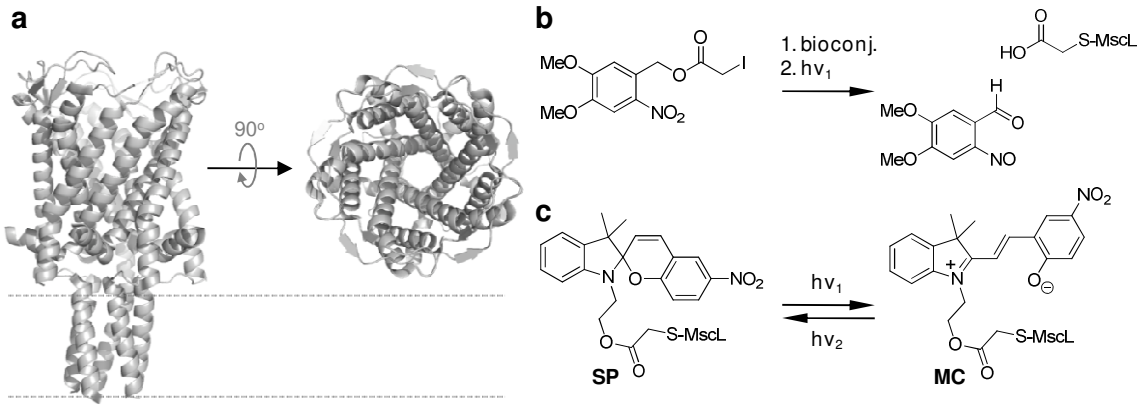

Figure 20. **Photosensitization of a bacterial mechanosensitive ion channel**. a) The structure of MsCl in its closed form in side and top view (pdb 2OAR). b) A caged acid used to trigger MscL opening. c) The SP and MC form of a photoswitch, used to reversibly gate MscL.

12. Summary and Outlook

From the preceding sections it is clear that there is certainly no shortage of protein targets that could be addressed with optochemical genetics. These include naturally occurring photoreceptors, such as the channelrhodopsins, which could be fitted with synthetic switches to tune their spectral properties. However, many variants of synthetic molecules attached to naturally blind receptors are also conceivable. For instance, all of the PTLs and PCLs presented herein are either agonists or blockers, but it should be possible to turn them into antagonists or find photochromic molecules that function as channel openers. In addition, photoswitchable cross-linkers could be developed that could be hooked up to two cysteines.[108] These have been used with great success to control the helical content of peptides[108b, 109] and they have already found applications in governing the activity of proteins.[[110]] It is entirely possible that this approach could be extended to transmembrane receptors, providing yet another way to control neural activity with light.

Other types of photoswitches, such as hemthioindigos or SPMCs, could be systematically explored an applied toward neurobiological relevant receptors. But even if one sticks with azobenzenes, much could be done, since azobenzenes can be easily tuned toward specific photophysical and thermal requirements. For instance, the red-shifted variants that operate far in the visible range of the spectrum and turn themselves off in the dark need to be further developed. Perhaps, one could even push the spectral sensitivity of azobenzenes into the near infrared, in keeping with Sir Francis' grand challenge. Even if it is not possible to develop single-photon switches that respond to these wavelengths, one could explore two-photon photoswitches that would also allow for the precise activation of PCLs in very small volumes. These could be used, for instance, to photochemically stimulate a single synaptic spine, which can be simultaneously monitored with two-photon fluorescence imaging.

Light, however, is not the only "unnatural" input signal that could be considered. For instance, one could reprogram a ligand-gated ion channel to respond to an orthogonal ligand, i.e. a molecule that does not interact with native receptors. This has already been done with much success with kinases and GPCRs and it should be possible to

extend this approach to other types of receptors.[111] One could even speculate about sensitizing ion channels to signals that can deeply penetrate tissues, such as radiofrequency electromagnetic fields or static magnetic fields.

Yet as tempting as these speculations are, light is, and will remain, the most interesting input signal for neuroscience. The technology needed to quickly modulate its wavelength and intensity is highly developed and new ways to deliver light with spatiotemporal control and deep within tissues continue to emerge. These includes digital micromirror arrays[112] and fiber-optic microendoscopy.[113] At the same time, genetic targeting through viral transfection is becoming increasingly precise and effective, and the application of synthetic photoswitches will certainly benefit from new drug delivery techniques. Thus, we expect that many neurobiological questions will be tackled with optochemical genetics in the future.

Much could be learned, for instance, about the innate function of receptors and their many Isoforms since the optical control of genetically defined receptor subtypes could clarify their individual contributions to various physiological processes (cf. Fig. 5). So far, this has been carried out with a variety of K_v channels (cf. section 6) but we anticipate that the optochemical genetic approach can be more broadly applied. Simple pharmacological approaches frequently fail due to a lack of selectivity, and genetic knock-out strategies are often inconclusive because of compensatory effects. Therefore, a knock-in animal, wherein the receptor of interest is substituted with a simple cysteine mutation for PTL attachment and can be conditionally activated and deactivated with light could be very useful.

In addition to basic neuroscience research, where the goal is to understand existing systems through systematic perturbation, one could apply optochemical genetics to what one could call “synthetic neurobiology”. Here, the emphasis lies on rewiring nervous systems and altering their components to create new forms of neural processing or sensory perception. For instance, the receptors that underlie our sense for temperature or mediate pain sensation could be reprogrammed to become photoreceptors. The mechanoreceptors responsible for our sense of hearing and

balance could be engineered in a similar fashion. Perhaps, the day is not far where taste receptors and odorant receptors can be stimulated with light!

This may sound a bit outlandish but such a philosophy may actually lead to useful human therapies. A premier therapeutic target would be the retina, which can be easily reached with light, viruses and small molecules. In many forms of blindness, such as retinitis pigmentosa, the natural photoreceptor cells of the retina, i.e. the rods and cones, have been destroyed but its remaining layers are largely intact. Their neurons express numerous receptors that could be persuaded to become light sensitive using PTLs or PCLs. Indeed, first attempts to use optochemical genetics in vision restoration are very promising (Fig. 21). In a recent study, LiGluR was expressed in the retinal ganglion cells of blind mice after transfection with adeno-associated virus (AAV). Following injection of **MAG-0** into the vitreous body, the retinal ganglion cells, which communicate directly with the brain trough the optical nerve, responded to light-stimulation. This information was relayed to the visual cortex and, as a consequence, the pupillary reflex as well as natural light-avoidance behavior of the animals was restored.[114] First experiences with PCLs have also been promising and bode well for applications of synthetic photoswitches in human therapy.

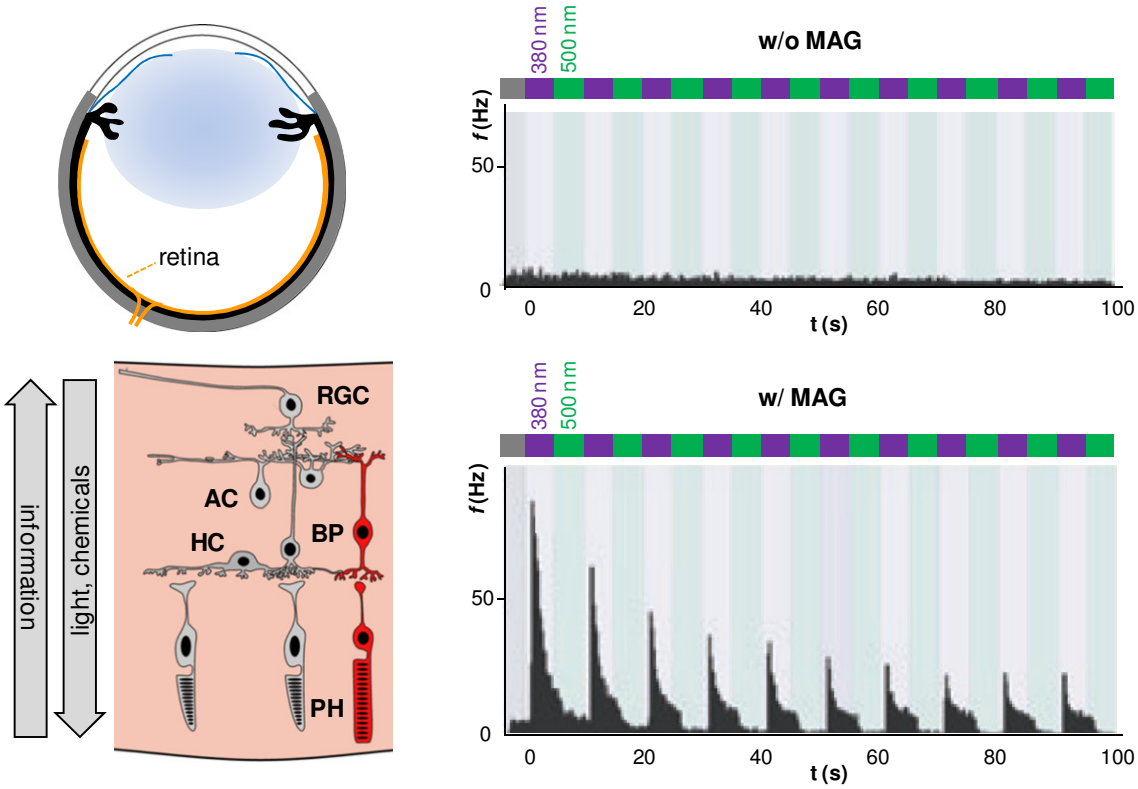

Figure 21. **Restoring visual responses with synthetic photoswitches.** a) Cross-section of a mouse eye with the retina shown in orange b) A schematic diagram of the retina that shows its layered architecture. RGC: retinal ganglion cell, AC: amacrine cell, BP: bipolar cell, HC: horizontal cell, PH: photoreceptor cells (rods and cones) c) and d) Electrical activity of RGCs expressing LiGluR before addition of MAG (c) and after addition if MAG (d).

For us, it is simply amazing that our attempts to teach old receptors new tricks have gone from a proof of principle to studies in vision restoration within seven years. This pace is likely to increase, as numerous new targets are on the horizon and a growing number of neurobiologists, biophysicists and chemists are drawn into the field. We are convinced that these highly collaborative efforts will yield many useful tools, with which to study neural networks or treat disorders of the nervous system. But usefulness aside, optochemical genetics will always remain an incredibly rewarding intellectual exercise and a nice demonstration that the complexities of life can be harnessed with comparatively simple synthetic chemistry (Figure 22).

Figure 22. **Harnessing the complexities of life.** a) A dog (a natural creature slightly modified through breeding) with a leash (a crude device used to control its behavior, with mixed success). b) LiGluR (a complex receptor slightly modified through genetic engineering) on a comparatively simple synthetic leash.

Acknowledgements

We would like to acknowledge our long-standing collaborators, with whom we have developed most of the systems presented, in particular Ehud Isacoff (UC Berkeley) and Richard Kramer (UC Berkeley). We also thank Herwig Baier (UCSF), John Flannery (UC Berkeley) and Xiang Zhang (UC Berkeley) for the stimulating collaborations and discussions we have had over the last years. Support by the National Institutes of Health, the European Science Foundation, and the German National Academic Foundation is gratefully acknowledged.

Abbreviations

AMPA	2-amino-3-hydroxy-5-methyl-4-isoxazolepropionic acid
AP	action potential
Ca_v	voltage-gated potassium channel
CL	caged ligand
GABA	γ-aminobutyric acid
GPCR	G-protein coupled receptor
K_v	voltage-gated potassium channel
MscL	Large-conductance mechanosensitive channel from *M. tuberculosis*
Na_v	voltage-gated sodium channel
NMDA	methyl-D-aspartate
pLGIC	pentameric ligand-gated ion channel
PTL	Photoswitchable tethered ligand
PCL	Photochromic ligand
SPMC	spiropyran/merocyanine photoswitch
TEA	Tetraethylammonium ion
TRPV1	Transient receptor potential channel, e.g. subtype V1

References

[1] F. Crick, *Phil. Trans. R. Soc. Lond. B* **1999**, *354*, 2021-2025.

[2] a) B. Feringa, *Molecular Switches, Vol. 1*, Wiley-VCH, Weinheim, **2001**; b) V. Balzani, M. Venturi, A. Credi, *Molecular Devices and Machines: A Journey into the Nanoworld*, 2 ed., Wiley-VCH, Weinheim, **2008**.

[3] M. Yoshida, E. Muneyuki, T. Hisabori, *Nat. Rev. Mol. Cell Biol.* **2001**, *2*, 669-667.

[4] T. A. Steitz, *Nat. Rev. Mol. Cell Biol.* **2008**, *9*, 242-253.

[5] a) P. Cramer, E. Arnold, *Curr. Opin. Struct. Biol.* **2009**, *19*, 680-682; b) G. Orphanides, D. Reinberg, *Nature* **2000**, *407*, 471-475.

[6] J. R. Kardon, R. D. Vale, *Nat. Rev. Mol. Cell Biol.* **2009**, *10*, 854-865.

[7] S. Choe, *Nat. Rev. Neurosci.* **2002**, *3*, 115-121.

[8] a) K. Deisseroth, *Nat Methods* **2011**, *8*, 26-29; b) S. Peron, K. Svoboda, *Nat. Methods* **2011**, *8*, 30-34; c) L. Sjulson, G. Miesenbock, *Chem. Rev.* **2008**, *108*, 1588-1602; d) F. Zhang, A. M. Aravanis, A. Adamantidis, L. de Lecea, K. Deisseroth, *Nat. Rev. Neurosci.* **2007**, *8*, 577-581.

[9] a) P. Gorostiza, E. Y. Isacoff, *Science* **2008**, *322*, 395-399; b) R. H. Kramer, D. L. Fortin, D. Trauner, *Curr. Opin. Neurobiol.* **2009**, *19*, 544-552.

[10] D. A. Doyle, J. Morais Cabral, R. A. Pfuetzner, A. Kuo, J. M. Gulbis, S. L. Cohen, B. T. Chait, R. MacKinnon, *Science* **1998**, *280*, 69-77.

[11] a) D. M. Rosenbaum, C. Zhang, J. A. Lyons, R. Holl, D. Aragao, D. H. Arlow, S. G. Rasmussen, H. J. Choi, B. T. Devree, R. K. Sunahara, P. S. Chae, S. H. Gellman, R. O. Dror, D. E. Shaw, W. I. Weis, M. Caffrey, P. Gmeiner, B. K. Kobilka, *Nature* **2011**, *469*, 236-240; b) T. Okada, M. Sugihara, A. N. Bondar, M. Elstner, P. Entel, V. Buss, *J. Mol. Biol.* **2004**, *342*, 571-583; c) F. Xu, H. Wu, V. Katritch, G. W. Han, K. A. Jacobson, Z. G. Gao, V. Cherezov, R. C. Stevens, *Science* **2011**, *332*, 322-327; d) E. Y. Chien, W. Liu, Q. Zhao, V. Katritch, G. W. Han, M. A. Hanson, L. Shi, A. H. Newman, J. A. Javitch, V. Cherezov, R. C. Stevens, *Science* **2010**, *330*, 1091-1095.

[12] A. I. Sobolevsky, M. P. Rosconi, E. Gouaux, *Nature* **2009**, *462*, 745-756.

[13] T. Kawate, J. C. Michel, W. T. Birdsong, E. Gouaux, *Nature* **2009**, *460*, 592-598.

[14] a) Y. Jiang, A. Lee, J. Chen, V. Ruta, M. Cadene, B. T. Chait, R. MacKinnon, *Nature* **2003**, *423*, 33-41; b) S. B. Long, E. B. Campbell, R. Mackinnon, *Science* **2005**, *309*, 897-903.

[15] a) N. Unwin, *J. Mol. Biol.* **2005**, *346*, 967-989; b) R. J. Hilf, R. Dutzler, *Nature* **2008**, *452*, 375-379; c) R. J. Hilf, R. Dutzler, *Nature* **2009**, *457*, 115-118.

[16] X. Chen, Q. Wang, F. Ni, J. Ma, *Proc. Natl. Acad. Sci. USA* **2010**, *107*, 11352-11357.

[17] E. R. Kandel, J. Schwartz, T. Jessell, *Principles of Neural Science*, 4 ed., Elsevier, **2000**; b) B. P. Bean, *Nat. Rev. Neurosci.* **2007**, *8*, 451-465; c) B. Hille, *Ionic Channels of Excitable Membranes*, 3 ed., Sinauer Associates, Inc., **2001.**

[18] C. Yue, Y. Yaari, *J. Neurosci.* **2004**, *24*, 4614-4624.

[19] W. M. Oldham, H. E. Hamm, *Nat. Rev. Mol. Cell Biol.* **2008**, *9*, 60-71.

[20] D. E. Nichols, C. D. Nichols, *Chem. Rev.* **2008**, *108*, 1614-1641.

[21] S. W. Hell, *Nat. Methods* **2009**, *6*, 24-32.

[22] W. Denk, J. H. Strickler, W. W. Webb, *Science* **1990**, *248*, 73-76.

[23] J. N. Kerr, W. Denk, *Nat. Rev. Neurosci.* **2008**, *9*, 195-205.

[24] B. V. Zemelman, G. A. Lee, M. Ng, G. Miesenbock, *Neuron* **2002**, *33*, 15-22.

[25] a) G. Nagel, T. Szellas, W. Huhn, S. Kateriya, N. Adeishvili, P. Berthold, D. Ollig, P. Hegemann, E. Bamberg, *Proc. Natl. Acad. Sci. USA* **2003**, *100*, 13940-13945; b) F. Zhang, L. P. Wang, E. S. Boyden, K. Deisseroth, *Nat. Methods* **2006**, *3*, 785-792.

[26] E. S. Boyden, F. Zhang, E. Bamberg, G. Nagel, K. Deisseroth, *Nat. Neurosci.* **2005**, *8*, 1263-1268.

[27] F. Zhang, L. P. Wang, M. Brauner, J. F. Liewald, K. Kay, N. Watzke, P. G. Wood, E. Bamberg, G. Nagel, A. Gottschalk, K. Deisseroth, *Nature* **2007**, *446*, 633-639.

[28] a) A. Berndt, P. Schoenenberger, J. Mattis, K. M. Tye, K. Deisseroth, P. Hegemann, T. G. Oertner, *Proc. Natl. Acad. Sci. USA* **2011**, *108*, 7595-7600; b) V. Gradinaru, F. Zhang, C. Ramakrishnan, J. Mattis, R. Prakash, I. Diester, I. Goshen, K. R. Thompson, K. Deisseroth, *Cell* **2010**, *141*, 154-165; c) L. A. Gunaydin, O. Yizhar, A. Berndt, V. S. Sohal, K. Deisseroth, P. Hegemann, *Nat. Neurosci.* **2010**, *13*, 387-392; d) A. Berndt, O. Yizhar, L. A. Gunaydin, P. Hegemann, K. Deisseroth, *Nat. Neurosci.* **2009**, *12*, 229-234; e) F. Zhang, M. Prigge, F. Beyriere, S. P. Tsunoda, J. Mattis, O. Yizhar, P. Hegemann, K. Deisseroth, *Nat. Neurosci.* **2008**, *11*, 631-633.

[29] B. Y. Chow, X. Han, A. S. Dobry, X. Qian, A. S. Chuong, M. Li, M. A. Henninger, G. M. Belfort, Y. Lin, P. E. Monahan, E. S. Boyden, *Nature* **2010**, *463*, 98-102.

[30] V. Gradinaru, M. Mogri, K. R. Thompson, J. M. Henderson, K. Deisseroth, *Science* **2009**, *324*, 354-359.

[31] V. Busskamp, J. Duebel, D. Balya, M. Fradot, T. J. Viney, S. Siegert, A. C. Groner, E. Cabuy, V. Forster, M. Seeliger, M. Biel, P. Humphries, M. Paques, S. Mohand-Said, D. Trono, K. Deisseroth, J. A. Sahel, S. Picaud, B. Roska, *Science* **2010**, *329*, 413-417.

[32] A. B. Arrenberg, D. Y. Stainier, H. Baier, J. Huisken, *Science* **2010**, *330*, 971-974.

[33] G. C. Ellis-Davies, *Nat. Methods* **2007**, *4*, 619-628.

[34] J. Noguchi, A. Nagaoka, S. Watanabe, G. C. Ellis-Davies, K. Kitamura, M. Kano, M. Matsuzaki, H. Kasai, *J. Physiol.* **2011,** *589*, 2447-2457.

[35] B. V. Zemelman, N. Nesnas, G. A. Lee, G. Miesenbock, *Proc. Natl. Acad. Sci. USA* **2003**, *100*, 1352-1357.

[36] P. J. Alaimo, M. A. Shogren-Knaak, K. M. Shokat, *Curr. Opin. Chem. Biol.* **2001**, *5*, 360-367; b) S. L. Schreiber, *Bioorg. Med. Chem.* **1998**, *6*, 1127-1152; c) B. R. Stockwell, *Nat. Rev. Genet.* **2000**, *1*, 116-125.

[37] M. J. Keiser, V. Setola, J. J. Irwin, C. Laggner, A. I. Abbas, S. J. Hufeisen, N. H. Jensen, M. B. Kuijer, R. C. Matos, T. B. Tran, R. Whaley, R. A. Glennon, J. Hert, K. L. Thomas, D. D. Edwards, B. K. Shoichet, B. L. Roth, *Nature* **2009**, *462*, 175-181.

[38] a) M. E. Hahn, T. W. Muir, *Trends. Biochem. Sci.* **2005**, *30*, 26-34; b) M. A. Shogren-Knaak, P. J. Alaimo, K. M. Shokat, *Annu. Rev. Cell. Dev. Biol.* **2001**, *17*, 405-433.

[39] M. R. Banghart, M. Volgraf, D. Trauner, *Biochemistry* **2006**, *45*, 15129-15141.

[40] F. Hamon, F. Djedaini-Pilard, F. Barbot, C. Len, *Tetrahedron* **2009**, *65*, 10105-10123.

[41] P. Gorostiza, M. Volgraf, R. Numano, S. Szobota, D. Trauner, E. Y. Isacoff, *Proc. Natl. Acad. Sci. USA* **2007**, *104*, 10865-10870.

[42] A. Mourot, M. Kienzler, M. Banghart, T. Fehrentz, F. Huber, M. S., R. H. Kramer, D. Trauner, *ACS. Chem. Neurosci.* **2011**, accepted for publication.

[43] a) P. V. Chang, J. A. Prescher, M. J. Hangauer, C. R. Bertozzi, *J. Am. Chem. Soc.* **2007**, *129*, 8400-8401; b) J. A. Prescher, C. R. Bertozzi, *Nat. Chem. Biol.* **2005**, *1*, 13-21; c)J. A. Prescher, D. H. Dube, C. R. Bertozzi, *Nature* **2004**, *430*, 873-877.

[44] F. Tombola, M. M. Pathak, E. Y. Isacoff, *Annu. Rev. Cell Dev. biol.* **2006**, *22*, 23-52.

[45] H. Wulff, N. A. Castle, L. A. Pardo, *Nat. Rev. Drug Discovery* **2009**, *8*, 982-1001.

[46] Y. Jiang, A. Lee, J. Chen, M. Cadene, B. T. Chait, R. MacKinnon, *Nature* **2002**, *417*, 515-522.

[47] a) M. Nishida, M. Cadene, B. T. Chait, R. MacKinnon, *EMBO J.* **2007**, *26*, 4005-4015; b) M. Nishida, R. MacKinnon, *Cell* **2002**, *111*, 957-965; c) S. Pegan, C. Arrabit, W. Zhou, W. Kwiatkowski, A. Collins, P. A. Slesinger, S. Choe, *Nat. Neurosci.* **2005**, *8*, 279-287.

[48] N. Shi, S. Ye, A. Alam, L. Chen, Y. Jiang, *Nature* **2006**, *440*, 570-574.

[49] a) T. Hoshi, W. N. Zagotta, R. W. Aldrich, *Science* **1990**, *250*, 533-538; b) W. N. Zagotta, T. Hoshi, R. W. Aldrich, *Science* **1990**, *250*, 568-571.

[50] a) L. G. Cuello, V. Jogini, D. M. Cortes, A. C. Pan, D. G. Gagnon, O. Dalmas, J. F. Cordero-Morales, S. Chakrapani, B. Roux, E. Perozo, *Nature* **2010**, *466*, 272-275; b) L. G. Cuello, V. Jogini, D. M. Cortes, E. Perozo, *Nature* **2010**, *466*, 203-208; c) L. Kiss, S. J. Korn, *Biophys. J.* **1998**, *74*, 1840-1849.

[51] C. Hammond, *Cellular and Molecular Neurophysiology*, 3 ed., Elsevier *Science*, **2008**.

[52] a) K. G. Chandy, M. Cahalan, M. Pennington, R. S. Norton, H. Wulff, G. A. Gutman, *Toxicon* **2001**, *39*, 1269-1276; b) M. A. Eriksson, B. Roux, *Biophys. J.* **2002**, *83*, 2595-2609.

[53] C. M. Armstrong, *J. Gen. Physiol.* **1971**, *58*, 413-437.

[54] M. J. Lenaeus, M. Vamvouka, P. J. Focia, A. Gross, *Nat. Struct. Mol. Biol.* **2005**, *12*, 454-459.

[55] M. Banghart, K. Borges, E. Isacoff, D. Trauner, R. H. Kramer, *Nat. Neurosci.* **2004**, *7*, 1381-1386.

[56] a) R. O. Blaustein, *J. Gen. Physiol.* **2002**, *120*, 203-216; b) R. O. Blaustein, P. A. Cole, C. Williams, C. Miller, *Nat. Struct. Mol. Biol.* **2000**, *7*, 309-311.

[57] J. J. Chambers, M. R. Banghart, D. Trauner, R. H. Kramer, *J. Neurophysiol.* **2006**, *96*, 2792-2796.

[58] D. L. Fortin, T. W. Dunn, A. Fedorchak, D. Allen, R. Montpetit, M. R. Banghart, D. Trauner, J. P. Adelman, R. H. Kramer, *J. Neurophysiol.* **2011**, *106*, 488-496.

[59] a) M. R. Banghart, A. Mourot, D. L. Fortin, J. Z. Yao, R. H. Kramer, D. Trauner, *Angew. Chem. Int. Ed.* **2009**, *48*, 9097-9101; b) D. L. Fortin, M. R. Banghart, T. W. Dunn, K. Borges, D. A. Wagenaar, Q. Gaudry, M. H. Karakossian, T. S. Otis, W. B. Kristan, D. Trauner, R. H. Kramer, *Nat. Methods* **2008**, *5*, 331-338.

[60] R. W. Gereau, G. T. Swanson, *The Glutamate Receptors*, Humana Press, **2008**.

[61] a) G. N. Barnes, J. T. Slevin, *Curr Med Chem* **2003**, *10*, 2059-2072; b) M. R. Farlow, *Geriatrics* **2004**, *59*, 22-27.

[62] S. F. Traynelis, L. P. Wollmuth, C. J. McBain, F. S. Menniti, K. M. Vance, K. K. Ogden, K. B. Hansen, H. Yuan, S. J. Myers, R. Dingledine, *Pharmacol. Rev.* **2010**, *62*, 405-496.

[63] M. L. Mayer, *Neuron* **2005**, *45*, 539-552.

[64] a) G. L. Collingridge, J. T. Isaac, Y. T. Wang, *Nat. Rev. Neurosci.* **2004**, *5*, 952-962; b) C. G. Lau, R. S. Zukin, *Nat. Rev. Neurosci.* **2007**, *8*, 413-426.

[65] P. Stawski, H. Janovjak, D. Trauner, *Bioorg. Med. Chem.* **2010**, *18*, 7759-7772.

[66] M. Volgraf, P. Gorostiza, R. Numano, R. H. Kramer, E. Y. Isacoff, D. Trauner, *Nat. Chem. Biol.* **2006**, *2*, 47-52.

[67] M. H. Nanao, T. Green, Y. Stern-Bach, S. F. Heinemann, S. Choe, *Proc. Natl. Acad. Sci. USA* **2005**, *102*, 1708-1713.

[68] S. Szobota, P. Gorostiza, F. Del Bene, C. Wyart, D. L. Fortin, K. D. Kolstad, O. Tulyathan, M. Volgraf, R. Numano, H. L. Aaron, E. K. Scott, R. H. Kramer, J. Flannery, H. Baier, D. Trauner, E. Y. Isacoff, *Neuron* **2007**, *54*, 535-545.

[69] R. Numano, S. Szobota, A. Y. Lau, P. Gorostiza, M. Volgraf, B. Roux, D. Trauner, E. Y. Isacoff, *Proc. Natl. Acad. Sci. USA* **2009**, *106*, 6814-6819.

[70] H. Janovjak, S. Szobota, C. Wyart, D. Trauner, E. Y. Isacoff, *Nat. Neurosci.* **2010**, *13*, 1027-1032.

[71] G. Q. Chen, C. Cui, M. L. Mayer, E. Gouaux, *Nature* **1999**, *402*, 817-821.

[72] C. Wyart, F. Del Bene, E. Warp, E. K. Scott, D. Trauner, H. Baier, E. Y. Isacoff, *Nature* **2009**, *461*, 407-410.

[73] M. Volgraf, P. Gorostiza, S. Szobota, M. R. Helix, E. Y. Isacoff, D. Trauner, *J. Am. Chem. Soc.* **2007**, *129*, 260-261.

[74] Z. R. Abrams, A. Warrier, D. Trauner, X. Zhang, *Front Neural Circuits* **2010**, *4*, 13.

[75] M. O. Ortells, G. G. Lunt, *Trends in Neurosci.* **1995**, *18*, 121-127.

[76] a) J. Bormann, A. Feigenspan, *Trends in Neurosci.* **1995**, *18*, 515-519; b) U. Rudolph, H. Mohler, *Annu. Rev. Pharm. Toxicol.* **2004**, *44*, 475-498; c) W. Sieghart, G. Sperk, *Curr. Top. in Med. Chem.* **2002**, *2*, 795-816.

[77] a) C. M. Becker, *The Neuroscientist* **1995**, *1*, 130-141; b) E. Y. Kim, N. Schrader, B. Smolinsky, C. Bedet, C. Vannier, G. Schwarz, H. Schindelin, *EMBO J.* **2006**, *25*, 1385-1395.

[78] a) P. J. Corringer, N. Le Novere, J. P. Changeux, *Annu. Rev. Pharm. Toxicol.* **2000**, *40*, 431-458; b) A. Karlin, *Nat. Rev. Neurosci.* **2002**, *3*, 102-114.

[79] D. Paterson, A. Nordberg, *Progress in Neurobiology* **2000**, *61*, 75-111.

[80] N. Unwin, *FEBS. Letters* **2003**, *555*, 91-95.

[81] a) Y. Bourne, T. T. Talley, S. B. Hansen, P. Taylor, P. Marchot, *The EMBO J.* **2005**, *24*, 1512-1522; b) K. Brejc, W. J. van Dijk, R. V. Klaassen, M. Schuurmans, J. van Der Oost, A. B. Smit, T. K. Sixma, *Nature* **2001**, *411*, 269-276; c) P. H. Celie, S. E. van Rossum-Fikkert, W. J. van Dijk, K. Brejc, A. B. Smit, T. K. Sixma, *Neuron* **2004**, *41*, 907-914; d) S. B. Hansen, G. Sulzenbacher, T. Huxford, P. Marchot, P. Taylor, Y. Bourne, *EMBO J.* **2005**, *24*, 3635-3646.

[82] M. Brams, A. Pandya, D. Kuzmin, R. van Elk, L. Krijnen, J. L. Yakel, V. Tsetlin, A. B. Smit, C. Ulens, *PLoS. Biol.* **2011**, *9*, e1001034.

[83] E. Bartels, N. H. Wassermann, B. F. Erlanger, *Proc. Natl. Acad. Sci. USA* **1971**, *68*, 1820-1823.

[84] H. A. Lester, H. W. Chang, *Nature* **1977**, *266*, 373-374.

[85] a) L. D. Chabala, H. A. Lester, *J. Physiol.* **1986**, *379*, 83-108; b) H. A. Lester, M. E. Krouse, M. M. Nass, N. H. Wassermann, B. F. Erlanger, *J. Gen. Physiol.* **1980**, *75*, 207-232.

[86] J. Payandeh, T. Scheuer, N. Zheng, W. A. Catterall, *Nature* **2011**.

[87] C. B. Felder, R. C. Graul, A. Y. Lee, H. P. Merkle, W. Sadee, *AAPS. PharmSci.* **1999**, *1*, E2.

[88] E. Michard, P. T. Lima, F. Borges, A. C. Silva, M. T. Portes, J. E. Carvalho, M. Gilliham, L. H. Liu, G. Obermeyer, J. A. Feijo, *Science* **2011**, *332*, 434-437.

[89] H. Janovjak, G. Sandoz, E. Y. Isacoff, *Nat. Commun.* **2011**, *2*, 232.

[90] H. Brauner-Osborne, P. Wellendorph, A. A. Jensen, *Curr. Drug. Targets* **2007**, *8*, 169-184.

[91] J. P. Pin, J. Kniazeff, V. Binet, J. Liu, D. Maurel, T. Galvez, B. Duthey, M. Havlickova, J. Blahos, L. Prezeau, P. Rondard, *Biochem. Pharmacol.* **2004**, *68*, 1565-1572.

[92] a) M. Behrens, W. Meyerhof, C. Hellfritsch, T. Hofmann, *Angew. Chem. Int. Ed.* **2011**, *50*, 2220-2242; b) G. Q. Zhao, Y. Zhang, M. A. Hoon, J. Chandrashekar, I. Erlenbach, N. J. Ryba, C. S. Zuker, *Cell* **2003**, *115*, 255-266.

[93] T. Muto, D. Tsuchiya, K. Morikawa, H. Jingami, *Proc. Natl. Acad. Sci. USA* **2007**, *104*, 3759-3764.

[94] X. L. He, A. Dukkipati, K. C. Garcia, *J. Mol. Biol.* **2006**, *361*, 698-714.

[95] J. Vicogne, J. P. Pin, V. Lardans, M. Capron, C. Noel, C. Dissous, *Mol. Biochem. Parasitol* **2003**, *126*, 51-62.

[96] V. Cherezov, D. M. Rosenbaum, M. A. Hanson, S. G. Rasmussen, F. S. Thian, T. S. Kobilka, H. J. Choi, P. Kuhn, W. I. Weis, B. K. Kobilka, R. C. Stevens, *Science* **2007**, *318*, 1258-1265.

[97] B. S. Khakh, *Nat. Rev. Neurosci.* **2001**, *2*, 165-174.

[98] Y. Yu, Z. Chen, W. G. Li, H. Cao, E. G. Feng, F. Yu, H. Liu, H. Jiang, T. L. Xu, *Neuron* **2010**, *68*, 61-72.

[99] a) E. B. Gonzales, T. Kawate, E. Gouaux, *Nature* **2009**, *460*, 599-604; b) J. Jasti, H. Furukawa, E. B. Gonzales, E. Gouaux, *Nature* **2007**, *449*, 316-323.

[100] L. Schild, *Biochim. Biophys. Acta* **2010**, *1802*, 1159-1165.

[101] A. I. Basbaum, D. M. Bautista, G. Scherrer, D. Julius, *Cell* **2009**, *139*, 267-284.

[102] M. J. Caterina, M. A. Schumacher, M. Tominaga, T. A. Rosen, J. D. Levine, D. Julius, *Nature* **1997**, *389*, 816-824.

[103] A. P. Christensen, D. P. Corey, *Nat. Rev. Neurosci.* **2007**, *8*, 510-521.

[104] A. Kocer, M. Walko, W. Meijberg, B. L. Feringa, *Science* **2005**, *309*, 755-758.

[105] G. Chang, R. H. Spencer, A. T. Lee, M. T. Barclay, D. C. Rees, *Science* **1998**, *282*, 2220-2226.

[106] a) K. Yoshimura, A. Batiza, C. Kung, *Biophys. J.* **2001**, *80*, 2198-2206; b) K. Yoshimura, A. Batiza, M. Schroeder, P. Blount, C. Kung, *Biophys. J.* **1999**, *77*, 1960-1972.

[107] J. H. Folgering, J. M. Kuiper, A. H. de Vries, J. B. Engberts, B. Poolman, *Langmuir* **2004**, *20*, 6985-6987.

[108] A. A. Beharry, L. Wong, V. Tropepe, G. A. Woolley, *Angew. Chem. Int. Ed.* **2011,** *50*, 1325-1327.

[109] J. A. Ihalainen, B. Paoli, S. Muff, E. H. Backus, J. Bredenbeck, G. A. Woolley, A. Caflisch, P. Hamm, *Proc. Natl. Acad. Sci. USA* **2008**, *105*, 9588-9593.

[110] F. Bonardi, G. London, N. Nouwen, B. L. Feringa, A. J. Driessen, *Angew. Chem. Int. Ed.* **2010**, *49*, 7234-7238.

[110] J. A. Ihalainen, B. Paoli, S. Muff, E. H. Backus, J. Bredenbeck, G. A. Woolley, A. Caflisch, P. Hamm, *Proc. Natl. Acad. Sci. USA* **2008**, *105*, 9588-9593.

[111] a) B. N. Armbruster, X. Li, M. H. Pausch, S. Herlitze, B. L. Roth, *Proc. Natl. Acad. Sci. USA* **2007**, *104*, 5163-5168; b) B. R. Conklin, E. C. Hsiao, S. Claeysen, A. Dumuis, S. Srinivasan, J. R. Forsayeth, J. M. Guettier, W. C. Chang, Y. Pei, K. D. McCarthy, R. A. Nissenson, J. Wess, J. Bockaert, B. L. Roth, *Nat. Methods* **2008**, *5*, 673-678.

[112] S. Wang, S. Szobota, Y. Wang, M. Volgraf, Z. Liu, C. Sun, D. Trauner, E. Y. Isacoff, X. Zhang, *Nano. Lett.* **2007**, *7*, 3859-3863.

[113] a) K. Deisseroth, G. Feng, A. K. Majewska, G. Miesenbock, A. Ting, M. J. Schnitzer, *J. Neurosci.* **2006**, *26*, 10380-10386; b) B. A. Wilt, L. D. Burns, E. T. Wei Ho, K. K. Ghosh, E. A. Mukamel, M. J. Schnitzer, *Annu. Rev. Neurosci.* **2009**, *32*, 435-506.

[114] N. Caporale, K. D. Kolstad, T. Lee, I. Tochitshy, D. Dalkara, D. Trauner, R. H. Kramer, Y. Dan, E. Y. Isacoff, J. C. Flannery, *Mol. Ther.* **2011**, *19*, 1212-1219.

II

Novel small molecule ENaC inhibitors as potential therapeutics in Cystic Fibrosis – a patent evaluation

Matthias Schönberger[1], and Mike Althaus[2]

[1]Department of Chemistry, Ludwig-Maximilians-Universität, and Center for Integrated Protein Science, 81377 Munich, Germany.

[2]Justus Liebig University Giessen, Institute of Animal Physiology, Giessen , Germany

Novel molecular platforms for ENaC modulators are claimed in six patents (WO2012035158(A1); WO2009074575(A2); WO2011028740(A1); WO2009150137(A2); WO2011079087(A1); WO2008135557(A1)). These ENaC inhibitors may be used in order to block transepithelial sodium and consequently water absorption across airway epithelia. This may result in airway re-hydration and enhanced mucociliary clearance in patients with cystic fibrosis (CF) lung disease. All inhibitors resemble the classical ENaC blocker amiloride but follow different strategies to increase structural diversity in a sterically tolerant region. These substitutions can be modified in order to 1) enhance potency of ENaC inhibition; 2) reduce epithelial permeability; and 3) broaden applicability in order to be used as potential drugs for CF therapy. Most of the claims and patent data are supported by the currently available literature. The patents deliver a solid chemical basis for a variety of chemical modifications of the ENaC inhibitor amiloride. These modifications may result in the development of a novel, applicable ENaC inhibitor which may have lasting effects on diseased airways and may achieve airway re-hydration and enhanced mucociliary clearance in CF lung disease.

Contents

1. Introduction

The Epithelial Sodium Channel (ENaC) is a sodium-selective, non-voltage gated ion channel consisting of three subunits, α,β,γ, and δ[1] which likely assemble as a heterotrimer in the plasma membrane[2]. This "classical" ENaC is found in various epithelia including those of the lung. In addition to the three classical ENaC subunits there is a fourth δ-subunit[3] which can replace the α-subunit and, together with β and γ, form ENaC-like ion channels with different pharmacological and biophysical properties[4–6]. The physiological role of δ-subunit containing ENaCs is as of yet insufficiently demonstrated; however, it is speculated that these channels may play an important role in the central nervous system. [6, 7]

In epithelia ENaCs represent the rate-limiting step for the uptake of sodium ions into epithelial cells and are thereby key factors in the transepithelial absorption of sodium. According to the classical epithelial transport model by Ussing and colleagues[8], sodium ions enter the epithelial cells via ENaCs located in the apical membrane. The driving force for this sodium entry is an electrochemical gradient which is mainly generated and maintained by the basolaterally located Na^+/K^+-ATPase as well as various types of basolateral potassium channels. The sodium ions which enter the cells via ENaCs are eventually pumped out at the basolateral membrane of the epithelium due to the activity of the Na^+/K^+-ATPase. This transepithelial net-movement of sodium ions creates osmotic forces which drive the transepithelial absorption of water. Therefore, ENaC is crucial for the physiology of sodium and water homeostasis in various organs – including the lung. [9]

All pulmonary epithelia are covered by a thin layer of liquid which is critical for lung physiology. In the airways, this so-called airway surface liquid (ASL) is important for mucociliary clearance.[10] The periciliary liquid (PCL) is a part of the ASL and surrounds the cilia of airway epithelial cells (Figure 1). According to the recently suggested "gel-on-brush model", the PCL contains tethered macromolecules which form a brush-like structure.[11] Due to these macromolecules, gel-like mucus forms a distinct layer on top of the PCL and serves as a trap for inhaled particles and pathogens. Due to ciliary beat and movement of the PCL, this mucus layer moves

continuously towards the larynx and thereby transports particles/pathogens out of the lung – a mechanism referred to as mucociliary clearance.[10, 12]

The liquid contents of the mucus layer and the PCL determine the efficacy of mucociliary clearance. The gel-like mucus layer serves as a liquid reservoir which helps maintain the PCL hydrated. However, when the mucus layer becomes severely dehydrated, liquid cannot be further transferred into the PCL. This results in squeezing of the cilia and failure of mucociliary clearance.[11–13] This indicates that the hydration status of the ASL/PCL critically determines mucociliary clearance in the airways.

Given the importance of ENaC for transepithelial salt and water absorption, ENaC activity and ASL/PCL homeostasis are also connected.[14] The salt-wasting syndrome type 1 pseudohypoaldosteronism (PHA1) is caused by mutations in ENaC subunits which lead to a decreased ENaC activity.[15] Aside from salt loss, patients with PHA1 display an increased ASL volume in the airways.[16] By contrast, transgenic mice which overexpress ENaCs in the airways show a reduced ASL volume, impaired mucociliary clearance and develop cystic fibrosis (CF)-like lung disease.[17] In addition, mutations that lead to increased ENaC activity have been identified in patients which develop CF-like symptoms (atypical CF).[18, 19] ENaC can thus be considered a regulator of sodium and water homeostasis of ASL/PCL. This makes ENaC an interesting molecular target for pharmacotherapy of Cystic Fibrosis lung disease.[20]

Cystic Fibrosis is the most common genetic disorder in the Caucasian population and is caused by mutations which lead to impaired function of the chloride channel CFTR (cystic fibrosis transmembrane conductance regulator). Despite its prevalence, the molecular mechanisms belying how impaired CFTR activity leads to pathogenesis and eventually CF-disease are still not completely understood.[14, 21] The pulmonary manifestations in cystic fibrosis patients are airway obstruction by thick and viscous mucus and chronic lung inflammation. These are the result of an airway ASL/PCL dehydration which leads to impaired mucociliary clearance and reduces the capability to remove mucus as well as pathogens out of the lung.[11, 12] Therefore, a well-accepted approach for the treatment of CF is the re-hydration of the airways in order to restore mucociliary clearance.[22] Air-way re-hydration can be achieved by the inhalation of

hypertonic saline or interference with ENaC-mediated salt and, consequently, liquid absorption across the airway epithelium.

Hypertonic saline will re-hydrate the airways by drawing fluid osmotically into the ASL (the PCL as well as the mucus layer). This would consequently avoid squeezing of the cilia and enhance mucociliary clearance. Beneficial effects due to the inhalation of hypertonic saline are indicated by results from clinical trials in CF patients[23] and have been summarized in a review article by Goralski *et al*..[22] Furthermore, preventive and late treatment with hypertonic saline effectively reduced mucus obstruction in the ENaC-overexpressing mouse model.[24] This indicates that hypertonic saline is an effective approach in order to re-hydrate the airway surfaces in CF.

In contrast to drawing water into the ASL by hyperosmotic agents, a reduction of liquid absorption by the airway epithelium can increase the liquid content of the ASL. This may be achieved by pharmacological interference with transepithelial sodium absorption and suggests that inhibitors of ENaC are potential pharmacological tools for decreasing fluid absorption across airway epithelia and thereby may contribute to airway re-hydration and stimulation of mucociliary clearance.

This patent evaluation addresses novel ENaC blockers and their potential use as therapeutic tools for treating condition in which inhibition of ENaC is desired.

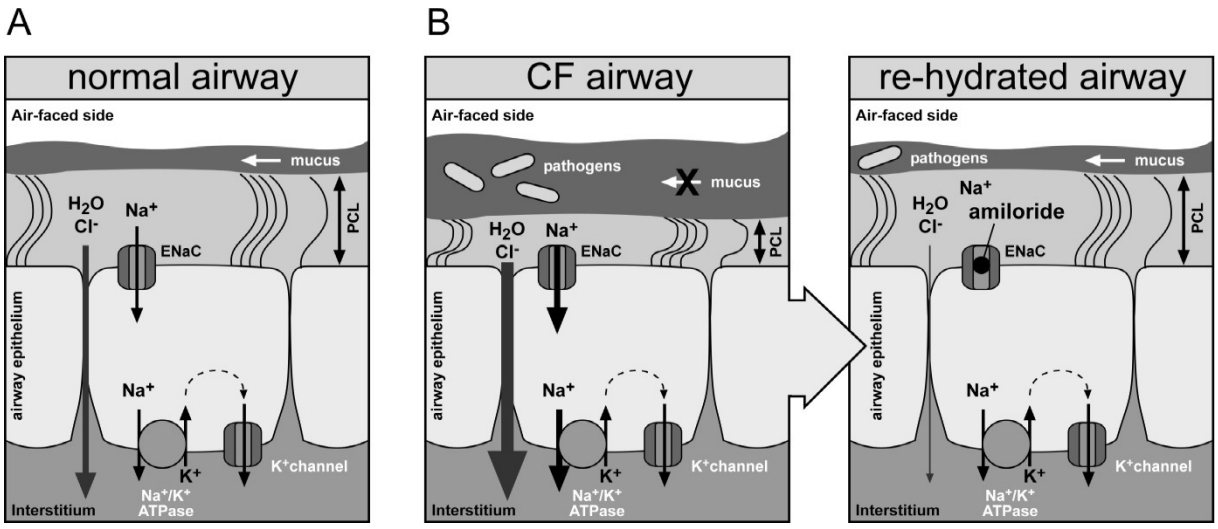

Figure 1. ENaC inhibitors as a tool for airway re-hydration in cystic fibrosis. A) Normal airways exhibit a balanced periciliary liquid (PCL) allowing efficient ciliary beat and mucus clearance from the airways. PCL volume is maintained by a balance of ENaC-mediated sodium and, consequently, water absorption as well as chloride secretion (not shown). **B)** In CF airways, the lack of chloride/water secretion as well as an enhanced sodium absorption leads to PCL depletion and impaired mucociliary clearance. ENaC inhibitors such as amiloride may be used in order to reduce sodium/water absorption and thereby re-hydrate the PCL and enhance mucociliary clearance.

2. Chemistry

Amiloride was disclosed in the 1960s as a potassium sparing diuretic able to inhibit transepithelial sodium absorption.[25–28] Decades later, ENaC was discovered as the primary protein target responsible for the diuretic effect[1, 29] and many other ion channels and transporters were also identified as amiloride sensitive. The molecular design of amiloride has been proven to be highly successful in blocking ENaC activity and in many cases novel ENaC blockers are amiloride derivatives or highly resemble the 3,5-diamino pyrazine (Figure 2).

Years of optimizing amiloride structure activity relationships have taught us that first, a protonated and thus positively charged guanidinium is needed for ENaC block and second, substitution at the guanidine nitrogen with hydrophobic moieties enhance potency.[30] Both of these finding are mirrored in the herein reported patents for new ENaC blockers, which follow different strategies of generating new molecular design platforms. Interestingly, the 3,5-diamino pyrazine core with a halogen or halogenoid in

6-position and a carboxy functional group in 2-position remains unchanged in all cases. In contrast, the apparent high structural tolerance for substituents extending from the center of positive charge allows for creative chemical design. These modifications may be used to modify bioavailability and pharmacodynamics, more specifically addressing certain organs or directing drug metabolism.

In compounds of series I, the guanidine is part of an imidazolidine, which forms a spiro cycle with an *N*-acyl-piperidine. The concept of integrating the guanidine into a heterocycle has in fact been followed by Novartis before as seen in series II. In this case, ring size has been varied from imidazolidines (5-membered) to 1,3-diazepanes (7-membered). Series I and II utilize an acyl guanidine as represented by amiloride, which would be protonated at physiological pH to a large extend leading to ENaC block. In their non-protonated form, however, these molecules would be comparatively permeable to membranes. Series III to V would instead install peralkylated nitrogen atoms leading to a permanent positive charge. Interestingly, this charge is one bond length further away from the pyrazine core as compared to the above described acyl guanidines. Series III and IV feature ethane-1,2-diamines, which are connected to the canonical pyrazinic acid through an amide bond. The permanent positive charge is then installed by quaternarization of the distal amine functionality. This feature resembles known cation channel blockers such as tetraethylammonium or QX-314. In physiological investigations, quaternary amine ENaC blockers have been shown to be comparable or superior to amiloride in terms of potency and efficacy.[31, 32] As a consequence of their permanent charge, these molecules have starkly increased polarity. This translates into higher solubility and hindered passive penetration across cell membranes or, for instance, the blood brain barrier. It has been hypothesized that as such quaternary amine ENaC blockers could be a promising platform for nebulizers enhancing mucociliary clearance in CF.[31] Series V again features molecules with a permanent positive charge, however, carried by an amidine. In this case it is represented by an *N*-alkylated benzimidazole. This patent is the only one in which the pyrazinic acid may be transformed to an amide or ester (in all other cases: amides), which might result in different hydrolysis rates. While all above mentioned structural platforms outline different strategies of generating a diamino pyrazine with a basic or

positively charged substituent in 2-position, series VI represents bivalent ligands. Two amiloride or amiloride like molecular fragments are presented on either side of a linker, which can be varied in lengths and flexibility.

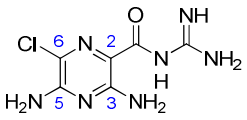

amiloride

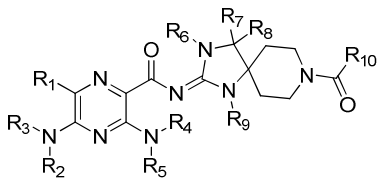

I

WO2012/035158 A1
NOVARTIS

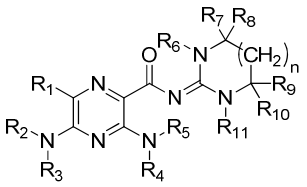

II

WO2009/074575 A2
NOVARTIS

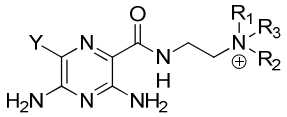

III

WO2011/028740 A1
GLAXO GROUP LTD

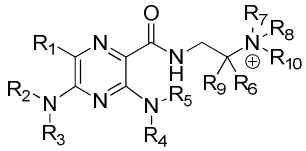

IV

WO2009/150137 A2
NOVARTIS

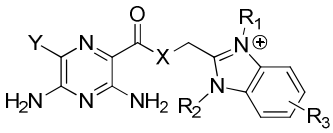

V

WO2011/079087 A1
GLAXO GROUP LTD

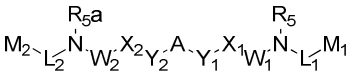

general structure

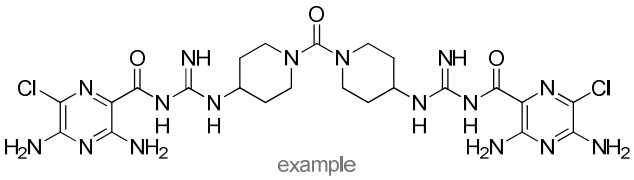

example

VI

WO2008/135557 A1
SENOMYX INC

Figure 2. The canonical blocker amiloride and patents on new chemical structures for ENaC block. Abbreviations and residues are reported identical to the patent literature.

3. Biology and action

Amiloride inhibits human lung ENaC with an IC_{50} value in the submicromolar range (~100 nM).[33] The high affinity towards ENaC makes amiloride an interesting

pharmacological tool for the interference of sodium absorption across airway epithelia. Various clinical trials have investigated the potential of amiloride inhalation in order to re-hydrate ASL/PCL and enhance mucociliary clearance in CF patients.[34–38] However, conflicting data have been reported and amiloride failed to become a therapeutic option due to its instability and rapid clearance from the airways.[38, 39]

Two amiloride-derivatives, benzamil and phenamil are more potent inhibitors of ENaC and sodium transport,[1, 40–42] however, they were not more effective than amiloride.[40] Despite the higher affinities of phenamil/benzamil for ENaC, their stability in the airways was low.[40] Third generation derivatives of amiloride were subsequently designed by substitutions at the guanidine nitrogen.[43] Those compounds displayed both higher affinity (IC_{50} values below 10 nM) and lower reversibility of ENaC block. One of those compounds, compound 552-02 (N-(3,5-diamino-6-chloropyrazine-2-carbonyl)-N'-4-[4-(2,3-dihydroxy-propoxy)phenyl] butyl-guanidine methane-sulfonate), was able to enhance mucociliary clearance in sheep and conserved ASL volume on CF bronchial epithelial cells.[44] These studies indicated its potential suitability for CF therapy and made 552-02 being investigated in clinical phase 1 and 2 trials (NCT00274313).

This example demonstrates that the guanidine nitrogen in amiloride can be substituted in order to alter the pharmacodynamics of the molecule without losing the potency of ENaC block. This is also mirrored in the herein addressed patents which are all effective blockers of ENaC (with IC_{50} values generally below 10 μM). Compounds of series III to V are especially interesting due to the installation of a permanent positive charge. Unprotonated amiloride is lipid soluble and can accumulate in or cross epithelial cells [30]. The cationic character of compounds III to V should decrease epithelial permeability, a major limitation for the airway efficacy of amiloride, phenamil and benzamil.[40] Furthermore, it has been hypothesized that the cationic character of the compounds makes them especially suitable for dry powder or nebulizer applications – which are desired in CF therapy.[31, 32]

4. Expert Opinion

The herein addressed patents represent novel interesting chemical platforms for small molecule ENaC blockers. The known structural freedom for lipophilic substitution beyond the guanidine nitrogen of amiloride has been translated into novel molecular designs. The guanidine may be part of different heterocycles which are further substituted. Alternatively, the guanidine may be replaced by a permanently charged, that is, peralkylated, amidine or amine which again may be further extended by various substituents. These substitutions allow a variety of chemical modifications which may achieve an enhanced potency of ENaC inhibition and a decreased epithelial permeability and thus clearance from the airways. As we learned from clinical trials using amiloride or its first generation derivatives benzamil/phenamil, both features are desired for an effective ENaC inhibitor which could be used for the treatment of CF lung disease. All of the discussed compounds are potent inhibitors of ENaC in airway epithelia (mainly tested in human bronchial epithelial cells), however, most of the data addressing the pharmacodynamics and potency of these ENaC inhibitors arise from electrophysiological recordings on airway epithelial preparations in Ussing chambers. It has to be kept in mind that the liquid environment in Ussing chambers is very different from the *in vivo* situation in the airways where air and mucus are obstacles to be overcome. Some of the compounds have already been evaluated with more physiological methods such as nasal potential measurement in guinea pigs.[31, 32] However, mucus becomes a way greater obstacle in the diseased CF airway. Thus appropriate animal models which develop CF-like symptoms such as the ENaC-overexpressing mouse[17] or the recently developed CFTR knock-out pig[45, 46] should be considered for the evaluation of the efficacy of these ENaC inhibitors in promoting airway re-hydration and mucociliary clearance in CF lung disease.

In addition to the choice of a disease-relevant model the timing of treatment is an important aspect which needs to be addressed. This is evident from a study which demonstrated that preventive but not late amiloride therapy has beneficial effects in ENaC-overexpressing transgenic mice.[20, 47] Amiloride may thus still have a potential for preventive therapy, especially in countries which conduct newborn screening for CF. This may also apply for the herein addressed novel small molecule ENaC

inhibitors and their efficacy in "preventive versus late" therapy should be investigated. Despite the potential of amiloride for preventive treatment of CF, Mall and colleagues recently highlighted that there is lack of data concerning the toxicity of amiloride in infants and its impact on neonatal development.[24] These aspects need to be addressed when novel ENaC inhibitors and their putative use for preventive CF treatment are evaluated.

Taken together, the herein addressed patents provide a broad basis for a variety of new generation ENaC inhibitors. These novel molecules may lead to enhanced pharmacodynamics and open new doors for applicable ENaC inhibitors with sustained effects on diseased airways. Such inhibitors may achieve ASL/PCL re-hydration and enhance mucociliary clearance in CF patients.

References

Papers of special note have been highlighted as either of interest (*) or of considerable interest (**) to readers.

1. Canessa CM, Schild L, Buell G, et al. Amiloride-sensitive epithelial Na+ channel is made of three homologous subunits. Nature 1994;367(6462):463–7

** **Original paper which described the cloning and molecular composition of ENaC**

2. Jasti J, Furukawa H, Gonzales EB, et al. Structure of acid-sensing ion channel 1 at 1.9 A resolution and low pH. Nature 2007;449(7160):316–23
3. Waldmann R, Champigny G, Bassilana F, et al. Molecular cloning and functional expression of a novel amiloride-sensitive Na+ channel. J Biol Chem 1995;270(46):27411–4
4. Wesch D, Miranda P, Afonso-Oramas D et al. The neuronal-specific SGK1.1 kinase regulates {delta}-epithelial Na+ channel independently of PY motifs and couples it to phospholipase C signaling. Am J Physiol Cell Physiol 2010;299(4):C779-90
5. Wesch D, Althaus M, Miranda P, et al. Differential N-termini in epithelial Na+ channel δ subunit isoforms modulate channel trafficking to the membrane. Am J Physiol Cell Physiol 2011
6. Giraldez T, Rojas P, Jou J, et al. The epithelial sodium channel δ-subunit: new notes for an old song. Am J Physiol Renal Physiol 2012;303(3):F328-38
7. Giraldez T, Domínguez J, Alvarez de La Rosa, D. ENaC in the brain-future perspectives and pharmacological implications. Curr Mol Pharmacol 2013
8. Koefoed-Johnsen V, Ussing HH. The nature of the frog skin potential. Acta Physiol Scand 1958;42(3-4):298–308

** **Original paper which established the model of transepithelial sodium absorption.**

9. Fronius M, Clauss WG, Althaus M. Why Do We have to Move Fluid to be Able to Breathe? Front Physiol 2012;3:146
10. Knowles MR, Boucher RC. Mucus clearance as a primary innate defense mechanism for mammalian airways. J Clin Invest 2002;109(5):571–7
11. Button B, Cai L, Ehre C, et al. A periciliary brush promotes the lung health by separating the mucus layer from airway epithelia. Science 2012;337(6097):937–41

**** This paper proposes a novel model of how the airway surface liquid is established by a macromolecular brush below the mucus layer**

12. Boucher RC. New concepts of the pathogenesis of cystic fibrosis lung disease. Eur Respir J 2004;23(1):146–58
13. Dickey BF. Biochemistry. Walking on solid ground. Science 2012;337(6097):924–5
14. Althaus M. ENaC inhibitors and airway re-hydration in cystic fibrosis: state of the art. Curr Mol Pharmacol 2013
15. Chang SS, Grunder S, Hanukoglu A, et al. Mutations in subunits of the epithelial sodium channel cause salt wasting with hyperkalaemic acidosis, pseudohypoaldosteronism type 1. Nat Genet 1996;12(3):248–53
16. Kerem E, Bistritzer T, Hanukoglu A, et al. Pulmonary epithelial sodium-channel dysfunction and excess airway liquid in pseudohypoaldosteronism. N Engl J Med 1999;341(3):156–62
17. Mall M, Grubb BR, Harkema JR, et al. Increased airway epithelial Na+ absorption produces cystic fibrosis-like lung disease in mice. Nat Med 2004;10(5):487–93

**** This paper demonstrated for the first time a link between ENaC-mediated sodium absorption and mucus plugging *in vivo*.**

18. Azad AK, Rauh R, Vermeulen F, et al. Mutations in the amiloride-sensitive epithelial sodium channel in patients with cystic fibrosis-like disease. Hum Mutat 2009;30(7):1093–103

*** This paper provides a direct link between abnormal ENaC activity and CF-like disease in humans.**

19. Rauh R, Diakov A, Tzschoppe A, et al. A mutation of the epithelial sodium channel associated with atypical cystic fibrosis increases channel open probability and reduces Na+ self inhibition. J Physiol (Lond) 2010;588(Pt 8):1211–25
20. Mall MA. Role of the amiloride-sensitive epithelial Na+ channel in the pathogenesis and as a therapeutic target for cystic fibrosis lung disease. Exp. Physiol 2009;94(2):171–4
21. Kunzelmann K, Schreiber R. Airway epithelial cells-Hyperabsorption in CF? Int J Biochem Cell Biol 2012;44(8):1232-5
22. Goralski JL, Boucher RC, Button B. Osmolytes and ion transport modulators: new strategies for airway surface rehydration. Curr Opin Pharmacol 2010;10(3):294–9

23. Donaldson SH, Bennett WD, Zeman KL, et al. Mucus clearance and lung function in cystic fibrosis with hypertonic saline. N Engl J Med 2006;354(3):241–50
24. Graeber SY, Zhou-Suckow Z, Schatterny J, et al. Hypertonic Saline is Effective in the Prevention and Treatment of Mucus Obstruction but not Airway Inflammation in Mice with Chronic Obstructive Lung Disease. Am J Respir Cell Mol Biol 2013
25. Baer JE, Jones CB, Spitzer SA, et al. The potassium-sparing and natriuretic activity of N-amidino-3,5-diamino-6-chloropyrazinecarboxamide hydrochloride dihydrate (amiloride hydrochloride). J Pharmacol Exp Ther 1967;157(2):472–85
26. Bull MB, Laragh JH. Amiloride. A potassium-sparing natriuretic agent. Circulation 1968;37(1):45–53
27. Bentley PJ. Amiloride: a potent inhibitor of sodium transport across the toad bladder. J Physiol (Lond) 1968;195(2):317–30
28. Salako LA, Smith AJ. Effects of amiloride on active sodium transport by the isolated frog skin: evidence concerning site of action. Br J Pharmacol 1970;38(4):702–18
29. Canessa CM, Horisberger JD, Rossier BC. Epithelial sodium channel related to proteins involved in neurodegeneration. Nature 1993;361(6411):467–70
30. Kleyman TR, Cragoe EJ. Amiloride and its analogs as tools in the study of ion transport. J Membr Biol 1988;105(1):1–21

**** This comprehensive review provides solid information on amiloride structure activity relationships on multiple targets.**

31. Hunt T, Atherton-Watson HC, Axford J, et al. Discovery of a novel chemotype of potent human ENaC blockers using a bioisostere approach. Part 1: quaternary amines. Bioorg Med Chem Lett 2012;22(2):929–32
32. Hunt T, Atherton-Watson HC, Collingwood SP, et al. Discovery of a novel chemotype of potent human ENaC blockers using a bioisostere approach. Part 2: α-Branched quaternary amines. Bioorg Med Chem Lett 2012;22(8):2877–9

*** This publication presents a novel bioisostere design in combination with optically active side chains, which increase potency of ENaC block.**

33. Fronius M, Bogdan R, Althaus M, et al. Epithelial Na+ channels derived from human lung are activated by shear force. Respir Physiol Neurobiol 2010;170(1):113–9

34. App EM, King M, Helfesrieder R, et al. Acute and long-term amiloride inhalation in cystic fibrosis lung disease. A rational approach to cystic fibrosis therapy. Am Rev Respir Dis 1990;141(3):605–12
35. Knowles MR, Church NL, Waltner WE, et al. A pilot study of aerosolized amiloride for the treatment of lung disease in cystic fibrosis. N Engl J Med 1990;322(17):1189–94
36. Köhler D, App E, Schmitz-Schumann M, et al. Inhalation of amiloride improves the mucociliary and the cough clearance in patients with cystic fibroses. Eur J Respir Dis Suppl 1986;146:319–26
37. Riedler J, Huttegger I. Pilotstudie zur Amiloridinhalation bei Kindern mit cystischer Fibrose. Klin Padiatr 1992;204(3):158–62
38. Graham A, Hasani A, Alton EW, et al. No added benefit from nebulized amiloride in patients with cystic fibrosis. Eur Respir J 1993;6(9):1243–8
39. Cuthbert AW. New horizons in the treatment of cystic fibrosis. Br J Pharmacol 2011;163(1):173–83
40. Hirsh AJ, Sabater JR, Zamurs A, et al. Evaluation of second generation amiloride analogs as therapy for cystic fibrosis lung disease. J Pharmacol Exp Ther 2004;311(3):929–38
41. Hofmann T, Stutts MJ, Ziersch A, et al. Effects of topically delivered benzamil and amiloride on nasal potential difference in cystic fibrosis. Am J Respir Crit Care Med 1998;157(6 Pt 1):1844–9
42. Rodgers HC, Knox AJ. The effect of topical benzamil and amiloride on nasal potential difference in cystic fibrosis. Eur Respir J 1999;14(3):693–6
43. Hirsh AJ, Molino BF, Zhang J, et al. Design, synthesis, and structure-activity relationships of novel 2-substituted pyrazinoylguanidine epithelial sodium channel blockers: drugs for cystic fibrosis and chronic bronchitis. J Med Chem 2006;49(14):4098–115
44. Hirsh AJ, Zhang J, Zamurs A, et al. Pharmacological properties of N-(3,5-diamino-6-chloropyrazine-2-carbonyl)-N'-4-[4-(2,3-dihydroxypropoxy)phenyl]butyl-guanidine methanesulfonate (552-02), a novel epithelial sodium channel blocker with potential clinical efficacy for cystic fibrosis lung disease. J Pharmacol Exp Ther 2008;325(1):77–88

45. Rogers CS, Stoltz DA, Meyerholz DK, et al. Disruption of the CFTR gene produces a model of cystic fibrosis in newborn pigs. Science 2008;321(5897):1837–41

**** This paper describes a porcine CF model.**

46. Rogers CS, Abraham WM, Brogden KA, et al. The porcine lung as a potential model for cystic fibrosis. Am J Physiol Lung Cell Mol Physiol 2008;295(2):L240-63

47. Zhou Z, Treis D, Schubert SC, et al. Preventive but not late amiloride therapy reduces morbidity and mortality of lung disease in betaENaC-overexpressing mice. Am J Respir Crit Care Med 2008;178(12):1245–56

*** This paper demonstrates the importance of a correct time point for pharmacological interference with ENaC activity in a CF model.**

III

Controlling Epithelial Sodium Channels with Light Using Photoswitchable Amiloride

Matthias Schönberger[1], Mike Althaus[2], Martin Fronius[2,3], Wolfgang Clauss[2] and Dirk Trauner[1*]

[1]Department of Chemistry and Center for Integrated Protein Science, Ludwig Maximilians-Universität München, Butenandtstraße 5–13 (F4.086), 81377 Munich (Germany);

[2]Institute of Animal Physiology, Justus Liebig University Giessen, Heinrich-Buff-Ring 26, 35392 Giessen, Germany.

[3]Department of Physiology, University of Otago, PO Box 913, Dunedin 9054, New Zealand

Amiloride is a widely used diuretic that blocks Epithelial Sodium Channels (ENaCs). These heterotrimeric transmembrane proteins, assembled from β, γ and α or δ subunits effectively control water transport across epithelia and sodium influx into non-epithelial cells. The functional role of δβγ–ENaC in neural processing and in the periphery is still poorly understood. Herein, we introduce a photo-switchable version of amiloride, termed PA1, that enables the optical control of ENaC channels, in particular the δβγ–isoform. It was used to demonstrate the functional expression of δβγENaC in a model for human lung epithelium.

Content

Introduction

The Epithelial Sodium Channel (ENaC) is a constitutively open sodium-selective ion channel that lacks voltage sensitivity and mediates sodium absorption across various epithelia.[1] Classical ENaCs are heterotrimers composed of three subunits, α, β and γ, which assemble as a sodium selective ion channel in the plasma membrane (Fig. 1).[2,3] In renal epithelia, ENaCs are important players in Na^+ reabsorption by the kidney and in maintaining extracellular volume and blood pressure. Gain-of-function mutations cause a hereditary form of hypertension (Liddle syndrome), whereas loss-of-function mutations give rise to the salt-wasting syndrome pseudohypoaldosteronism type 1.[4,5] ENaC-mediated sodium absorption by the pulmonary epithelium drives lung liquid clearance and is thus a critical regulator of pulmonary water content. Increased ENaC activity in the airways is the cause for cystic-fibrosis-like lung disease, whereas decreased ENaC activity in the distal lung leads to impaired alveolar fluid clearance and the development of pulmonary edema.[6-9] As such, ENaCs are a primary target for drugs that affect electrolyte and water homeostasis, such as diuretics or edema medications.[10-13]

An additional ENaC δ-subunit has been identified in 1995.[14] There is only scarce knowledge about its physiological function, however, it can assemble with the β and γ subunits to form channels with high open probability.[14-16] Expression of δENaC and other ENaCs has been confirmed in various non-epithelial tissues, most prominently the central nervous system of primates.[17-20] It has been speculated that δ-containing ENaCs play a role in communicating ischemic and hypoxic signals in neurons, as well as adjusting nervous excitability.[21,22] Complicating its analysis, mice and rats do not have a gene for the δ-subunit. Furthermore, no pharmacological tools are available for functional differentiation between α and δ-containing ENaCs. Thus, in contrast to αβγ, little is known about the physiological function of δβγENaC and in particular the (putative) function of δENaC in the brain is obscure.[22]

ENaCs belong to a large group of ion channels, the ENaC/degenerin (ENaC/deg) protein family that also includes neuronal acid sensing ion channels (ASIC).[23,24] The latter has recently been elucidated with X-ray crystallography, which confirmed a

trimeric architecture that probably applies to all channels of the family (Fig. 1).[25] Every individual ENaC subunit comprises only two trans-membrane helices (TM 1,2) with relatively short intracellular C and N-termini and a large, cysteine-rich, extracellular domain.

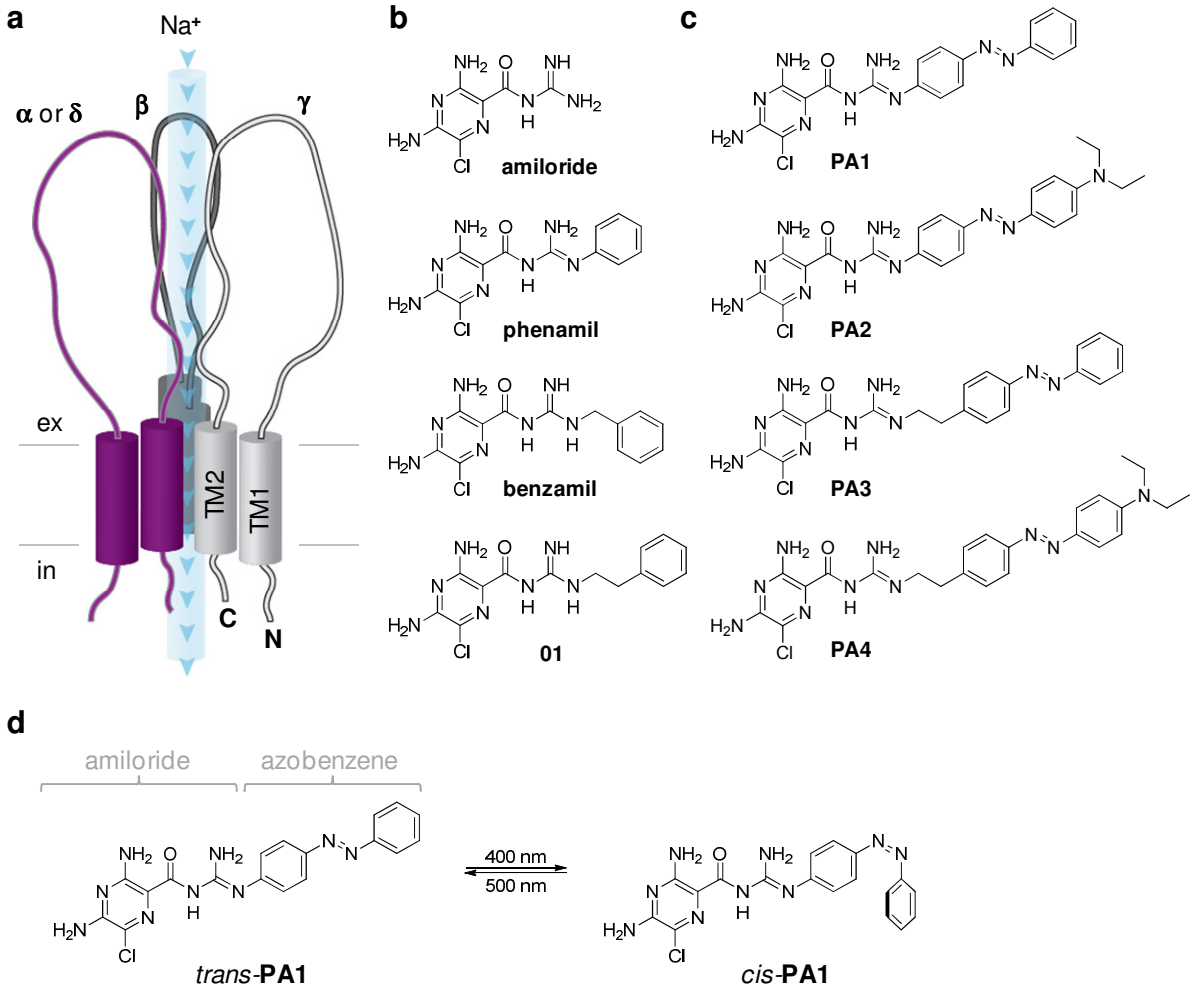

Figure 1. Epithelial sodium channels (ENaCs) and their blockers. a, Schematic drawing of a heterotrimeric αβγENaC and δβγENaC, respectively. Each subunit contains two transmembrane helices TM1 and TM2, relatively short C and N-termini at the intracellular site and a large extracellular loop. **b**, Chemical structure of **amiloride** and more potent derivatives **phenamil**, **benzamil** and **01**. **c**, Proposed structures of photo-switchable amiloride derivatives containing an azobenzene functional group. **d**, Photo-isomerization of Photo-amiloride-1 (**PA1**). Illumination with 400 nm induces isomerization to *cis*-**PA1**, which is the thermodynamically less stable form. The cis-isomer can relax back to the *trans*-state thermally, or spatiotemporally controlled using 500 nm light.

Although ENaC/deg channels respond to a variety of input signals, none of them are inherently sensitive toward light. In recent years, our group has succeeded in developing a range of synthetic photo-switches that can confer light sensitivity to native or slightly modified receptor proteins. These can either function as freely diffusible photochromic ligands (PCLs) or as photo-switchable tethered ligands (PTLs) that are covalently attached to the target protein.[26] Using either strategy, we have been able to effectively turn voltage-gated potassium, sodium, and calcium channels, ionotropic and metabotropic glutamate receptors as well as nicotinic acetylcholine receptors into photoreceptors.[27-31]

We now show that an entirely new class of transmembrane proteins, *viz*. trimeric ENaC/deg channels, are amenable to the PCL approach. To this end we have designed, synthesized and characterized a small series of photo-switchable azobenzene derivatives of amiloride and identified one candidate that can be used to control δβγENaC-activity with light. Our photochromic ligands provide insights into the structure-activity relationships of ENaC blockers and could be used to functionally discriminate between isoforms.

Results and Discussion

Design and Synthesis of Photoamilorides. Amiloride was introduced as a potassium sparing diuretic in the 1960s without particular knowledge of its molecular target.[32] ENaC in kidney epithelia was subsequently established as the ion channel primarily responsible for the potassium sparing diuretic effect.[3] To date, countless amiloride analogs have been synthesized and tested, providing insights into its structure-activity-relationships.[33,34] Most importantly, it has been found that lipophilic substitution at the terminal guanidine nitrogen boost both potency and selectivity for ENaC. In fact, the potency gained by an aromatic substituent increases with linker length, Fig. 1b.[35] Accordingly, we designed photochromic amiloride derivatives that have an azobenzene unit directly attached to the guanidine, which gave photoamiloride-1 (**PA1)** and photoamiloride-2 (**PA2**) resembling the drug phenamil, Fig. 1. Phenamil is known to irreversibly block ENaCs to a certain extent, possibly through cell uptake, and has been used to determine channel density.[36] In addition, we designed compounds photoamiloride-3 (**PA3**) and photoamiloride-4 **(PA4**), which bear an azobenzene moiety linked through an ethylene spacer and resemble the known amiloride analogue **01**.[37] In **PA2** and **PA4**, the azobenzenes are further substituted in the 4′-position with a diethylamino substituent, which is known to red-shift the action spectra for photo-switching.[38] The photo-switching of **PA1** between its *trans and cis* configuration is shown in Fig. 1c.

The synthesis of the shorter photoamilorides **PA1** and **PA2** started from 4-nitroaniline **s1**, which was oxidized using oxone and condensed with a respective aniline using Mills conditions (see supporting information). Sodium sulfide reduction then yielded 4-amino azobenzenes **02** and **03**, respectively, which were converted to aryl guanidines **s4** and **s5** using cyanamide (Fig. 2a). The resulting guanidine hydrochlorides were deprotonated and condensed with an active ester of pyrazinic acid **4a**, which yielded **PA1** and **PA2**, respectively.

To generate the requisite phenethylamine building blocks for the longer photoamilorides, primary amine **s6** was first chemoselectively protected to **05**, then condensed with commercially available nitrosobenzene **s7** in a Mills-reaction and

subsequently deprotected to yield **06** (SI, Fig. 2b). Alternatively, oxidation of **05** and condensation with *p*-diethylamino aniline **s8** followed by deprotection gave azobenzene **07.** With two azobenzene-amine building blocks in hand, the guanidine functional moiety was installed using carboxamidine **s9**. The resulting guanidinium salts were deprotonated via basic work-up and directly added to an ethanolic solution of ester **09**. Heating to reflux then yielded **PA3** and **PA4**, respectively. Interestingly, attempts to furnish **PA3** or **PA4** under the same coupling conditions as **PA1** and **PA2** (and *vice versa*) failed. Likewise, attempts to condense 4-amino azobenzenes **02** and **03** with carboxamidine **s9** did not yield the corresponding guanidines.

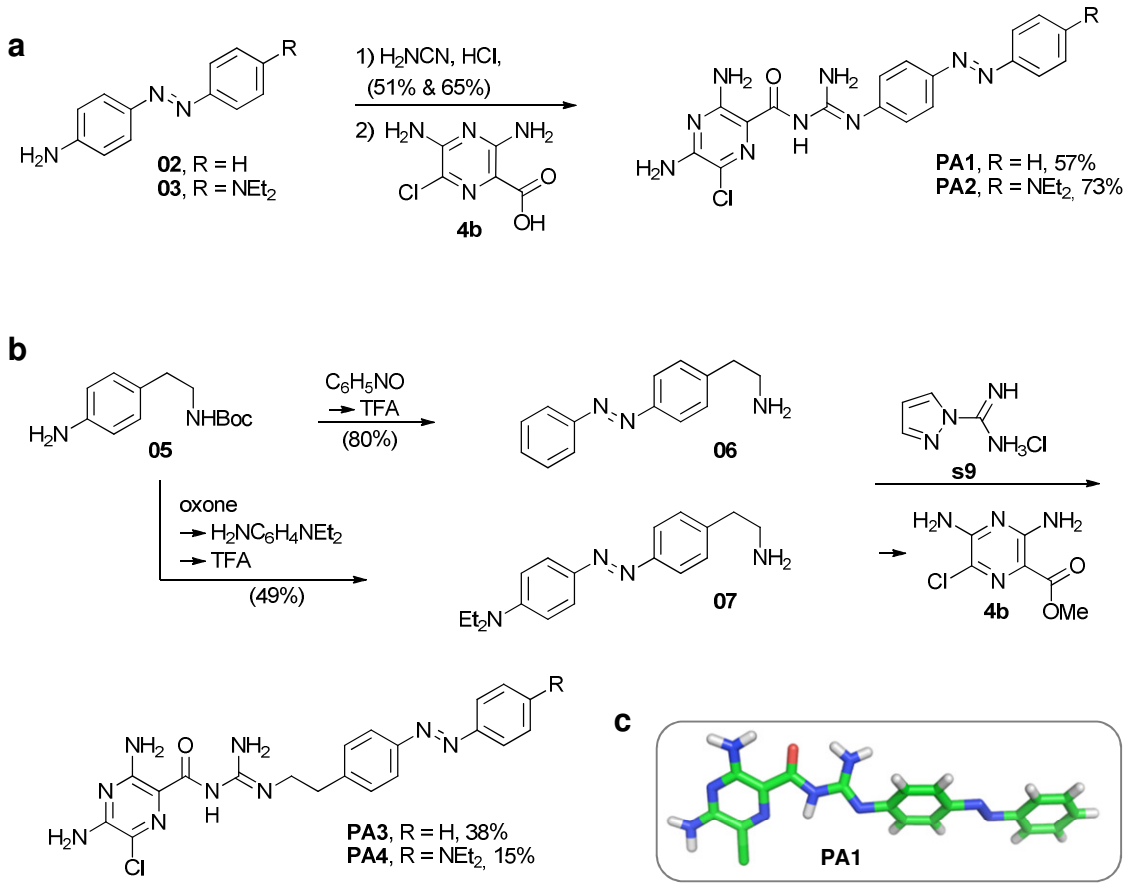

d

Switching wavelengths (nm)

	λ(*cis*)	λ(*trans*)
PA1	400	500
PA2	440	600
PA3	360	500
PA4	420	560

e

IC_{50} values (nM)

	αβγ	δβγ	δ/α
PA1	90	390	4.3
PA2	346	8000	23.1
PA3	36	80	2.2
PA4	4	14	3.5

Figure 2. Photo-switchable amiloride (PA) synthesis and characterization. a, synthesis of **PA1** and **PA2** starts with 4-amino azobenzenes **02** and **03**, respectively. Reaction with cyanamide installs the guanidine functional group. Guanidines (**s4** & **s5**) can be coupled to the active ester of **4b** (HATU activation) yielding **PA1** and **PA2**. **b**, Synthesis of **PA3** and **PA4** starts from boc-protected phenethylamine **05**, which can be either condensed with nitrosobenzene **s7**, or oxidized itself to condense with 4-aminodiethylaniline **s8**. After acidic deprotection, primary amine building blocks **06** and **07** are functionalized to guanidines, which can react with ester **4a** yielding **PA3** and **PA4**. **c**, X-Ray structure of **PA1** indicates an extended hydrogen bond network, a slightly rotated azobenzene and the guandine double bond directed to the latter. **d**, Ideal wavelengths for photo-switching were investigated using UV/Vis. Generally, the more conjugated candidates **PA1** and **PA2** are more red-shifted than their corresponding homologs **PA3** and **PA4**. Substitution with the electron donating diethylaniline functionality leads to a red-shift compared to unsubstituted candidates (**PA2** and **PA4** vs. **PA1** and **PA3**). e) IC_{50} values of **PA**s in their dark-adapted *trans* form as determined in dose response experiments using microelectrode recordings. **PA4** is the most and **PA2** as the least potent ENaC blocker. All **PA** molecules are more potent on the αβγ isoform. **PA2** discriminates the most between αβγ and δβγENaC with 23 fold selectivity for the former.

A single crystal X-ray structure of **PA1** is shown in Fig. 2c. It provides the first structural data of an amiloride derivative substituted at the terminal guanidine nitrogen and reveals an extended hydrogen-bonding network involving an amine on the pyrazine, the adjacent carbonyl, and the guanidine.

Photophysical Characterization of Photoamilorides. To determine absorption maxima and the optimal wavelengths for photo-switching, solutions of **PA1**-**4** (50 μM, dissolved in DMSO) were irradiated at different wavelengths using a monochromator (Till Photonics Polychrome 5000), Fig. S1. DMSO was chosen as a solvent to slow down thermal relaxation in order to resolve absorption spectra of *cis* and *trans*-isomers for red-shifted candidates.[39] Thus, it was possible to identify wavelengths leading to the highest *cis* and *trans*-content for each molecule (Fig. 2d).

Electrophysiological Characterization of Photoamilorides in the Dark. To identify the amiloride derivative that would be the best photochromic ENaC blocker, we performed microelectrode recordings on *Xenopus* oocytes expressing human αβγ and δβγENaCs for all molecules (Fig. S2). Without monochromatic illumination and at dimmed room light (i.e. *trans*-enriched), a series of increasing ligand concentrations was applied, followed by full block using a 100 μM amiloride solution. This enabled both the determination of IC_{50} values and the relative block compared to the full blocker amiloride (Fig. S2 & Fig. 2e). It was found that all photochromic ligands synthesized are ENaC blockers with higher affinity for α-containing than δ-containing ENaCs. **PA4** is the most potent molecule with IC_{50} values of 4 and 14 nM for αβγ and δβγENaC, respectively. The weakest blocker is **PA2** with an IC_{50} of 346 and 8000 nM, respectively. For comparison, amiloride has IC_{50} values of 100 nM and 2600 nM on αβγ and δβγENaC channels in a similar experimental setting.[22]

The structure-activity relationships of our small molecular series revealed interesting trends (Fig. 2e). As hypothesized above, the addition of a C-2-linker markedly

increased ligand affinity, as **PA3** and **PA4** are substantially more potent than their shorter analogues. Addition of a substituent in 4'-position in **PA4** further increases potency compared to the unsubstituted **PA3**. However, this trend is reversed when there is no linker between the guanidine and the azobenzene moiety.

It can be argued that the flexible linker in **PA3** and **PA4** enables the azobenzene moiety to optimally interact with amino acids in the vicinity of the amiloride binding site. Affinity is increased by the diethylaniline substituent suggesting an extended hydrophobic pocket in line with previous studies.[37] In contrast, with no flexible linker (as in **PA1**), the stiff azobenzene functional group is forced into a comparatively unfavorable orientation. The additional loss in affinity by addition of the diethylaniline functionality (**PA2**) suggests that an extension in this particular region results in repulsive interactions. Interestingly, this effect is more pronounced on δβγENaC yielding in a 23-fold decrease in potency, compared with a 2 to 4-fold decrease in the case of αβγENaC channels (Fig. 2e). This new finding could be helpful for developing an amiloride derivative that is selective for αβγ or δβγENaC.

Photocurrents elicited with PA1. To investigate which compound elicits the most pronounced photoeffect, we first performed electrophysiological recordings on ENaC-expressing *Xenopus* oocytes in combination with monochromatic illumination. Each compound was applied at concentrations higher than the previously determined IC_{50} values in order to obtain an on-off-like photoeffect. Illumination wavelengths were then switched in 1 min intervals while perfusion was stopped (Fig. S3). When **PA1**-**4** was applied to the αβγ or δβγENaC isoform, compound **PA1** emerged as an excellent photochromic blocker, especially of the δβγ isoform, where effects were not only more pronounced, but also more robust, Fig. 3. Illumination with 400 nm immediately triggered a strong reduction in current. This effect could be reversed by switching back to 500 nm light (Fig. S4a). Thus, **PA1** functions as a *cis*-blocker of the δβγENaC. This observation adds to the trend of an increased potency going from the 4'-substituted **PA2** to the shorter **PA1** and the even shorter *cis*-**PA1**. We found that the overall switching amplitude evoked by PA1 is consistent between 1 and 10 μM and decided to

settle on 10 μM as a working concentration, which allows photoswitching close to the amiloride baseline (Fig. S4b). Control experiments using oocytes expressing ENaC channels showed no innate sensitivity to light (Fig. S5). Likewise, ENaC expressing oocytes blocked by a 100 μM solution of amiloride did not react to varying illumination, even though applied wavelengths are known to evoke amiloride fluorescence.[40]

Fig. 3a shows the effect of **PA1** on δβγENaC–mediated current in real time. Wavelengths and consequentially currents were switched in 10 and 5 second intervals, respectively. With light-mediated activation, perfusion-induced mechanical effects can be avoided, which has been recently demonstrated for ENaCs, as well as other members of the ENaC/deg family.[41-43]

The photostationary state of azobenzenes, *i.e*. their *cis*/*trans*-ratio, is a function of the illumination wavelength, which allows for controlling their effective concentrations with light. As a consequence, the degree to which δβγENaC channels are blocked by **PA1** also depends on the wavelength applied (Fig. 4b, S6). Switching in 20 nm steps between a given wavelength and 500 nm results in a graded effect on the current, which is not dependent on the order applied. In line with our previous UV/VIS experiments, 400 nm light emerged as the most effective blocking wavelength.

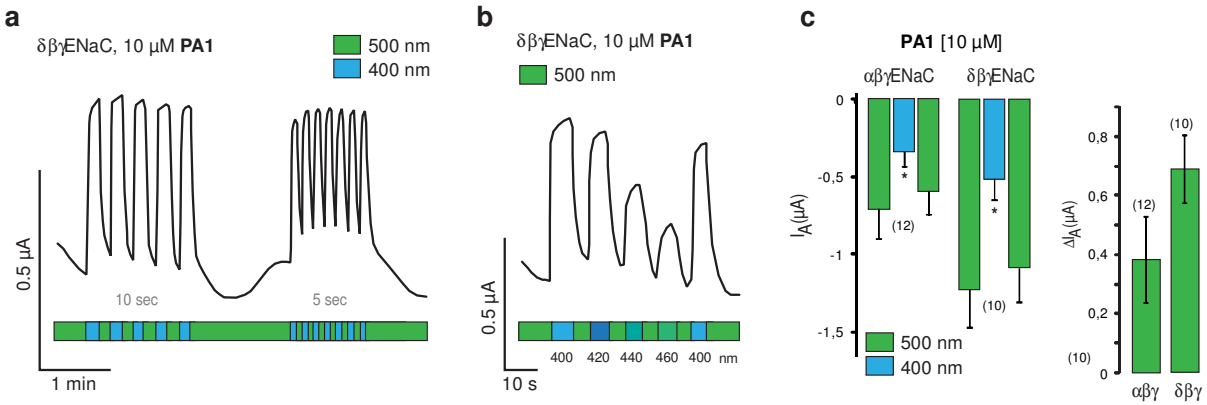

Figure 3. PA1 photo-switching. a, Reversible block of of δβγENaC currents evoked by photo-isomerization of **PA1** (10 µM). **b**, Action spectrum of **PA1**. Wavelengths were switched between 500 nm and 400 + x(20)nm (x = 0,1,2,3). Largest photo-switchable currents are observed when 500 and 400 nm are used as illumination wavelengths for *cis* and *trans*-isomerization. **c**, Photo-switching of **PA1** tested on amiloride-sensitive current (I_A) of αβγ (left) and δβγENaC (right) expressing *Xenopus* oocytes by two electrode voltage clamp (TEVC) recordings. Perfusion was stopped and illumination wavelengths were switched between 500 and 400 nm in 1 min intervals. Current values were taken at the end of each interval and averaged (n = 12 and 10, respectively). Error bars indicate SEM, significance refers to switching from 400 nm to 500 nm (*: $p < 0.05$). There is a reversible photo-switching-effect on both αβγENaC and δβγENaC. However, the amplitude of **PA1** evoked photoswitching is higher on δβγENaC.

Photoswitching evoked by 10 µM **PA1** could be detected on both αβγ and δβγENaC expressing oocytes (Fig. 3c). However, switching events were generally more robust and amplitudes were higher on δβγENaC. Given the interesting and vaguely understood role of existence δβγENaC, especially in primates, we next turned to HEK293t (HEK) cells as a mammalian expression system. Additionally, in the light of a smaller and transparent cell, we expected faster and more pronounced effects compared to the non-transparent pigmented oocytes where only a fraction of the membrane surface can be illuminated. As depicted in Fig. 4, **PA1** is an excellent photoswitch for δβγENaC expressing HEK cells.

In line with the data from *Xenopus* oocytes, 400 nm translates into a rapid block of ENaC currents, which can be released repeatedly with 500 nm. As expected, this process occurs on the time scale of only a few seconds (Fig S7). In current clamp mode, the action of **PA1** on δβγENaC translates into a pronounced and fast light-dependend change in membrane potential. Interestingly, this effect was also found in *Xenopus*

oocytes even though no starting potential could be set so effects were only driven by the chemical potential (Fig. S8). A comparison of δβγ and αβγENaC expressing HEK cells revealed that the average amplitude of photocurrents is ~180 pA on the former and ~10 pA on the latter isoform (Fig. S9). Likewise, the average change in membrane potential was ~57 mV for δβγENaCs and ~4 mV for αβγENaCs in HEK cells. Thus, the general trends and effects that were found in *Xenopus* oocytes could also be observed in HEK cells, however, much more pronounced and faster, as was expected from the smaller transparent system that can be entirely illuminated.

When addressing the thermal stability of the thermodynamically less stable *cis*-**PA1**, we found that after being switched to *cis* using 400 nm, **PA1** relaxes back on a fast time scale even without additional energy. Thus, our novel optical tool can be operated by turning on and off a simple light source emitting between 380 and 400 nm. As determined in oocytes, Fig 3b, intermediate wavelengths between 400 and 500 nm translate to graded effects. We were thus able to induce current and voltage steps in δβγENaC expressing HEK cells by switching between 400, 433, 466 and 500 nm, respectively.

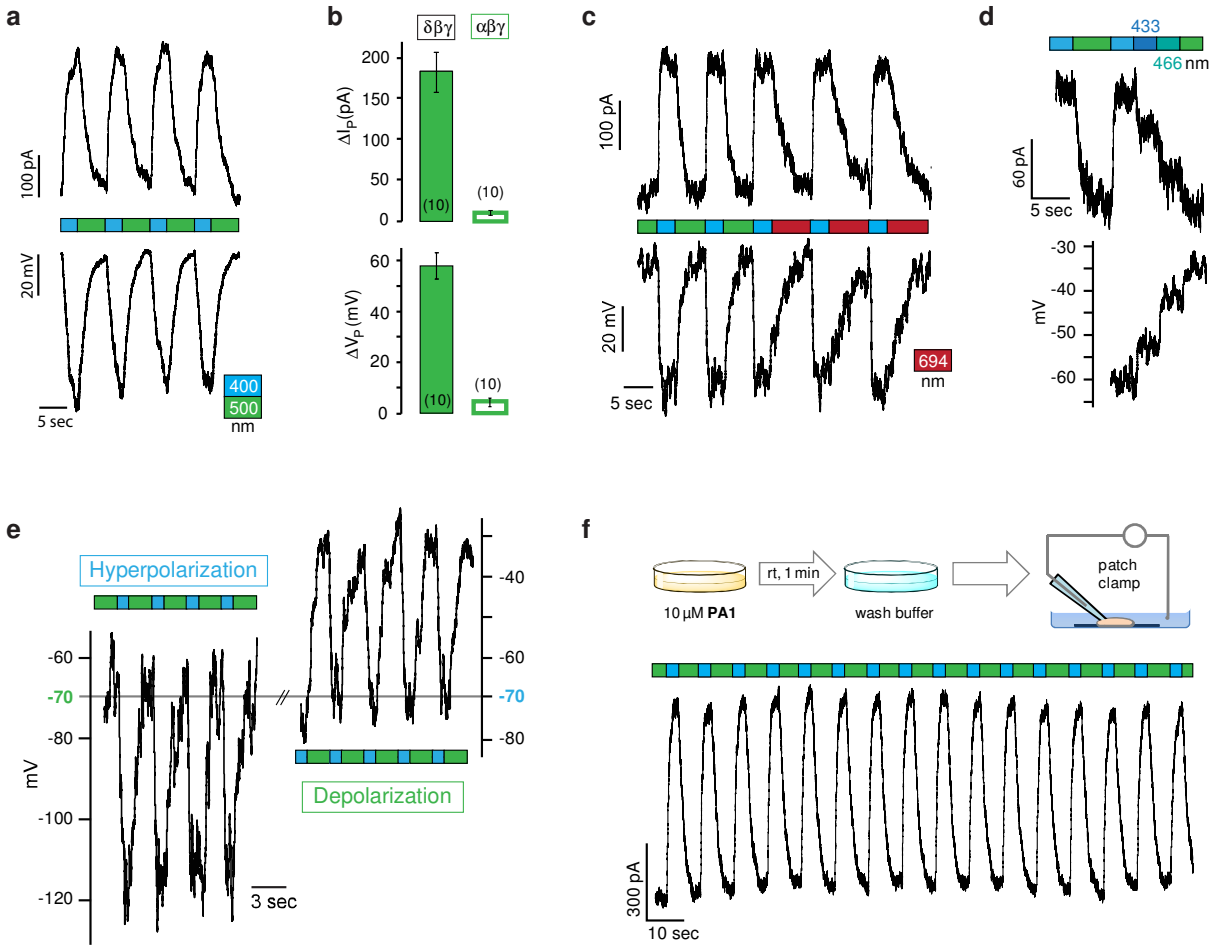

Figure 4. Switching δβγENaC in HEK cells using 10 µM **PA1**. **a**, Photoswitching mediated by **PA1** on δβγENaC expressing HEK cells. By switching between 400 and 500 nm both large currents (upward deflection = inhibition) and potentials (downward deflection = hyperpolarization) can be controlled by light. **b**, The average current amplitude of photoswitching (ΔI_P) is 182 pA on for δβγENaC and 9 pA for αβγENaC. The average ampitude of light mediated membrane potential (ΔV_P) is 57 mV and 4 mV, respectively (currents and potentials were recorded from the same cell, n = 10 biological repeats from 3 independent transfections, holding potential was -60 mV). **c**, Comparison between light-induced and thermal relaxation. **d**, Action spectrum of **PA1** on δβγENaC expressing HEK cells demonstrates graded effects on both currents and membrane potential. **e**, **PA1** can be used as a tool for not only hyperpolarization, but also depolarization. **f**, **PA1** can be loaded into HEK cells by short incubation. After 1 min incubation at room temperature (rt) in 10 µM **PA1** (yellow petry dish) and subsequent wash (blue petry dish), cells are ready for photo-experiments using the patch clamp technique.

To further determine the potential of **PA1** as a phototool for adjusting membrane potential, we set the starting potential in current clamp mode at -70 mV under blue or green light illumination (Fig. 4e). Starting from these conditions, **PA1** can be used not only to hyperpolarize (switching from 500 to 400 nm), but also to depolarize a cell

(switching from 400 to 500 nm). This feature is especially interesting as de- and hyperpolarization are key triggers in cell communication including action potential firing and vesicle release. Therefore, the δβγENaC-**PA1**-system could be used as a mammalian derived tool for investigating cellular communication that roots in de or hyperpolarization, or as a trigger in optical screening platforms.

In the course of our switching experiments using **PA1** on δβγENaC expressing HEK cells, we found that photoswitching remains, even after wash out of **PA1** from the external recoding solution (Fig. S10). There are different mechanisms by which this observation could be explained. First, protonated **PA1** could stay in the channel pore, second, **PA1** could be integrated into the membrane forming a reservoir and third, **PA1** could be internalized and act from inside the cell. To exclude that this finding results from **PA1** contamination in the tubing or recording chamber, we pre-incubated coverslips with HEK cells that were transiently transfected with δβγENaC for 1 min at room temperature in 10 µM **PA1** (Fig. 4f). Coverslips were then washed 3 times and investigated using patch clamp experiments.

Interestingly, we obtained a fully functional photoswitchable system with strong, persistent ENaC-photo-currents. Up to this point, no perfusion and only a very small amount of **PA1** was needed to perform an experiment with ENaC under optical control. Figure 4f further illustrates the rapid robust and reversible action of **PA1** on δβγENaC that would be difficult to achieve with conventional tools. Intriguingly, cells prepared in such manner could be blocked and unblocked by amiloride without affecting photoswitching (Fig S11). This rules out a place of enrichment were **PA1** and amiloride compete such as the channel pore.

To test if **PA1** may be internalized by the cell and act from the inside, we loaded **PA1** through the patch pipettel (Fig. 12). Photoswitching was possible instantaneously and a reversible amiloride block was conserved. Additional **PA1** delivered by perfusion did not enhance the photo-effect. It is thus possible that PA1 acts from inside the cell or within the membrane. In fact, recent investigations point out an amiloride binding site in the transmembrane region.[44]

In contrast to lipophilic amiloride derivatives such as phenamil, the innate light-mediated reversibility of **PA1** allows for block and unblock even after cell uptake. The three different modes of **PA1** delivery – perfusion, incubation and loading through the patch pipette – allow for versatile applications.

With the ability of **PA1** to switch ENaC currents and to differentiate between αβγ and δβγENaC in HEK cells, we next wanted to employ **PA1** in a mammalian cell model, which endogenously expresses ENaC subunits. Human H441 bronchiolar epithelial cells were the model of choice since these cells were (a) human, (b) express all ENaC subunits including δENaC,[16] and (c) form a polarized epithelium which allows the electrophysiological assessment of sodium transport across an intact cell monolayer. Furthermore, despite the molecular evidence for δENaC expression in pulmonary epithelia, a functional contribution of this isoform to transepithelial sodium transport is highly controversial.[22]

To address the functional role of δβγENaC in these cells, we measured the transepithelial potential of H441 monolayers which were cultured on permeable membrane supports. First, we determined the magnitude of the overall amiloride-sensitive transepithelial potential (VE) (in average ~4 mV, Fig. 5c). We then exchanged the apical bath solution for 10 µM **PA1** and switched between 400 and 500 nm, and 400 nm and dark (694 nm) for three cycles, respectively. Results were identical for the different wavelength protocols and the overall magnitude was ~0.4 mV of photo-sensitive transepithelial potential (Fig. 5b).

This finding hints towards a small amount of functional δβγENaC. To investigate whether the photoeffect comes from δβγENaC or is a small effect on αβγENaC, we addressed the lithium conductivity of either isoform. The ratio between lithium and sodium conductivity is 0.64 for δβγENaC and 2.0 for αβγENaC.[45] Thus, we expected decreased photoeffects for the δ-containing isoform and increased effects for the latter when sodium is replaced by lithium. We verified this hypothesis using *Xenopus* oocytes (Fig. 5d), which had shown photoeffects for either isoform before. Likewise, δβγENaC-photocurrents were significantly reduced in HEK cells by extracellular lithium (Fig S13).

When sodium was substituted by lithium at the apical side of the H441 monolayer, **PA1**-mediated photoeffects decreased from 0.4 to 0,15 mV for both wavelength protocols, Fig. 5c. Thus, the photo-sensitive fraction of VE is due to δβγENaC rather than αβγENaC. These data strongly indicate functional δβγENaC in H441 cells and underline the ability of PA1 for functional differentiation between αβγ and δβγENaC.

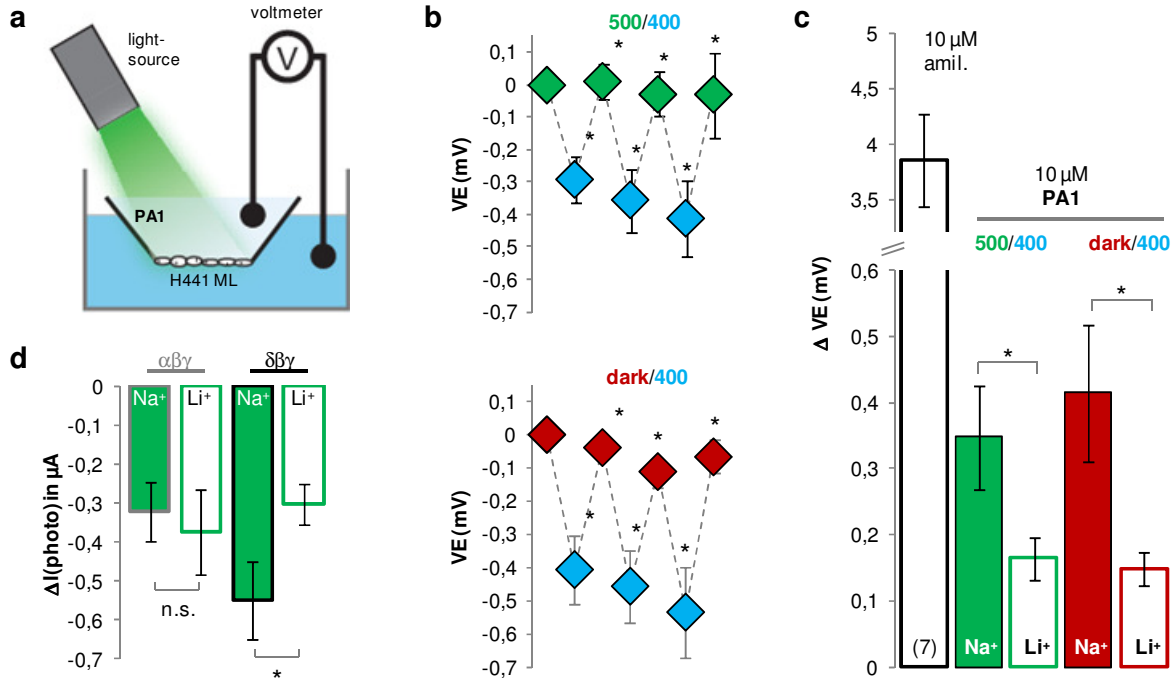

Figure 5. **Switching the transepithelial potential in H441 monolayers**. **a**, Experimental setup with H441 monolayer (ML) on a filter. The apical compartment contains 10 µM **PA1** in sodium or lithium based buffer and was illuminated with a monochromator. The transepithelial potential VE between the apical and basolateral compartment was measured by a voltmeter. **b**, Switching VE with both 500/400 nm (top) and 694(=dark)/400 nm light (bottom). 400 nm were applied for 10 sec, the longer wavelengths for 20 sec and voltage was recorded at the end of each illumination period. Photoeffects are robust and reversible for both protocols **c**, Comparison of the entire amiloride sensitive VE, and **PA1** mediated photosensitive VE with apical sodium or lithium using both 400/500nm and 400nm/dark switching. (for one filter, first 400/500 nm and 400nm/dark switching was performed. Then the same series was repeated with Li-based buffer, n = 7) **d**, Comparison of extracellular lithium on αβγ and δβγENaC photocurrents in *Xenopus* oocytes (n ≥ 7).

Summary and Outlook

In summary, the photoswitchable ENaC blocker **PA1** has been designed, synthesized, and functionally characterized using electrophysiology on *Xenopus* oocytes, HEK cells and H441 cells. Our results provide new insights into the structure-activity relationships of the amiloride class of diuretics and outline a strategy to selectively address the αβγ and δβγ isoforms of ENaC channels. **PA1** can be used to optically control δβγENaCs by switching between blue and green light, or by turning on and off blue light. We showed that **PA1**, acts from the intracellular site and can be applied by perfusion, cell incubation or loading through the patch pipette. This offers additional spatial control and allows reversibly addressing intracellular ENaC gating, which would not be possible by conventional methods. We used **PA1** to address the controversial role of different ENaC isoforms in H441 monolayers and identified functional δβγENaC. The combination of photoswitchable **PA1** and the non-voltage-gated δβγENaC is a powerful tool to precisely control the membrane potential with light, allowing not only hyper but also depolarization. With its unique function, **PA1** will deliver new insights into δβγENaC function and will enable new non-invasive means to investigate these channels in non-epithelial tissue such as the primate brain.

Methods

Chemical synthesis. See supporting information.

Cell culture and Electrophysiology. *HEK293t cells* were cultured in dulbeco´s modified eagle medium with 10% fetal bovine serum in a 10% CO_2 37°C incubator. At 90-95% confluency, cells were splitted and used for transient transfection using the jetPRIME polyplus transfection reagent following the supplier´s protocol. Poly-L-lysine coated acid etched glass coverslips were placed in a 24-well plate and consecutively treated with the DNA-mix (150 ng of each ENaC subunit and 50 ng YFP) and 30k to 50k cells in growth medium. After 2-4 hours, the supernatant was removed and growth medium supplemented with 10 μM amiloride was added. Cells were used for electrophysiological recordings 12 – 48 hours post transfection. Only YFP-positive cells with an amiloride sensitive current were used for experiments.

Whole cell patch clamp experiments were performed using a standard electrophysiology setup equipped with a HEKA Patch Clamp EPC10 USB amplifier and patch master software. Micropipettes were generated from "Science Products GB200-F-8P with filament" pipettes using a vertical puller. Resistance varied between 5-8 MΩ. Bath solution contained in mM: 140 NaCl, 3 KCl, 2 CaCl2, 1 MgCl2, D-Gluc 10, 20 HEPES (NaOH to pH 7.4). Pipette solution contained in mM: 90 K-gluconate, 10 NaCl, 10 KCl, 1 MgCl2, 10 EGTA, 60 HEPES (KOH to pH 7.3). Photoswitchable ligands and reference agonist were dissolved in bath solution from a 1000 x DMSO stock.

H441 cells were purchased from American Type Culture Collection in the 65th passage and cultured under liquid/air conditions in the presence of 200 nM dexamethasone as previously described.[46] For experiments, H441 containing cell culture inserts were placed in 6-well plates containing H441 saline (2ml in the basolateral, and 500 μl in the apical compartment). H441 saline contained in mM: 130 NaCl, 2.7 KCl, 1.5 KH2PO4, 1 mM CaCl2, 0.5 MgCl2, 10 HEPES, and 10 glucose (37°C, pH 7.35 (TRIZMA)). In some experiments sodium was substituted by equivalent concentrations of lithium. Transepithelial voltage (VE) was measured with an epithelial voltohmmeter (EVOM; World Precision Instruments). When VE was stable, amiloride was added to the apical compartment to a final concentration of 100 μM in order to investigate the amiloride-

sensitive fraction of VE. Monolayers were washed 3 times with H441 saline and afterwards 10 μM PA1 was added to the apical compartment. When VE stabilized again, the EVOM was zeroed (for better comparability between cell preparations) and monolayers were exposed to different wavelengths of light. Afterwards, cells were rinsed with lithium containing saline and the same measurement protocol was employed. Experiments were performed at 37°C on seven H441 monolayers from two independent cell preparations.

Irradiation was performed a TILL Photonics Polychrome 5000 monochromator. In patch clapm experiments, the light beam was guided through the microscope objective and operated by the amplifier and patch master software. In all other experiments, a light fiber was positioned in proximity to the object of interest and the monochromator was operated using the PolyCon 3.1 software.

Heterologous expression of ENaC subunits and microelectrode recordings. Defolliculated oocytes (stages V/VI) which were derived from female South African Clawed Frogs (*Xenopus laevis*) were injected with 20-30 nl of cRNA encoding the αβγ or δ1βγ subunits of human ENaC (the splice variant δ1βγ is referred to as δβγ in this report). The RNA concentration was 10 ng/μl per subunit. Oocytes were incubated for 24-48 h in a solution containing (in mM): 10 NaCl, 1 KCl, 2 $CaCl_2$, 80 NMDG-Cl, 5 HEPES, 2.5 sodium pyruvate, 0.06 penicillin G, 0.02 streptomycinsulfate (pH 7.4-HCl). Microelectrode recordings were performed with the two-electrode voltage-clamp technique (TEVC). ENaC-expressing oocytes were placed into a lucite chamber and perfused with oocyte ringer solution (ORI) containing (in mM): 90 NaCl, 1 KCl, 2 $CaCl_2$, 5 HEPES, 2.5 sodium pyruvate (pH 7.4-NaOH). Glass capillaries with an outer diameter of 1.2 mm were pulled to microelectrodes and filled with 1 M KCl. Chloride-coated silver wires served as bath electrodes. Electrodes were connected to a TEVC amplifier (Warner Instruments, Hamden, CT, USA). In order to measure the transmembrane ion currents (I_M), the membrane potential of ENaC-expressing oocytes was clamped to -60 mV. The membrane potential (V_M) as well as transmembrane current (I_M) were continuously recorded with a strip chart recorder (Kipp&Zonen, Delft, The Netherlands). For statistical measurements, oocytes from at least two animals were used.

References

1. de la Rosa, D.A., Canessa, C.M., Fyfe, G.K. & Zhang, P. Structure and Regulation of Amiloride-Sensitive Sodium Channels. *Annual Review of Physiology* **62**, 573-594 (2000).
2. Canessa, C.M., Merillat, A.M. & Rossier, B.C. Membrane topology of the epithelial sodium channel in intact cells. *Am J Physiol* **267**, C1682-90 (1994).
3. Canessa, C.M. et al. Amiloride-sensitive epithelial Na+ channel is made of three homologous subunits. *Nature* **367**, 463-7 (1994).
4. Bubien, J.K. Epithelial Na+ channel (ENaC), hormones, and hypertension. *J Biol Chem* **285**, 23527-31 (2010).
5. Chang, S.S. et al. Mutations in subunits of the epithelial sodium channel cause salt wasting with hyperkalaemic acidosis, pseudohypoaldosteronism type 1. *Nat Genet* **12**, 248-253 (1996).
6. Boucher, R.C. New concepts of the pathogenesis of cystic fibrosis lung disease. *European Respiratory Journal* **23**, 146-158 (2004).
7. Hummler, E. et al. Early death due to defective neonatal lung liquid clearance in [alpha]ENaC-deficient mice. *Nat Genet* **12**, 325-328 (1996).
8. Scherrer, U. et al. High-altitude pulmonary edema: from exaggerated pulmonary hypertension to a defect in transepithelial sodium transport. *Adv Exp Med Biol* **474**, 93-107 (1999).
9. Althaus, M., Clauss, W.G. & Fronius, M. Amiloride-sensitive sodium channels and pulmonary edema. *Pulm Med* **2011**, 830320 (2011).
10. Althaus, M. ENaC inhibitors and airway re-hydration in cystic fibrosis: state of the art. *Curr Mol Pharmacol*.
11. Fronius, M. Treatment of Pulmonary Edema by ENaC Activators/Stimulators. *Curr Mol Pharmacol* (2013).
12. BULL, M.B. & LARAGH, J.H. Amiloride: A Potassium-Sparing Natriuretic Agent. *Circulation* **37**, 45-53 (1968).
13. Schoenberger, M. & Althaus, M. Novel small molecule epithelial sodium channel inhibitors as potential therapeutics in cystic fibrosis - a patent evaluation. *Expert Opinion on Therapeutic Patents* **23**, 1383-1389 (2013).

14. Waldmann, R., Champigny, G., Bassilana, F., Voilley, N. & Lazdunski, M. Molecular cloning and functional expression of a novel amiloride-sensitive Na+ channel. *J Biol Chem* **270**, 27411-4 (1995).
15. Giraldez, T. et al. Cloning and functional expression of a new epithelial sodium channel delta subunit isoform differentially expressed in neurons of the human and monkey telencephalon. *J Neurochem* **102**, 1304-15 (2007).
16. Wesch, D. et al. Differential N termini in epithelial Na+ channel delta-subunit isoforms modulate channel trafficking to the membrane. *Am J Physiol Cell Physiol* **302**, C868-79 (2012).
17. Teruyama, R., Sakuraba, M., Wilson, L.L., Wandrey, N.E. & Armstrong, W.E. Epithelial Na(+) sodium channels in magnocellular cells of the rat supraoptic and paraventricular nuclei. *Am J Physiol Endocrinol Metab* **302**, E273-85 (2012).
18. Ji, H.-L. et al. dENaC: a novel divergent amiloride-inhibitable sodium channel. *American Journal of Physiology - Lung Cellular and Molecular Physiology* **303**, L1013-L1026 (2012).
19. Yamamura, H., Ugawa, S., Ueda, T., Nagao, M. & Shimada, S. A novel spliced variant of the epithelial Na+ channel delta-subunit in the human brain. *Biochem Biophys Res Commun* **349**, 317-21 (2006).
20. Miller, R.L., Wang, M.H., Gray, P.A., Salkoff, L.B. & Loewy, A.D. ENaC-expressing neurons in the sensory circumventricular organs become c-Fos activated following systemic sodium changes. *Am J Physiol Regul Integr Comp Physiol* **305**, R1141-52 (2013).
21. Giraldez, T., Dominguez, J. & Alvarez de la Rosa, D. ENaC in the brain--future perspectives and pharmacological implications. *Curr Mol Pharmacol* **6**, 44-9 (2013).
22. Giraldez, T., Rojas, P., Jou, J., Flores, C. & Alvarez de la Rosa, D. The epithelial sodium channel Î´-subunit: new notes for an old song. *American Journal of Physiology - Renal Physiology* **303**, F328-F338.
23. Kellenberger, S. & Schild, L. Epithelial sodium channel/degenerin family of ion channels: a variety of functions for a shared structure. *Physiol Rev* **82**, 735-67 (2002).

24. Waldmann, R., Champigny, G., Bassilana, F., Heurteaux, C. & Lazdunski, M. A proton-gated cation channel involved in acid-sensing. *Nature* **386**, 173-177 (1997).
25. Jasti, J., Furukawa, H., Gonzales, E.B. & Gouaux, E. Structure of acid-sensing ion channel 1 at 1.9 A resolution and low pH. *Nature* **449**, 316-23 (2007).
26. Fehrentz, T., Schonberger, M. & Trauner, D. Optochemical genetics. *Angew Chem Int Ed Engl* **50**, 12156-82 (2011).
27. Banghart, M., Borges, K., Isacoff, E., Trauner, D. & Kramer, R.H. Light-activated ion channels for remote control of neuronal firing. *Nat Neurosci* **7**, 1381-6 (2004).
28. Mourot, A. et al. Rapid optical control of nociception with an ion-channel photoswitch. *Nat Methods* **9**, 396-402.
29. Volgraf, M. et al. Allosteric control of an ionotropic glutamate receptor with an optical switch. *Nat Chem Biol* **2**, 47-52 (2006).
30. Levitz, J. et al. Optical control of metabotropic glutamate receptors. *Nat Neurosci* **16**, 507-16.
31. Tochitsky, I. et al. Optochemical control of genetically engineered neuronal nicotinic acetylcholine receptors. *Nat Chem* **4**, 105-111.
32. Cragoe, E.J., Woltersd.Ow, Bicking, J.B., Kwong, S.F. & Jones, J.H. Pyrazine Diuretics .2. N-Amidino-3-Amino-5-Substituted L-Halopyrazinecarboxamides. *Journal of Medicinal Chemistry* **10**, 66-& (1967).
33. Kleyman, T.R. & Cragoe, E.J., Jr. Amiloride and its analogs as tools in the study of ion transport. *J Membr Biol* **105**, 1-21 (1988).
34. Cuthbert, A.W., Fanelli, G.M. & Scriabine, A. *Amiloride and epithelial sodium transport*, (Urban & Schwarzenberg, 1979).
35. Li, J.H., Cragoe, E.J., Jr. & Lindemann, B. Structure-activity relationship of amiloride analogs as blockers of epithelial Na channels: II. Side-chain modifications. *J Membr Biol* **95**, 171-85 (1987).
36. Garvin, J.L., Simon, S.A., Cragoe, E.J., Jr. & Mandel, L.J. Phenamil: an irreversible inhibitor of sodium channels in the toad urinary bladder. *J Membr Biol* **87**, 45-54 (1985).

37. Hirsh, A.J. et al. Design, synthesis, and structure-activity relationships of novel 2-substituted pyrazinoylguanidine epithelial sodium channel blockers: drugs for cystic fibrosis and chronic bronchitis. *J Med Chem* **49**, 4098-115 (2006).

38. Sadovski, O., Beharry, A.A., Zhang, F. & Woolley, G.A. Spectral tuning of azobenzene photoswitches for biological applications. *Angew Chem Int Ed Engl* **48**, 1484-6 (2009).

39. Mourot, A. et al. Tuning photochromic ion channel blockers. *ACS Chem Neurosci* **2**, 536-43.

40. PulgarÄ±Ì n, J.A.M., Molina, A.A.Ã.n. & LÃ³pez, P.F.n. Direct analysis of amiloride and triamterene mixtures by fluorescence spectrometry using partial-least squares calibration. *Analytica Chimica Acta* **449**, 179-187 (2001).

41. Althaus, M., Bogdan, R., Clauss, W.G. & Fronius, M. Mechano-sensitivity of epithelial sodium channels (ENaCs): laminar shear stress increases ion channel open probability. *FASEB J* **21**, 2389-99 (2007).

42. Fronius, M., Bogdan, R., Althaus, M., Morty, R.E. & Clauss, W.G. Epithelial Na+ channels derived from human lung are activated by shear force. *Respir Physiol Neurobiol* **170**, 113-9.

43. Geffeney, S.L. et al. DEG/ENaC but not TRP channels are the major mechanoelectrical transduction channels in a C. elegans nociceptor. *Neuron* **71**, 845-57.

44. Shi, S. & Kleyman, T.R. Gamma subunit second transmembrane domain contributes to epithelial sodium channel gating and amiloride block. *American Journal of Physiology - Renal Physiology* **305**, F1585-F1592 (2013).

45. Giraldez, T., Rojas, P., Jou, J., Flores, C. & Alvarez de la Rosa, D. The epithelial sodium channel d-subunit: new notes for an old song. *American Journal of Physiology - Renal Physiology* **303**, F328-F338 (2012).

46. Althaus, M. Gasotransmitters: Novel regulators of epithelial Na+ transport? *Frontiers in Physiology* **3**(2012).

Acknowledgements

MA is supported by grants from the German Research Foundation (AL1453/1-1 and AL1453/1-2), MF and WC are grant holder of a grant provided by the Federal State of Hessen/Germany (LOEWE Research Focus, Non-neuronal cholinergic systems). MS acknowledges the support of Katharina Hüll during chemical synthesis, the International Max Planck Research School (IMPRS-LS) and the financial support from the German National Academic Foundation. We want to thank Dr. Diego de la Rosa for providing constructs of all ENaC subunits in pcDNA3.1.

Author Contributions

DT conceived of the project. MS designed and synthesized the molecules and performed the UV/Vis and patch clamp experiments. MS and MA performed the TEVC and VE experiments. MS and DT wrote the manuscript. MF and WC provided resources.

Competing financial interest

The authors declare no competing financial interest.

III.i

Supporting Information

to

Controlling Epithelial Sodium Channels with Light Using Photoswitchable Amiloride

Matthias Schönberger[1], Mike Althaus[2], Martin Fronius[2,3], Wolfgang Clauss[2] and Dirk Trauner[1*]

[1]Department of Chemistry and Center for Integrated Protein Science, Ludwig Maximilians-Universität München, Butenandtstraße 5–13 (F4.086), 81377 Munich (Germany).

[2]Institute of Animal Physiology, Justus Liebig University Giessen, Heinrich-Buff-Ring 26, 35392 Giessen, Germany.

[3]Department of Physiology, University of Otago, PO Box 913, Dunedin 9054, New Zealand

Additional Photoswitching Experiments

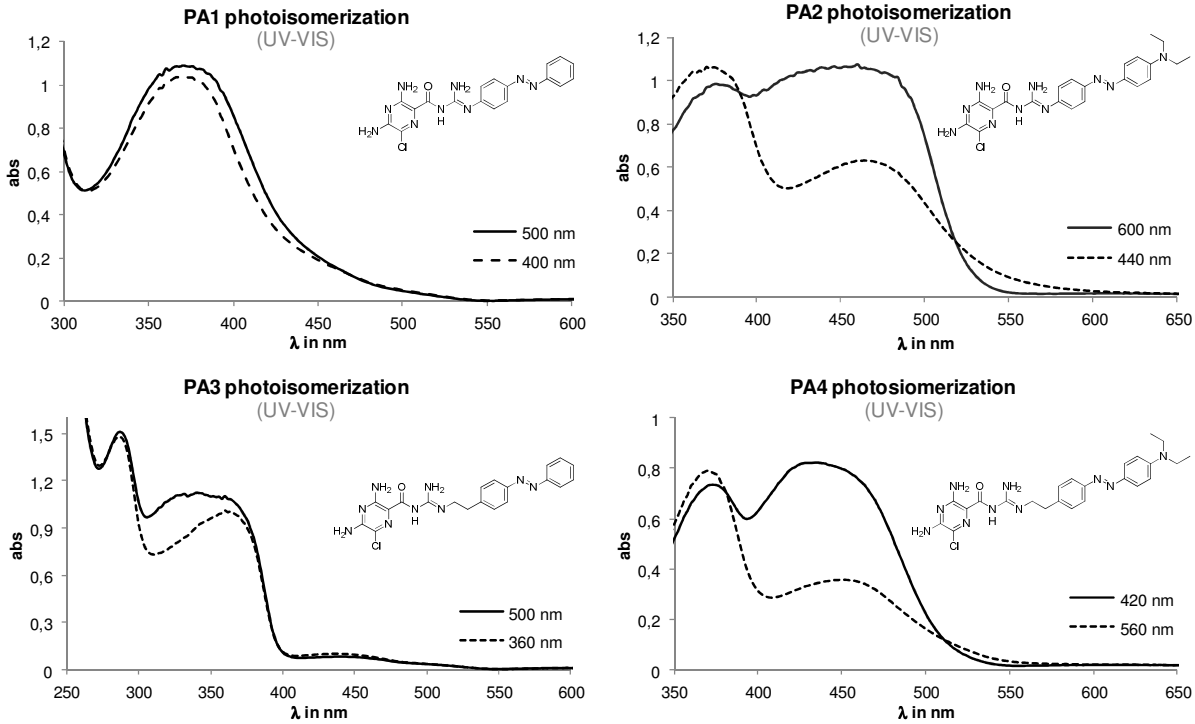

Figure S1. UV-VIS characterization of photo-isomerization of photo-switchable amilorides **PA1**-**4**. 50 µM solutions of **PA1**-**4** in DMSO were placed in a 1 mL quartz cuvette (10 mm diameter, VAIRAN Cary 50 Scan UV/Vis Spectrophotometer). A light-fiber cable connected to a Till Photonics Polychrome 5000 monochromator was placed in the cuvette. The light fiber cable was positioned in a way that it just penetrates the surface of the **PA**-solution in order to avoid diffraction at the liquid/air interface. Monochromatic illumination was screened from wavelengths higher than the n→p* transition (500 to 600 nm) to those smaller than the π→π* transition (300 to 400 nm) in 20 nm steps going from higher to smaller wavelengths. Every wavelength was applied for 2 min before a UV-Vis-scan was recorded. Illumination conditions yielding the highest π→π* absorption were used for maximal trans-enrichment (solid line). Illumination conditions yielding the lowest π→π* absorption were used for maximal *cis*-enrichment (dashed line).

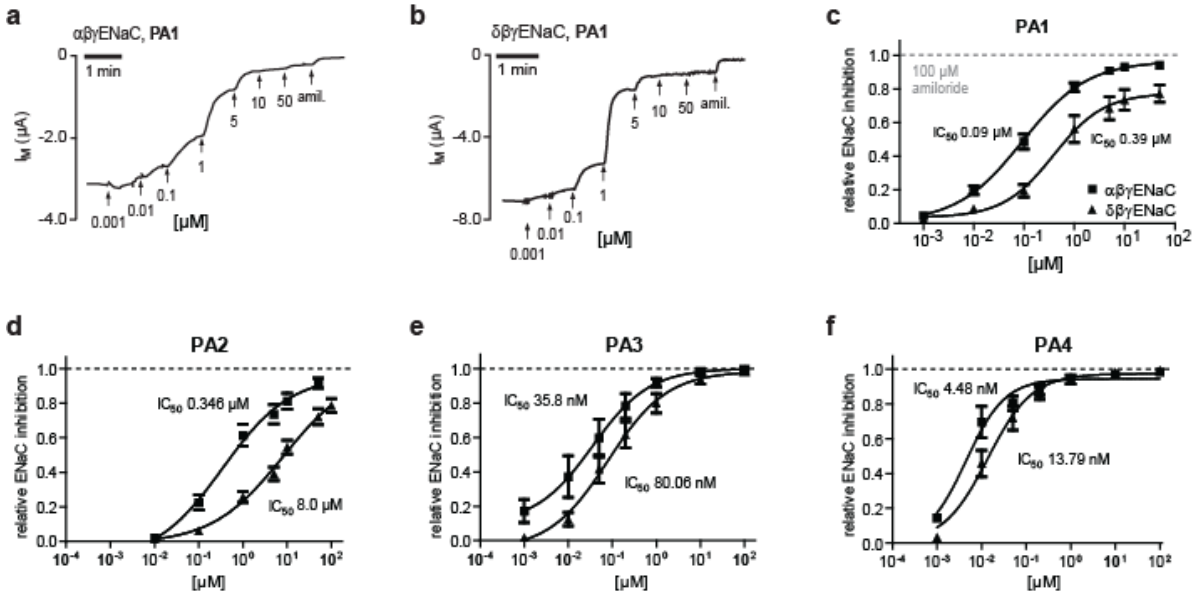

Figure S2. Microelectrode recordings for Electrophysiological characterization of PAs. a, Single current trace of an αβγENaC expressing *Xenopus* oocytes sequentially treated with increasing concentrations of **PA1** followed by saturating amiloride under dimmed room light (trans-enriched, I_M = membrane current). **b**, Same experiments with δβγENaC. **c**, Dose response curves of **PA1** on αβγ and δβγENaC calculated from experiments as described in a) and b). Trans-enriched solutions of **PA1** fully block αβγENaC, but only partially block δβγENaC (dashed line indicates amiloride baseline). **d-f,** Dose response curves of **PA2-4** on αβγ (square) and δβγENaC (triangle), respectively. IC_{50} values were obtained from a sigmoidal concentration-response fit according to the Hill equation using Graphpad Prism (version 4), at least 5 biological repeats ,at least two donor animals.

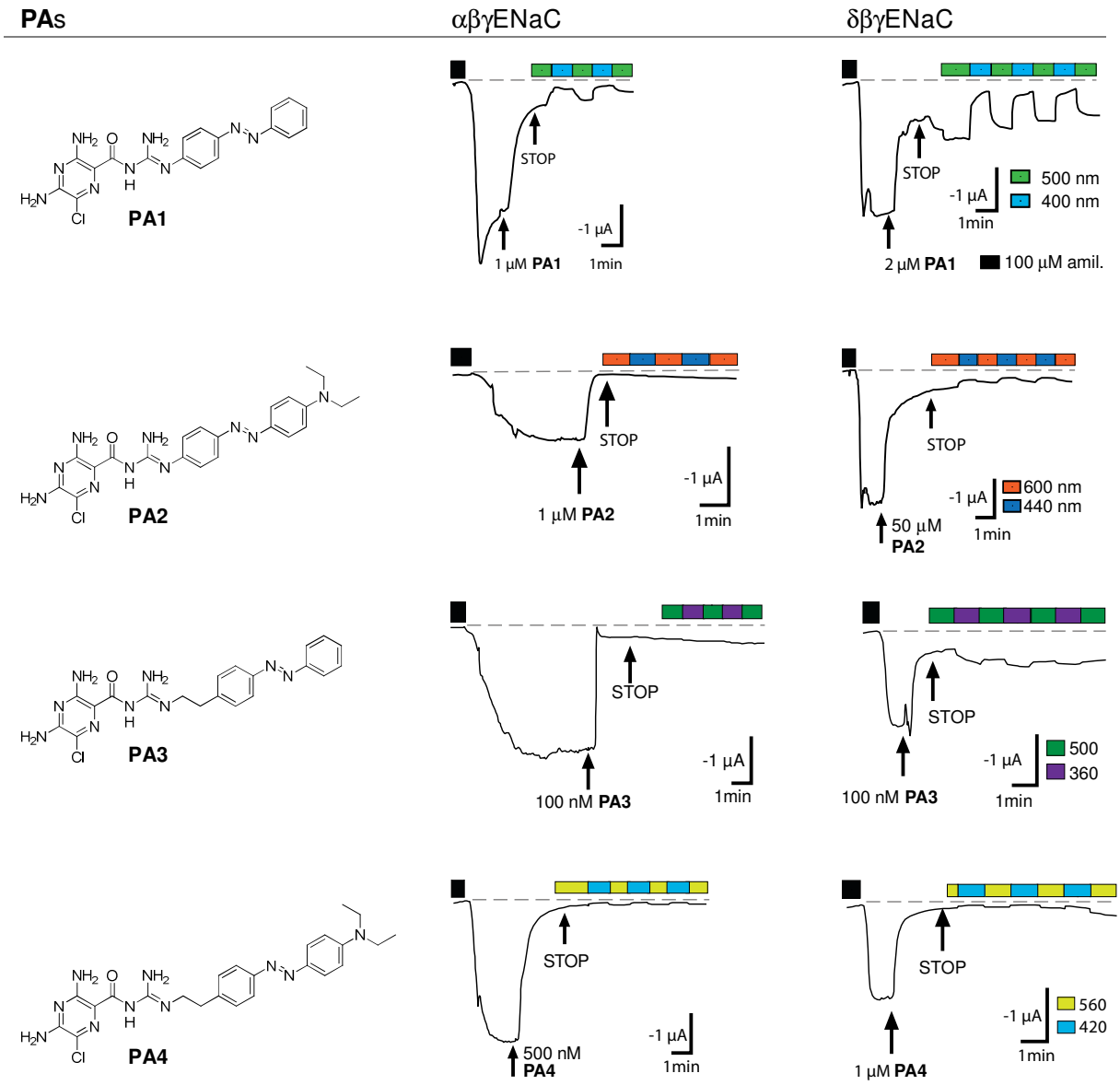

Figure S3. Two electrode voltage clamp recordings from ENaC expressing *Xenopus* oocytes – **PA**x Screen. Photoswitchable amiloride derivatives **PA1**-**PA4** (left column) were tested on αβγENaC (middle column) and δβγENaC (right column).Testing concentrations were chosen based on the previously determined IC_{50} values in order to obtain photoswitching events close to the amiloride baseline (dashed) (Fig. S2). Switching wavelengths were chosen based on previous UV/Vis experiments (Fig. S1). For all **PA**s, photoswitching effects were more pronounced on δβγENaC, even though overall currents were comparable. **PA1** gave the best results in terms of overall photocurrent magnitude. Depicted current traces show identical amiloride sensitive currents for either ENaC isoform. However, photoswitching is more pronounced on δβγENaC. Interestingly, for **PA1**, **PA2** and **PA4**, the *cis*-isomer (illumination with the shorter wavelength) was the better blocker. In the case of **PA3**, however, the *trans*-isomer (longer wavelength) blocked δβγENaC currents more efficiently. Based on the presented series, there is no structural rational for explaining this result, especially with no X-ray structure of the ion channel and the binding site at hand. Based on this screen, we settled on **PA1** and δβγENaC for further experiments. (Depicted traces are representative. At least two concentrations were tested for every molecule. Every experiment was repeated at least two times).

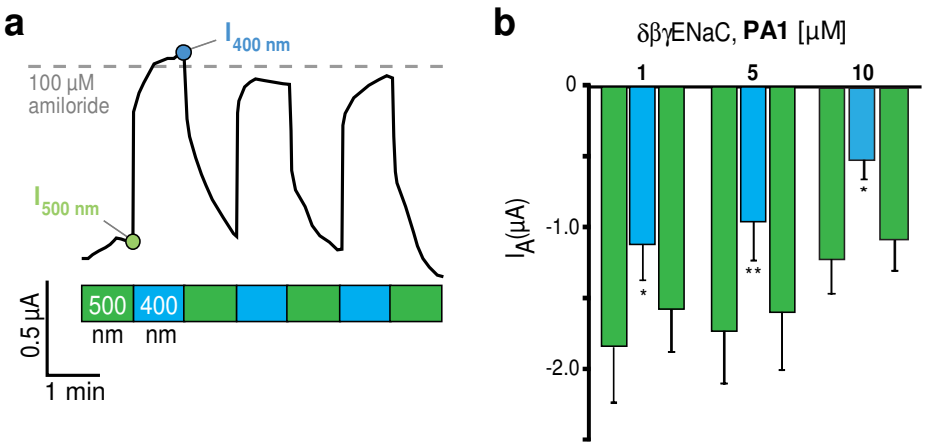

Figure S4. Photo-switching of **PA1** (10 µM) on δβγENaC investigated using microelectrode recordings. **a**, Photocurrents: Perfusion was stopped and illumination was switched between 500 and 400 nm in 1 min intervals. At the end of each illumination period, current values were taken ($I_{500\ nm}$ & $I_{400\ nm}$). These data are summarized in Fig. 3**b**. **b**, Photoswitching of **PA1** on δβγENaC. The amplitude of photocurrents is stable over the range of tested concentrations. However, events occur closer to the amiloride baseline when 10 µM **PA1** are applied indicated by a small residual amiloride sensitive current I_A under 400 nm. (n ≥ 6, *: $p < 0.05$, **: $p < 0.01$).

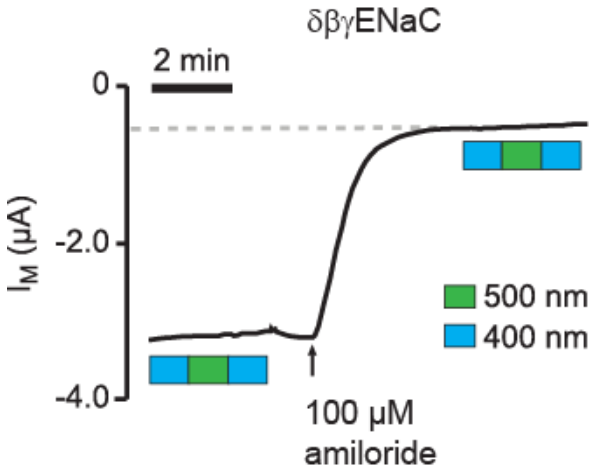

Figure S5. Control experiment. δβγENaC expressing Xenopus oocytes do not show innate sensitivity to light in both unblocked and blocked state. (n = 3, αβγENaC analogous).

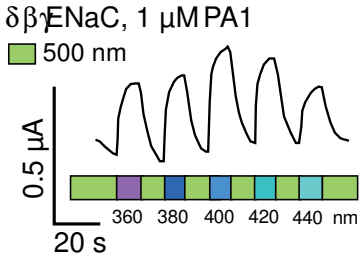

Figure S6. Action spectrum of **PA1** on a δβγENaC expressing oocyte. Wavelengths were switched between 500 nm and 360, 380, 400, 420 and 440 nm. 400 nm illumination translates to the most pronounced photo-current.

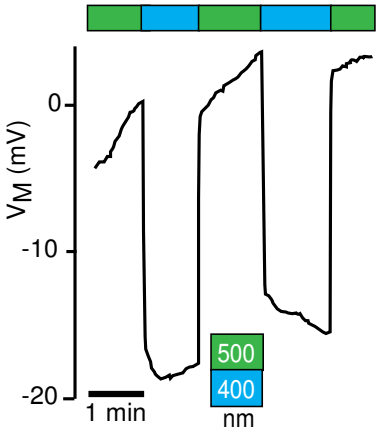

Figure S7. Switching voltage using **PA1** on δβγENaC expressing oocytes. As expected from photocurrents, switching to 400 nm (blocking ENaCs) polarizes the oocytes, which can be reversed by switching to 500 nm. (representative trace).

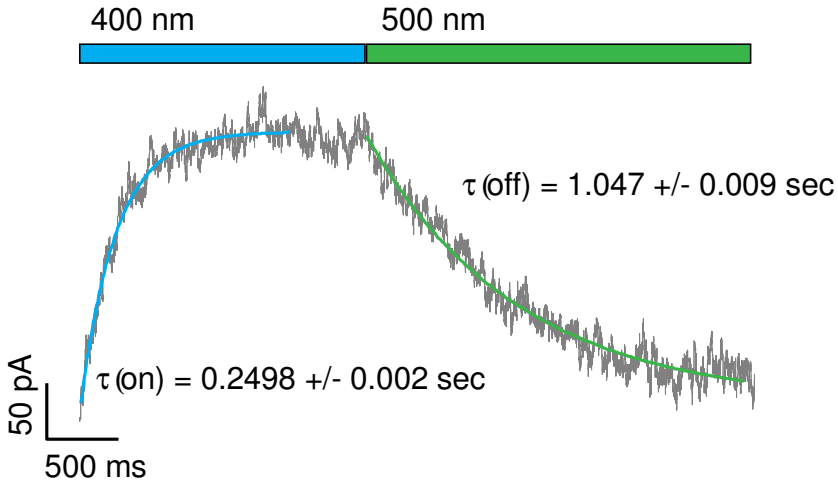

Figure S8. Photoswitching of 10 µM **PA1** on δβγENaC expressing HEK cells occurs on the timescale of seconds. Exponential curve fitting demonstrates that channel block mediated by 400 nm illumination is considerably faster than unblock by 500 nm (τ = 250 ms vs 1 sec).

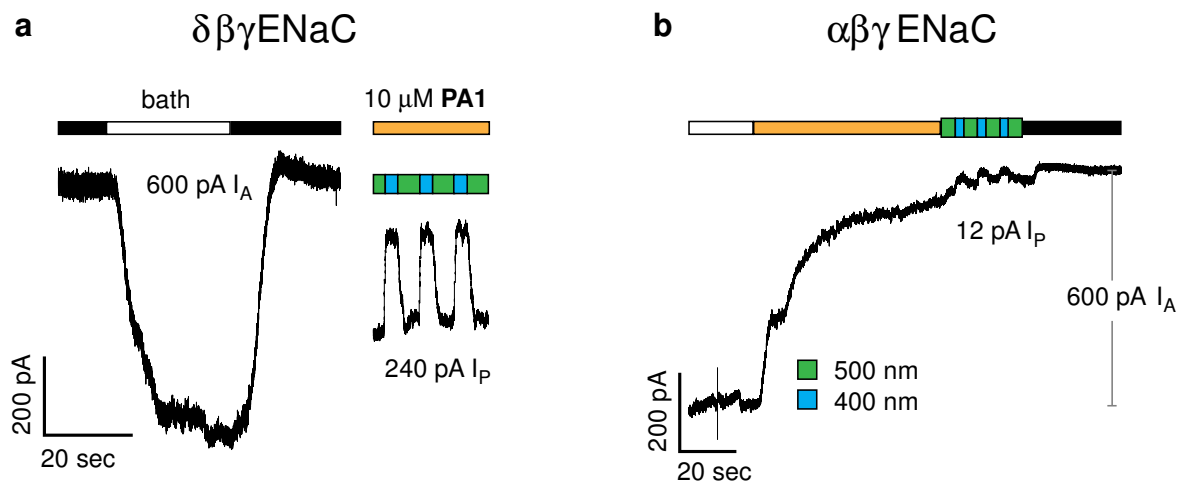

Figure S9. Comparison of Amiloride sensitive current I_A and photocurrent.I_P on αβγENaC (a) and δβγENaC (b) expressing HEK cells (black bar indicates perfusion with 10 µM amiloride). Both representative traces have 600 pA I_A. IP on δβγENaC is 240 pA (compare: average I_P = 180 pA, Fig. 4a). I_P on αβγENaC is 12 pA (compare: average I_P = 9 pA, Fig 4a). This bias of **PA1**-mediated photoswitching on δβγENaC is in line with data from *Xenopus* oocytes (e.g. Fig S3). Selectivity is probably higher in HEK cells because the entire cell can be illuminated.

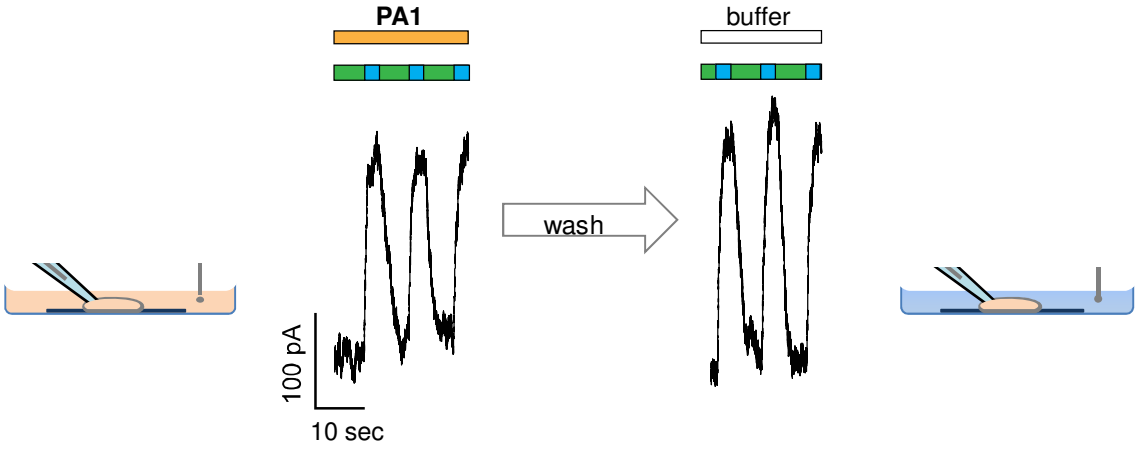

Figure S10. Photoswitching occurs in presence of extracellular **PA1** (orange color of bath solution) and remains after wash out (blue color). This indicates uptake in the cell as indicated by the orange cytoplasm.

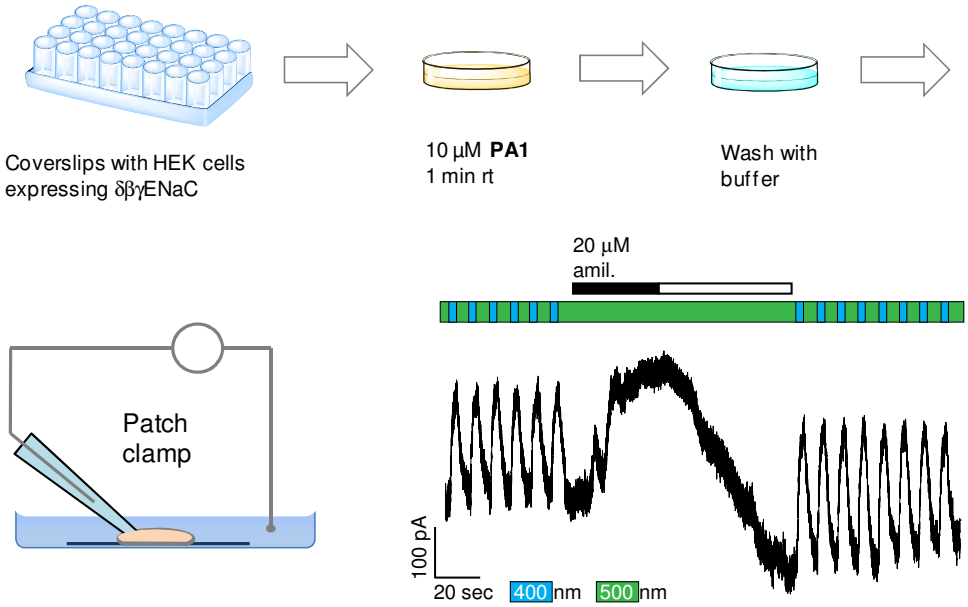

Figure S11. **PA1** cell uptake by short incubation. 24h after transfection, coverslips with HEK cells expressing δβγENaC were transferred to a petry dish containing a 10 µM **PA1** solution (orange color) in extracellular recording buffer. After incubation for 1 min at room temperature, the coverslip was washed with extracellular recording buffer (blue color) and investigated using the patch clamp technique. Photocurrents could be evoked without further treatment. Cells could be fully blocked and unblocked with amiloride.

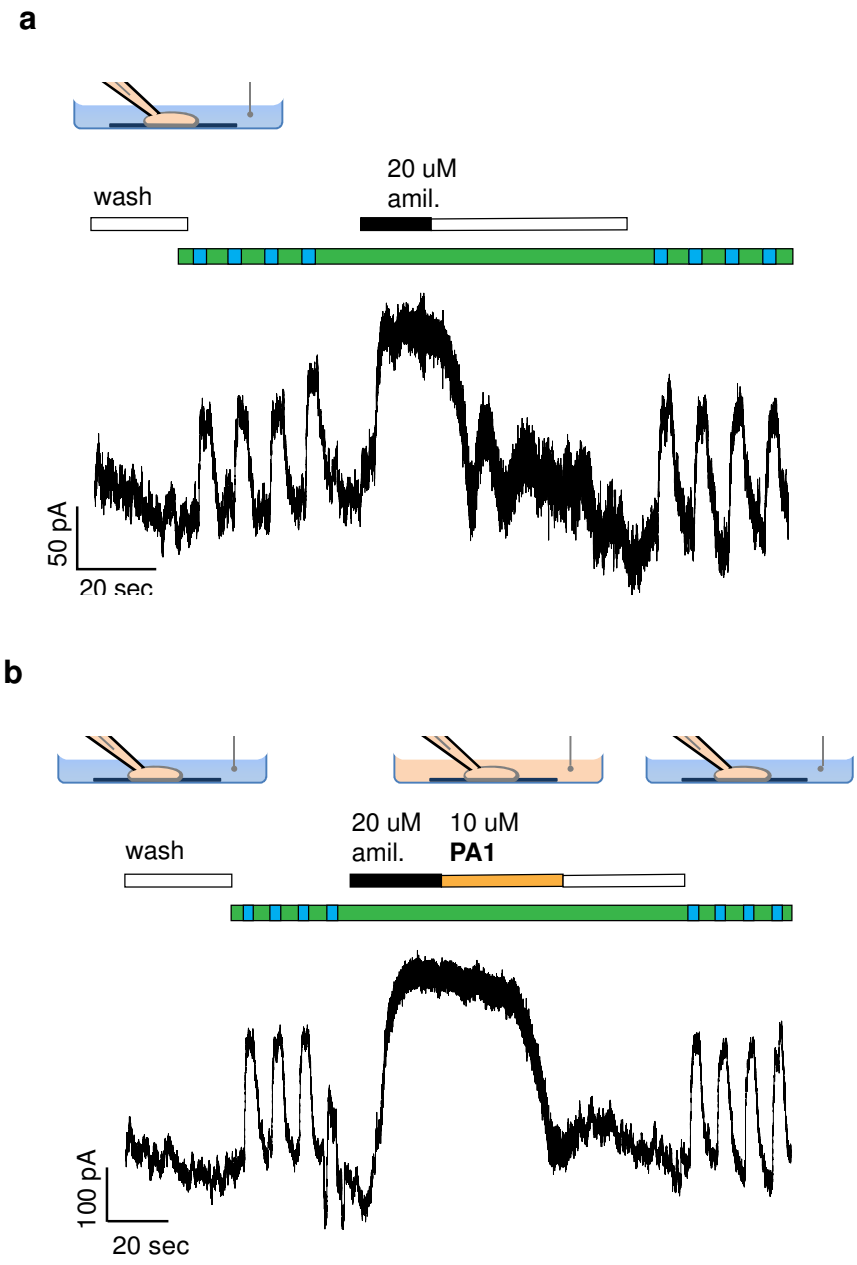

Figure S12. Loading **PA1** through the patch pipette. Pipettes were loaded with 10 µM PA1 and HEK cells expressing δβγENaC where investigated in whole cell mode. Photocurrents could be triggered immediately. **a**, photoswitching takes place before and after amiloride block with identical amplitudes analogously to Fig. S8. **b**, external amiloride can be displaced by **PA1**. After consecutive wash out of **PA1**, photocurrents have the same magnitude. It can thus be assumed that externally applied **PA1** is taken up by cells and acts from the intracellular site.

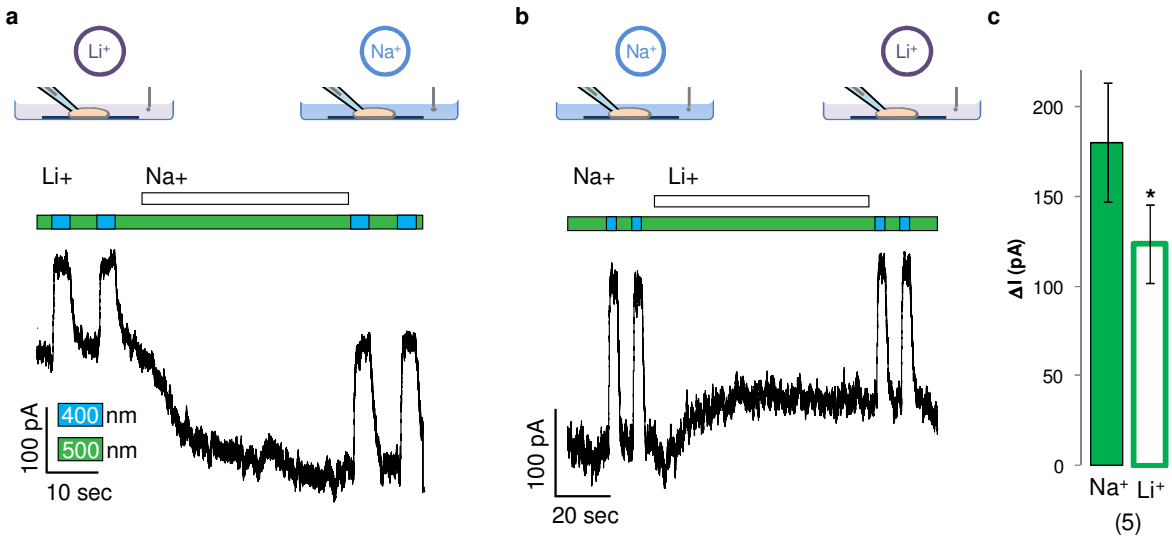

Figure S13. Effect of external lithium on overall and photocurrents (δβγENaC, HEK cells, biological repeats). HEK cells loaded with **PA1** as described in Fig. S8 were switched with lithium or sodium containing external solution. **a**, in line with reported data on δβγENaC lithium conductivity, washing out external lithium increases the overall current. **b**, washing in lithium has the opposite effect and decreases both overall and photocurrents. **c**, the average photocurrent amplitude is significantly reduced when external sodium is exchanged for lithium (* $p < 0.05$).

Experimental procedures for chemical syntheses

4-Nitro-azobenzene s2 and **s3**

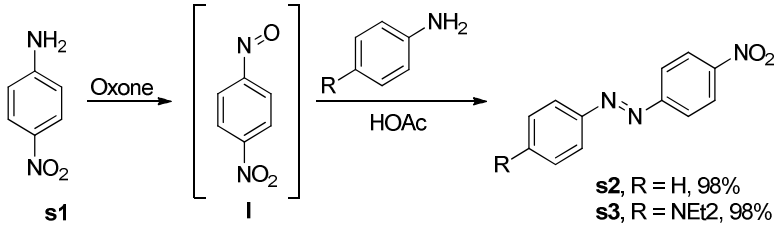

Oxone oxidation. To a solution of 4-nitroaniline **s1** (5.94 g, 43.0 mmol, 1 eq) in 150 mL CH_2Cl_2 was added an aqueous solution of oxone (26.4 g, 43.0 mmol, 1 eq, 150 mL). The biphasic mixture was stirred vigorously under N_2 atmosphere. After 3 hours, phases were separated and the aqueous phase was extracted 2x with CH_2Cl_2 (30 mL aliquots). Pooled organic phases were washed with 1x 1 M HCl, 1x sat. NaCl (75 mL aliquots), dried over Na_2SO_4 and concentrated to 30 mL under reduced pressure. The resulting yellow-black solution of nitrosobenzene **I** in CH_2Cl_2 was carried on to the next step immediately.

Mills condensation. To the freshly prepared nitrosobenzene solution in DCM described above was added sequentially the respective aniline (21.5 mmol, 1 eq) and glacial AcOH (6.15 mL, 107.5 µL, 5 eq). The reaction mixture was allowed to stir for 15 hours under N_2 atmosphere, after which time the reaction mixture was found to be an orange-black suspension. EtOAc (150 mL) was added and the organic phase was washed with 3x 1-M-NaOH, 2x sat. $NaHCO_3$, 2x sat. NaCl (50 mL aliquots). The organic phase was then dried over Na_2SO_4 and concentrated under reduced pressure. Crude material was purified by flash column chromatography (silica gel, dry loading on bulk sorbent, gradient: 1% → 5% →10% EtOAc in Hexanes), affording compounds **s2** and **s3** (21.0 mmol, 98%), as orange solids.

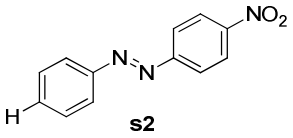

^{1}H NMR (400 MHz, $CDCl_3$): δ 8.46 – 8.28 (m, 2H), 8.06 – 7.99 (m, 2H), 7.99 – 7.91 (m, 2H), 7.58 – 7.49 (m, 3H). Lim, Y.-K., Lee, K.-S. & Cho, C.-G. Novel Route to Azobenzenes via Pd-Catalyzed Coupling Reactions of Aryl Hydrazides with Aryl Halides, Followed by Direct Oxidations. *Organic Letters* **5**, 979-982 (2003).

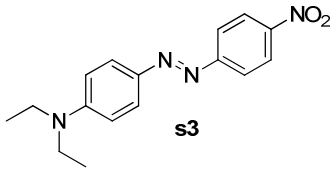

s3

^{1}H NMR (200 MHz, $CDCl_3$): δ 8.35 – 8.23 (m, 2H), 7.97 – 7.82 (m, *J*=4.8, 2.6, 4H), 6.72 (d, *J*=9.3, 2H), 3.47 (q, *J*=7.1, 4H), 1.24 (t, *J*=7.1, 6H). Sigman, M.E. & Leffler, J.E. Supercritical carbon dioxide. The cis to trans relaxation and .pi.,.pi.* transition of 4-(diethylamino)-4'-nitroazobenzene. *The Journal of Organic Chemistry* **52**, 3123-3126 (1987).

4-Amino-azobenzene 02 and **03**

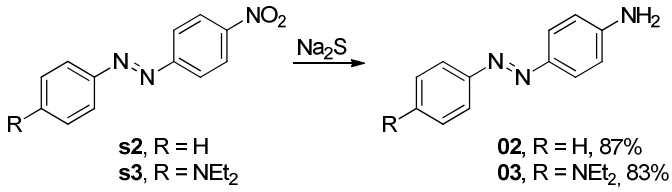

s2, R = H
s3, R = NEt_2

02, R = H, 87%
03, R = NEt_2, 83%

To a solution of nitrobenzene **s2** or **s3** (9.16 mmol, 1 eq) in 3:1 THF:H_2O (120 mL) was added Na_2S (2.14 g, 27.5 mmol, 3 eq). The red-black reaction suspension was allowed to stir for 3h hours at reflux temperature. THF was removed under reduced pressure, and the remaining aqueous material was partitioned between EtOAc (150 mL) and 1-M-NaOH (50 mL). The organic phase was further washed with 1-M-NaOH, sat. $NaHCO_3$ and brine (50 mL aliquots). An orange precipitate was removed through vacuum filtration before the filtrate was dried over Na_2SO_4 and concentrated *in vacuo*, affording anililnes **02** and **03**, respectively, as dark orange solids (**02**, 87%. **03**, 83%).

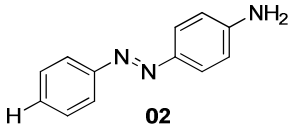

02

^{1}H NMR (300 MHz, $CDCl_3$): δ 7.89 – 7.75 (m, 5H), 7.54 – 7.33 (m, 2H), 6.82 – 6.69 (m, 2H), 4.04 (s, 2H). Bahulayan, D., John, L. & Lalithambika, M. Modified Clays as Efficient Acid-Base Catalyst Systems for Diazotization and Diazocoupling Reactions. in *Synthetic Communications* Vol. 33 863 (Taylor & Francis Ltd, 2003).

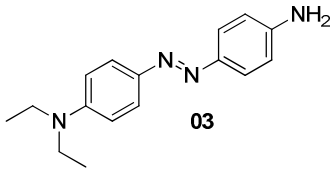

03

^{1}H NMR (599 MHz, $CDCl_3$): δ 7.81 – 7.75 (m, 2H), 7.74 – 7.69 (m, 2H), 6.75 – 6.67 (m, 4H), 3.88 (s, 2H), 3.42 (q, *J*=7.1, 4H), 1.20 (t, *J*=7.1, 6H). Mourot, A. et al. Tuning photochromic ion channel blockers. *ACS Chem Neurosci* **2**, 536-43.

Arylguanidines **s4** and **s5**

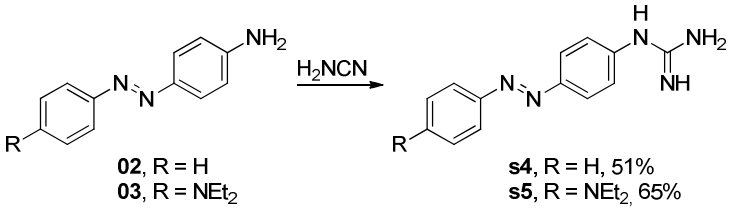

02, R = H
03, R = NEt_2

s4, R = H, 51%
s5, R = NEt_2, 65%

Aniline 02 or **03** (2.02 mmol, 1.0 eq) was suspended in ethanol (1.3 mL), and a 75 % ethanolic cyanamide solution (227 µL, 4.06 mmol, 2.0 eq) was added, followed by HCl (4 M in dioxane, 507 µL, 2.02 mmol, 1.0 eq). After refluxing for 24 h, the reaction mixture was diluted with EtOAc (450 mL), washed with 5-M-NaOH (3 x 20 mL), $NaHCO_3$ (20 mL) and brine (20 mL), dried over Na_2SO_4 and concentrated using rotary evaporation. The crude product was purified by column chromatography (SiO_2, gradient: 10 % NH_3/MeOH (1:3) →20 % NH_3/MeOH (1:3)/EtOAc) yielding guanidines **s4** and **s5**, respectively, as orange amorphous solids.

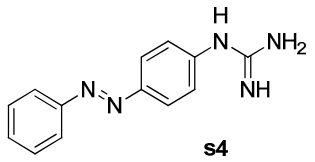

s4

TLC (SiO_2, EtOAc:MeOH:$NH_{3(aq)}$, 80:15:5 v/v/v): R_f = 0.27 (UV); ^{1}H NMR (400 MHz, CD_2Cl_2): δ 7.91 – 7.84 (m, 4H), 7.52 (t, *J*=7.3, 2H), 7.48 – 7.42 (m, 1H), 7.04 (d, *J*=8.7, 2H), 3.58 (s, 4H); ^{13}C NMR (100 MHz, CD_2Cl_2): δ 153.37, 153.31, 151.92, 148.56, 130.90, 129.59, 124.92, 124.11, 123.01; IR (Diamond-ATR, neat): 3324, 3028, 2760, 1665, 1622, 1562, 1491, 1456, 1429, 1406, 1307, 1123, 982, 862 cm^{-1}; HRMS (m/z): $[M+H]^+$ calcd. for $C_{13}H_{14}N_5$, 240.1244; found, 240.1242.

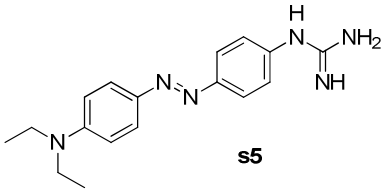

s5

TLC (SiO_2, EtOAc:MeOH:$NH_{3(aq)}$, 80:15:5 v/v/v): R_f = 0.16 (UV); ^{1}H NMR (400 MHz, CD_2Cl_2): δ 7.83 – 7.73 (m, 4H), 7.04 – 6.97 (m, 2H), 6.78 – 6.69 (m, 2H), 3.46 (q, *J*=7.1, 4H), 1.23 (t, *J*=7.1, 6H); ^{13}C NMR (101 MHz, CD_2Cl_2): δ 151.41, 149.99, 149.81, 148.70, 142.92, 124.70, 123.43, 123.33, 110.90, 44.61, 12.37; IR (Diamond-ATR, neat): 3400 – 2700 (m, br), 3323, 3050, 2972, 1658, 1569, 1551, 1512, 1446, 1392, 1352, 1266, 1194, 1137, 1074, 1009 cm^{-1}; HRMS (m/z): $[M+H]^+$ calcd. for $C_{17}H_{23}N_6$, 311.1979; found, 311.1976;

Pyrazinic acid 4b

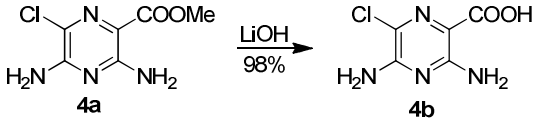

4a **4b**

The title compound was prepared as described in patent literature.[1] Analytical data matched those reported.

^{13}C NMR (101 MHz, DMSO-d_6) δ 167.69, 156.32, 153.61, 119.07, 110.50. IR (Diamond-ATR, neat): 3476, 3422, 3356, 3296, 3194, 2867, 2548, 1665, 1609, 1514, 1442, 1308, 1250, 1144, 790 cm^{-1}; HRMS (m/z): $[M-H]^-$ calcd. for $C_5H_5ClN_4O_2$, 187.0023; found, 187.0028.

N-Boc-phenethylamine 05

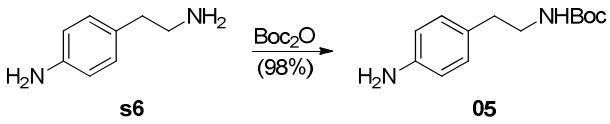

s6 **05**

Aminophenethylamine **s6** (1.0 g, 7.3 mmol, 1 eq) was dissolved in 50 mL THF and a solution of Boc_2O (1.7 g, 7.7 mmol, 1.05 eq) in THF (30 mL) was added dropwise. After stirring for 2 h at room temperature, the mixture was diluted with EtOAc (400 mL), washed with 1-M-HCl (100 mL), 1-M-NaOH (150 mL), sat. $NaHCO_3$ (150 mL) and brine (150 mL) and dried over Na_2SO_4. The solvent was removed by rotary evaporation and

[1] WO2008106692 (A1) — 2008-09-04 „PIM KINASE INHIBITORS AND METHODS OF THEIR USE".

the crude was purified using silica gel chromatography (gradient: 0 to 30 % EtOAc in hexanes) yielding the title **05** compound as a pale white solid (1.7 g, 7.2 mmol. 98%)

TLC (SiO_2, EtOAc:hexanes, 1:1 v/v): R_f = 0.48 (UV + ninhydrin stain); ^{1}H NMR (300 MHz, $CDCl_3$) δ 7.00 (d, *J*=8.3, 2H), 6.69 – 6.62 (m, 2H), 4.53 (s, 1H), 3.62 (s, 2H), 3.33 (d, *J*=6.4, 2H), 2.70 (t, *J*=7.0, 2H), 1.45 (s, 9H). Hah, J.-M., Martasek, P., Roman, L.J. & Silverman, R.B. Aromatic Reduced Amide Bond Peptidomimetics as Selective Inhibitors of Neuronal Nitric Oxide Synthase. *Journal of Medicinal Chemistry* **46**, 1661-1669 (2003).

Primary amine 06

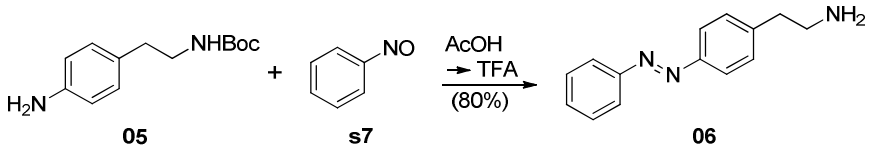

05 **s7** **06**

Aniline **05** (5.13 g, 21.7 mmol, 1.0 eq) was dissolved in DCM (30 mL) and nitrosobenzene **s7** (2.56 g, 23.9 mmol, 1.1 eq) was added followed by AcOH (12.4 mL, 217 mmol, 10 eq). After stirring over night at room temperature, the reaction mixture was diluted with EtOAc (300 mL) and the organic phase was washed with 1-M-HCl (50 mL), 1-M-NaOH (50 mL), sat. $NaHCO_3$ (50 mL) and brine (1 x 50 mL). After drying over Na_2SO_4, solvent was removed *in vacuo*. The resulting orange oil was redissolved in 10 mL DCM and TFA (16 mL, 217 mmol; 10 eq) was added for Boc-deprotection. After stirring for 1 h, the mixture was basified with 5-M-NaOH (60 mL) and extracted with EtOAc (4 x 150 mL). Pooled organic phases were washed with sat. $NaHCO_3$ (50 mL) and brine (50 mL). The EtOAc layer was filtered and concentrated *in vacuo*, followed by purification using flash column chromatography (SiO_2; 10 % MeOH, 90% DCM + 1 % TEA), yielding primary amine **06** (3.93 g; 17.5 mmol, 80 %) as orange solid (3.93 g; 17.5 mmol, 80 %).

TLC (SiO_2, DCM:MeOH, 1:1 v/v, + 1 % TEA): R_f = 0.26 (UV); ^{1}H NMR (400 MHz, CD_3OD) δ 7.92 – 7.85 (m, 4H), 7.56 – 7.48 (m, 3H), 7.48 – 7.43 (m, 2H), 3.26 – 3.19 (m, 2H), 3.07 – 3.01 (m, 2H); ^{13}C NMR (101 MHz, DMSO-d_6) δ 151.72, 150.77, 140.01, 130.03, 128.45, 128.01, 122.01, 121.50, 39.98, 33.56; IR (Diamond-ATR, neat): 2936, 1668, 1554, 1203, 1171, 1130, 1075, 1021, 1013, 943, 839 cm^{-1}; HRMS (m/z): $[M+H]^+$ calcd. for $C_{14}H_{16}N_3$, 226.1339; found, 226.1339.

Primary amine 07

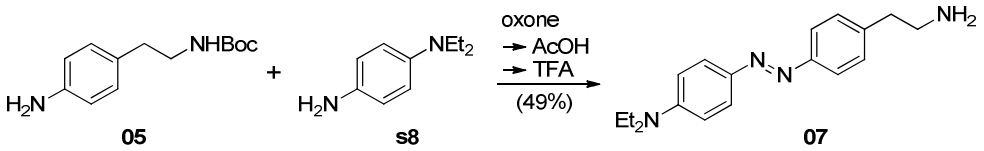

05 s8 07

Aniline **05** (1.1 g, 4.7 mmol, 1 eq) was dissolved in 100 mL DCM and water (50 mL) was added followed by an aqueous solution of oxone (3.2 g, 5.1 mmol, 1.1 eq, in 50 mL). The heterogeneous mixture was stirred vigorously for 3h before phases were separated. The DCM layer was dried over Na_2SO_4 and concentrated to ~30 mL. Aniline **s8** (0.77 mL, 4.7 mmol, 1 eq) was added to the nitrosobenzene solution followed by AcOH (1.3 mL, 23.3 mmol, 5 eq). After 1h, TLC analysis (SiO_2, 1:1 EtOAc/hexanes) showed complete azobenzene formation. TFA (4 mL, 53.5 mmol, 12 eq) was added and the purple mixture was stirred over night. 100 mL EtOAc were added and the organic phase was washed with 30 mL aliquots of 2x 5-M-NaOH, 1-M-NaOH and brine. After drying over Na_2SO_4 and concentrating under reduced pressure, the crude material was purified using silica gel chromatography (10% MeOH, 90% DCM, + 1% TEA) yielding the product **07** as an orange amorphous solid (668 mg, 2.3 mmol, 49%).

TLC (SiO_2, DCM:MeOH, 1:1 v/v, + 1 % TEA): R_f = 0.55 (UV + ninhydrin stain); ^{1}H NMR (300 MHz, $CDCl_3$) δ 7.87 – 7.80 (m, 2H), 7.76 (d, *J*=8.4, 2H), 7.30 (d, *J*=8.4, 2H), 6.69 (t, *J*=6.3, 2H), 5.30 (s, 2H), 3.44 (q, *J*=7.1, 4H), 3.11 (t, *J*=7.2, 2H), 2.94 (t, *J*=7.2, 2H), 1.22 (t, *J*=7.1, 6H); ^{13}C NMR (75 MHz, $CDCl_3$) δ 152.18, 150.05, 143.11, 139.19, 129.38, 125.24, 122.42, 110.96, 44.67, 42.07, 36.55, 12.66; IR (Diamond-ATR, neat): 3363, 3202, 2964, 2923, 2850, 1660, 1633, 1601, 1516, 1399, 1140, 820, 801 cm^{-1}; HRMS (EI): [M] calcd. for $C_{18}H_{24}N_4$, 296.2001; found, 296.1997.

Photo-Amiloride-1 and **2**

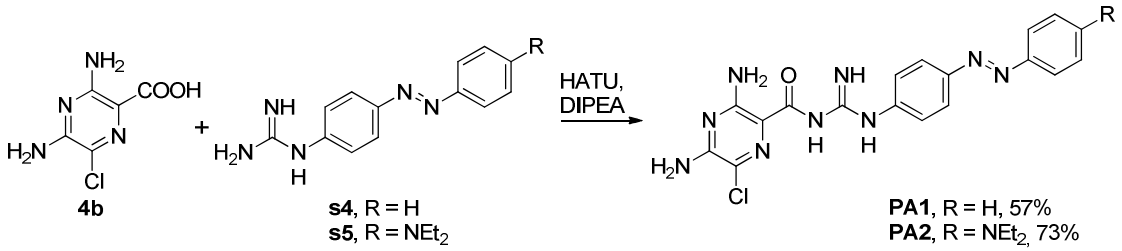

Pyrazinic acid **4b** (18.2 mg, 0.097 mmol, 1.0 eq) was dissolved in anhydrous DMF and treated with DIPEA (50 µL, 0.29 mmol, 3.0 eq) followed by HATU (36.7 mg, 0.097 mmol, 1.0 eq). After stirring at rt for 10 min, respective guanidine (**s4** or **s5**) (30.0 mg, 0.097 mmol, 1.0 eq) was added as a solid. The reaction mixture was allowed to stir at rt for 24 h under N2-atm and was then diluted with 30 mL EtOAc. For removal of DMF, the solution was extracted 3x with 10% $NaCl_{(aq)}$. The organic layer was separated, dried with NaSO4 and concentrated under reduced pressure. The crude material was purified using flash chromatography (Al_2O_3, gradient 0 to 5% MeOH in $CHCl_3$) affording the title compound as an orange oil (34 mg, 0.071 mmol, 73% yield). **PA1** was transformed to the formic acid (FA) salt using lyophilization of **PA1** dissolved in an aqueous FA solution.

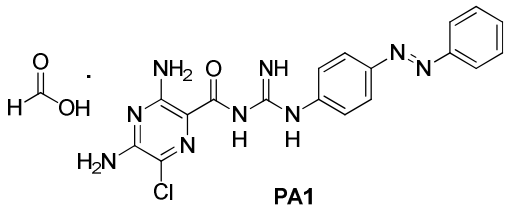

TLC (Al_2O_3, DCM:MeOH, 9:1 v/v): R_f = 0.60 (UV); ^{1}H NMR (599 MHz, DMSO-d_6) δ 8.14 (s, 1H), 7.87 – 7.79 (m, 4H), 7.58 – 7.52 (m, 2H), 7.52 – 7.47 (m, 1H), 7.43 (s, 2H), 7.24 (s, 2H); ^{13}C NMR (101 MHz, DMSO-d_6) δ 169.19, 163.71, 155.73, 153.66, 152.56, 151.21, 148.19, 147.64, 131.20, 129.79, 124.36, 122.83, 122.67, 118.95, 113.15; IR (Diamond-ATR, neat): 3429, 3325, 3159, 1719, 1683, 1580, 1504, 1417, 1350, 1241, 1096, 763, 678 cm^{-1}; HRMS (m/z): $[M+H]^+$ calcd. for $C_{18}H_{16}ClN_9O$, 410.1245; found, 410.1238.

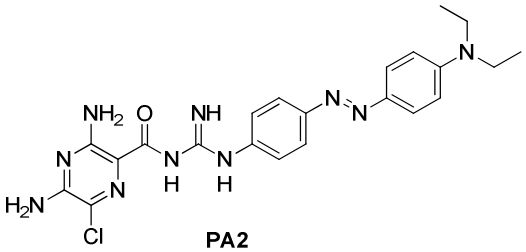

PA2

TLC (Al_2O_3, DCM:MeOH, 9:1 v/v): R_f = 0.64 (UV); ^{1}H NMR (599 MHz, $CDCl_3$) δ 7.86 – 7.79 (m, 4H), 7.08 (d, *J*=8.5, 2H), 6.71 (d, *J*=9.3, 2H), 5.38 (s, 2H), 3.43 (q, *J*=7.1, 4H), 1.21 (t, *J*=7.1, 6H); ^{13}C NMR (151 MHz, $CDCl_3$) δ 154.61, 152.83, 149.77, 149.42, 148.26, 143.19, 124.97, 123.66, 123.22, 119.74, 113.27, 110.98, 44.65, 12.66, (guanidine and carbonyl signal not detected); IR (Diamond-ATR, neat): 3467, 3324, 3182, 2966, 2923, 1639, 1591, 1512, 1393, 1375, 1251, 1138, 1072, 821 cm^{-1}; HRMS (m/z): $[M+H]^+$ calcd. for $C_{22}H_{25}ClN_{10}O$, 481.1980; found, 481.1967.

Photo-amiloride-3 and 4

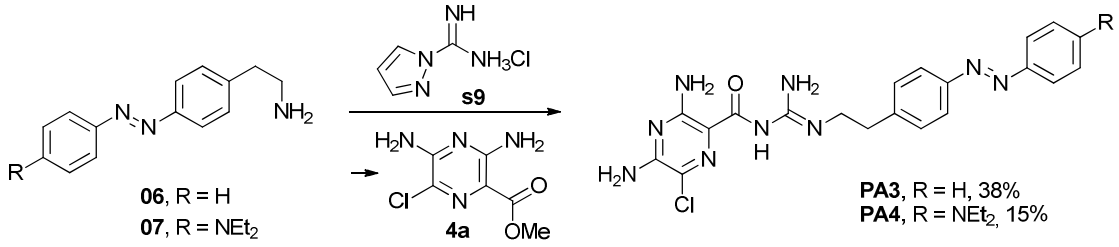

Guanidine formation (500 mg to 2 g scale).[37] Primary amine **06** or **07** (4.44 mmol, 1.0 eq) was suspended in DMF (5 mL), followed by addition of 1-*H*-pyrazole-carboxamidine chloride **s9** (775 mg; 5.02 mmol; 1.1 eq) as well as DIPEA (1.7 mL; 10.2 mmol; 2.3 eq) and the mixture was stirred over night at room temperature. LCMS analysis showed quantitative conversion to a less polar species with expected UV/VIS spectrum and mass (Agilent 1260 Infinity, C-18, gradient: 20% to 80% MeCN in H_2O + 0.1% formic acid buffer). The crude product was precipitated from the clear, red solution by addition of diethyl ether, yielding red oil. Oil and supernatant were separated by decantation and the product was dried under high vacuum to yielding the corresponding guanidine hydrochloride as an orange solid.

Acylguanidine formation (20 to 300 mg scale). Freshly prepared guanidine hydrochloride described above (1.40 mmol, 2.0 eq) was converted to the free base by basic aqueous work up using EtOAc and 5-M-NaOH. After drying under high vacuum,

the guanidine was suspended in ethanol (5 mL) followed by addition of pyrazinic ester **4a** (142 mg, 7.01 mmol, 1.0 eq) and the mixture was heated to 100 °C for 48 h. The solution was diluted with EtOAc (400 mL), washed with sat. $NaHCO_3$ (3 x 20 mL) and brine (1 x 20 mL), dried over Na_2SO_4 and concentrated by rotary evaporation. The crude material was purified using column chromatography, loaded from bulk sorbens (SiO_2, gradient: 5 % $NH_{3(aq)}$/MeOH (1:3) → 20 % $NH_{3(aq)}$/MeOH (1:3)/EtOAc). The solvent was removed *in vacuo* and water was added before the product was lyophilized yielding **PA3** and **PA4**, respectively, as amorphous orange-red solids (38 % and 15%).

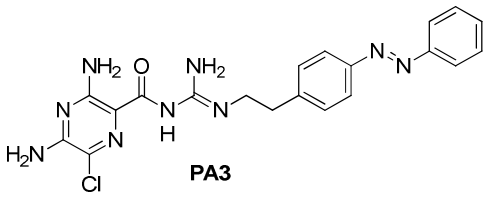

PA3

TLC (SiO_2, EtOAc:MeOH:$NH_{3(aq)}$, 80:15:5 v/v/v): R_f = 0.69 (UV); ^{1}H NMR (400 MHz, DMSO-d_6) δ 10.58 (s, 1H), 9.44 (t, *J*=6.0, 1H), 9.01 (s, 2H), 7.91 – 7.85 (m, 4H), 7.63 – 7.54 (m, 5H), 7.42 (s, 2H), 3.67 (q, *J*=13.6, 6.7, 2H), 3.01 (t, *J*=7.3, 2H); ^{13}C NMR (101 MHz, DMSO-d_6) δ 165.77, 156.35, 154.68, 153.76, 152.35, 151.17, 142.44, 131.86, 130.42, 129.89, 123.10, 122.90, 120.12, 109.46, 42.37, 34.08; IR (Diamond-ATR, neat): 3286, 3176, 2362, 2339, 1577, 1420, 1375, 1242, 1155, 1069, 904, 808 cm^{-1}; HRMS (m/z): $[M+H]^+$ calcd. for $C_{20}H_{21}ON_9Cl$, 438.1552; found, 438.1549.

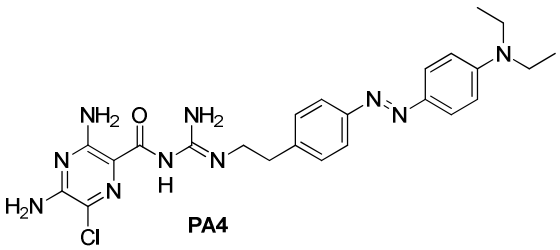

PA4

TLC (SiO_2, EtOAc:MeOH:$NH_{3(aq)}$, 80:15:5 v/v/v): R_f = 0.60 (UV); ^{1}H NMR (599 MHz, DMSO-d_6) δ 8.26 (s, 1H), 7.72 (d, *J*=9.2, 2H), 7.69 (d, *J*=8.3, 2H), 7.41 (d, *J*=8.3, 2H), 6.95 (s, 1H), 6.76 (d, *J*=9.3, 2H), 3.46 (s, 2H), 3.42 (q, *J*=7.0, 4H), 2.89 (s, 2H), 1.12 (t, *J*=7.0, 6H); ^{13}C NMR (101 MHz, DMSO-d_6) δ 171.09, 164.83, 158.79, 155.56, 152.68, 151.62, 150.41, 142.51, 140.61, 130.04, 125.44, 122.22, 118.73, 111.40, 44.47, 42.33, 34.54, 12.93; IR (Diamond-ATR, neat): 3420, 3309, 3175, 2966, 1678, 1597, 1514, 1425, 1397, 1353, 1245, 1195, 1138, 1076, 1012, 821, 787, 734 cm^{-1}; HRMS (m/z): $[M+H]^+$ calcd. for $C_{24}H_{29}ClN_{10}O$, 509.2293; found, 509.2283.

Analytical Spectra

^{1}H-NMR, 4-Nitro-azobenzene **s2**

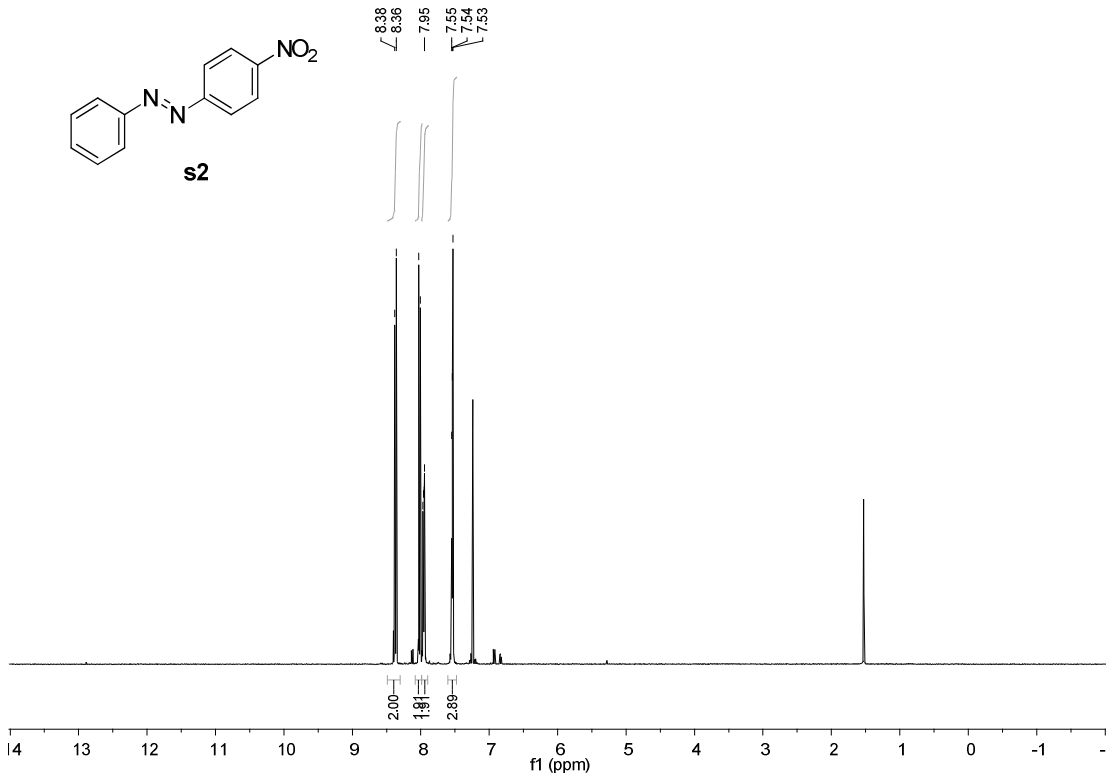

^{1}H-NMR, 4-Nitro-azobenzene **s3**

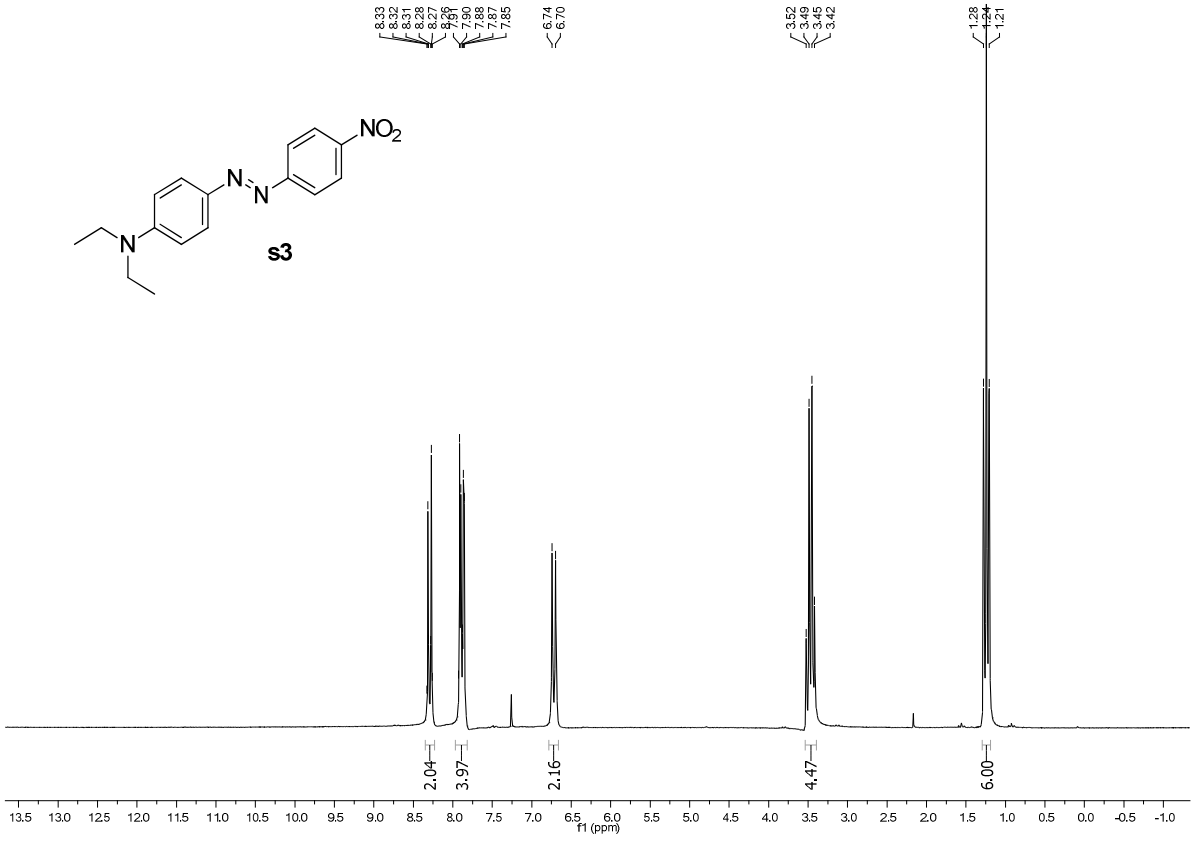

^{1}H-NMR, 4-Amino-azobenzene **02**

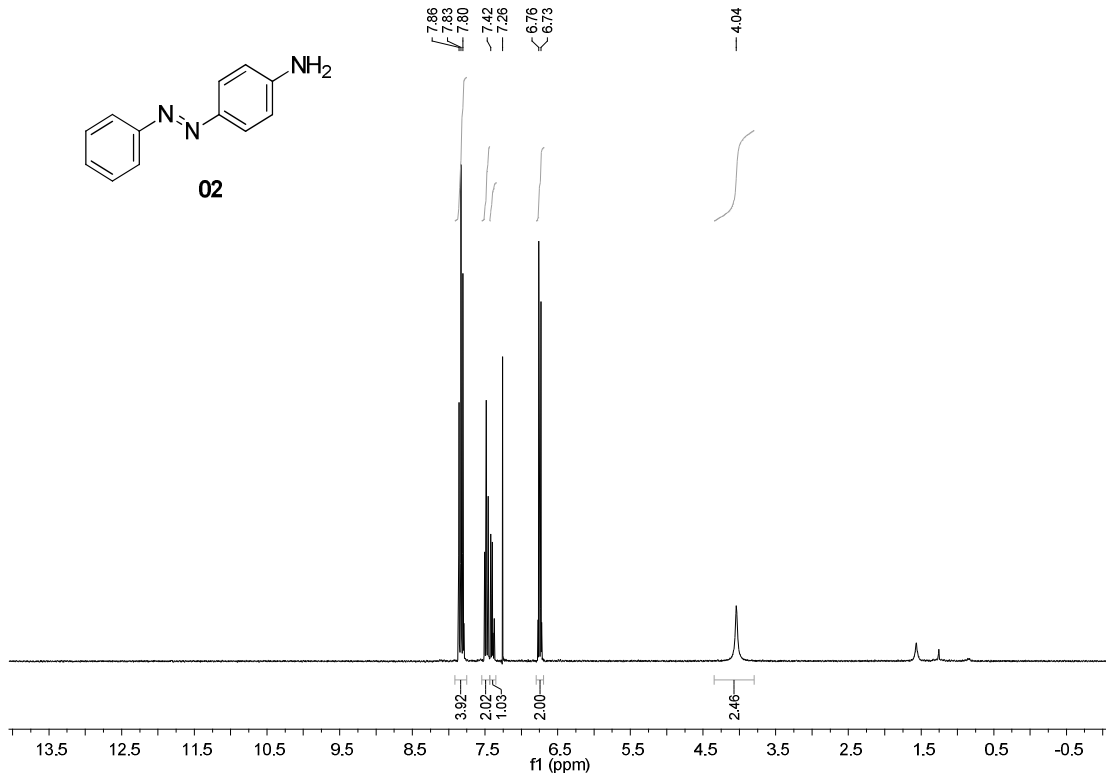

^{1}H-NMR, Aniline **03**

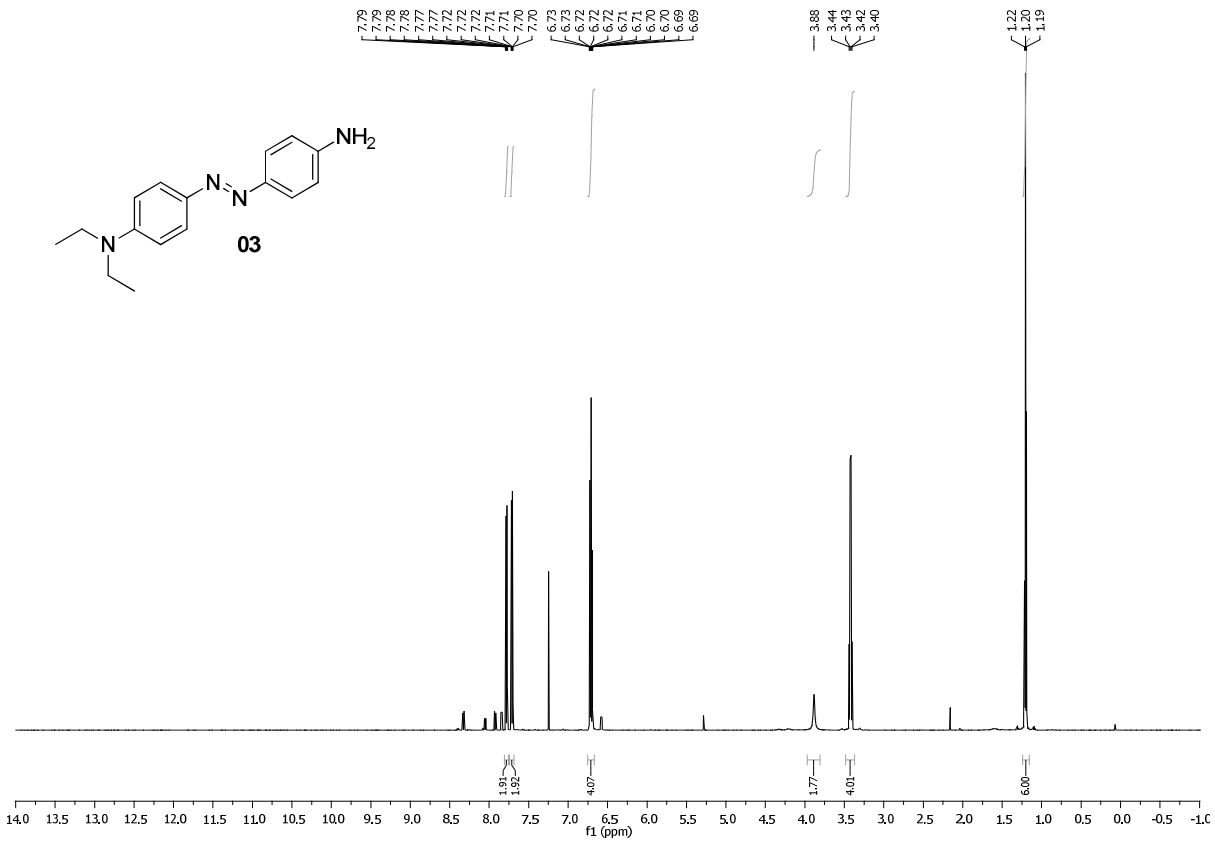

^{1}H-NMR, Arylguanidine **s4**

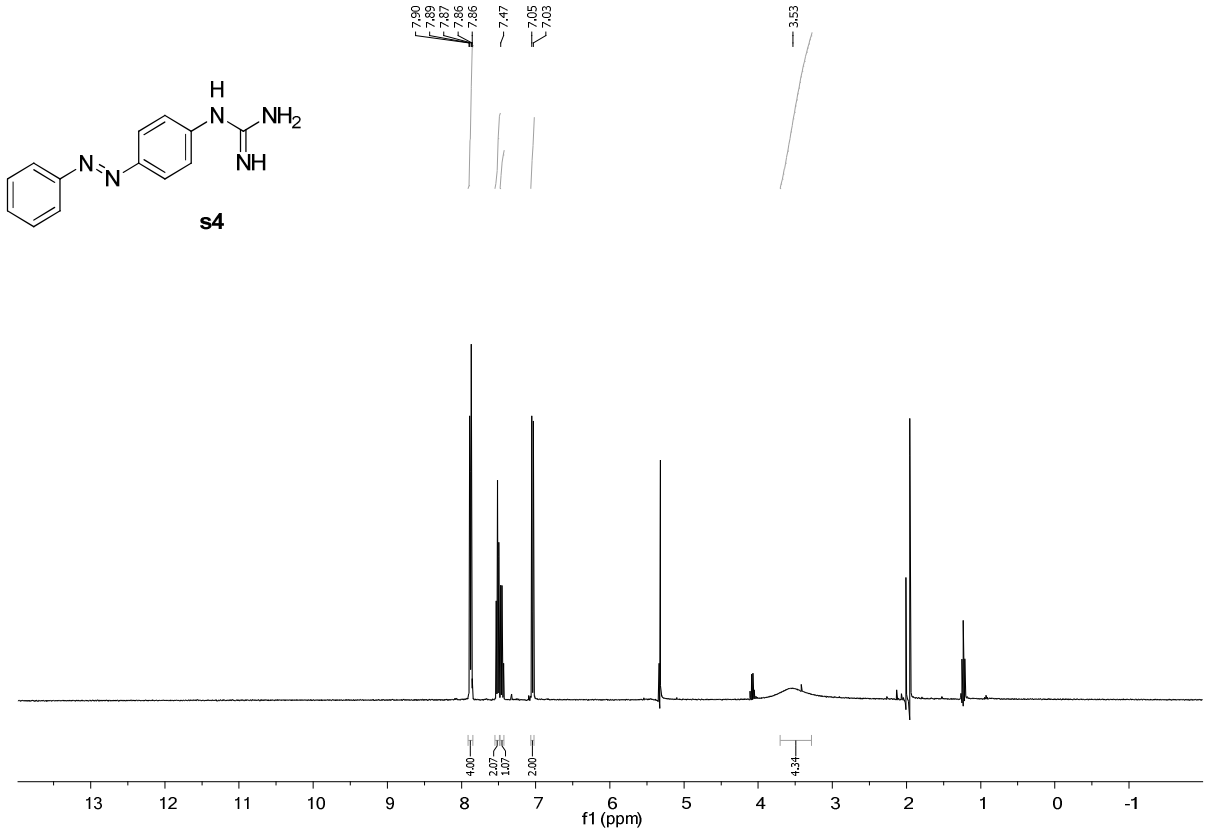

^{13}C-NMR, Arylguanidine **s4**

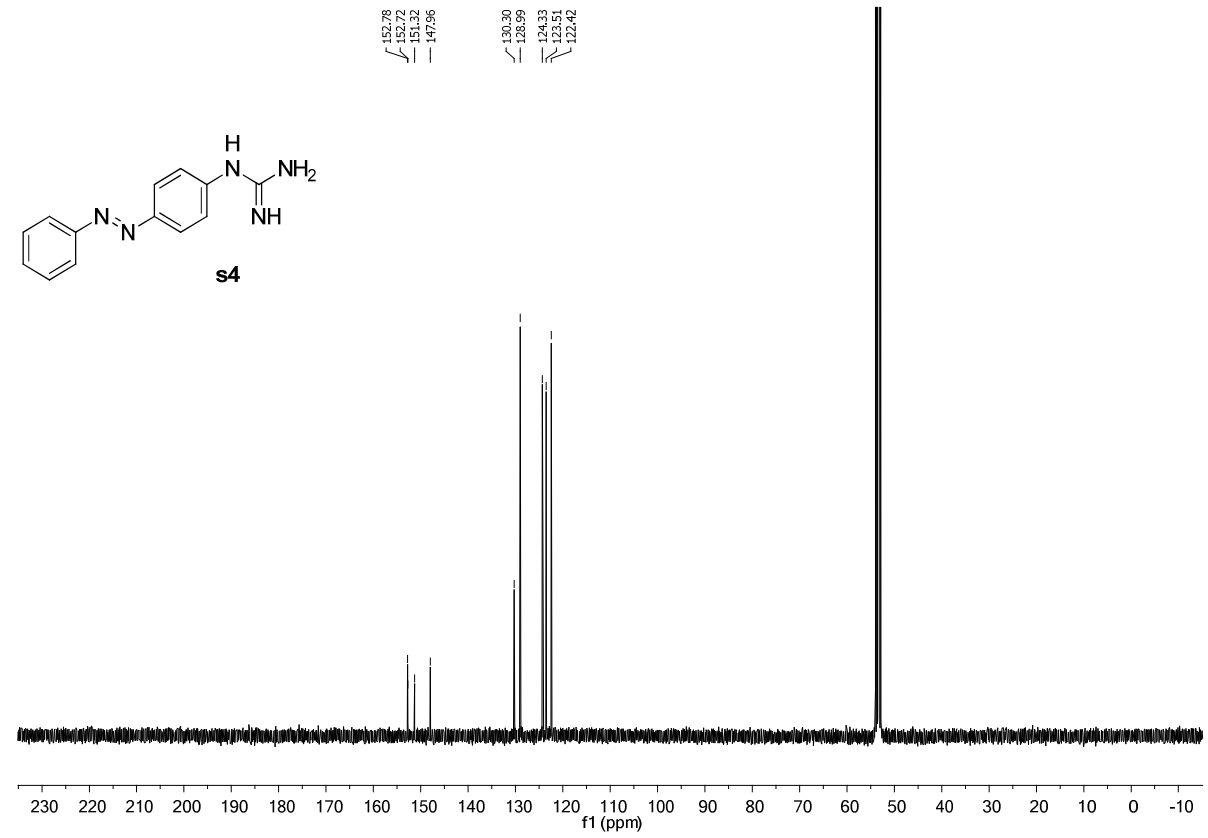

^{1}H-NMR, Arylguanidine **s5**

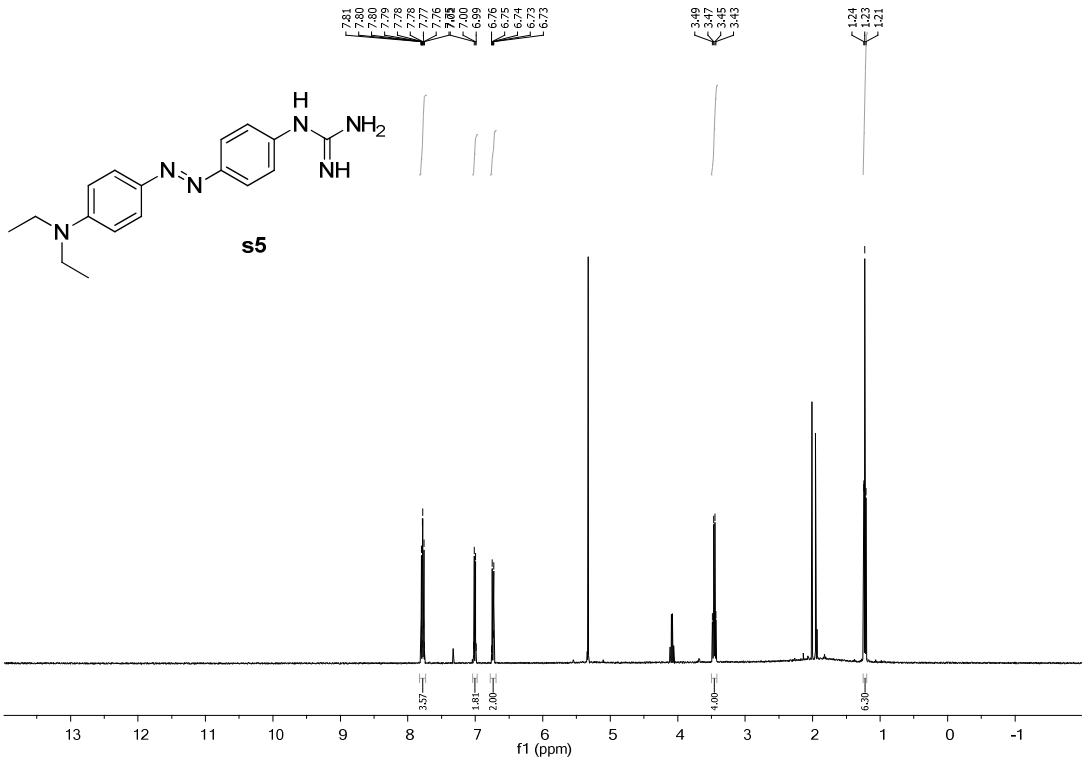

^{13}C-NMR, Arylguanidine **s5**

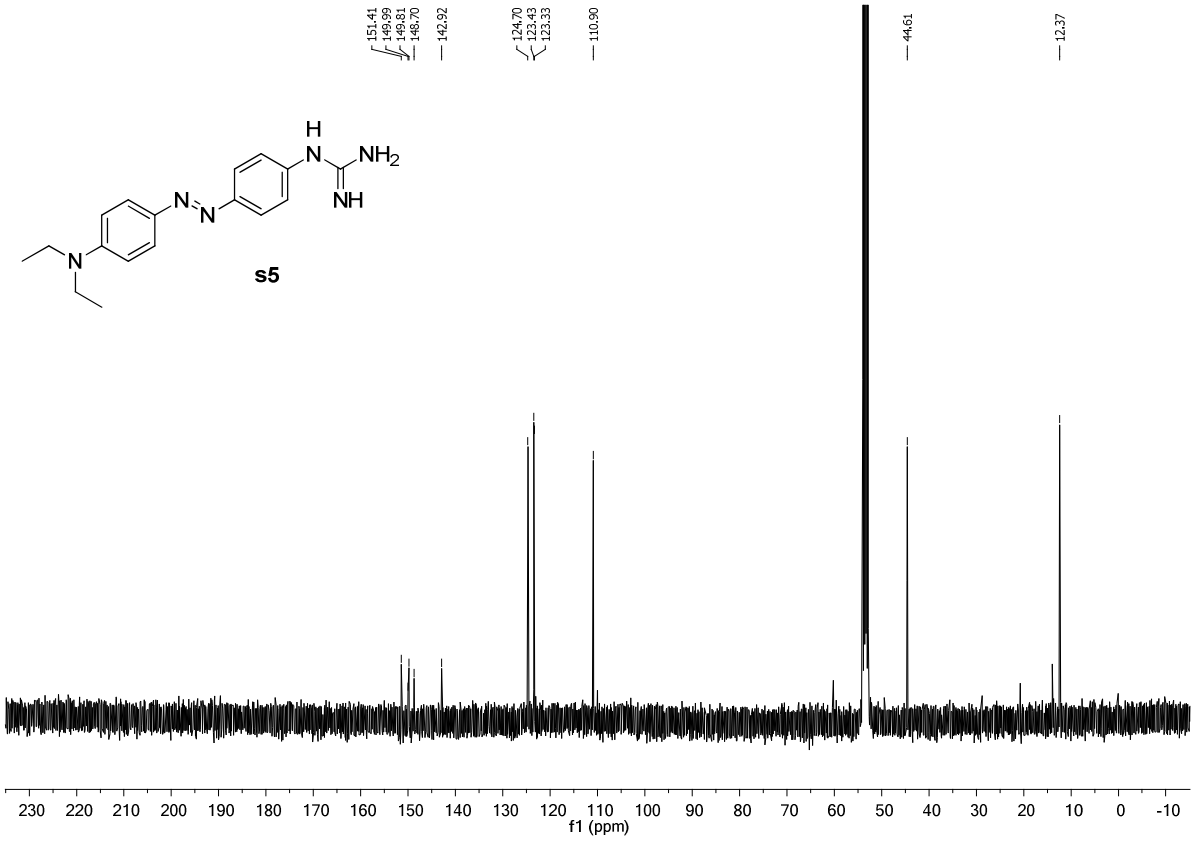

^{13}C-NMR, pyrazinoic acid **4b**

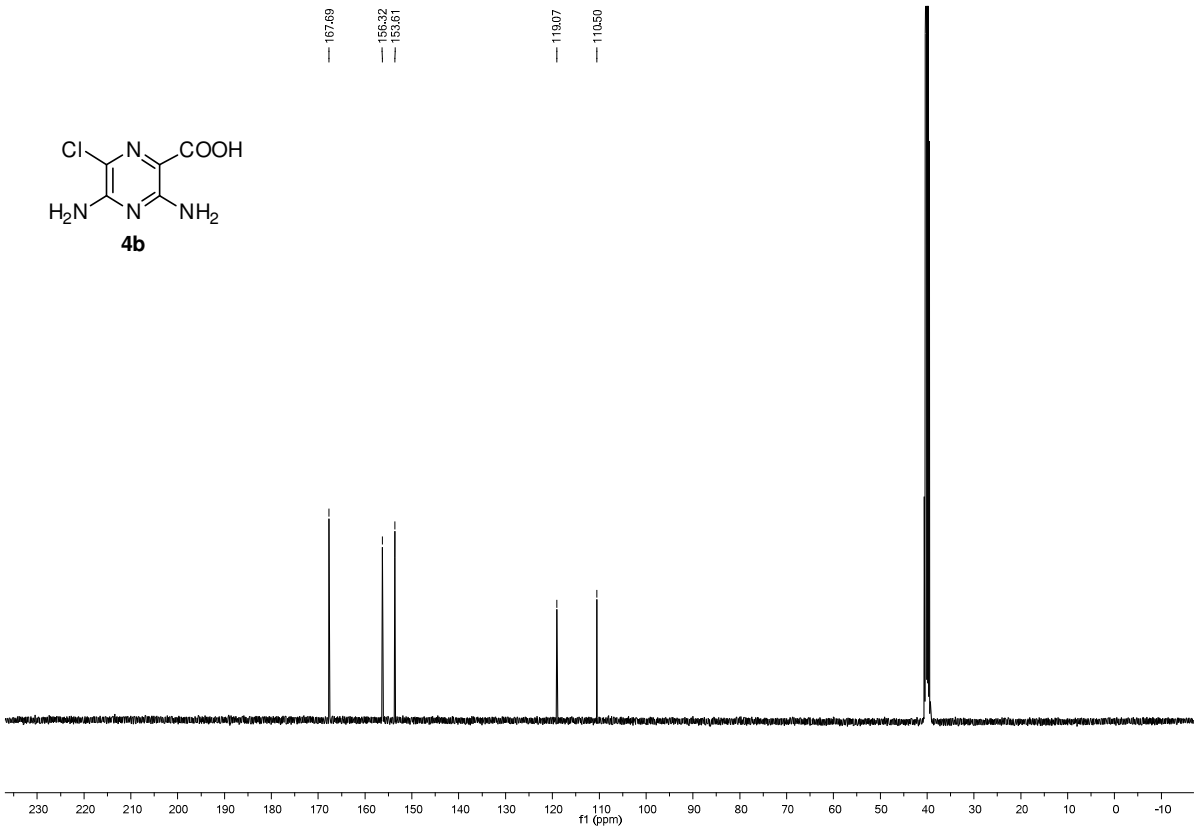

^{1}H-NMR, Boc-protected amine **05**

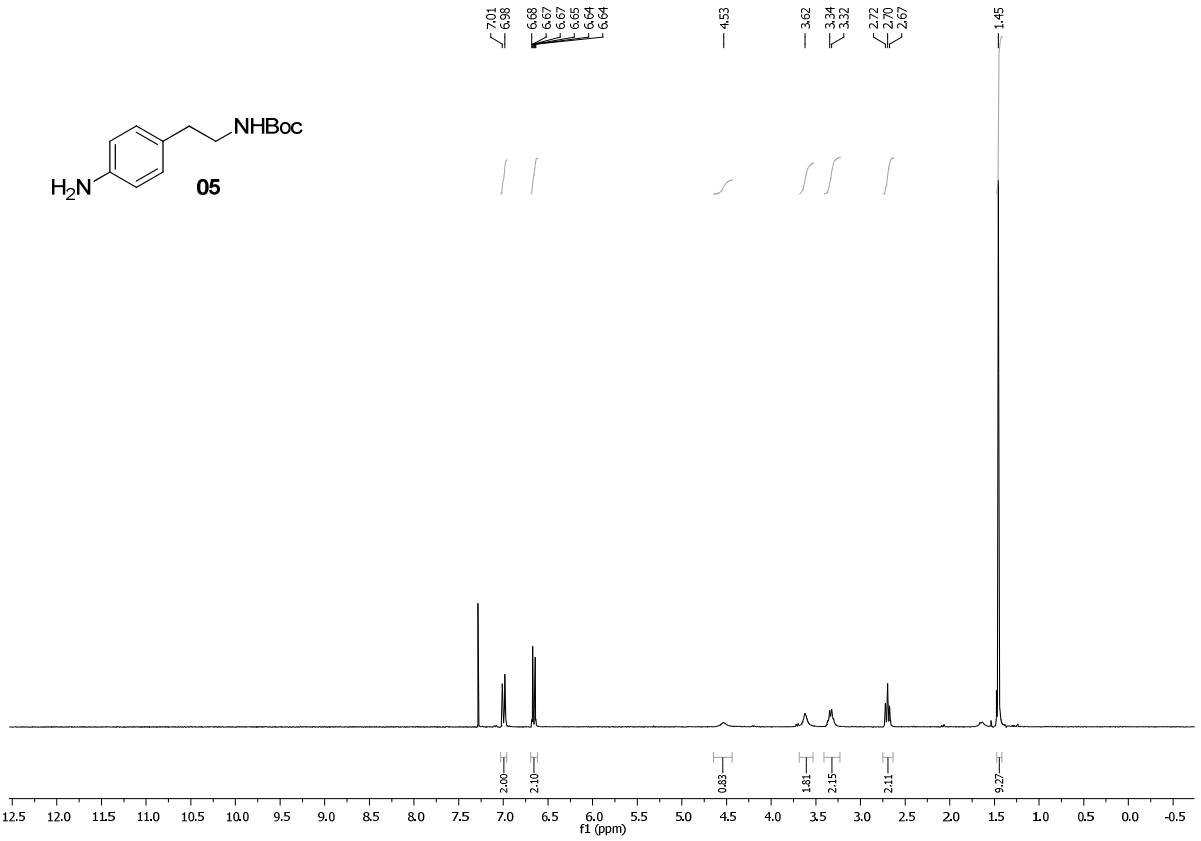

[1]H-NMR, primary amine building block **06**

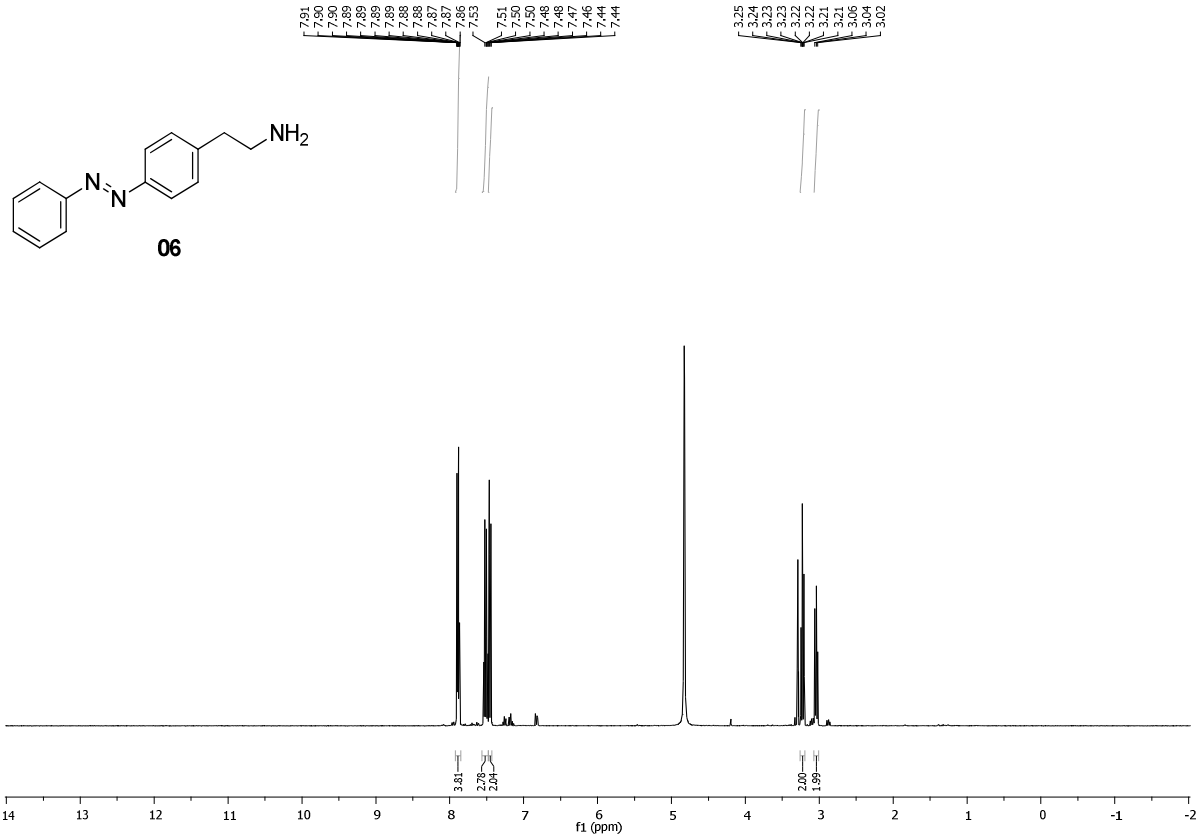

[13]C-NMR, primary amine building block **06**

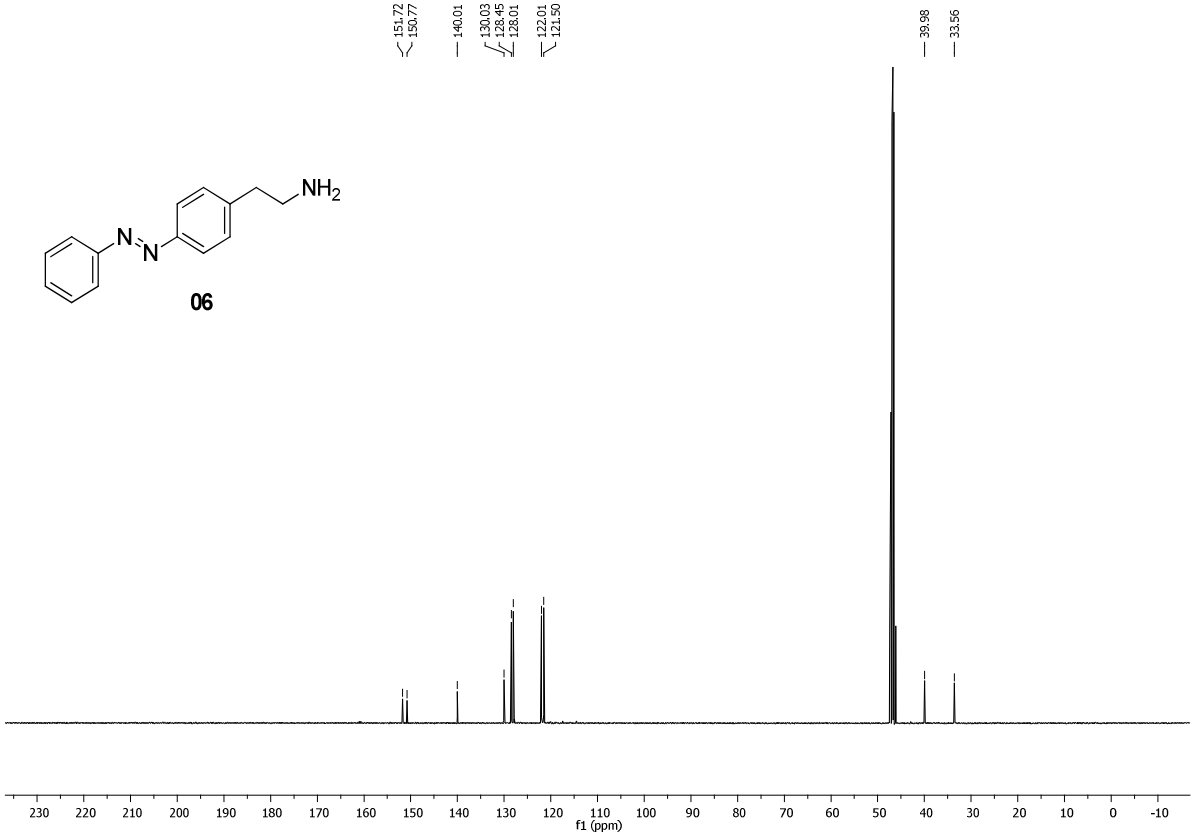

^{1}H-NMR, primary amine **07**

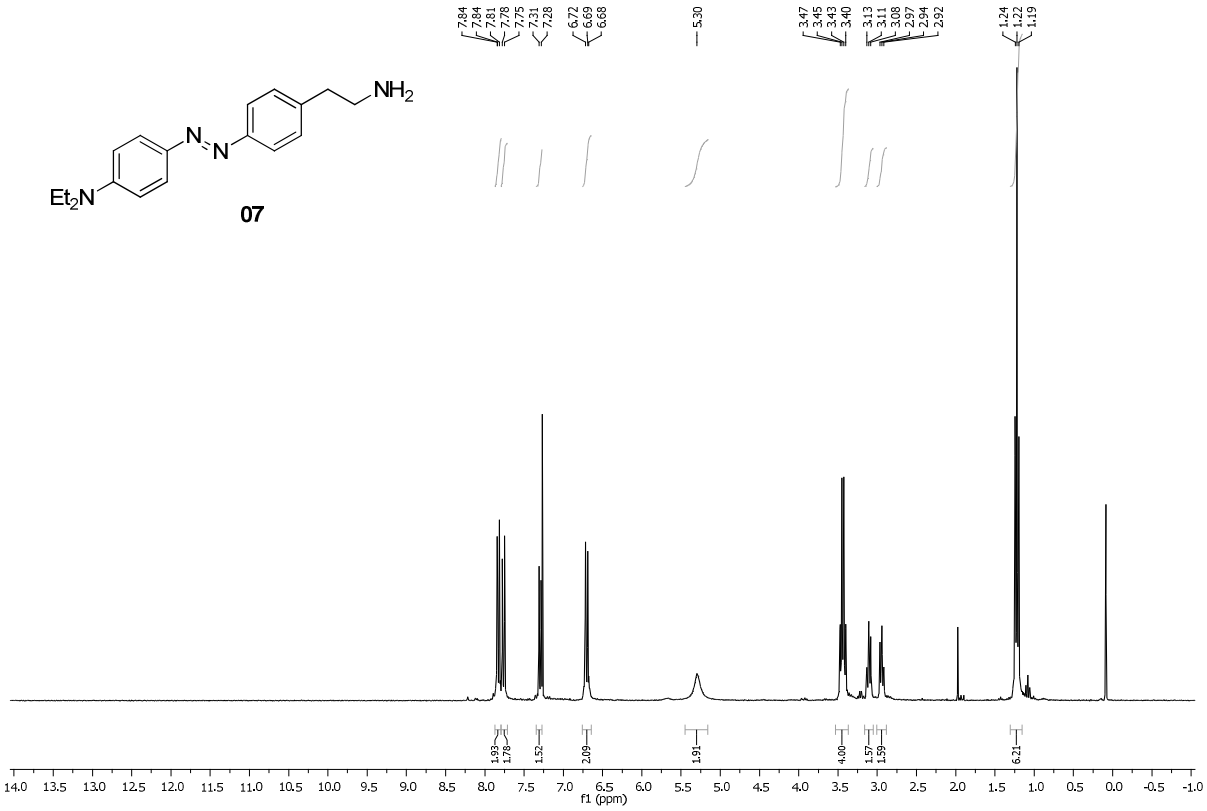

^{13}C-NMR, primary amine **07**

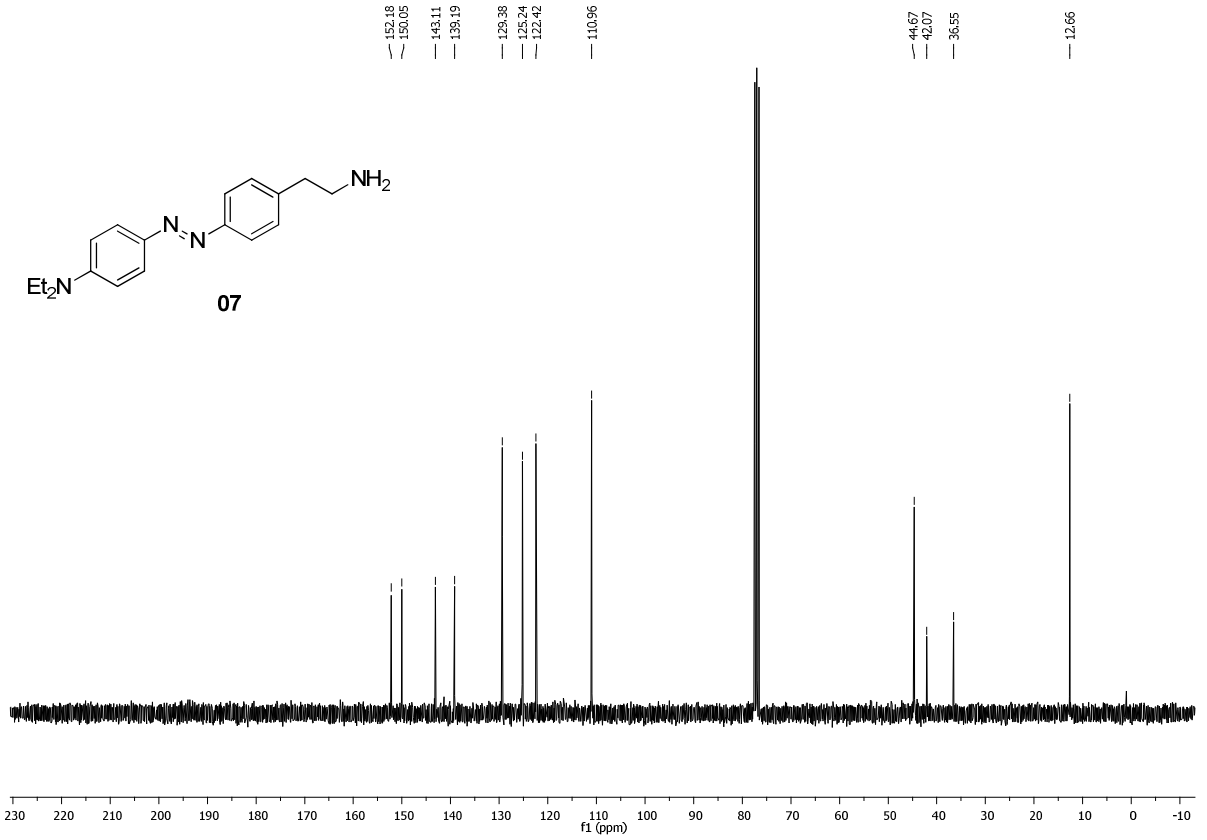

[1]H-NMR PA1

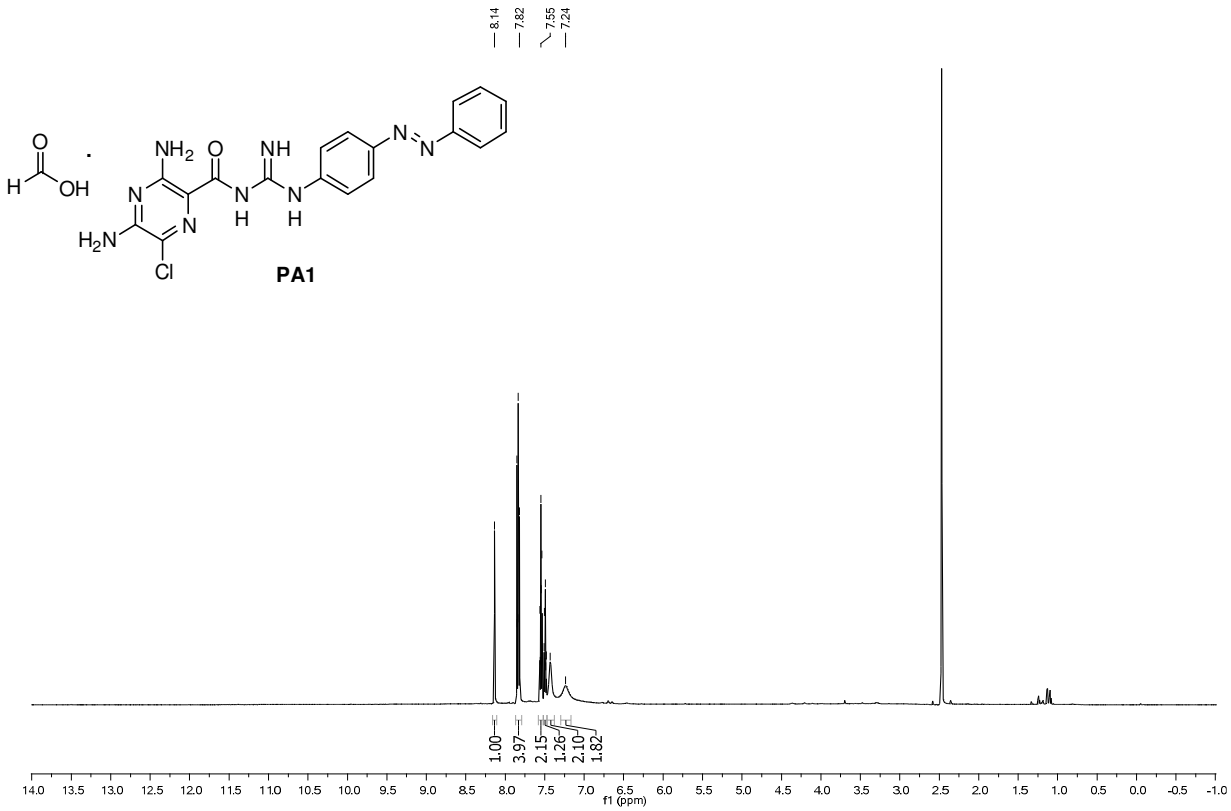

[13]C-NMR PA1

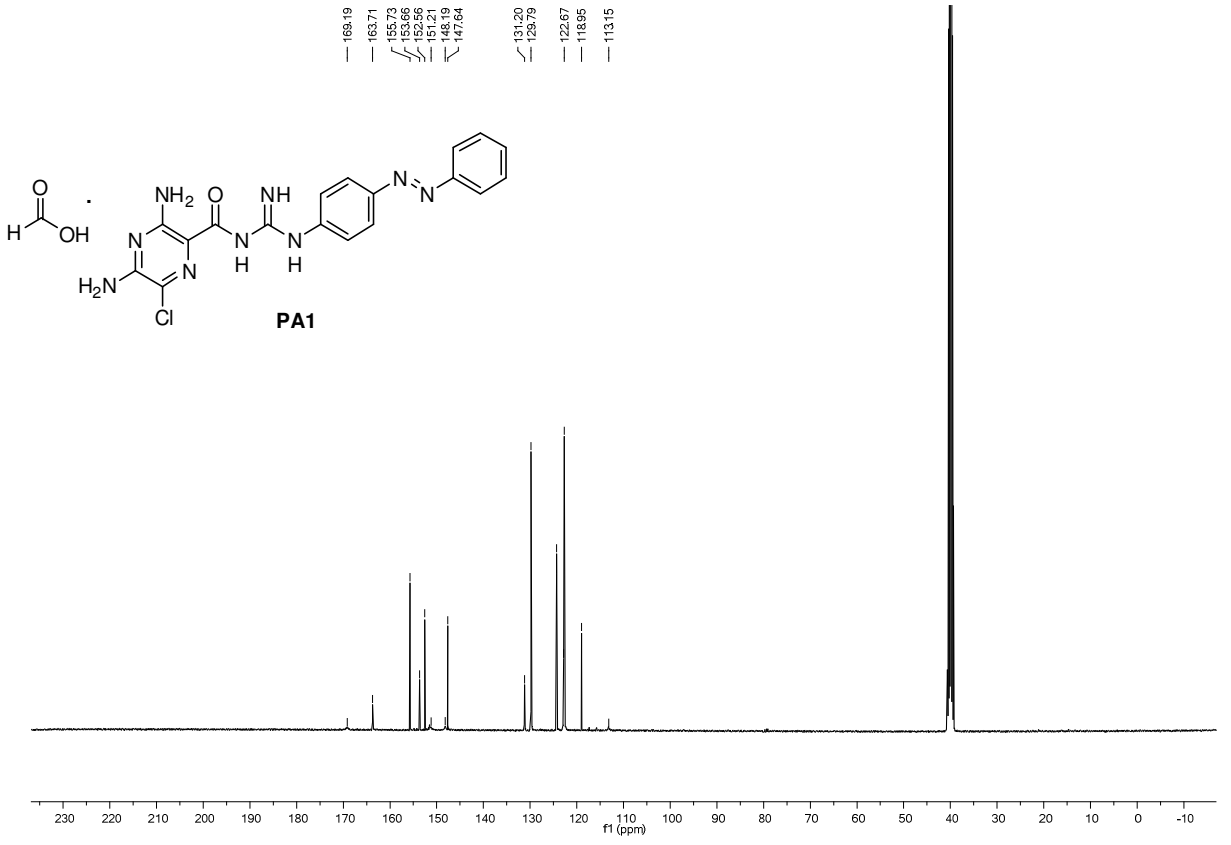

[1]H-NMR PA2

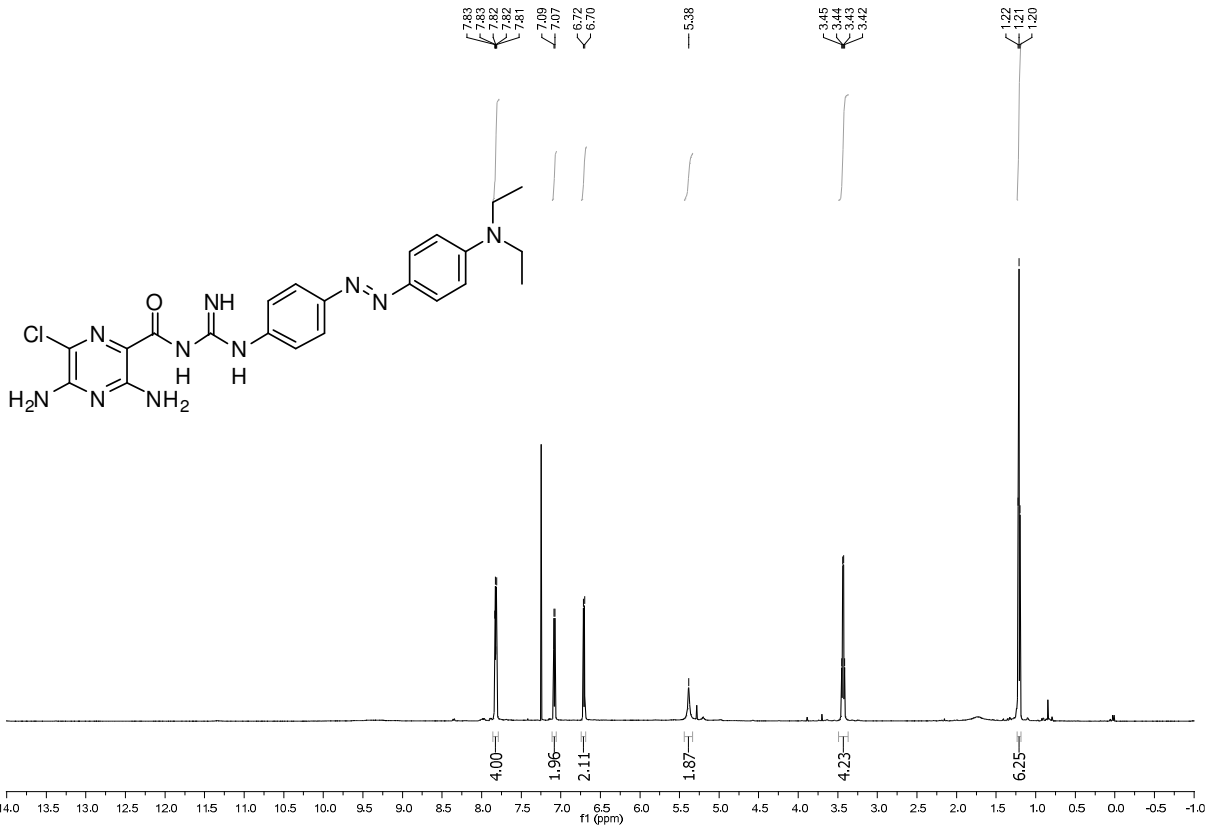

[13]C-NMR PA2

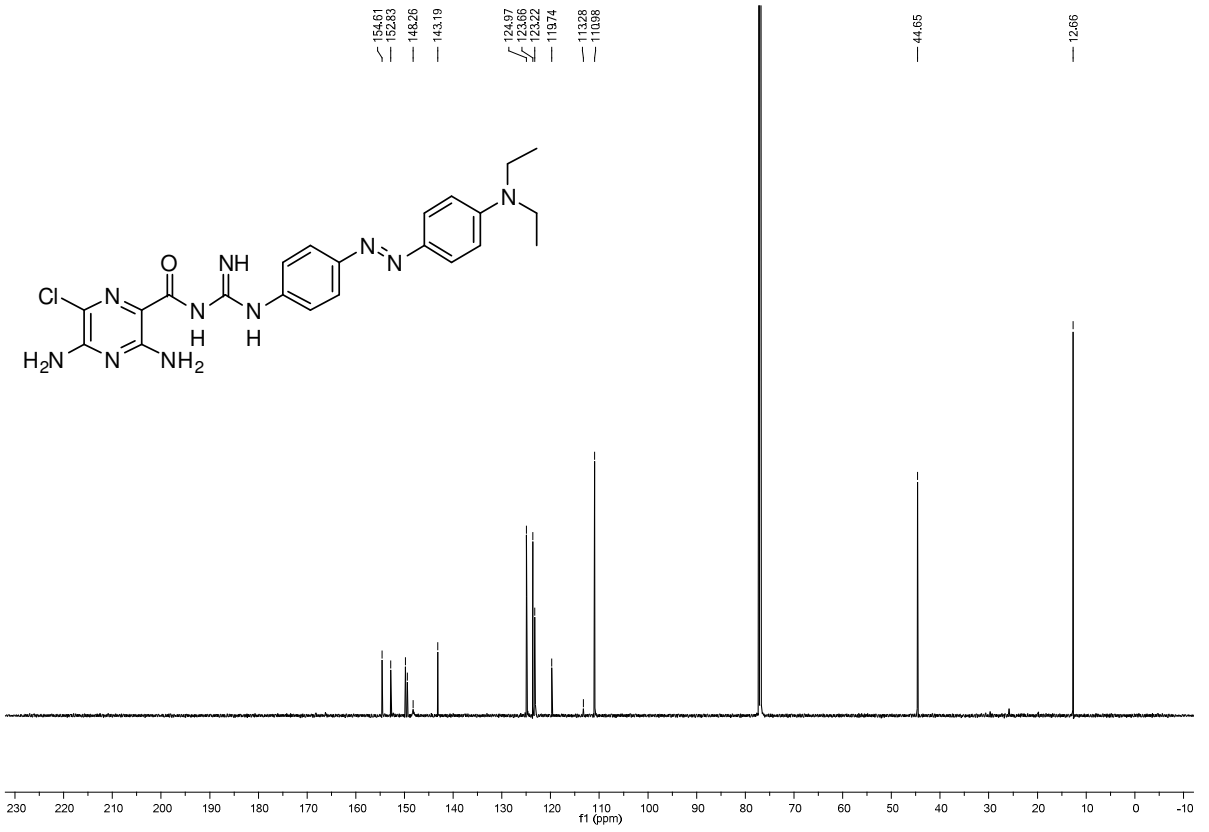

[1]H-NMR PA3

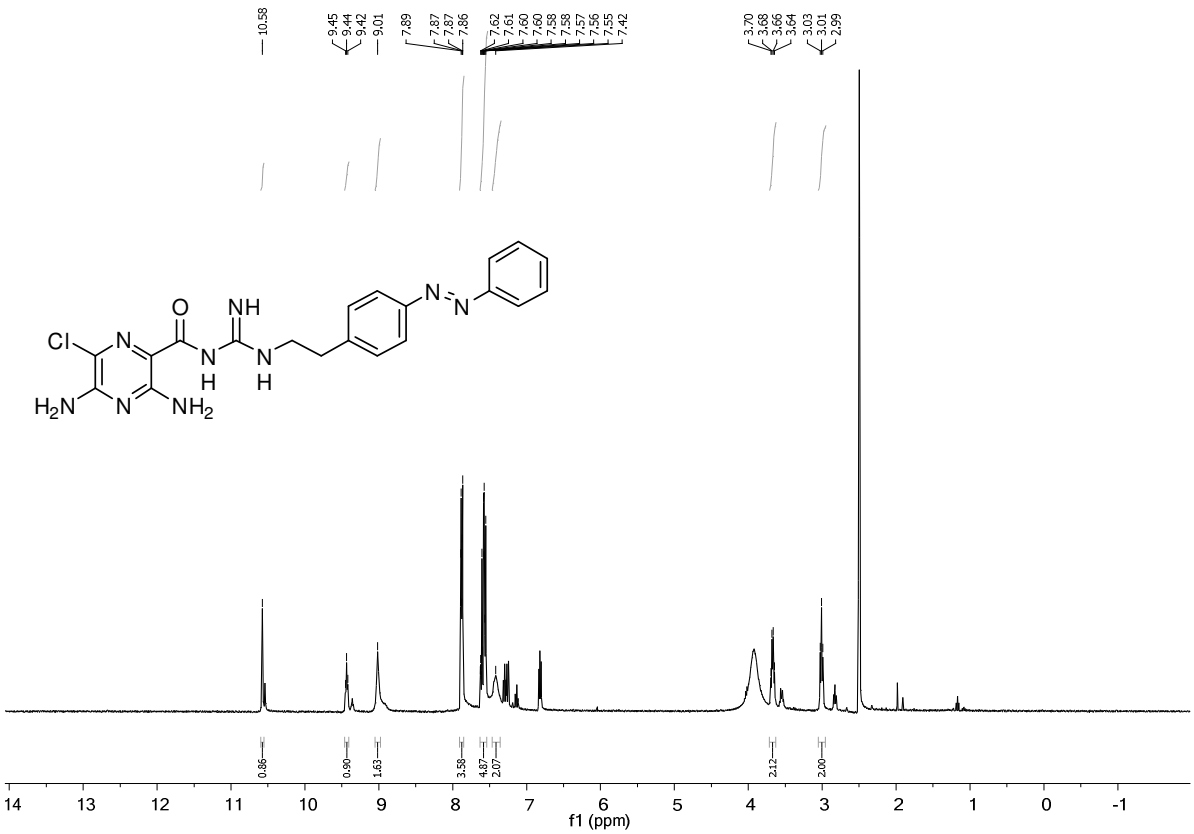

[13]C-NMR PA3

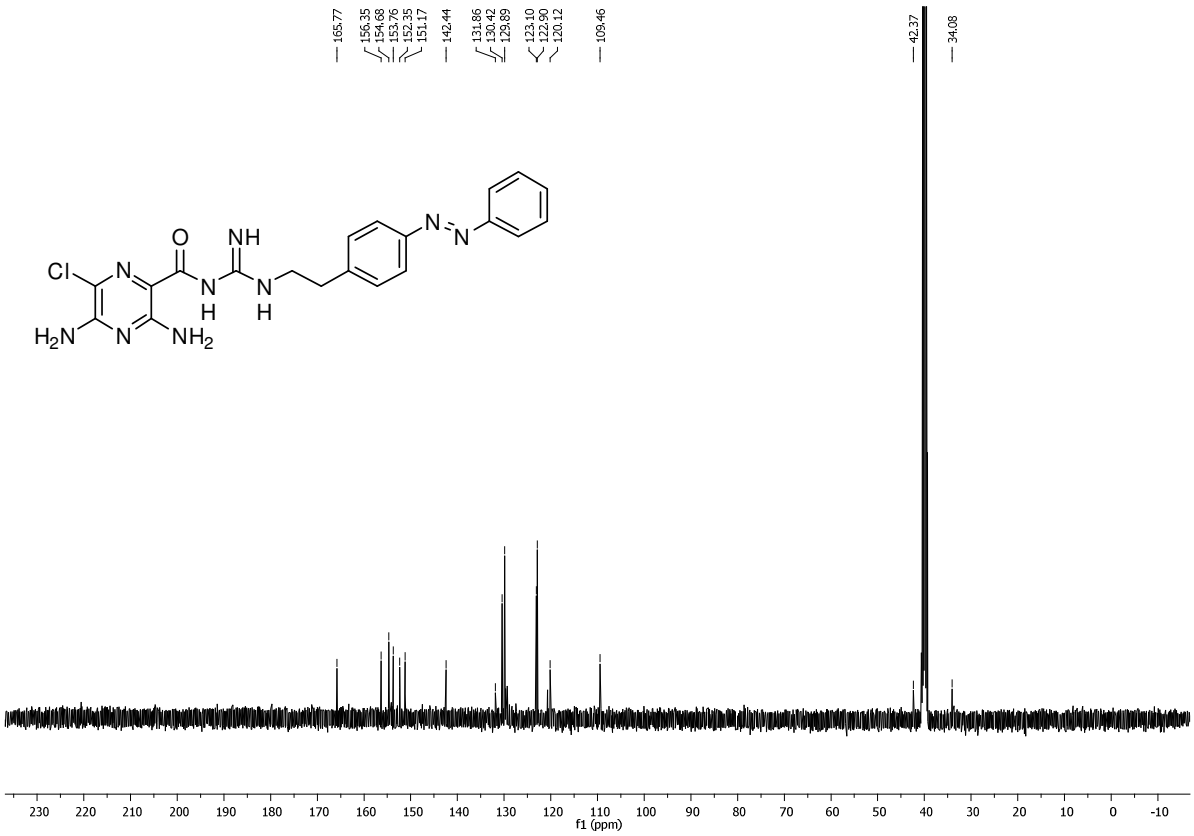

^{1}H-NMR PA4

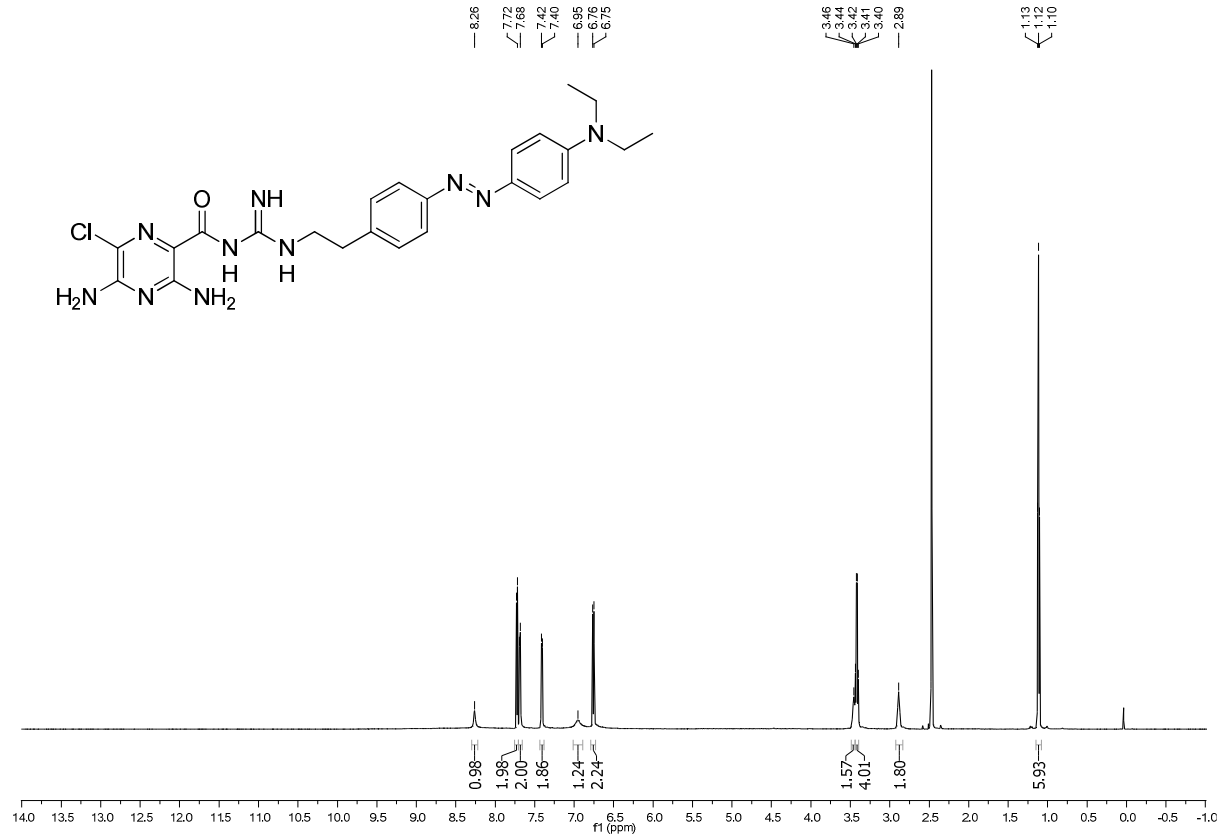

^{13}C-NMR PA4

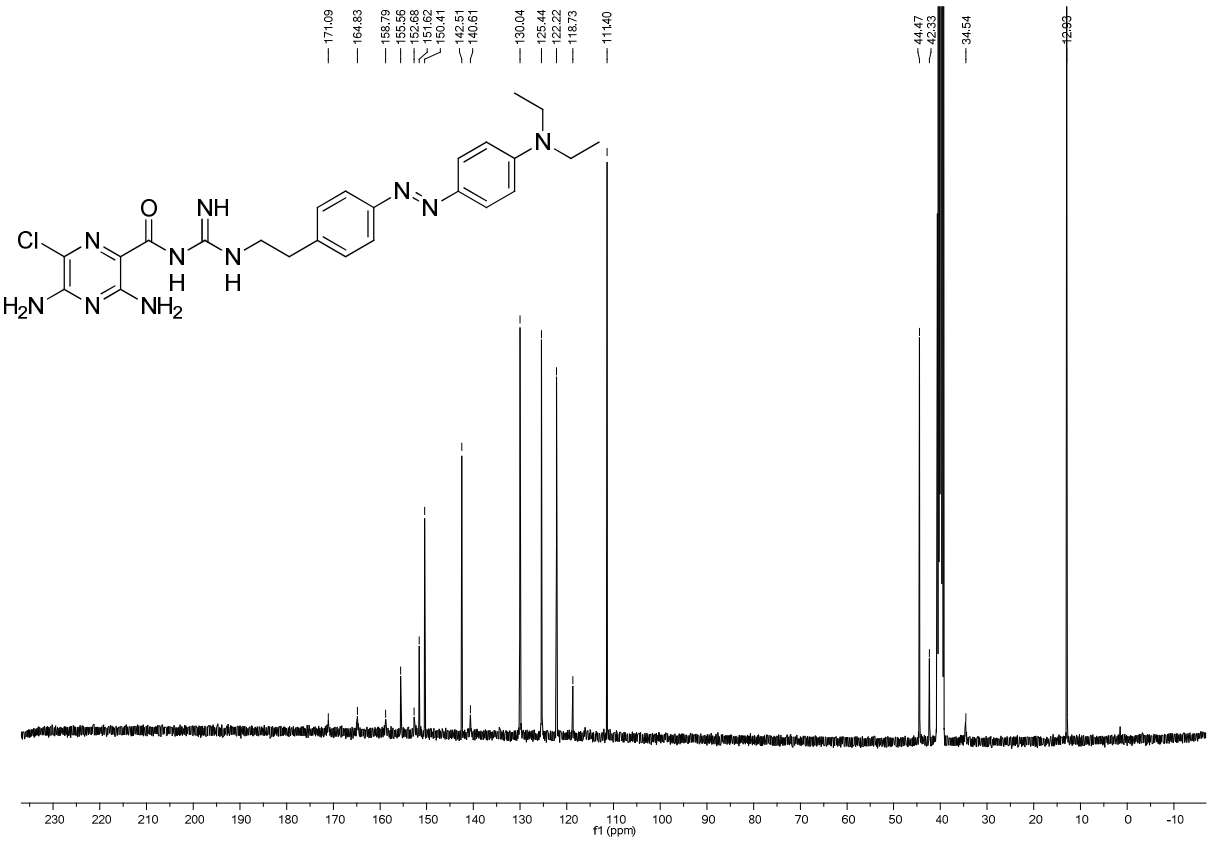

X-Ray PA1

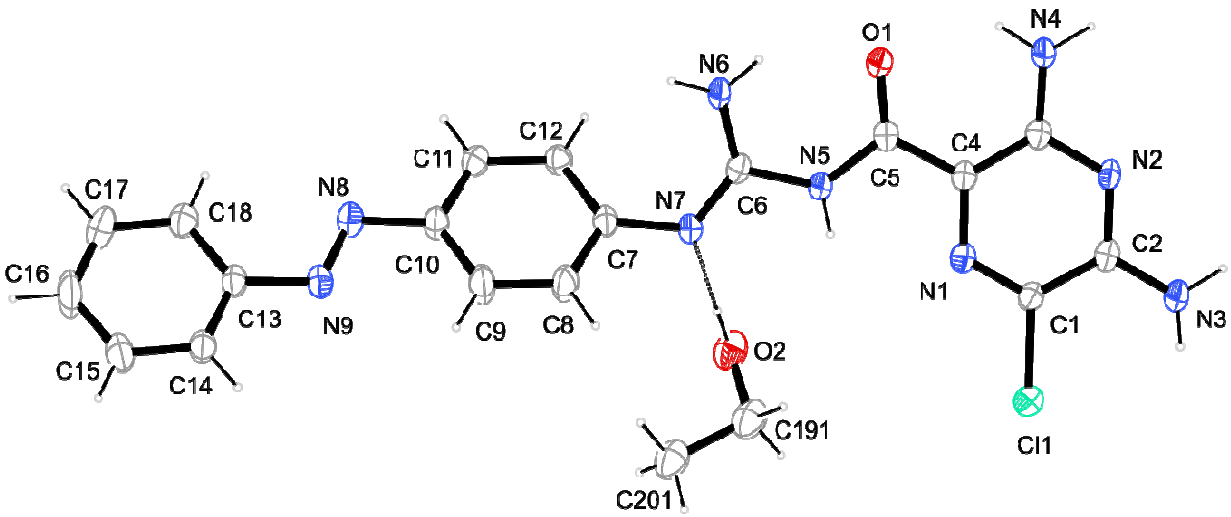

(crystallized from methanl/ethanol by slow evaporation at 4 °C)

Table 1.

1. Crystallographic data **PA1**. This structure is also available at CCDC 976534

	1
net formula	$C_{19.36}H_{20.73}ClN_9O_2$
M_r/g mol^{-1}	446.934
crystal size/mm	0.20 × 0.16 × 0.02
T/K	100(2)
radiation	'Mo Kα
diffractometer	'Bruker D8Venture'
crystal system	monoclinic
space group	$C2/c$
a/Å	25.833(3)
b/Å	9.8281(12)
c/Å	17.894(2)
α/°	90
β/°	110.041(4)
γ/°	90
V/Å^3	4267.9(9)
Z	8
calc. density/g cm^{-3}	1.3912(3)
μ/mm^{-1}	0.217
absorption correction	multi-scan
transmission factor range	0.8968–0.9579
refls. measured	36579
R_{int}	0.0783
mean σ(I)/I	0.0459
θ range	2.40–25.06
observed refls.	2790
x, y (weighting scheme)	0.0415, 5.2715
hydrogen refinement	mixed
refls in refinement	3761
parameters	327
restraints	0
$R(F_{obs})$	0.0399
$R_w(F^2)$	0.1012
S	1.006
shift/error$_{max}$	0.001
max electron density/e Å^{-3}	0.204
min electron density/e Å^{-3}	−0.225

C-bound H: constr, N- and O-bound H: refall.

0.36% EtOH, 0.64% MeOH, CH3-group of MeOH disordered. Figure shows EtOH only.

IV

Fotocaine – a new type of Photochromic Ion Channel Blocker

Matthias Schoenberger[1], Arunas Damjionaitis[1], Zinan Zhang[2], Daniel Nagel[3], and Dirk Trauner[‡,1]

[1]Department of Chemistry, Ludwig-Maximilians-Universität München, Munich, Germany

[2]Department of Chemistry, Princeton University, Princeton, NJ 08544, USA

[3]Department Molecules - Signaling - Development, Max-Planck Institute of Neurobiology, Martinsried, Germany

Photochromic blockers of voltage gated ion channels are powerful tools for the exploration of neuronal systems with high spatial and temporal precision. We now introduce fotocaine, a novel type of photochromic channel blocker that is based on the long lasting and not permanently charged surface anesthetic fomocaine. Fotocaine enables the optical control of action potential firing by switching between 350 and 450 nm light.

Content

Introduction

Optical methods for investigating neuronal function have boosted neuroscience in recent years.[1-3] Photoswitchable azobenzene versions of local anesthetics have proven to be powerful tools for addressing native voltage gated ion channels[4,5] and have been used in pain research and vision restoration.[6-8] For instance, the doubly-charged QAQ and singly-charged DENAQ are in essence derivatives of lidocaine and its permanently charged congener QX-314.[9] A common feature of these compounds is there permanent charge, which may limit their ability to cross biological barriers. In our ongoing efforts to develop new and improved photoswitchable ligands, we therefore looked for alternative pharmacophores. Local anesthetics research dates back centuries and is a very active field of research to date.[10-13] Initially, for example the psychoactive alkaloid **cocaine** was used in ophthalmology.[14] **Novocaine** is a representative of the ester local anesthetics resembling the anilid local anesthetic **lidocaine** with a diethylated tertiary amine. Our attention was drawn to **fomocaine**, which is a representative of ether local anesthetics with a morpholino group as a pharmacophore that has been used for decades as a long-lasting surface anesthetic.[14] With its unique structure and function in mind, we decided to develop a photoswitchable version of **fomocaine**.

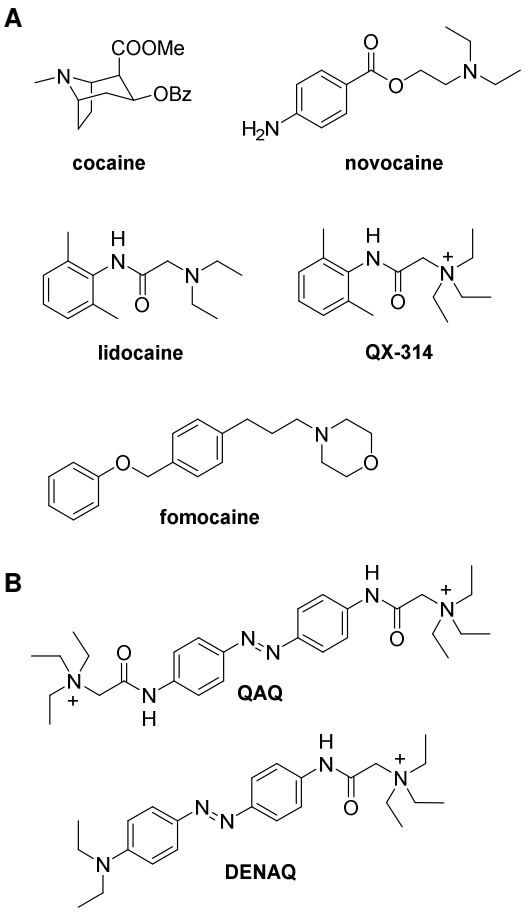

Figure 1. A) Structures of known local anesthetics. **Cocaine** is a piperidine alkaloid, **novocaine** is a ester local anesthetic and **lidocaine** is a anilid local anesthetic. All of these compounds feature a tertiary amine pharmacophore. **QX-314** is a permanently charged derivative of **lidocaine**. Fomocaine is an ether local anesthetic with a morpholino functional group. B) Photoswitchable azobenzene derivatives of local anesthetics **QAQ** and **DENAQ** that are used as photoswitchable blockers of voltage gated ion channels.

Results and Discussion

Fomocaine especially evoked our interest, since it abides to our philosophy of "azologization", i.e. the rational introduction of azobenzenes in drugs (Figure 2). Obvious targets for azologization are stilbenes, 1,2-diphenyl ethers, 1,2.diphenyl hydrazines, *N*-benzyl anilines, benzyl-phenyl ethers, benzyl-phenyl thioethers, diaryl esters and diaryl amides (Figure 2A). Those "azosters" can be strategically replaced by azobenzenes giving access to photoswitchable ligands that highly resemble their parent coumpounds in size and shape. We have applied this logic to **fomocaine**, which

features a benzyl-phenyl ether, by replacing the C-O-bridge with a diazene unit giving the azobenzene derivative **fotocaine** (synthesis see supporting information).

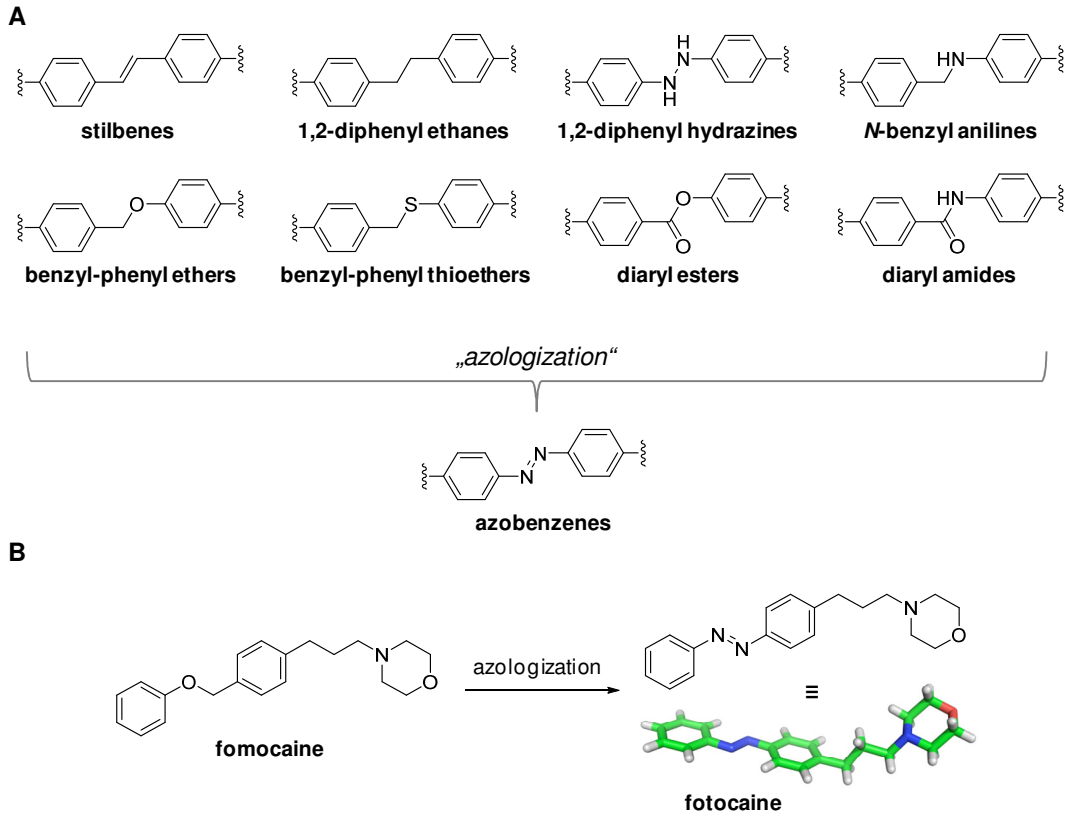

Figure 2. Azologization. A) Prime isosters of azobenzenes, i.e. azosters, are stilbenes, 1,2-diphenyl ethers, 1,2.diphenyl hydrazines, N-benzyl anilines, benzyl-phenyl ethers, benzyl-phenyl thioethers, diaryl esters and diaryl amides. B) Application of the concept of azologization to **fomocaine**. Strategic replacement of the benzyl-phenyl ether bridge by a diazene yields the azobenzene derivative **fotocaine**.

We hypothesized that combining the local anesthetics properties of fomocaine with the photoisomerization of azobenzenes in this way would yield a photoswitchable ion channel blocker. To test **fotocaine**'s photoswitching properties, we first utilized UV/Vis spectroscopy (Figure 3). A 50 μM solution of **fotocaine** in DMSO was placed in a quartz cuvette with 1 cm diameter and illuminated from above using a monochromator. The light-induced isomerization of **fotocaine** and the corresponding absorption spectra of *cis* and *trans*-isomers are depicted in Figure 3A. As a classical azobenzene, isomerization could be followed by monitoring the π to π* transition at 330 nm over time. Switching between 350 nm and 450 nm light reversibly turned the molecule into its *cis* and *trans*-state, respectively, Figure 3C (i). Wavelengths between 400 and 360 nm could be used to install mixtures with different *cis*/*trans* ratios, Figure 3C (ii). As expected from an azobenzene devoid of major electronic substituents, the thermodynamically less stable *cis*-state could be maintained in the dark, Figure 3C (iii).[15,16] Thus, **fotocaine** provides the desired reversible light-mediated *cis*/*trans*-isomerization. As an added advantage, it stays in its *cis*-state at least for several minutes even without UV-illumination.

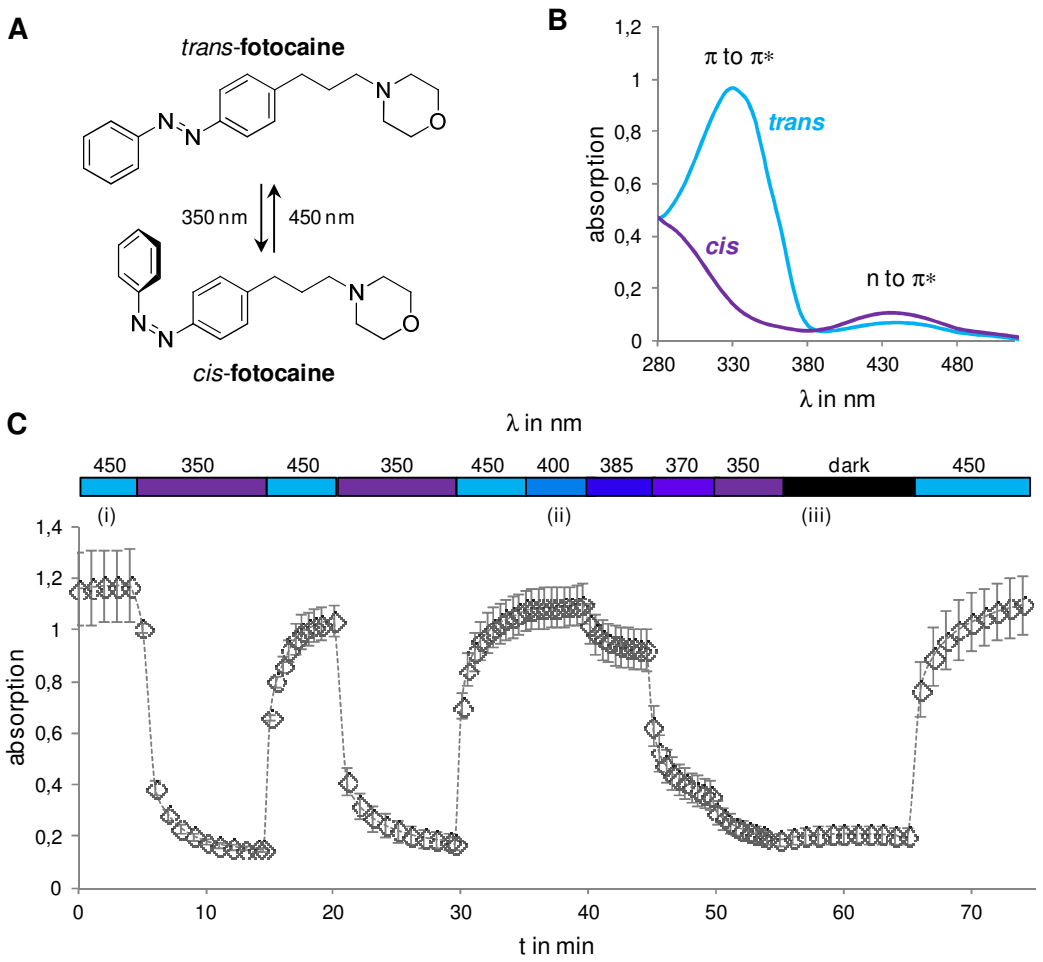

Figure 3. Photoswitching of **fotocaine** followed by UV/Vis spectroscopy. **A**) UV-light (e.g. 350 nm) isomerizes the azobenzene functional group in fotocaine to its *cis*-isomer, which is the thermodynamically less stable state. Blue light (e.g. 450 nm) triggers isomerization to *trans*. **B**) Absorption spectra of *trans*-**fotocaine** (blue line) and *cis*-**fotocaine** (purple line) are distinct. The π to π* band decreases starkly upon isomerization to *cis*, while the n to π* band slightly increases. **C**) In-time photoswitching by following the **fotocaine** absorption at 330 nm. **Fotocaine** can be reversibly isomerized by switching between, e.g., 450 and 350 nm (i). Wavelengths between 400 and 350 nm lead to graded effects (ii). Once switched to *cis*, **fotocaine** stays in its excited state without further illumination (iii). No decay was detected for the investigated time of 10 min. (n = 3, error bar indicates standard deviation)

To test if **fotocaine** provides photoswitching of neuronal function as hypothesized above, we investigated dissociated mouse hippocampal neurons using patch clamp experiments (Figure 2). Under 450 nm illumination at a starting potential of -80 mV, action potential (AP) firing of neurons induced by 50 pA current injection was inhibited. When switching to 350 nm, however, AP firing triggered by the same current did take place. This process could be repeated reversibly at any desired illumination protocol and the same effects were observed when applying 100 μM fotocaine, Figure S1. The single action potential at the beginning of each current injection under 450 nm indicates that *trans*-**fotocaine** acts as an open channel blocker as is the case for its permanently charged relatives.[9,17]

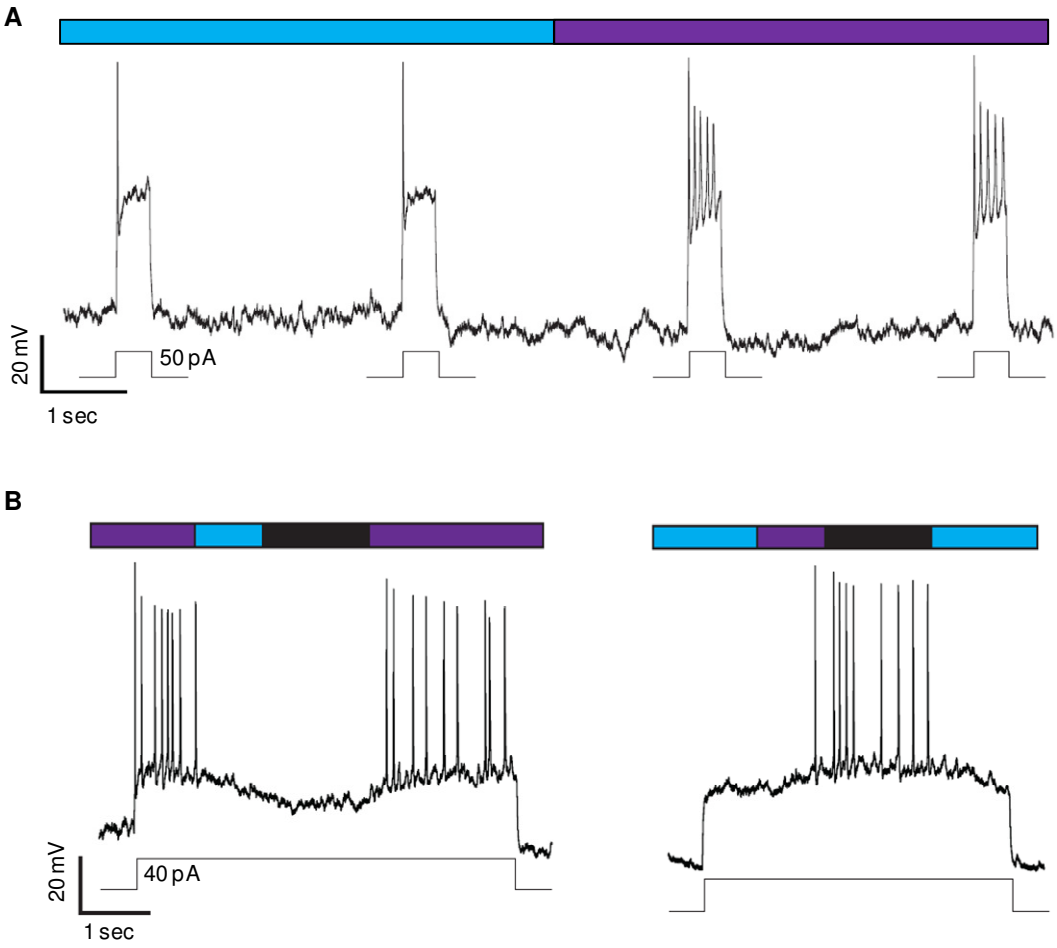

Figure 4. Photocontrol of action potential (AP) firing mediated by **fotocaine** investigated in whole cell patch clamp experiments (representative traces). A) Dissociated mouse hippocampal neurons, current clamp mode, 50 µM **fotocaine**. AP-firing was triggered by injecting 50 pA for 300 ms (cells were held at -80 mV). Under 450 nm (*trans*-**fotocaine**), AP-firing was suppressed, while and 350 nm illumination (*cis*-**fotocaine**), allowed AP-firing. The initial AP under 450 nm is indicative of the action of an open channel blocker. B) Acute mouse brain slice, hippocampal CA1 neurons, current clamp mode, after 10 min wash-out of **fotocaine**. 40 pA currents were injected and illumination wavelengths were changed simultaneously. Effects of *cis*- and *trans*-**fotocaine** were identical to A). In addition, when 350 nm or 450 nm were turned off after short application, the thereby installed effect maintained.

To test the action of **fotocaine** *in vivo* and investigate cell both uptake and bistability, we performed patch clamp experiments using acute hippocampal mouse brain slices. First, the tissue was treated with 100 µM **fotocaine** for 5 minutes. Then, buffered ringer solution was perfused for 10 min to remove the photoswitchable blocker from the extracellular solution. As hypothesized and desired by chemical design, fotocaine was taken up by the cell and photocontrol of AP firing was possible without extracellular **fotocaine** (Figure 2B). AP firing was triggered by injecting a 40 pA current for several seconds and illumination wavelengths where switched during this activation period. In line with our observations using dissociated neurons, AP firing was inhibited by 450 nm illumination and enabled by 350 nm. Furthermore, the bistability that was observed during UV/Vis-switching also applied to this physiological experiment. When a short pulse of 450 nm or 350 nm light was followed by darkness, the respective effect maintained and could be reversed.

Summary and Outlook

Taken together, we have introduced our philosophy of azologization, which is the strategic introduction of azobenzenes in drugs. We have applied this logic to the local anesthetic **fomocaine** and thereby developed the novel photochromic ion channel blocker **fotocaine**. It features a non-permanently charged morpholine functional group that provides novel pharmacodynamics compared to existing permanently charged photoswitches. We demonstrated that **fotocaine** gets readily taken up by cells and can be used to control action potential firing with light when present extracallularly or after cell-loading. Its relatively simple structure will serve as a versatile platform to chemically design new photoswitching properties such as cis-stability and red-shifted action spectra. As such, fotocaine represents another chemical tool for addressing the BRAIN Initiative.[18] These investigations and the application of **fotocaine** in neuroscience and vision restoration will be reported in due course.

METHODS

UV/Vis Spectroscopy was performed using a VARIAN Cary 50 Scan UV/Vis spectrometer. PCL solution was placed in a standard quartz cuvette (d = 1 cm) illuminated by a light fibre cable from above.

Cell and Tissue Preparation. Dissociated mouse hippocampal neurons were prepared and cultured using an astrocyte feeder layer as reported elsewhere.[19] For acute mouse hippocampal brain slices, BL6 wild type mice (postnatal days 9 to 13) of either sex, were quickly decapitated, the brain was removed, and 250 µm horizontal slices were prepared using a vibrating microtome (7000smz-2, Campden Instruments). Slices were incubated for 30 min at 34°C in carbogenated (5% CO_2, 95% O_2) sucrose medium (mM: 87 NaCl, 2.5 KCl, 7 $MgCl_2$, 0.5 $CaCl_2$, 25 Gluc, 1.25 NaH_2PO_4, 25 $NaHCO_3$, 75 sucrose, (319 mOsm)). Slices were perfused with 100 µM Fotocaine in bath solution for 5 min, followed by 10 min perfusion with bath solution. Whole cell patch clamp recordings where performed on CA1 hippocampal neurons.

Electrophysiology. Whole cell patch clamp recordings where performed using a standard electrophysiology setup equipped with a HEKA Patch Clamp EPC10 USB amplifier and patch master software. Micropipettes were generated from "Science Products GB200-F-8P with filament" pipettes using a vertical puller (PC-10, Narishige). Resistance varied between 5-7 MΩ. Bath solution for dissociated hippocampal neurons contained in mM: 140 NaCl, 3 KCl, 2 $CaCl_2$, 1 $MgCl_2$, D-Gluc 10, 20 HEPES (NaOH to pH 7.4). Pipette solution for dissociated hippocampal neurons contained in mM: 107 KCl, 1.2 $MgCl_2$, 1 $CaCl_2$, 10 EGTA, 5 HEPES, 2 MgATP, 0.3 Na_2GTP (KOH to pH 7.2). Bath solution for acute brain slice contained in mM: 125 NaCl, 2.5 KCl, 1 $MgCl_2$, 2 $CaCl_2$, 10 Glucose, 1.25 NaH_2PO_4, 26 $NaHCO_3$, (290 - 295 mOsm). Pipette solution for acute brain slice contained in mM: 140 K-gluconate, 4 NaCl, 12 KCl, 10 HEPES, 4 MgATP, 0.4 Na_2ATP (KOH to pH 7.3). Action Potentials (APs) were induced with 50 pA current injection. **Fotocaine** was dissolved in bath solution from a 1000 x DMSO stock for either tissue preparation.

Illumination. Irradiation during electrophysiology and UV/Vis experiments was performed using a TILL Photonics Polychrome 5000 monochromator operated by the PolyCon software or by the patch clamp amplifier, respectively..

ASSOCIATED CONTENT

Representative traces of AP-firing using different concentrations of **fotocaine** and illumination timing (Figure S1). Synthesis and characterization of organic compounds This material is available free of charge via the Internet at http://pubs.acs.org.

AUTHOR INFORMATION

‡Corresponding author

Email: dirk.trauner@lmu.de, phone: +49 89 2180-77800

Author Contributions

M.S. conceived of the study, planed the chemical synthesis, performed the UV/Vis experiments, the electrophysiology on dissociated neurons and wrote the manuscript. A.D. performed the electrophysiology on acute mouse brain slice. Z.Z. performed the chemical synthesis, D.N. prepared the dissociated mouse hippocampal neurons. D.T. provided funding and equipment.

Notes

The authors declare no competing financial interest.

REFERENCES

1. Deisseroth, K. Optogenetics. *Nat Methods* **8**, 26-9 (2011).

2. Zemelman, B.V., Lee, G.A., Ng, M. & Miesenbock, G. Selective photostimulation of genetically chARGed neurons. *Neuron* **33**, 15-22 (2002).

3. Fehrentz, T., Schonberger, M. & Trauner, D. Optochemical genetics. *Angew Chem Int Ed Engl* **50**, 12156-82 (2011).

4. Banghart, M.R. et al. Photochromic blockers of voltage-gated potassium channels. *Angew Chem Int Ed Engl* **48**, 9097-101 (2009).

5. Banghart, M., Borges, K., Isacoff, E., Trauner, D. & Kramer, R.H. Light-activated ion channels for remote control of neuronal firing. *Nat Neurosci* **7**, 1381-6 (2004).

6. Mourot, A. et al. Rapid optical control of nociception with an ion-channel photoswitch. *Nat Methods* **9**, 396-402 (2012).

7. Polosukhina, A. et al. Photochemical restoration of visual responses in blind mice. *Neuron* **75**, 271-82 (2012).

8. Tochitsky, I. et al. Restoring Visual Function to Blind Mice with a Photoswitch that Exploits Electrophysiological Remodeling of Retinal Ganglion Cells. *Neuron* **81**, 800-813 (2014).

9. Mourot, A. et al. Tuning photochromic ion channel blockers. *ACS Chem Neurosci* **2**, 536-43 (2011).

10. Moldovan, M., Alvarez, S., Romer Rosberg, M. & Krarup, C. Axonal voltage-gated ion channels as pharmacological targets for pain. *European Journal of Pharmacology* **708**, 105-112 (2013).

11. Wulff, H., Castle, N.A. & Pardo, L.A. Voltage-gated potassium channels as therapeutic targets. *Nat Rev Drug Discov* **8**, 982-1001 (2009).

12. Wang, Y. et al. Development and Characterization of Novel Derivatives of the Antiepileptic Drug Lacosamide That Exhibit Far Greater Enhancement in Slow Inactivation of Voltage-Gated Sodium Channels. *ACS Chemical Neuroscience* **2**, 90-106 (2011).

13. Wang, Y. et al. Merging Structural Motifs of Functionalized Amino Acids and α-Aminoamides Results in Novel Anticonvulsant Compounds with Significant Effects

on Slow and Fast Inactivation of Voltage-Gated Sodium Channels and in the Treatment of Neuropathic Pain. *ACS Chemical Neuroscience* **2**, 317-332 (2011).

14. Oelschlager, H. [Fomocaine from the chemical, pharmacokinetic and pharmacologic viewpoint: current status and overview]. *Pharm Unserer Zeit* **29**, 358-64 (2000).

15. Sadovski, O., Beharry, A.A., Zhang, F. & Woolley, G.A. Spectral tuning of azobenzene photoswitches for biological applications. *Angew Chem Int Ed Engl* **48**, 1484-6 (2009).

16. Schonberger, M. & Trauner, D. A Photochromic Agonist for mu-Opioid Receptors. *Angew Chem Int Ed Engl*, in press (2014).

17. Nau, C. & Wang, G.K. Interactions of local anesthetics with voltage-gated Na+ channels. *J Membr Biol* **201**, 1-8 (2004).

18. Andrews, A.M., Schepartz, A., Sweedler, J.V. & Weiss, P.S. Chemistry and the BRAIN Initiative. *Journal of the American Chemical Society* (Article ASAP).

19. Kaech, S. & Banker, G. Culturing hippocampal neurons. *Nat. Protocols* **1**, 2406-2415 (2006).

IV.i

Fotocaine – a new type of Photochromic Ion Channel Blocker

Matthias Schoenberger[1], Arunas Damjionaitis[1], Zinan Zhang[2], Daniel Nagel[3], and Dirk Trauner[‡,1]

[1]Department of Chemistry, Ludwig-Maximilians-Universität München, Munich, Germany

[2]Department of Chemistry, Princeton University, Princeton, NJ 08544, USA

[3]Department Molecules - Signaling - Development, Max-Planck Institute of Neurobiology, Martinsried, Germany

SUPPORTING INFORMATION

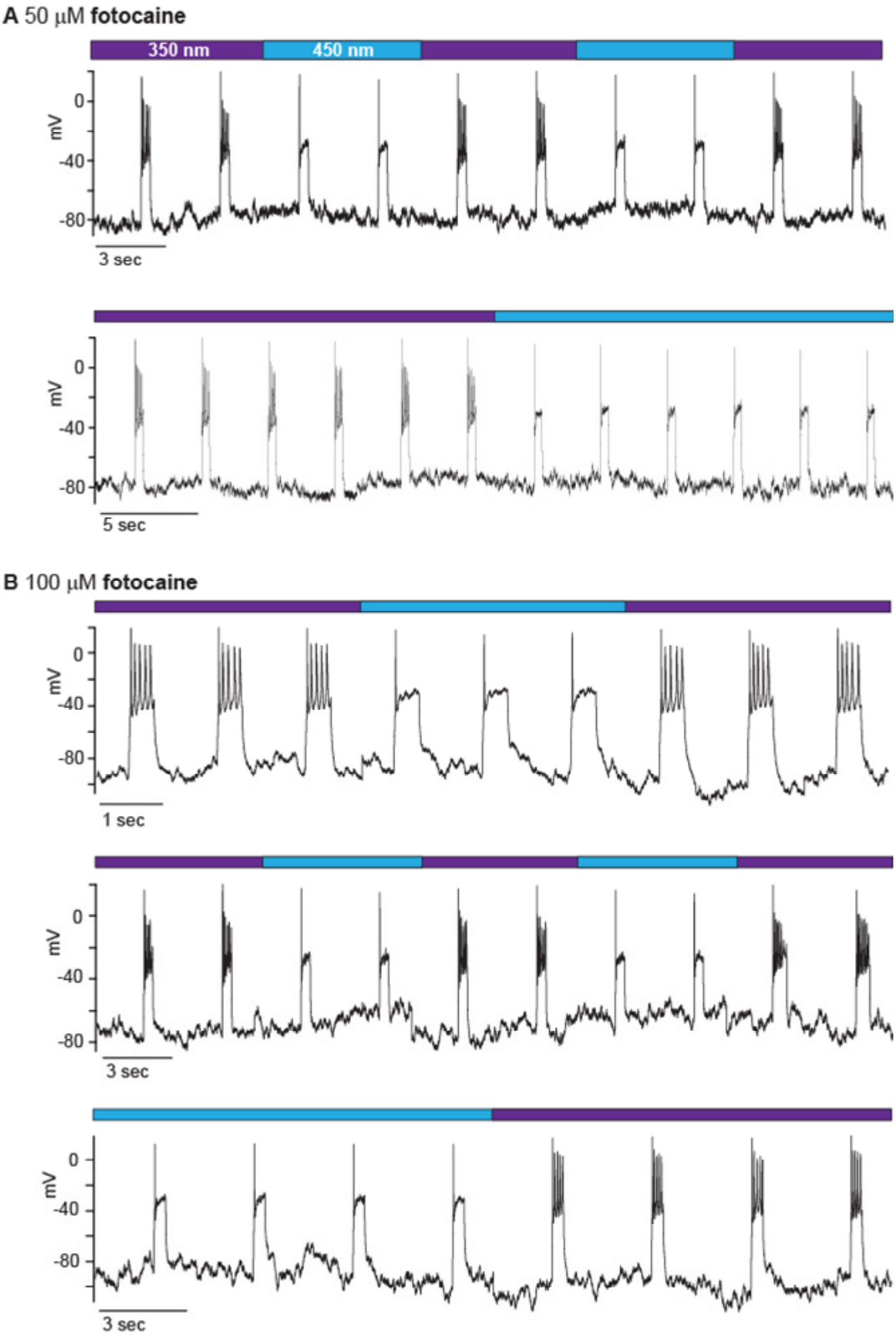

Figure S1. Optical control of AP firing using 50 µM fotocaine (A) or 100 µM fotocaine (B). APs were evoked by 50 pA current injection and enabled or blocked by 350 and 450 nm, respectively.

Chemical Synthesis

All reactions were performed in oven-dried glassware. All reagents were purchased from commercial sources and used without further purification. Chemical shifts (δ) are reported using parts per million (ppm) with $CDCl_3$ (δ= 7.26 ppm for ^{1}H NMR and δ= 77.0 ppm for ^{13}C NMR) as an internal reference.

Preparation of nitrobenzene (1)

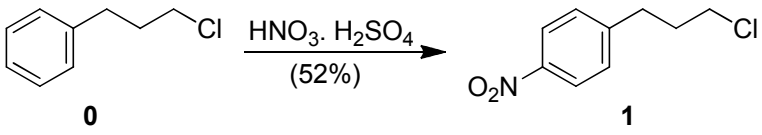

0 **1**

$C_9H_{10}ClNO_2$
199,63 g/mol

1-chloro-3-phenylpropane **0** (34.9 mmol, 5 mL) was placed in a flame-dried 100 mL round bottom flask and cooled to 0°C. A 1:1 mixture of concentrated nitric acid and sulfuric acid (20 mL) was slowly added. The reaction mixture was stirred for 4 hours and warmed to room temperature. The crude product was extracted using dichloromethane (50 mL), dried over Na_2SO_4, and the solvent was removed under reduced pressure. The crude product was purified using normal phase column chromatography (SiO_2; gradient 0 to 20% EtOAc in Hex) affording 3.6 g of the desired product as a colorless oil (18 mmol, 52% yield).

TLC (SiO_2, 8% EtOAc in Hex) *Rf* = 0.49 (UV)

^{1}H NMR (200 MHz, $CDCl_3$) δ = 8.17 (d, *J*=8.8, 2H), 7.37 (d, *J*=10.6, 2H), 3.54 (t, *J*=6.3, 2H), 2.98 – 2.84 (m, 2H), 2.13 (tt, *J*=13.1, 6.4, 2H).

Previously characterized: Baraldi, P., Cacciari,B., Romagnoli, R., Spalluto, G., Monopoli, A., Ongini, E., Varani, K., and Borea P. *J. Med. Chem.* 2002, 45, 115-126

Preparation of azobenzene (2)

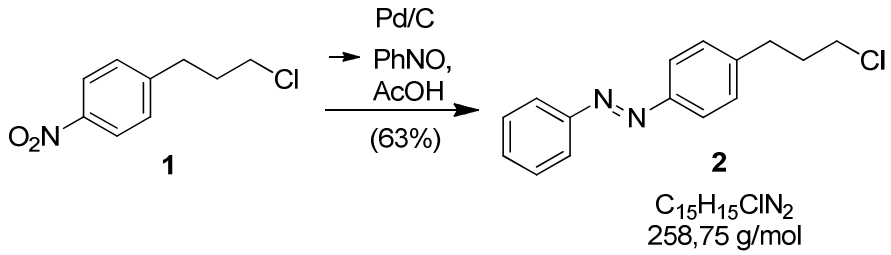

(i) Reduction

Nitrobenzene **1** (4.0 mmol, 0.800 g) was dissolved in methanol (64 mL) and acetic acid (16 mL) was added followed by ammonium formate (20 mmol, 1.28 g). The reaction mixture was stirred under nitrogen atmosphere at room temperature and then Pd/C (0.08 mmol, 0.112 g) was added. The reaction mixture was stirred for 4 hours or overnight, filtered through celite and concentrated to approximately 15 mL. This solution of the crude product was moved on directly to the next step.

(ii) Mills coupling

The crude methanolic aniline solution described above was added to a solution of acetic acid (16 mL) in dichloromethane (20 mL). Nitrosobenzene (4.0 mmol, 0.430 g) was added and the reaction mixture was stirred at room temperature overnight. After concentrating under reduced pressure, the crude product was diluted using ethyl acetate. The organic layer was washed with distilled water (2 x 15 mL), 1M HCl (2 x 15 mL), 1M NaOH (2 x 15 mL), and brine (20 mL), dried over Na_2SO_4, and the solvent was removed under reduced pressure. The crude product was purified using normal phase column chromatography (SiO_2; gradient 1 to 3% EtOAc in Hex). 650 mg (2.51 mmol, 63% yield) of an orange amorphous solid.

TLC (SiO_2, 5% EtOAc in Hex) *Rf* = 0.51 (UV and Vis)

IR: $\tilde{\nu}$ = 3063 (w), 2929 (w), 1601 (w), 1473 (s), 1437 (s), 1328 (w), 1299 (m), 1221 (w), 1154 (m) cm^{-1}.

^{1}H NMR (599 MHz, $CDCl_3$) δ = 7.93 – 7.84 (m, 4H), 7.55 – 7.45 (m, 3H), 7.37 – 7.33 (m, 2H), 3.56 (t, *J*=6.4, 2H), 2.89 – 2.85 (m, 2H), 2.14 (dt, *J*=14.8, 6.4, 2H).

^{13}C NMR (151 MHz, $CDCl_3$) δ = 152.68, 151.25, 144.11, 130.81, 129.24, 129.05, 123.03, 122.74, 44.05, 33.78, 32.63.

LRMS (ESI): m/z (M+H)+ 259.1. Calculated mass of C15H15ClN2 is 258.09.

Preparation of fotocaine

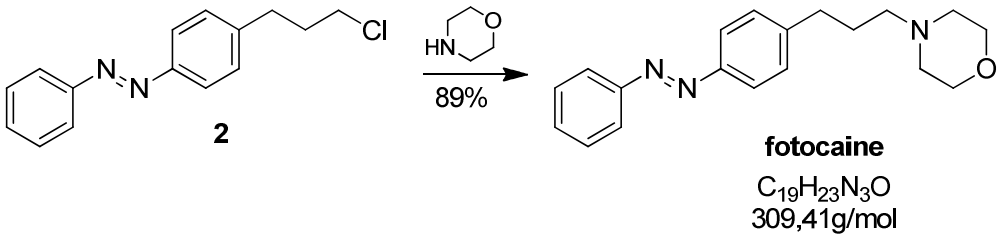

Azobenzene **2** (0.9 mmol, 0.233 g) was dissolved in acetonitrile (20 mL) and treated with morpholine (9 mmol, 0.776 mL) and diisopropylethylamine (13.5 mmol, 2.40 mL). The reaction mixture was stirred at reflux for 48 hours and then concentrated. The crude product was diluted using ethyl acetate. The organic layer was washed with distilled water, 1M NaOH, and brine, dried over Na_2SO_4, and the solvent was removed under reduced pressure. The crude product was purified using normal phase column chromatography (SiO_2; gradient 5 - 15% MeOH in CH_2Cl_2). 248 mg (0.8 mmol, 89% yield) of an orange amorphous solid.

TLC (SiO_2, 10% MeOH in DCM) *Rf* = 0.49 (UV and Vis)

IR: $\tilde{\nu}$ = 2944 (m), 2854 (m), 2807 (m), 1601 (w), 1499 (w), 1444 (m), 1358 (w), 1304 (w), 1274 (w), 1168 (s), 1070 (w) cm^{-1}.

^{1}H NMR (400 MHz, cdcl$_3$) δ = 7.93 – 7.80 (m, 4H), 7.54 – 7.41 (m, 3H), 7.35 – 7.28 (m, 2H), 3.77 – 3.69 (m, 4H), 2.76 – 2.68 (m, 2H), 2.48 – 2.41 (m, *J*=4.3, 4H), 2.41 – 2.34 (m, 2H), 1.86 (dt, *J*=15.1, 7.6, 2H).

^{13}C NMR (101 MHz, cdcl$_3$) δ = 152.69, 151.05, 145.53, 130.71, 129.08, 129.01, 122.89, 122.69, 66.91, 58.12, 53.65, 33.42, 27.92.

HRMS: m/z (M+H)+ 310.1916. Calculated mass of C19H23N3O is 309.1919.

Analytical Spectra[2]

^{1}H-NMR of **0**

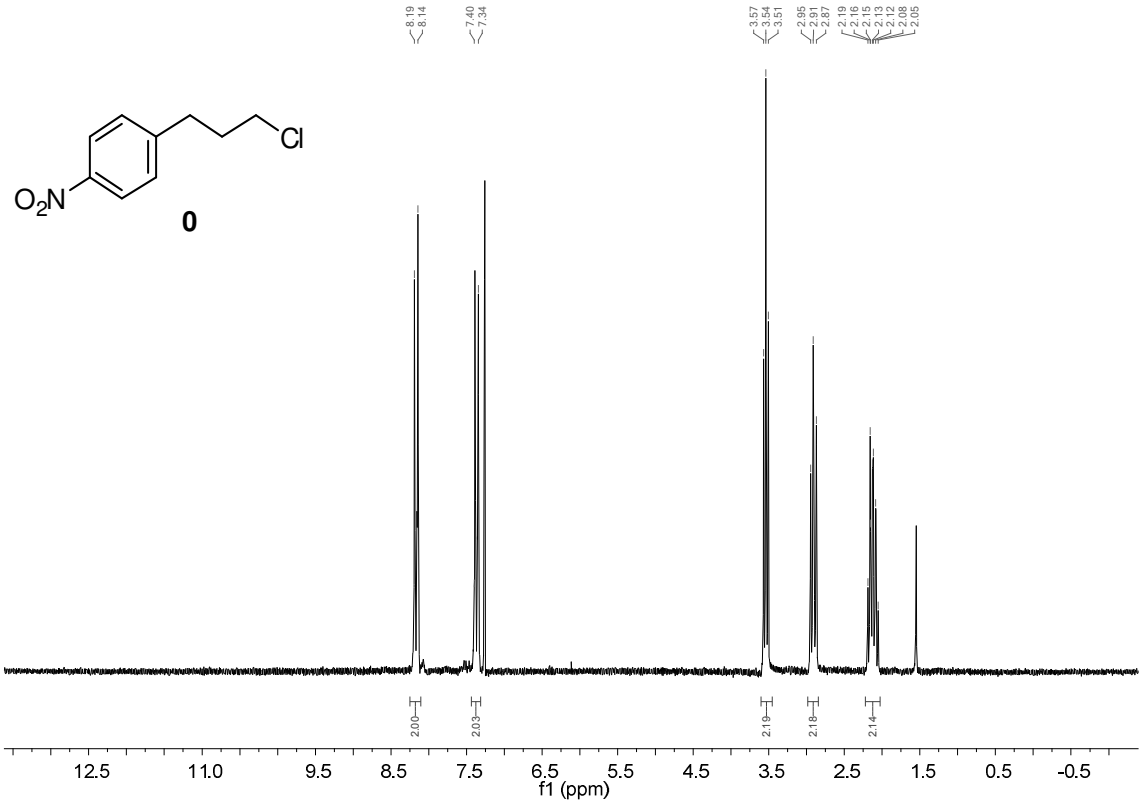

[2]NMR spectra of azobenzenes **2** and **fotocaine** contain signals of their corresponding *cis*-isomers ("mirrored" peaks, slightly from the major *trans*-signals). This is a common observation and those peaks were not included in integration or peak list.

^{1}H-NMR of **2**

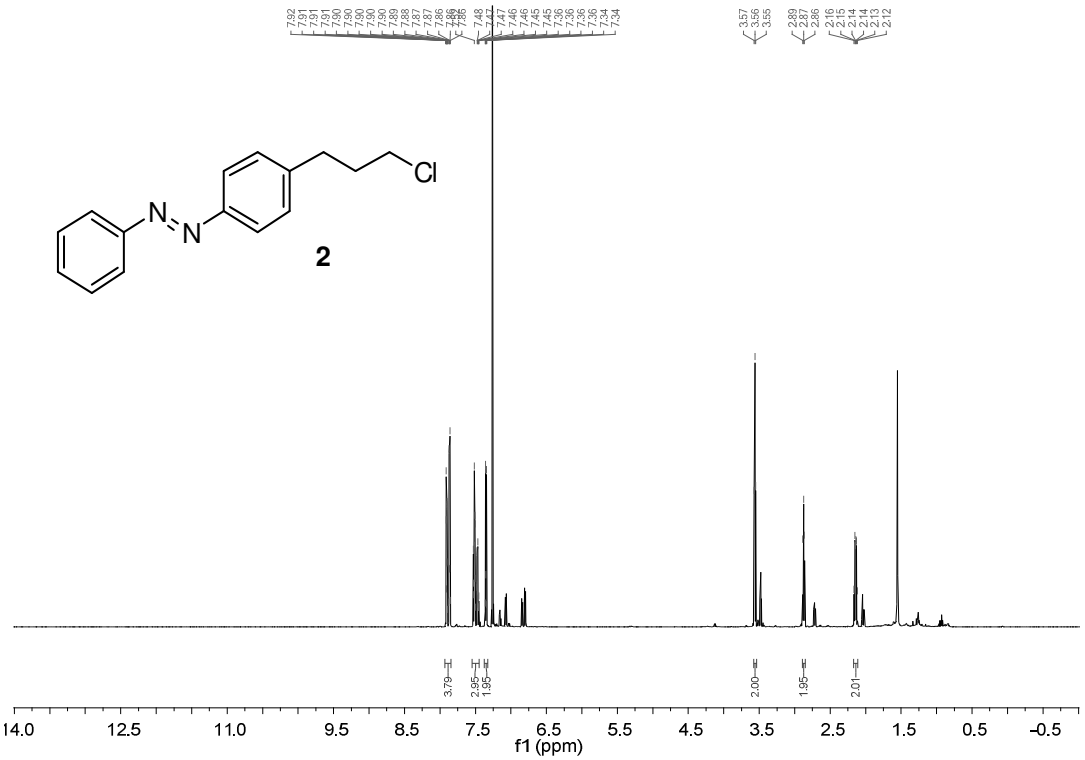

^{13}C-NMR **2**

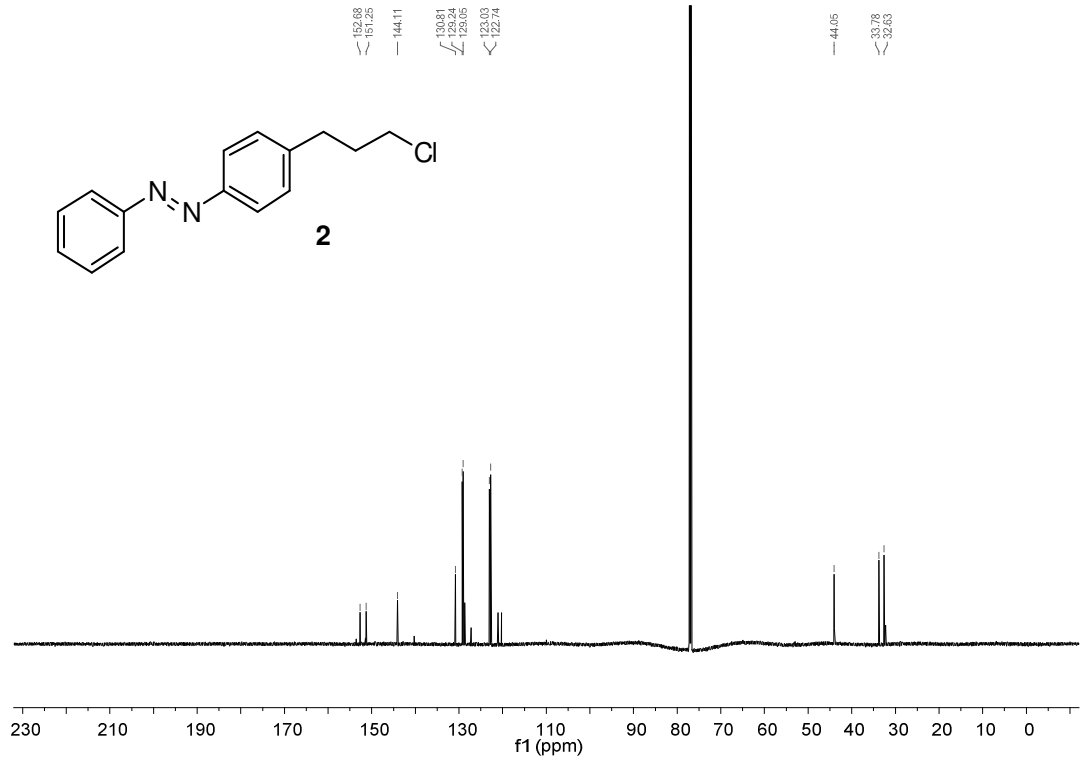

^{1}H-NMR of **fotocaine**

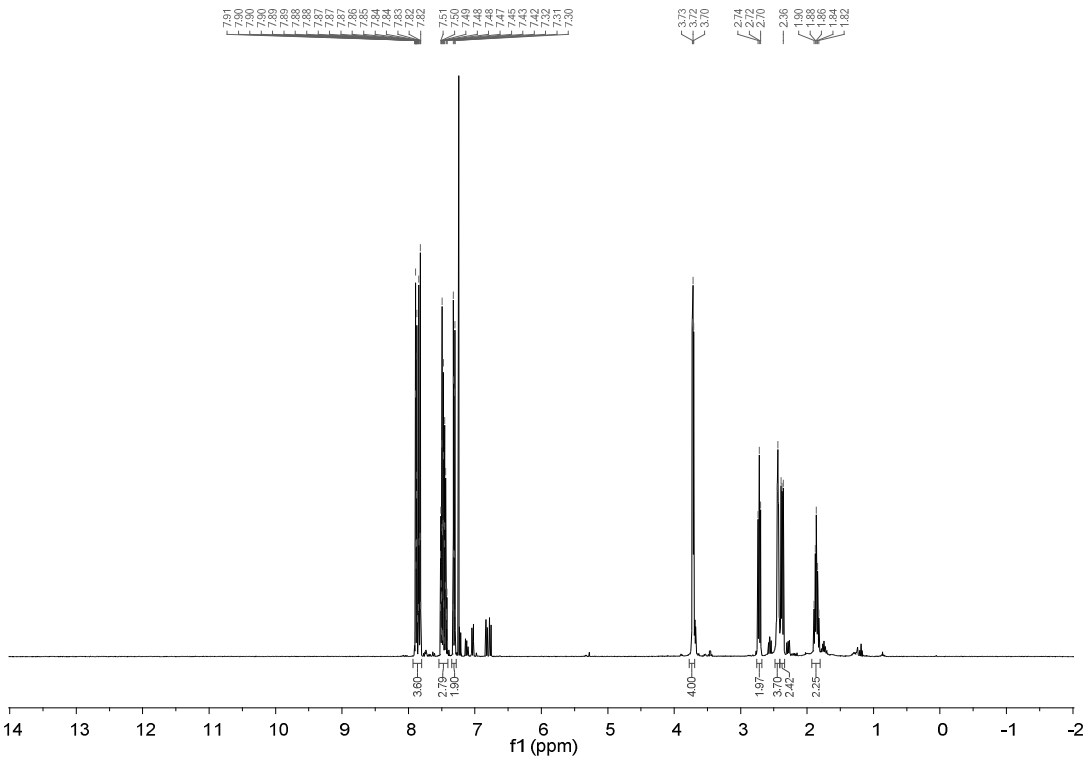

^{13}C-NMR **fotocaine**

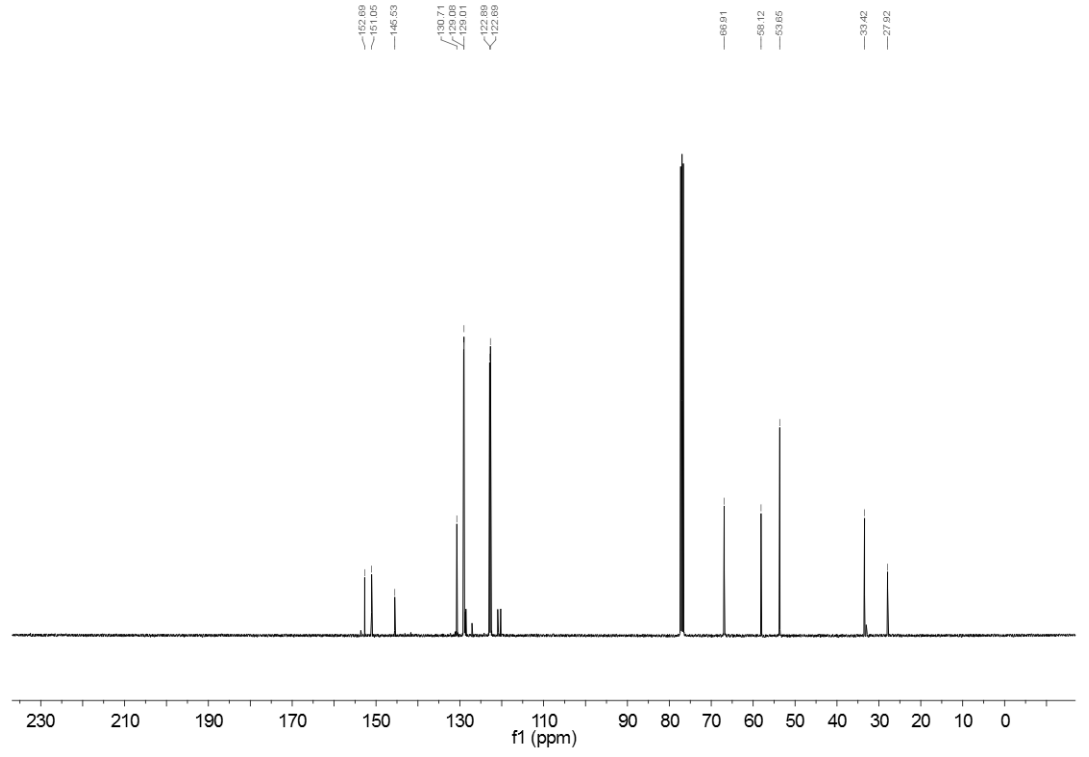

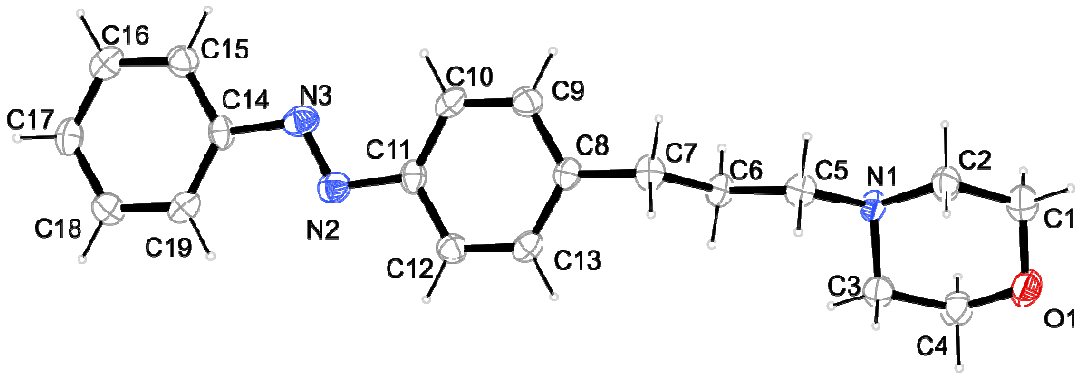

Crystallographic data. **fotocaine**

	fotocaine
net formula	$C_{19}H_{23}N_3O$
M_r/g mol^{-1}	309.406
crystal size/mm	0.211 × 0.189 × 0.014
T/K	173(2)
radiation	'Mo Kα
diffractometer	'Bruker D8Quest'
crystal system	monoclinic
space group	$P2_1/c$
a/Å	29.621(4)
b/Å	4.8529(7)
c/Å	11.3696(16)
α/°	90
β/°	94.356(3)
γ/°	90
V/Å^3	1629.6(4)
Z	4
calc. density/g cm^{-3}	1.2611(3)
μ/mm^{-1}	0.080
absorption correction	multi-scan
transmission factor range	0.8937–0.9580
refls. measured	18433
R_{int}	0.0796
mean σ(I)/I	0.0777
θ range	2.76–25.44
observed refls.	1722
x, y (weighting scheme)	0.0430, 0.0696
hydrogen refinement	constr
refls in refinement	2986
parameters	208
restraints	0
$R(F_{obs})$	0.0516
$R_w(F^2)$	0.1046
S	1.017
shift/error$_{max}$	0.001
max electron density/e Å^{-3}	0.205
min electron density/e Å^{-3}	–0.224

V

A Photochromic Agonist for μOpioid Receptors

Matthias Schönberger, and Dirk Trauner

Department of Chemistry, Ludwig-Maximilians-Universität, and Center for Integrated Protein Science, 81377 Munich, Germany.

Photofentanyl-1 is a photochromic version of the well-known analgesic fentanyl. It is a potent agonist in the dark (or when illuminated with blue light) and looses activity when irradiated with UV light. It can be used to optically control the μ-opioid receptor, converting a G-protein coupled receptor (GPCR) into a photoreceptor. As such, it represents a potentially general strategy to convert family A GPCRs, other than the rhodopsins, into photoreceptors

Content

Introduction

Opioids have a long cultural and medicinal history and belong to the most useful drugs available to humanity. Their best-known member, morphine, has been employed since antiquity to alleviate pain and induce euphoria (Fig. 1A).[1, 2] With the advent of modern organic chemistry, many synthetic or semisynthetic opioids, such as fentanyl, became available, some of which enabled the pharmacological discrimination of receptor subtypes.[3, 4] Subsequently, these transmembrane proteins were systematically explored through molecular cloning. Today, four human opioid receptor (OR) subtypes, *viz.* δ, μ, κ and NOP, are known, all of which have been recently characterized by X-ray crystallography.[5-10] The X-ray structure of a μ–opioid receptor (MOR) in conjunction with the covalently bound antagonist β-funaltrexamine provided insights into how morphine and its derivatives bind and helped explain some of the structure-activity data accumulated over decades (Fig. 1).

Results and Discussion

Opioid receptors belong to the Family A of G-protein coupled receptors (GPCRs), which includes many important drug targets.[11-13] GPCRs of this type are closely related to the rhodopsin photoreceptors, which enable vision and shape the circadian rhythm in humans.[14] The MOR is the major target of morphine and is endogenously activated by small peptides, such as Leu-enkephaline (LE), β-endorphin and the dynorphins.[15, 16] Upon binding of an agonist, it catalyzes the dissociation of a heterotrimeric $G_{i/o}$–protein into $G_{\alpha i}$ and $G_{\beta\gamma}$ subunits (Fig. 1B). The former inhibits adenylyl cyclase, resulting in decreased cAMP levels, and the latter activates G-protein-coupled-inward-rectifying potassium (GIRK) cannels.[17] Both actions translate into hyperpolarization and decreased neuronal excitability.[15, 18]

Given the importance of opioids in medicine and their role in drug abuse, the development of new agonists and antagonists for ORs continues to be a very active field. One important goal, for instance, is to untangle the analgesic properties of

opioids form their euphoric and addictive side effects. Another goal is to take advantage of the high precision light provides to elucidate the biological function of endogenous opioids and their receptors. Recently, photocaged versions of the enkephalins have been used to gain insight into the spatiotemporal scale at which neuropeptides act in the brain.[19] A caged version of the antagonist naloxone has been employed to reveal opioid deactivation kinetics.[20] To date, however, photoswitchable versions of opioids, i.e. compounds that can reversibly turned on and off with light, have not been described. We now introduce an azobenzene derivative of the potent OR-agonist fentanyl that can be used to optically control MOR in a reversible fashion.[21]

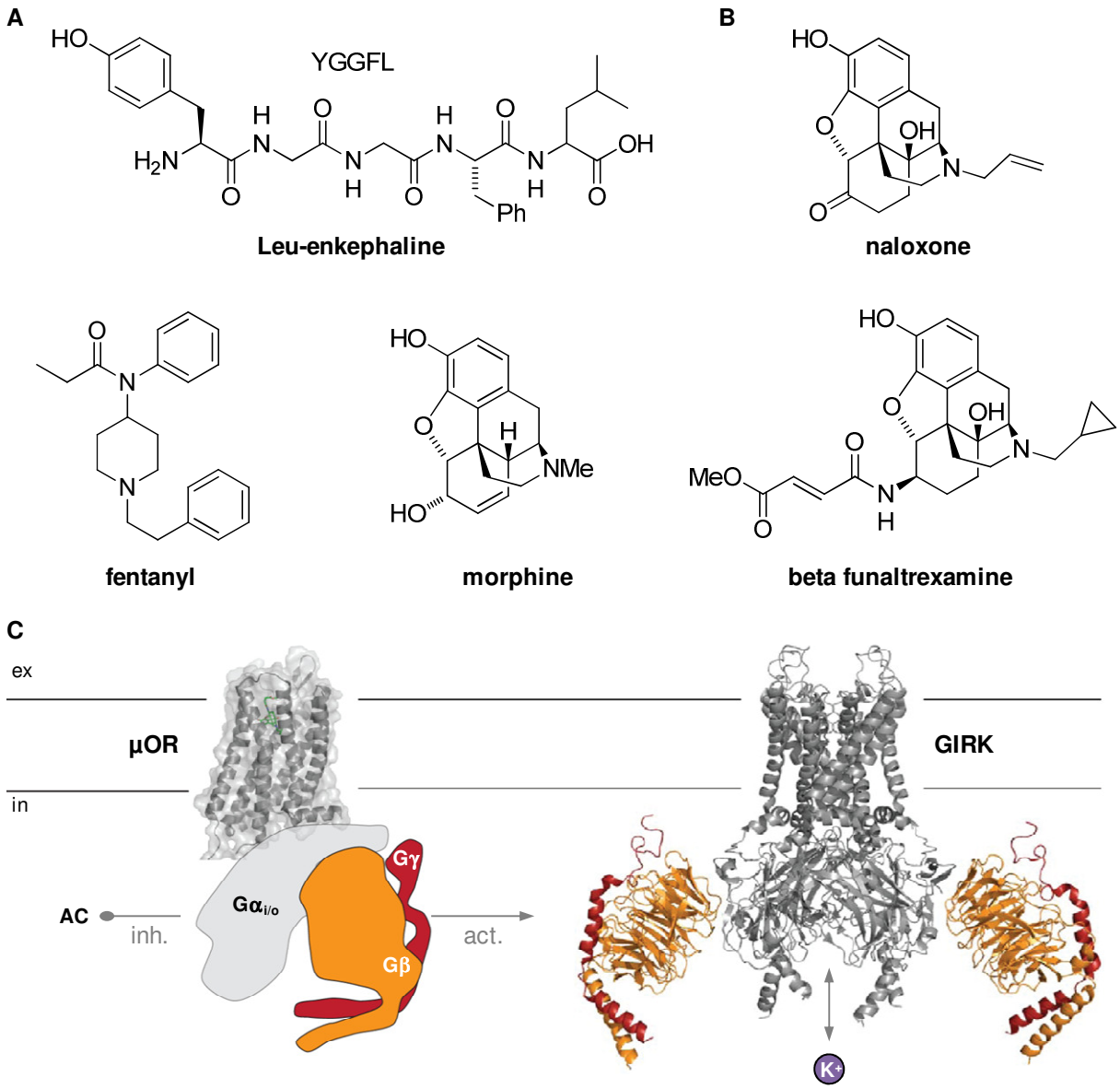

Figure 1. μ-Opioid (MOR) receptor pharmacology, structure, and function. A) MOR ligands. Beta funaltrexamine is a covalently bound agonist. Its binding mode is shown from the extracellular side below its molecular formula. Leu-enkephaline is an endogenous ligand, whereas morphine and fentanyl is a naturally occurring and synthetic agonist, respectively. B) Functional features of MOR. When activated by agonists, MOR acts as a nucleotide exchange factor on heterotrimeric $G_{i/o}$ G-proteins, which results in dissociation of the G_{α} and $G_{\beta\gamma}$ subunits. While G_{α} has an inhibitory effect on the adenylyl cyclase (AC), the $G_{\beta\gamma}$ complex activates G-protein coupled inward rectifying potassium channels (GIRK channels). Both modes lead to decreased neuronal activity.

Although derivatives of morphine were initially considered,[22, 23] fentanyl was ultimately chosen as a platform for the design of our photochromic ligands. This was due to its potency, its relatively simple structure, and the presence of two aryl rings that could be extended to azobenzene photoswitches. As in the design of other photochromic ligands (PCLs), the photoswitch had to be installed in such a fashion that the biological activity of the ligand was not completely abrogated, whilst aiming for a maximum change of its efficacy upon photoisomerization.[21] Scheme 1 shows the structure of two candidates, photofentanyl 1 (**PF1**) and photofentanyl 2 (**PF2**), which we designed, synthesized and evaluated for their biological activities.

Our synthesis of **PF1** started from commercially available *N*-benzyl piperidone **1**, which underwent reductive amination with aniline, followed by acylation and deprotection to yield piperidine **2** (Scheme 1 and Supporting Information). Reductive amination with azobenzene aldehyde **3**[24] then provided **PF1**. The synthesis of **PF2** started from commercially available *N*-Boc piperidone **5**, which underwent reductive amination with 4-amino azobenzene **4** to afford 4-amino piperidine **6**. Acylation using propionic acid anhydride then gave access to propionamide **7**. Finally, deprotection under acidic conditions, followed by reductive amination of the resulting piperidine **8** with phenyl acetaldehyde gave **PF2**.

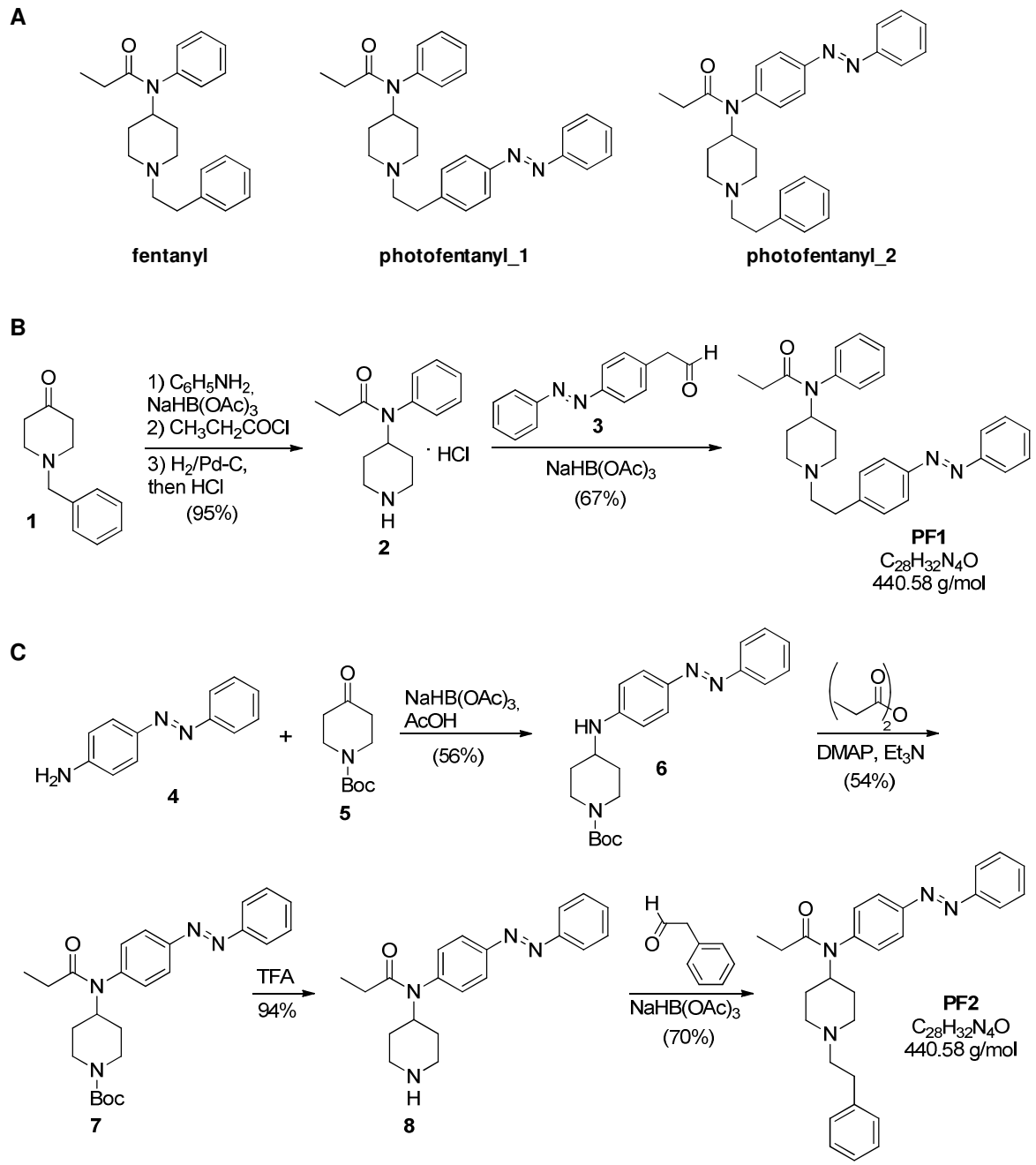

Scheme 1. PCL design and synthesis. A) The known synthetic opiate fentanyl was used as a platform for photochromic MOR agonists **PF1** and **PF2**. B) Synthesis of **PF1** started from *N*-benzyl piperidone **1**, which was reductively amminated, N-propionated, deprotected and reductively amminated with aldehyde **3**. C) Synthesis of PF2 opened with a reductive amination followed by propionation, deprotection and another reductive amination.

Preliminary pharmacological testing showed that **PF2** is an excellent μOR agonist. **PF1**, on the other hand, lacked MOR agonism at all concentrations. We therefore decided to focus on **PF2** for further physical and biological characterization.

Using UV/VIS spectroscopy, we first determined that **PF2** has all the hallmarks of a "regular" azobenzene (Fig. 2). As shown in Figure 2A, the π→π* and n→π* transitions

are well separated, allowing for clean photoswitching upon irradiation with 420 nm and 340 nm respectively (Fig. S1). **PF2** in its *cis* form was also found to be thermally stable in Ringer solution (Fig. 2B). After allowing to relax in the dark for 90 min, no back-isomerization to *trans* was detected. This feature might be helpful in physiological or pharmacological experiments were prolonged illumination times might be undesired.

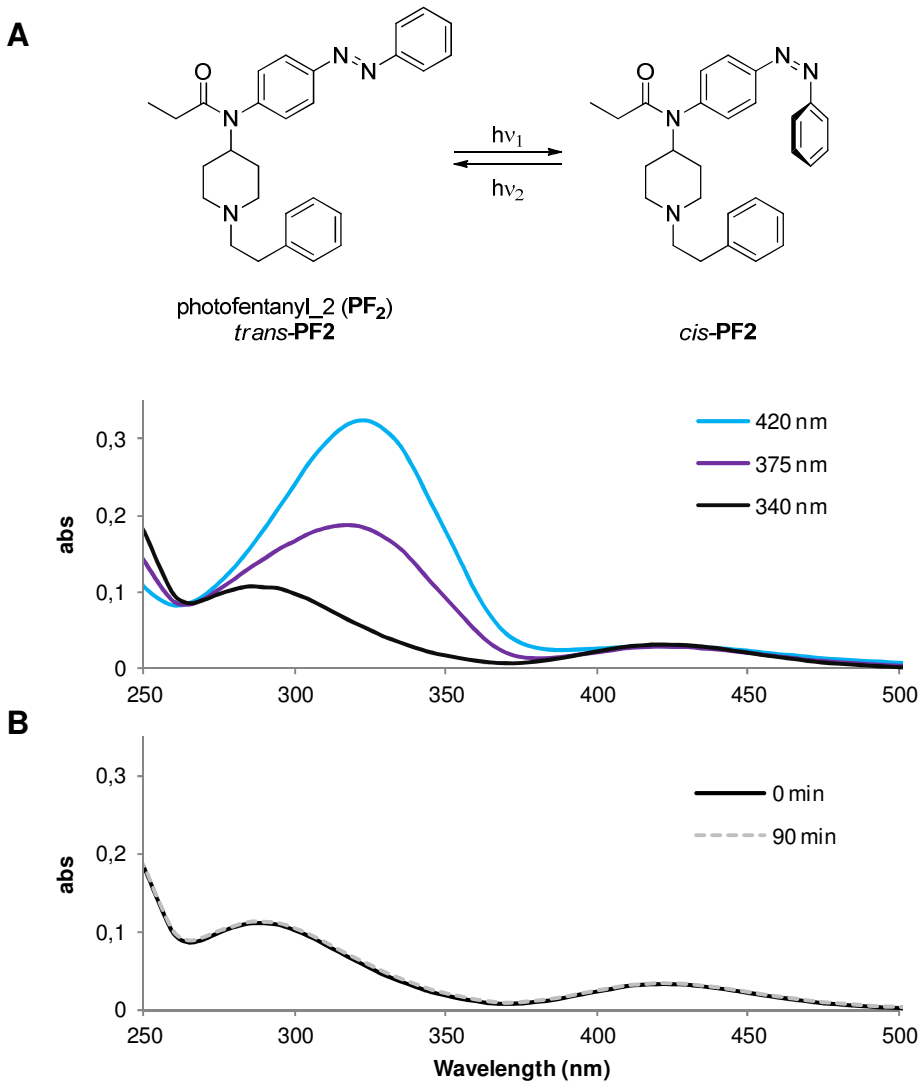

Figure 2. Photoswitching and thermal stability of PFII. A) Light induced isomerization can be followed by UV/Vis spectroscopy. Illumination of a 50 µM PF2 solution in Ringer with different wavelengths leads to distinct absorption spectra. B) A solution of PF2 that was previously switched to *cis* stays at this state over hours.

We next turned our attention to the functional characterization of **PF2**. Although GPCRs can be assayed with a variety of methods, we decided to use electrophysiology, due to its compatibility with optical stimulation protocols (Fig. 3).[26] To this end, human MOR was transiently transfected into HEK293t cells together with the G-protein coupled inward rectifier channels GIRK1 and GIRK2.[17] These channels are typical effectors in Gi/o signaling and native signaling partner of MORs in the locus coeruleus.[18, 27] Upon testing several concentrations, we found that 25 μM **PF2** gave optimal results for photoswitching. As shown in Figure 3A, *trans*-**PF2**, which predominates in the dark or at 420 - 480 nm, acts as an effective agonist of MOR. By contrast, *cis*-**PF2** which predominates at 360 nm, is much less active. As a consequence, switching from 360 nm to blue light immediately triggers a potassium influx by the action of GIRK channels (high external potassium concentrations were applied). This process can be terminated by switching back to 360 nm light, which stops MOR activation. Thus GIRK currents cease as βγ-G-proteins re-associate with inactive GDP bound $G_{\alpha i/o}$ subunits. Interestingly, GIRK currents evoked by 360 nm through the action of **PF2** maintain at a plateau and do not sensitize as is the case for certain GPCRs and respective agonists.[17]

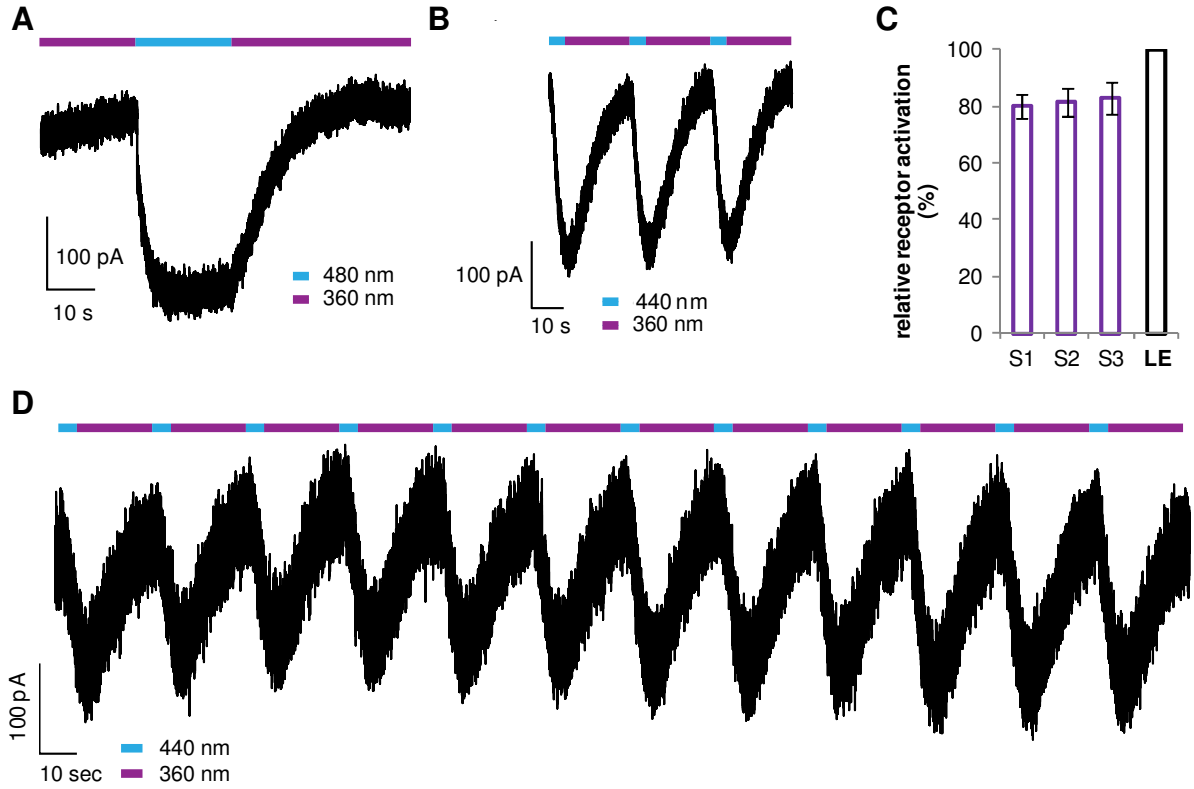

Figure 3. Light-dependent activation of MOR by **PF2** . HEK293t cells were transiently transfected with the human MOR and both GIRK1 and GIRK2 channels. A) Illuminating a 25 µM solution of **PF2** with 360 nm light keeps the system in an inactivated state. Switching to 480 nm quickly activates the receptor. B) Rapid, repeated photoactivation of GIRK by action of MOR and **PF2**. C) Comparison of photocurrents (consecutive stimulation with a 10 µM solution of the native agonist LE (n = 11, one error bar indicates ± SEM). D) Photoswitching can be repeated over many cycles without noticeable decrease in photocurrent.

The nature of azobenzene based PCLs allows for multiple repetition of this process at a timescale that is dictated by the illumination protocol. For example, photocurrents can be evoked by switching from 360 to 440 nm and stopped immediately after reaching the maximal current amplitude by illuminating with 360 nm. Comparison between photocurrents of three such consecutive fast switching cycles and subsequent activation of the same cell with saturating concentration of **LE** revealed that **PF2** is an excellent photoswitch (Fig. 3B, C). First, there was no decrease in overall photocurrents within a switching cycle despite rapid, consecutive activation (Fig. 3B). In fact, photoactivation could be repeated for a arbitrary number of times demonstrating the stability of the disclosed system, (Fig 3D). Second, the magnitude of **PF2** induced photocurrents was in average 80 % of the full **LE** response (Fig. 3C and S2). Since **PF2** acts as a "*trans*-agonist", the pharmacologically active isomer is, at the same time, the

thermodynamically more stable one. Therefore, a broad range of wavelengths can be applied to induce MOR agonism with light as shown in the action spectrum of **PF2** (Fig. S1). Switching between 360 nm and wavelengths between 400 and 500 nm leads to rapid and reliable photoactivation allowing for user-friendly application with comparatively simple light sources. In addition, exposure to 360 nm light can be kept at a minimum as **PF2** provides thermal stability not only in solution (Fig. 2B), but also during the pharmacological experiment (Fig. S3). In general, activation and deactivation occurred at timescales that can be expected for a metabotropic receptor.[26] As azobenzene photoswitching is known to occur on ms timescale or faster[21] and MOR ligands dissociate rapidly,[19] it can be assumed that the rate limiting step for the presented read out is the signaling cascade between MOR and GIRK by the action of G-proteins. As such, PF2 provides the first optical tool allowing precise and repeated photoactivation of native MORs. The combination of a broad activation spectrum and thermal stability further add to its applicability.

Recently, we described photochromic tethered ligands (PTLs) that are covalently attached to Family C GPCRs, *viz*. metabotropic glutamate receptors.[26] This system, termed LimGluR, was used to effectively control neuronal excitability with light. Our new results described herein should enable the extension of this concept to family A GPCRs. These "LiGPCRs" could provide a valuable alternative to genetically encodable light-sensitive GPCRs (Opto-XRs), which are based on a fusion of rhodopsin with other Family A GPCRs. [25]

Summary and Outlook

In conclusion, we have developed a method to optically control MORs with a photochromic ligand, **PF2**. In a sense, our PCL imparts the logic of rhodopsin onto a light-insensitive family A GPCR. Rhodopsin is a member of this transmembrane protein family that uses retinal as covalently bound photoswitchable inverse agonist. Our work outlines a potentially general chemical strategy to turn other members of Family A GPCRs, such as dopamine receptors or adrenergic receptors, into photoreceptors, laying the foundation for a photopharmacology of these targets. **PF2** itself could be used to investigate the role of ORs in various parts of the brain and the periphery in a precise spatiotemporal fashion. Its application in neuroscience as well as its potential use as a "photoanalgesic" is currently under investigation and will be disclosed in due course.

Acknowledgements

We thank Dr. Matthew Banghart (Harvard University) for assistance with the pharmacological testing of **PF2** and for helpful discussions. M. S. is grateful to the Studienstiftung des Deutschen Volkes for a Ph.D. fellowship. This work was supported by the European Science Foundation (ERC grant No 268795 to D.T.).

Literature

[1] H. Kalant, *Addiction* **1997**, *92*, 267.

[2] C. B. Pert, S. H. Snyder, *Science* **1973**, *179*, 1011.

[3] W. F. Simonds, *Endocr Rev* **1988**, *9*, 200.

[4] Y. S. Lee, J. Nyberg, S. Moye, R. S. Agnes, P. Davis, S. W. Ma, J. Lai, F. Porreca, R. Vardanyan, V. J. Hruby, *Bioorg Med Chem Lett* **2007**, *17*, 2161.

[5] P. L. Wood, *Neuropharmacology* **1982**, *21*, 487.

[6] M. Filizola, L. A. Devi, *Nature*, *485*, 314.

[7] S. Granier, A. Manglik, A. C. Kruse, T. S. Kobilka, F. S. Thian, W. I. Weis, B. K. Kobilka, *Nature*, *485*, 400.

[8] A. Manglik, A. C. Kruse, T. S. Kobilka, F. S. Thian, J. M. Mathiesen, R. K. Sunahara, L. Pardo, W. I. Weis, B. K. Kobilka, S. Granier, *Nature*, *485*, 321.

[9] A. A. Thompson, W. Liu, E. Chun, V. Katritch, H. Wu, E. Vardy, X. P. Huang, C. Trapella, R. Guerrini, G. Calo, B. L. Roth, V. Cherezov, R. C. Stevens, *Nature*, *485*, 395.

[10] H. Wu, D. Wacker, M. Mileni, V. Katritch, G. W. Han, E. Vardy, W. Liu, A. A. Thompson, X. P. Huang, F. I. Carroll, S. W. Mascarella, R. B. Westkaemper, P. D. Mosier, B. L. Roth, V. Cherezov, R. C. Stevens, *Nature*, *485*, 327.

[11] R. Fredriksson, H. B. Schioth, *Mol Pharmacol* **2005**, *67*, 1414.

[12] M. C. Lagerstrom, H. B. Schioth, *Nat Rev Drug Discov* **2008**, *7*, 339.

[13] K. L. Pierce, R. T. Premont, R. J. Lefkowitz, *Nat Rev Mol Cell Biol* **2002**, *3*, 639.

[14] K. P. Hofmann, P. Scheerer, P. W. Hildebrand, H. W. Choe, J. H. Park, M. Heck, O. P. Ernst, *Trends Biochem Sci* **2009**, *34*, 540.

[15] M. Connor, M. J. Christie, *Clinical and Experimental Pharmacology and Physiology* **1999**, *26*, 493.

[16] H. H. Loh, A. P. Smith, *Annu Rev Pharmacol Toxicol* **1990**, *30*, 123.

[17] E. A. Johnson, S. Oldfield, E. Braksator, A. Gonzalez-Cuello, D. Couch, K. J. Hall, S. J. Mundell, C. P. Bailey, E. Kelly, G. Henderson, *Molecular Pharmacology* **2006**, *70*, 676.

[18] R. A. North, J. T. Williams, A. Surprenant, M. J. Christie, *Proc Natl Acad Sci U S A* **1987**, *84*, 5487.

[19] M. R. Banghart, B. L. Sabatini, *Neuron*, *73*, 249.

[20] M. R. Banghart, J. T. Williams, R. C. Shah, L. D. Lavis, B. L. Sabatini, *Molecular Pharmacology*, *84*, 687.

[21] T. Fehrentz, M. Schonberger, D. Trauner, *Angew Chem Int Ed Engl*, *50*, 12156.

[22] J. Mulzer, G. Dürner, D. Trauner, *Angewandte Chemie* **1996**, *108*, 3046.

[23] G. W. Kirby, *Science* **1967**, *155*, 170.

[24] H. Muxfeldt, W. Rogalski, G. Klauenberg, *Chemische Berichte* **1965**, *98*, 3040.

[25] R. D. Airan, K. R. Thompson, L. E. Fenno, H. Bernstein, K. Deisseroth, Nature 2009, 458, 1025.

[26] J. Levitz, C. Pantoja, B. Gaub, H. Janovjak, A. Reiner, A. Hoagland, D. Schoppik, B. Kane, P. Stawski, A. F. Schier, D. Trauner, E. Y. Isacoff, *Nat Neurosci*, *16*, 507.

[27] R. Sadja, N. Alagem, E. Reuveny, *Neuron* **2003**, *39*, 9.

V.i

Supporting Information

to

A Photochromic Agonist for the μ-Opioid Receptor

Matthias Schönberger, and Dirk Trauner

Department of Chemistry, Ludwig-Maximilians-Universität, and Center for Integrated Protein Science, 81377 Munich, Germany.

Additional Photoswitching Experiments

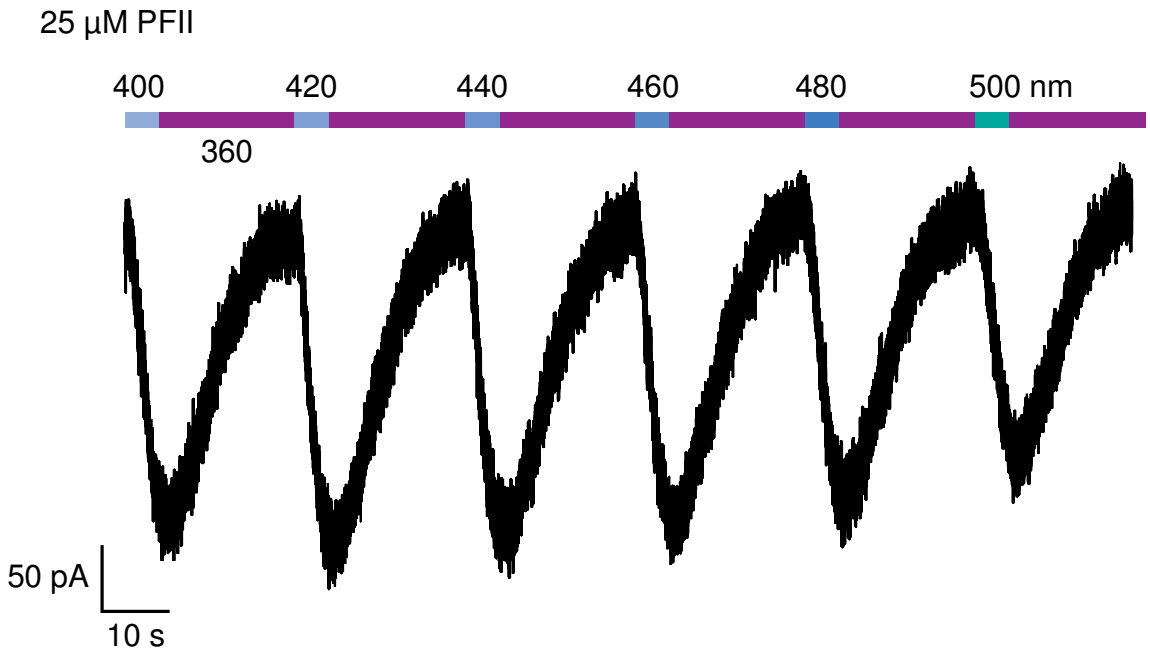

Figure S1. Action spectrum of **PF2**. At the electrophysiological setup, 360 nm gave the best results for switching to *cis*-**PF2**. As for switching to the active *trans*-state, wavelengths between 420 and 480 nm gave optimal results. (HEK293t cells transiently transfected with hµOR, GIRK1/2 and YFP).

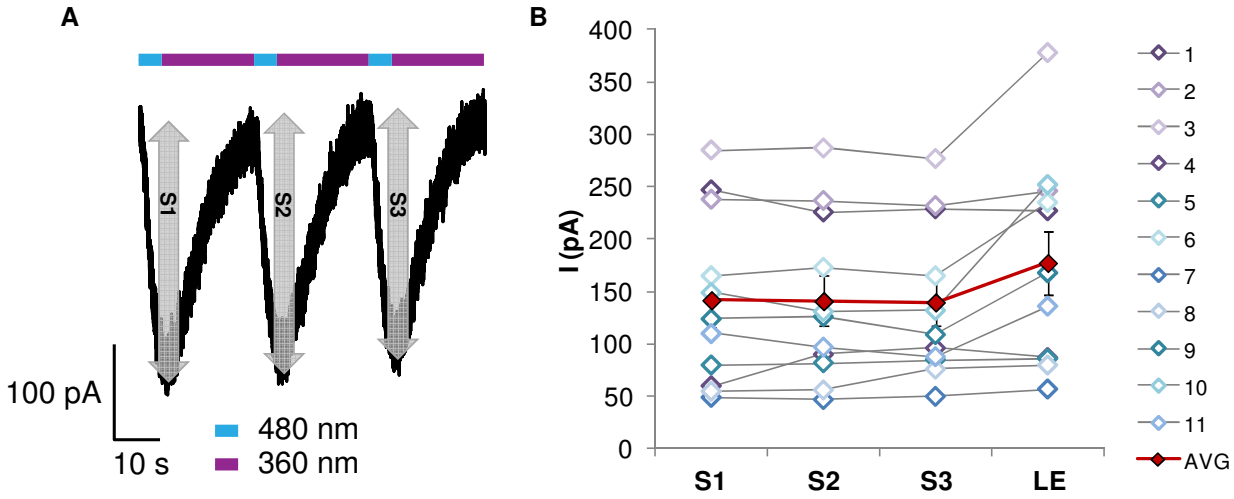

Figure S2. PF2-photoswitching compared to LE activation. A) HEK293t cells transiently transfected with hµOR, GIRK1/2 and YFP were treated with 10 µM PF2 and switched for three consecutive cycles. B) The same cell was then perfused with bath solution until PF2 was washed out and 10 µM LE were applied. Comparison between the overall LE-current to photocurrents S1-3 is shown for 11 cells.

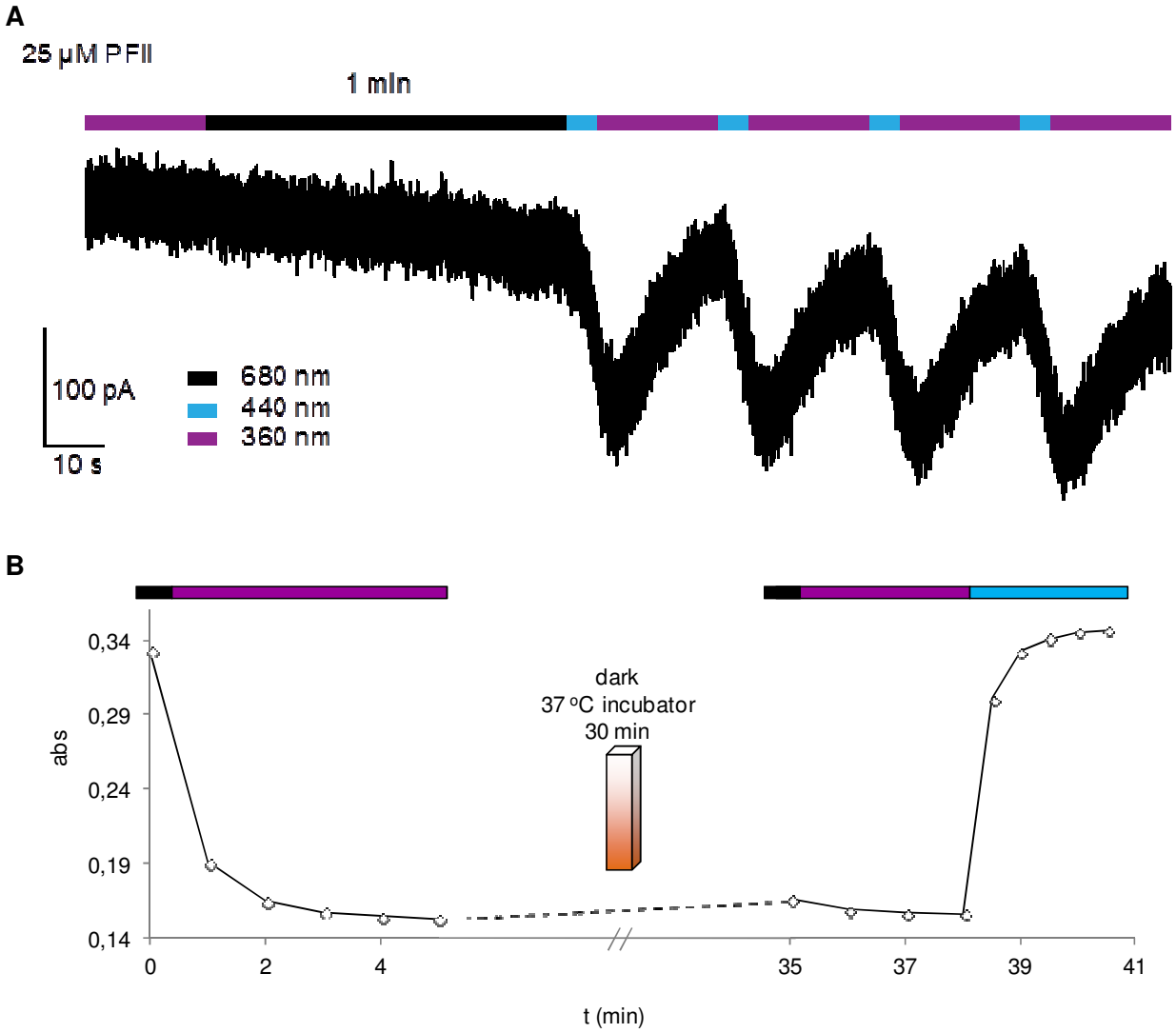

Figure S3. Thermal stability of *cis*-**PF2**. A) Patch Clamp Recordings. After switching to "cis" using 360 nm illumination, PF2 remains in the thermodynamically less stable state. Consecutive photoswitching can occur by alternating between 360 nm and blue light. This feature is beneficial as illumination times with near-UV light can be minimized. (HEK293t cells transiently transfected with hµOR, GIRK1/2 and YFP). B) UV/Vis spectroscopy. A 25 µM solution of **PF2** in extracellular recording buffer was switched to *cis* using 360 nm light. The cis-contend was nearly unchanged after 30 min incubation at 37 °C.

Experimental Procedures

Cell culture and electrophysiology. HEK293t cells were incubated in dulbeco´s minimal essential medium + 10% FBS and splitted at 80 to 90% confluency. For detachment, growth medium was removed, cells were washed with calcium free PBS buffer and cells were treated with trypsin solution at 37 °C for 2 min. Detached cells were diluted with growth medium and singularized by pipetting. For transfection, acid-etched coverslips were coated with poly-*L*-lysin and placed in a 24-well plate. 50.000 cells were added to each well in 500 µL standard growths medium. DNA (per coverslip: 50 ng hµOR, 450 ng GIRK1/2 and 50 ng YFP) was mixed with 1 µL polyplus jetprime in 50 µL jetprime buffer. After standing at room temperature for 10-15 min, the DNA-mix was added to the cells shortly after seeding them into the abovementioned 24-well-plate. After 3-5 hours, medium was exchanged for standard growth medium. Cells were used for electrophysiological recordings 24 to 72 hours post transfection.

Whole cell patch clamp experiments were performed using a standard electrophysiology setup equipped with a HEKA Patch Clamp EPC10 USB amplifier and patch master software. Micropipettes were generated from "Science Products GB200-F-8P with filament" pipettes using a vertical puller. Resistance varied between 5-7 MΩ. Bath solution contained in mM: 140 KCl, 2.6 $CaCl_2$, 1.2 $MgCl_2$, 5 HEPES (KOH to pH 7.4). Pipette solution contained in mM: 107 KCl, 1.2 $MgCl_2$, 1 $CaCl_2$, 10 EGTA, 5 HEPES, 2 MgATP, 0.3 Na_2GTP (KOH to pH 7.2).[3]

Photoswitchable ligands and reference agonist were dissolved in bath solution from a 1000 x DMSO stock.

Irradiation during electrophysiology and UV/Vis experiments was performed using a TILL Photonics Polychrome 5000 monochromator.

[3] J. L. Leaney, A. Benians, S. Brown, M. Nobles, D. Kelly, A. Tinker, *Am J Physiol Cell Physiol* **2004**, *287*, C182.

Chemicals and Instrumentation

Commercially available materials were used without further purification. Solvents such as ethyl acetate, methanol, dichloromethane and hexane were distilled prior to use.

Abbreviations

DCM	Dichloromethane
DMP	Dess Martin Periodinane
DCE	Dichloroethane
DIPEA	Diisopropylethylamine
TEA	Triethylamine
TFA	Trifluoroacetic acid
TLC	Thinlayer chromatography

Chemical syntheses

PHOTO-FENTANYL-I

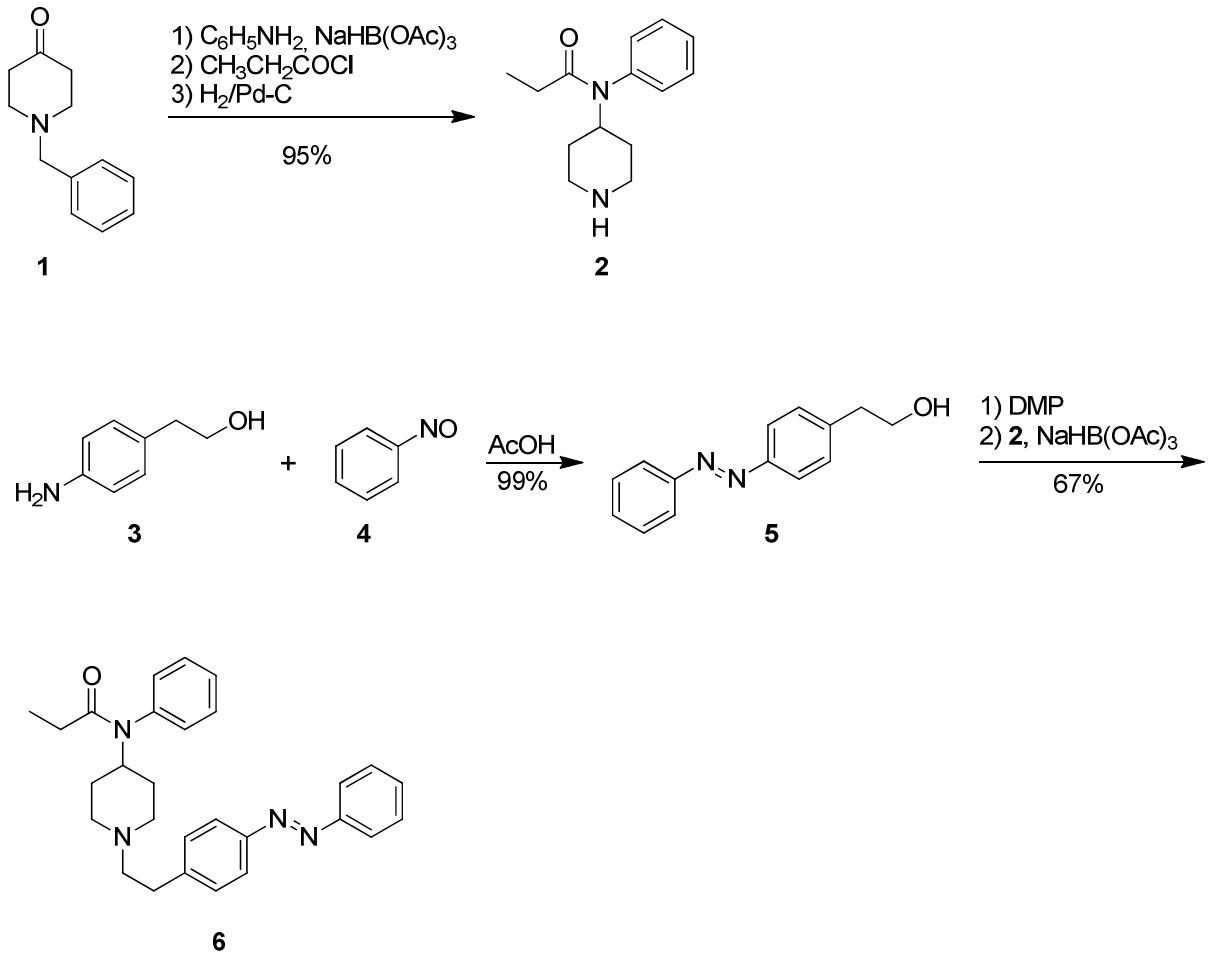

Scheme 1. Photo-Fentanyl-I synthesis.

Aminopiperidine 2

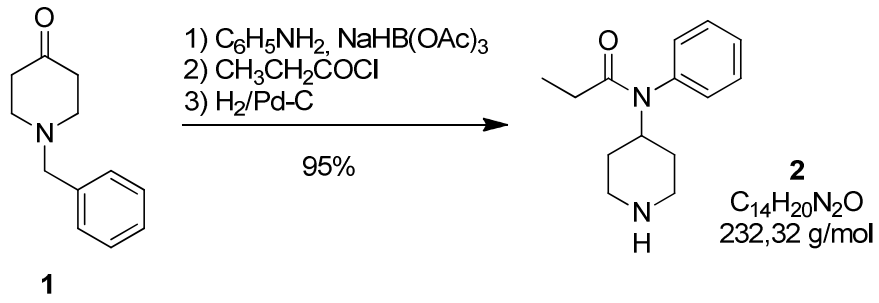

The synthesis of aminopiperidine **2** was based on a procedure reported in the literature and conducted with minor changes.[4] (stored as HCl salt)

TLC (90% CH_2Cl_2, 10% MeOH +1% Et_3N) *Rf* = 0.25 (UV + ninhydrine)
^{1}H-NMR (200 MHz, DMSO-d^6): δ = 7.47 - 7.44 (m, 3H), 7.21 - 7.17 (m, 2H), 4.59 – 4.44 (m, 1H), 2.92 - 2.86 (m, 2H), 1.80 (q, *J* = 7.5 Hz, 2H), 1.66 - 1.61 (m, 2H), 1.08 (m, 2H), 0.87 (t, *J* = 7.4 Hz, 3H).

Phenethylalcohol 5

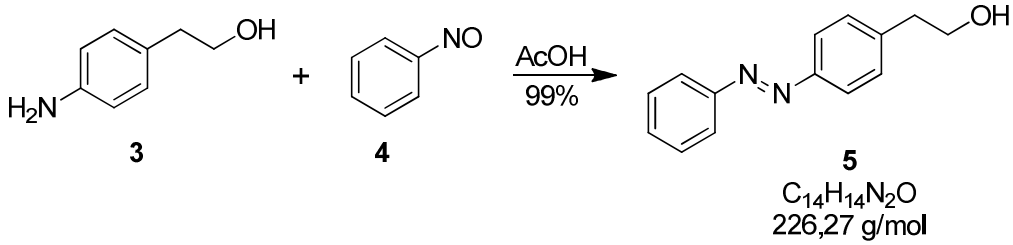

4-Aminophenethylalcohol **3** (0.647 g, 4.91 mmol, 1.0 eq) and nitrosobenzene **4** (0.526 g, 4.91 mmol, 1.0 eq) were dissolved in dichloromethane (10 mL) and treated with acetic acid (1.50 mL, 26.2 mmol, 5.42 eq). The reaction mixture was stirred for overnight, diluted with EtOAc and washed with 1 M HCl (2 x 25 mL), 1 M NaOH (2 x 25 mL) and brine (2 x 25 mL). The organic layer was separated, dried over Na_2SO_4 and concentrated using rotary evaporation yielding the title compound **5** as an orange powder (1.104 g, 4.88 mmol, 99% yield). Analytical data matched those reported previously.[5]

TLC (50% EtOAc, 50% hexanes) *Rf* = 0.50 (UV)

[4] Lee, Y. S., J. Nyberg, et al. (2007). "Understanding the structural requirements of 4-anilidopiperidine analogues for biological activities at μ and δ opioid receptors." Bioorganic & Medicinal Chemistry Letters 17(8): 2161-2165.
[5] Yu, B.-C., Y. Shirai, et al. (2006). "Syntheses of new functionalized azobenzenes for potential molecular electronic devices." Tetrahedron **62**(44): 10303-10310.

^{1}H NMR (200 MHz, $CDCl_3$) δ = 7.97 – 7.82 (m, *J*=8.2, 4H), 7.58 – 7.44 (m, *J*=7.4, 3H), 7.38 (d, *J*=8.2, 2H), 3.92 (t, *J*=6.5, 2H), 2.95 (t, *J*=6.5, 2H).

Photo-Fentanyl-1 (PF1)

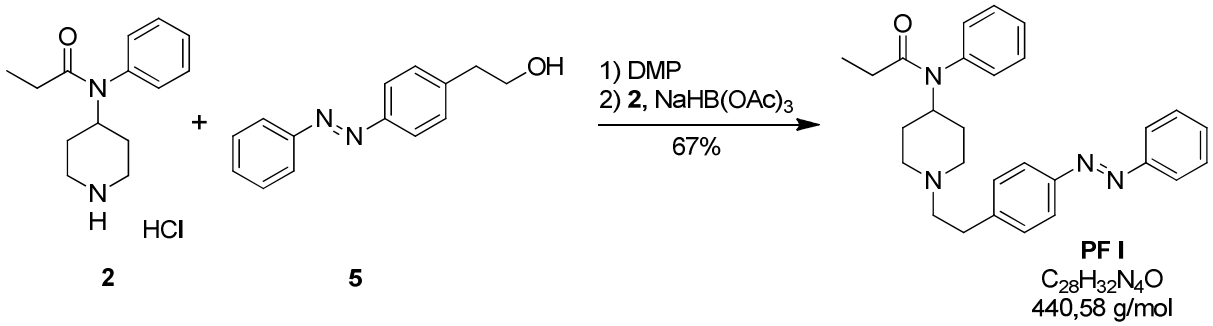

2 **5**

Fresh Aldehyde Preperation

Alcohol **5** (50 mg, 0.221 mmol, 1.0 eq) was dissolved in 1 mL DCM and DMP (187 mg, 0.44 mmol, 2.0 eq) was added. The reaction mixture was diluted with EtOAc after 3 h and subsequently extracted with concentrated $Na_2S_2O_{3(aq)}$, 1-M-NaOH and brine. The organic layer was dried over Na_2SO_4 and concentrated in vacuo.

Reductive Amination

The HCl salt of aminopiperidine **2** (63 mg, 0.22 mmol, 1.0 eq) was dissolved in 1 mL DCE and DIPEA (115 µL, 0.66 mmol, 3.0 eq). The freshly prepared aldehyde (described above) was added as a solution in 2 mL DCE before $NaHB(OAc)_3$ was added. The reaction suspension was stirred under N_2-atm at rt overnight before being quenched by partitioning between EtOAc and concentrated $NH_4Cl_{(aq)}$. The organic layer was further washed with 1-M-$NaOH_{(aq)}$, concentrated $NaHCO_{3(aq)}$ and brine. Evaporation of the solvent yielded the crude product, which was purified using silica gel chromatography (isogratic, 50% EtOAc, 50% hexanes + 1% TEA) affording the title compound **PF1** as an orange oil (65 mg, 0.15 mmol, 67%).

TLC (SiO_2, 50% EtOAc, 50% hexanes) *Rf* = 0.17 (UV).

^{1}H NMR (400 MHz, $CDCl_3$) δ = 7.92 – 7.84 (m, 2H), 7.84 – 7.78 (m, 2H), 7.54 – 7.42 (m, 3H), 7.42 – 7.31 (m, 3H), 7.30 – 7.25 (m, 2H), 7.10 – 7.03 (m, 2H), 4.68 (tt, *J*=12.2, 3.9, 1H), 2.99 (d, *J*=11.6, 2H), 2.78 (dd, *J*=10.0, 6.4, 2H), 2.60 – 2.52 (m, 2H), 2.17 (dd, *J*=11.9, 10.0, 2H), 1.98 – 1.86 (m, 2H), 1.80 (d, *J*=13.4, 2H), 1.51 – 1.34 (m, 2H), 1.05 – 0.96 (m, 3H).

^{13}C NMR (101 MHz, $CDCl_3$) δ = 173.52, 152.64, 151.10, 143.76, 138.79, 130.76, 130.39, 129.32, 129.28, 129.03, 128.26, 122.93, 122.72, 60.07, 53.09, 52.09, 33.71, 30.54, 28.51, 9.62.

HRMS (ESI) calcd for $C_{28}H_{33}N_4O$ $[M+H]^+$: 441.2654; found: 441.2644.

UV/VIS λ_{max} (π to π^*)= 325 nm.

Analytical Spectra PF1

^{1}H-NMR, **2**

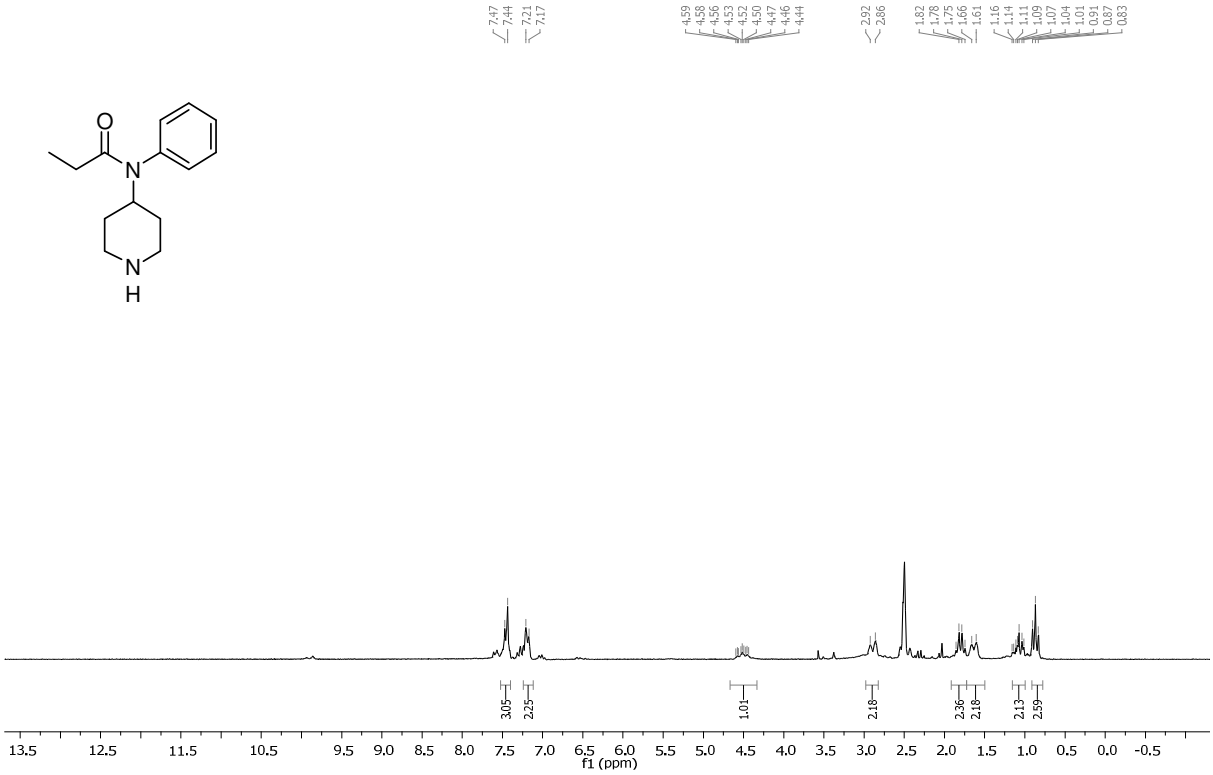

^{1}H-NMR, **5**

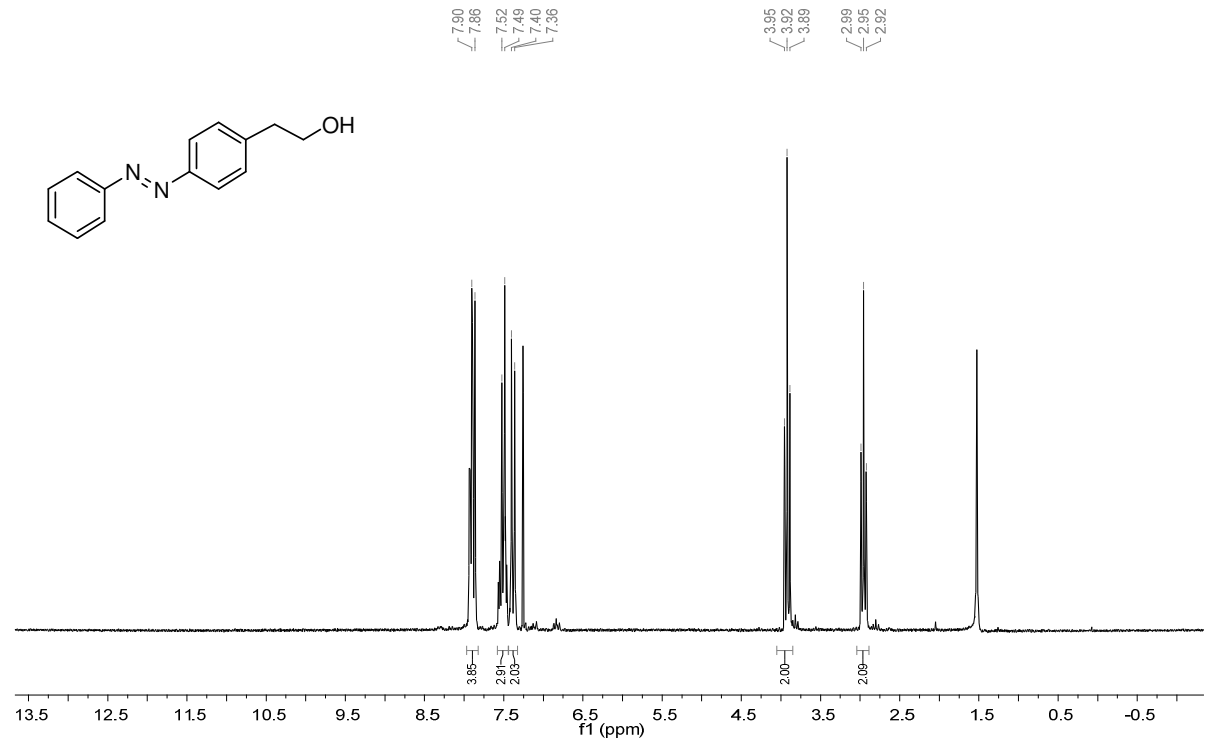

^{1}H-NMR, **Photo-Fentanyl-1**

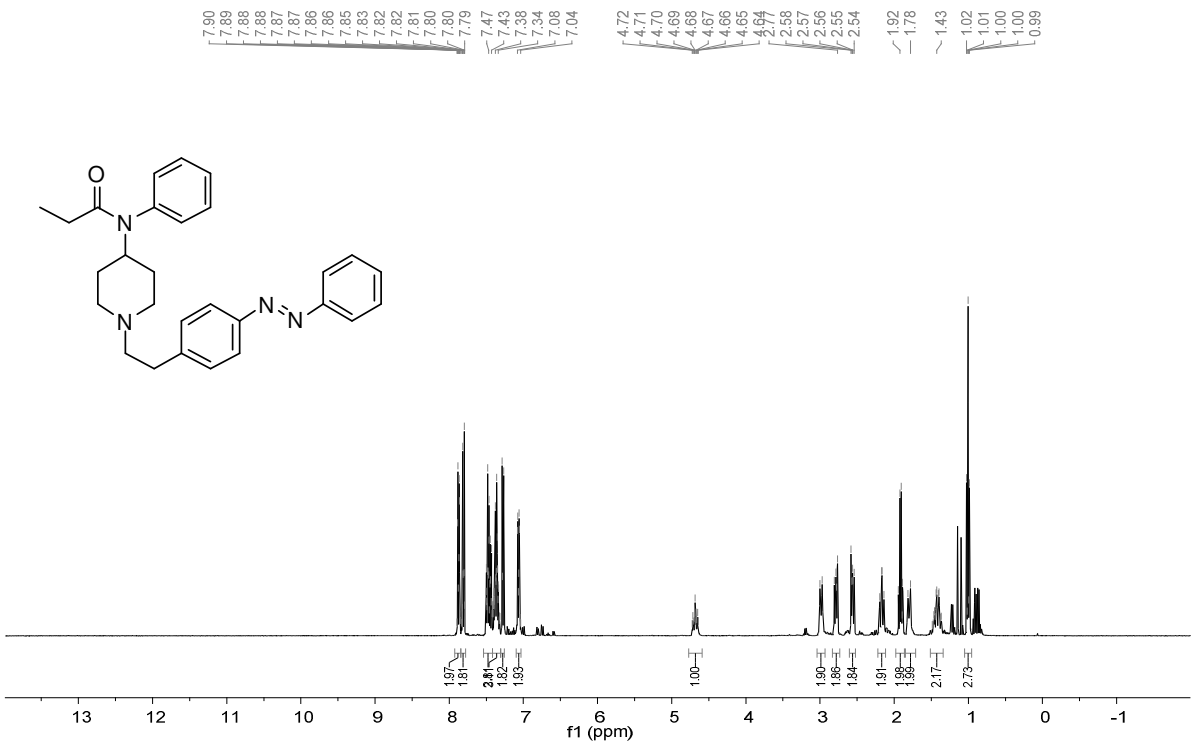

^{13}C-NMR, **Photo-Fentanyl-1**

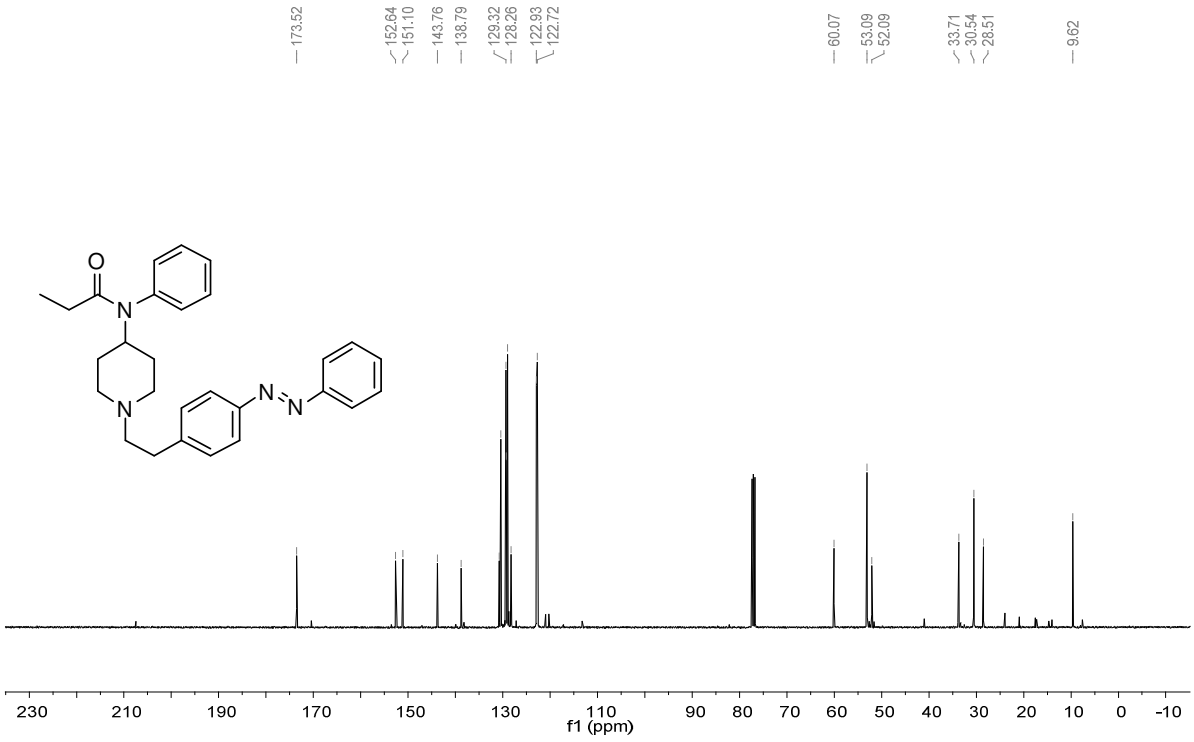

PHOTO-FENTANYL-2

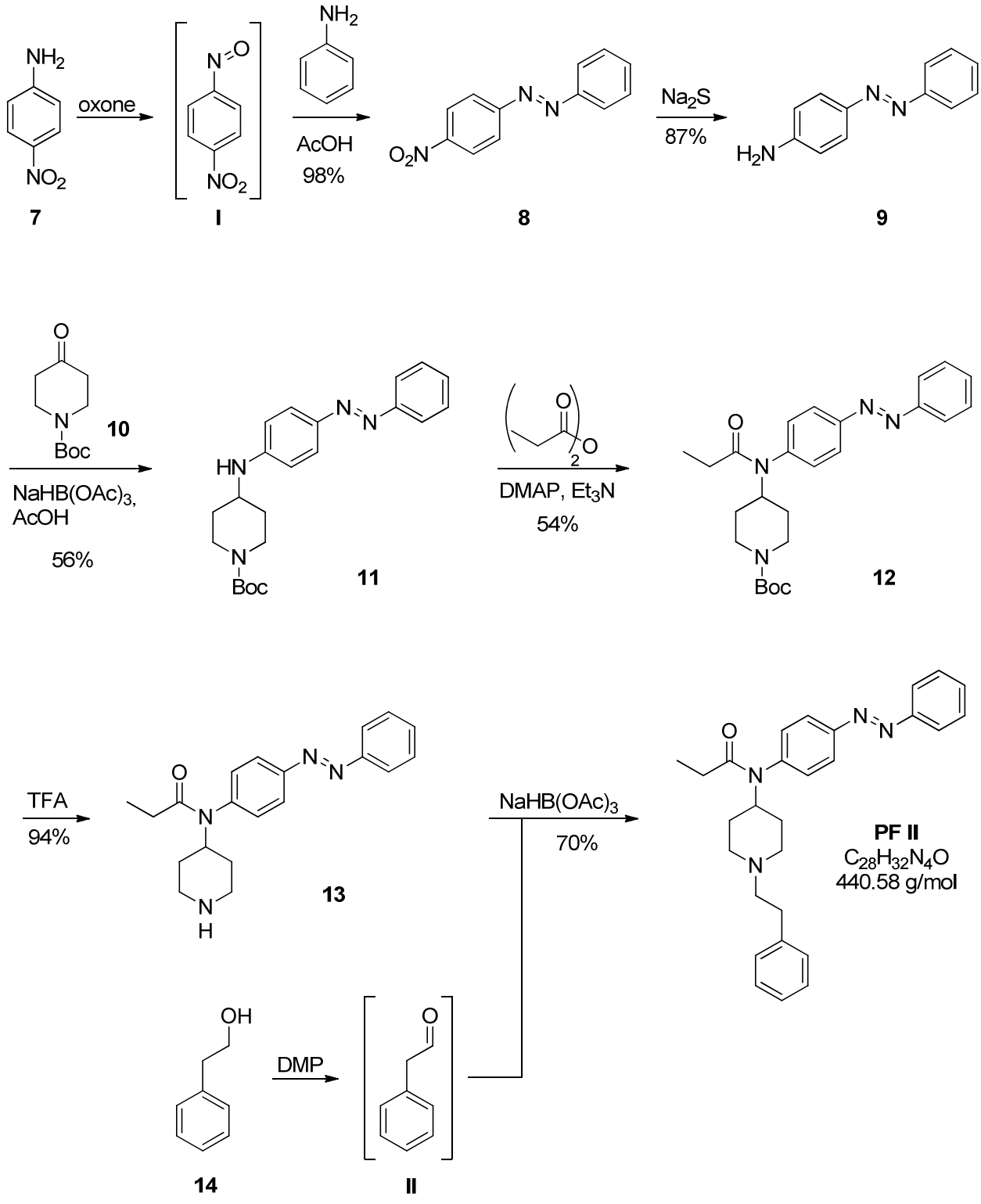

Scheme 1. Photo-Fentanyl-2 synthesis.

1-nitro-4-nitrosobenzene I

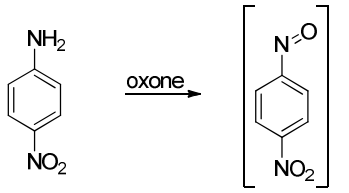

7 **I**

$C_6H_4N_2O_3$
152.11 g/mol

To a solution of 4-nitroaniline **7** (5.94 g, 43.0 mmol, 1.0 equiv) in CH_2Cl_2 (150 mL) was added Oxone (potassium peroxymonosulfate, 26.4 g, 43.0 mmol, 1.0 equiv) as a solution in H_2O (150 mL). The green, biphasic suspension was allowed to stir under N_2 atmosphere. After 3 hours, organic and aqueous phases were separated. The aqueous phase was extracted 2x with CH_2Cl_2 (30 mL aliquots). Pooled organic phase was washed with 1x 1 M HCl, 1x sat. NaCl (75 mL aliquots). The organic phase was then dried over Na_2SO_4 and concentrated to 30 mL under reduced pressure. The resulting yellow-black solution of **I** in CH_2Cl_2 was carried on to the next step immediately, without characterization.

1-(4-nitrophenyl)-2-phenyldiazene 8

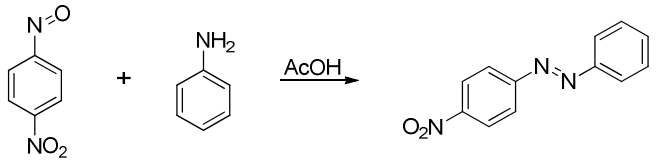

I **7** **8**

$C_{12}H_9N_3O_2$
227.22 g/mol

To a solution of **I** (6.53 g, 43.0 mmol, 2.0 equiv) in CH_2Cl_2 (30 mL) was added sequentially aniline **7** (1.96 mL, 21.5 mmol, 1.0 equiv) and glacial AcOH (6.15 mL, 107.5 µL, 5.0 equiv). The yellow-black solution was allowed to stir for 15 hours under N_2 atmosphere, after which time the reaction mixture was found to be an orange-black suspension. The reaction was diluted with EtOAc (150 mL) and washed with 3x 1M NaOH, 2x sat. $NaHCO_3$, 2x sat. NaCl (50 mL aliquots). The organic phase was then dried over Na_2SO_4 and solvent removed under reduced pressure. Crude material was purified by flash column chromatography (silica gel, dry loading on bulk sorbent, gradient 1% → 5% →10% EtOAc in Hexanes), affording compound **8** (4.765 g, 21.0 mmol, 98%), as an orange solid.

TLC (SiO_2, 10% EtOAc, 90% hexanes) R_f = 0.55 (UV)

HRMS (EI) calcd for $C_{12}H_9N_3O_2$ $[M]^{+\cdot}$: 227.0695; found: 227.0693

^{1}H NMR (400 MHz, $CDCl_3$) δ 8.46 – 8.28 (m, 2H), 8.06 – 7.99 (m, 2H), 7.99 – 7.91 (m, 2H), 7.58 – 7.49 (m, 3H).

^{13}C NMR (101 MHz, $CDCl_3$) δ 155.68 , 152.36 , 148.69 , 132.36 , 129.26 , 124.69 , 123.39 , 123.37.

4-(phenyldiazenyl)aniline 9

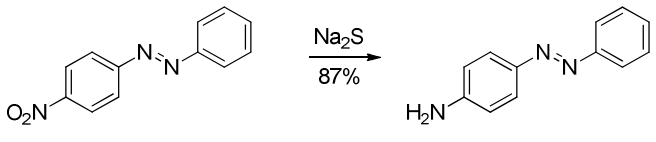

8 **9**
$C_{12}H_{11}N_3$
197.24 g/mol

To a solution of **8** (2.08 g, 9.16 mmol, 1.0 equiv) in 3:1 THF:H_2O (120 mL) was added Na_2S (2.14 g, 27.5 mmol, 3.0 equiv). The red-black suspension was allowed to stir for 3h hours at reflux, at which point TLC monitoring indicated the reaction had reached completion. THF was removed under reduced pressure, and the remaining aqueous material diluted with EtOAc (150 mL) and 1M NaOH (50 mL). The organic phase was isolated and washed with 1x 1M NaOH, 1x sat. $NaHCO_3$ and 1x brine (50 mL aliquots). An orange precipitate was removed through vacuum filtration, the filtrate dried over Na_2SO_4 and solvent removed *in vacuo*, affording **9** as a dark orange solid (1.568 g, 7.95 mmol, 87%).

TLC (SiO_2, 20% EtOAc, 80% hexanes) R_f = 0.25 (UV)

HRMS (EI) calcd for $C_{12}H_{11}N_3$ $[M]^{+\cdot}$: 197.0953; found: 197.0953

^{1}H NMR (300 MHz, $CDCl_3$) δ 7.89 – 7.75 (m, 5H), 7.54 – 7.33 (m, 2H), 6.82 – 6.69 (m, 2H), 4.04 (s, 2H).

^{13}C NMR (75 MHz, $CDCl_3$) δ 152.94 , 149.53 , 145.56 , 129.78 , 128.95 , 125.09 , 122.32 , 114.61

tert-butyl 4-((4-(phenyldiazenyl)phenyl)amino)piperidine-1-carboxylate 11

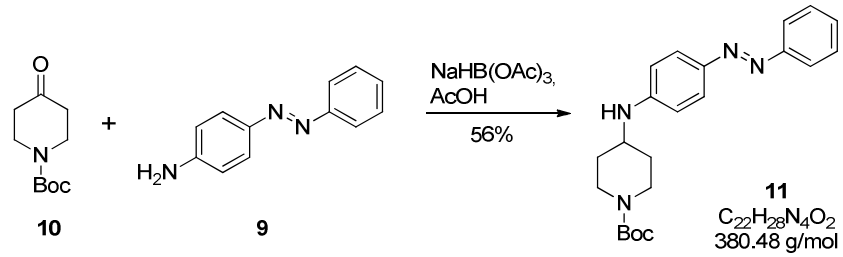

To a solution of **10** (500 mg, 2.51 mmol, 1.0 equiv) was added sequentially **9** (520 mg, 2.63 mmol, 1.05 equiv), $Na(AcO)_3BH$ (745 mg, 3.51 mg, 1.4 equiv) and glacial AcOH (144 µL, 2.51 mmol, 1.0 equiv). The bright-orange reaction mixture was allowed to stir overnight. After 15 hours, TLC monitoring indicated complete consumption of **10**, and the reaction mixture appeared to have become a suspension. The reaction mixture was diluted with EtOAc (125 mL) and washed with 2x 1M NaOH, 1x sat. $NaHCO_3$, 1x sat. NaCl (50 mL aliquots). The organic phase was dried over Na_sSO_4 and solvent removed under reduced pressure. Crude material was purified by normal phase chromatography on a Biotage Isolera system (Chromabond 120 g SiOH cartridge, 3% → 30% linear gradient EtOAc in hexanes over 10 column volumes), affording **11** as a bright orange solid (534 mg, 1.40 mmol, 56%).

TLC (SiO_2, 40% EtOAc, 60% hexanes) R_f = 0.63 (UV)

HRMS (ESI) calcd for $C_{22}H_{28}N_4O_2$ $[M+H]^+$: 381.2285; found: 381.2285

^{1}H NMR (599 MHz, $CDCl_3$) δ 7.89 – 7.78 (m, 4H), 7.47 (t, *J* = 7.7 Hz, 2H), 7.38 (t, *J* = 7.3 Hz, 1H), 6.66 (d, *J* = 8.4 Hz, 2H), 4.29 – 3.87 (m, 3H), 3.59 – 3.50 (m, 1H), 2.96 (t, *J* = 12.6 Hz, 2H), 2.14 – 1.98 (m, 2H), 1.48 (s, 9H), 1.43 – 1.34 (m, 2H).

^{13}C NMR (151 MHz, $CDCl_3$) δ 154.71, 153.00, 149.44, 144.71, 129.55, 128.93, 125.32, 122.20, 112.58, 79.74, 49.99, 42.63, 32.21, 28.43.

IR ν_{max}: 3341, 2975, 2929, 2857, 1674, 1601, 1518, 1428, 1410, 136, 1338, 1316, 1274, 1234, 1170, 1137, 1096, 868, 829, 767, 690

***tert*-butyl-4-(*N*-(4-(phenyldiazenyl)phenyl)propionamido)piperidine-1-carboxylate**

12

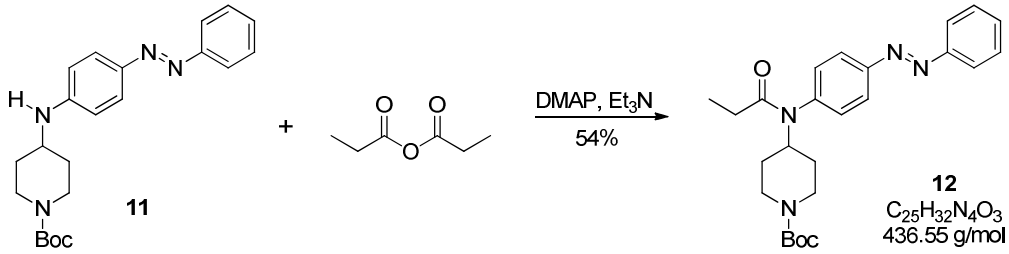

To a solution of **11** (200 mg, 0.526 mmol, 1.0 equiv.) in dry toluene (5.0 mL) was added sequentially DMAP (128 mg, 1.05 mmol, 2.0 equiv), Et_3N (365 µL, 2.63 mmol, 5.0 equiv.) and propionanhydride (137 µL, 1.05 mmol, 2.0 equiv.). The bright orange reaction mixture was allowed to stir for 15 hours under N_2 atmosphere, after which time the reaction was purified directly by flash column chromatography (silica gel, gradient10% → 20% → 30% → 40% EtOAc in hexanes) affording **12** as an orange oil (123 mg, 0.282 mmol, 54%). Yield based on recovered starting material: 73%.

TLC (SiO_2, 40% EtOAc, 60% hexanes) R_f = 0.36 (UV)

HRMS (ESI) calcd for $C_{25}H_{32}N_4O_3$ $[M+Na]^+$: 459.2367; found: 459.2367

^{1}H NMR (400 MHz, $CDCl_3$) δ 7.99 – 7.89 (m, 4H), 7.58 – 7.47 (m, 3H), 7.25 – 7.19 (m, 2H), 4.80 (tt, *J*=12.7, 3.8, 1H), 4.12 (s, 2H), 2.80 (t, *J*=12.0, 2H), 1.99 (q, *J*=7.4, 2H), 1.80 (d, *J*=13.7, 2H), 1.41 (s, 2H), 1.38 (s, 9H), 1.04 (t, *J*=7.4, 3H).

^{13}C NMR (101 MHz, $CDCl_3$) δ 212.92, 173.23, 154.46, 152.46, 152.14, 140.99, 131.51, 131.06, 129.17, 123.67, 122.99, 79.57, 52.51, 43.19, 30.59, 28.65, 28.34, 9.56.

IR ν_{max}: 3061, 3026, 2935, 2805, 2766, 1656, 1596, 1498, 1449, 1374, 1340, 1258, 1242, 1149, 1093, 1053, 1018, 981, 928, 862, 772, 749, 700, 689

***N*-(4-(phenyldiazenyl)phenyl)-*N*-(piperidin-4-yl)propionamide 13**

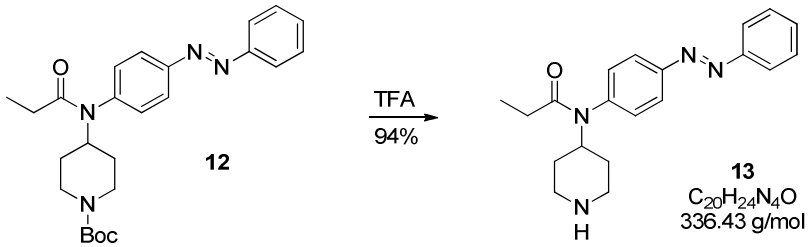

12 (102 mg, 0.234 mmol) was treated with a 1:1 mixture of TFA:DCM (2.0 mL). After 1 h, TLC monitoring indicated complete deprotection of **12**. The reaction mixture was cooled to 0 ℃ and quenched with 1 M NaOH. Combined organic and aqueous phase were transferred to a separatory funnel and aqueous phase removed. The organic phase was then washed with 1x 1M NaOH, 1x sat. $NaHCO_3$ and 1x brine (5 mL aliquots). Organic phase was dried of Na_2SO_4 and solvent removed *in vacuo*, affording **13** as an orange oil (74 mg, 0.220 mmol, 94%).

TLC (SiO_2, 10% MeOH, 90% DCM), R_f = 0.12 (UV)

HRMS (ESI) calcd for $C_{22}H_{28}N_4O_2$ $[M+H]^+$: 381.2285; found: 381.2285

^{1}H NMR (400 MHz, $CDCl_3$) δ 7.97 – 7.89 (m, 4H), 7.56 – 7.46 (m, 3H), 7.24 – 7.20 (m, 2H), 4.83 – 4.70 (m, 1H), 3.10 (d, *J*=12.2, 2H), 2.75 (td, *J*=12.4, 2.2, 2H), 2.53 (s, 1H), 1.98 (q, *J*=7.4, 2H), 1.84 (d, *J*=13.6, 2H), 1.34 (qd, *J*=12.4, 4.2, 2H), 1.03 (t, *J*=7.4, 3H).

^{13}C NMR (101 MHz, $CDCl_3$) δ 173.11, 152.46, 152.06, 141.17, 131.45, 131.11, 129.15, 123.62, 122.98, 52.45, 45.89, 31.59, 28.67, 9.58.

IR ν_{max}: 3421, 2938, 2817, 2726, 2493, 1651, 1596, 1499, 1461, 1377, 1265, 1154, 1099, 1071, 1039, 1012, 864, 808, 772, 690

Photo-Fentanyl-2

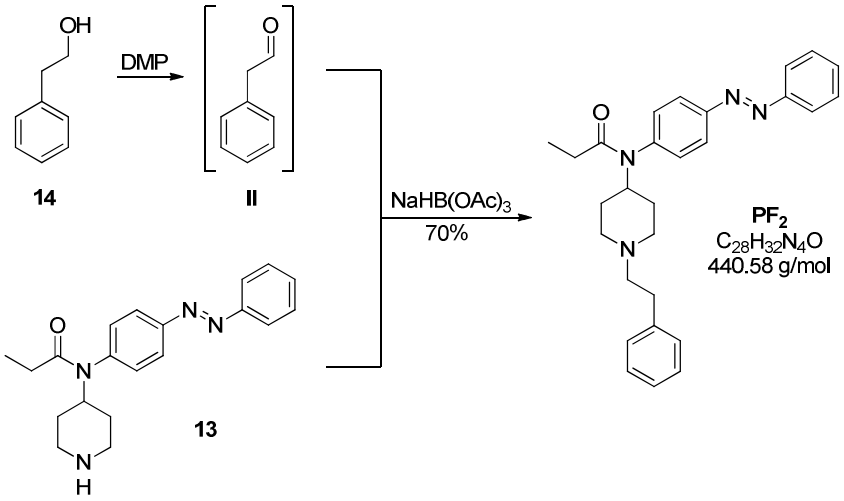

DMP Oxidation

A suspension of DMP (189 mg, 0.446 mmol, 3.0 equiv.) was cooled to 0 °C. To this was added phenethyl alcohol **14** (26.7 µL, 0.223 mmol, 1.5 equiv.) and the reaction was allowed to stir at RT under N_2 atmosphere. TLC monitoring at 1 hour indicated complete consumption of **14**. The reaction mixture was transferred to a separatory funnel and diluted with EtOAc (15 mL). Organic phase was washed with 1x sat. NaS_2O_3, 1x 1M NaOH, 1x brine (5 mL aliquots). Organic phase was then dried over Na_2SO_4 and solvent removed under removed pressure, affording phenylacetaldehyde **II** as a fragrant, colourless oil (100% conversion assumed). **II** was carried on to the next step immediately without characterization.

Reductive Amination

To a solution of **13** (50 mg, 0.149 mmol, 1.0 equiv.) in DCE (1.0 mL) was added **II** (0.223 mmol, 1.5 equiv.) as a solution in DCE (1.5 mL). To this was added $Na(AcO)_3BH$ (189 mg, 0.892 mmol, 6.0 equiv.) The bright orange suspension was allowed to stir for 15 hours at RT under N_2 atmosphere. TLC monitoring at this time indicated near-complete consumption of **13**. The reaction was transferred to a separatory funnel and diluted with EtOAc (15 mL). Organic phase was washed with 2x 1 M NaOH, 1x sat. $NaHCO_3$, 1x brine (5 mL). Organic was dried over Na_2SO_4 and solvent removed *in vacuo*. Crude material was purified by column chromatography (silica gel, gradient 1% → 2% →4% → 6% → 8% MeOH in DCM) affording **PF2** as an orange oil (46 mg, 0.104 mmol, 70%). Yield based on recovered starting material: 81%.

TLC (SiO_2, 10% MeOH, 90% DCM) R_f = 0.38 (UV)

HRMS (ESI) calcd for $C_{28}H_{32}N_4O$ $[M+H]^+$: 441.2649; found: 441.2649

^{1}H NMR (300 MHz, $CDCl_3$) δ 8.00 – 7.88 (m, 4H), 7.61 – 7.46 (m, 2H), 7.31 – 7.21 (m, 5H), 7.21 – 7.09 (m, 3H), 4.80 – 4.61 (m, 1H), 3.12 – 2.93 (m, 2H), 2.80 – 2.65 (m, 2H), 2.64 – 2.46 (m, 2H), 2.29 – 2.09 (m, 2H), 2.00 (q, *J* = 7.4 Hz, 2H), 1.86 (ddd, *J* = 11.8, 4.4, 2.3 Hz, 2H), 1.50 (qd, *J* = 14.0, 13.1, 4.6 Hz, 2H), 1.05 (t, 3H).

^{13}C NMR (75 MHz, $CDCl_3$) δ 173.24, 152.50, 152.09, 141.16, 140.13, 131.42, 131.19, 129.14, 128.60, 128.36, 126.02, 123.61, 122.99, 60.35, 53.05, 52.48, 33.75, 30.58, 28.68, 9.59.

IR ν_{max}: 3061, 3026, 2935, 2805, 2766, 1656, 1596, 1498, 1449, 1374, 1340, 1258, 1242, 1149, 1093, 1053, 1018, 862, 772, 749, 700, 689

Analytical Spectra[6]

^{1}H-NMR, **8**

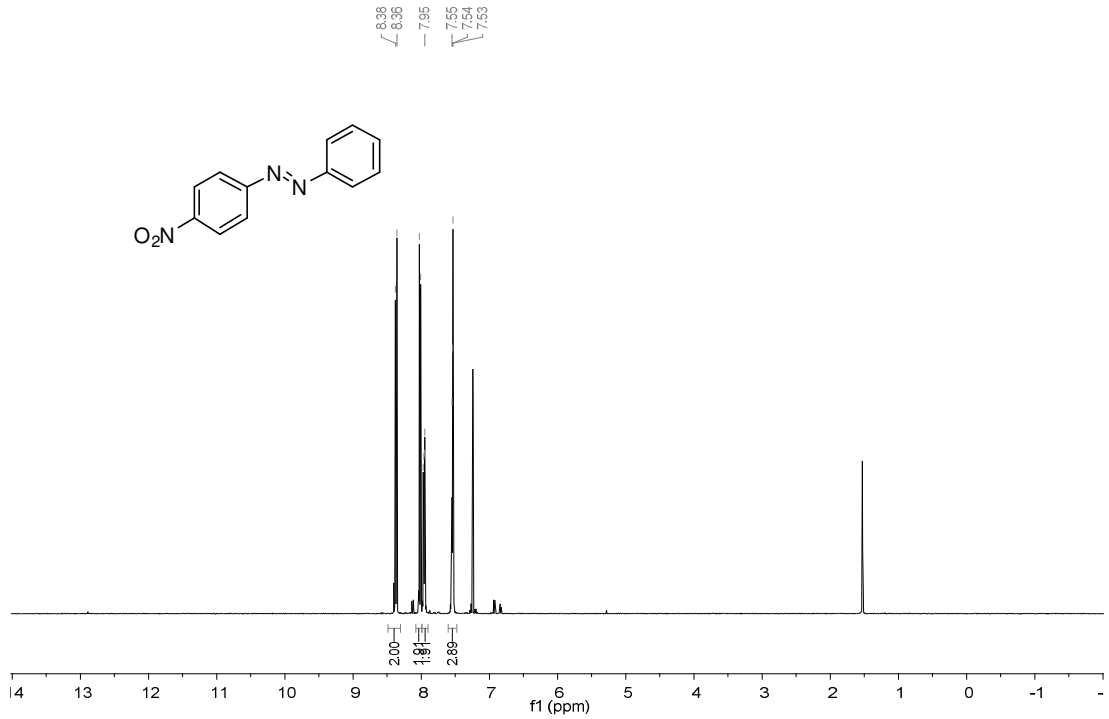

^{13}C-NMR, **8**

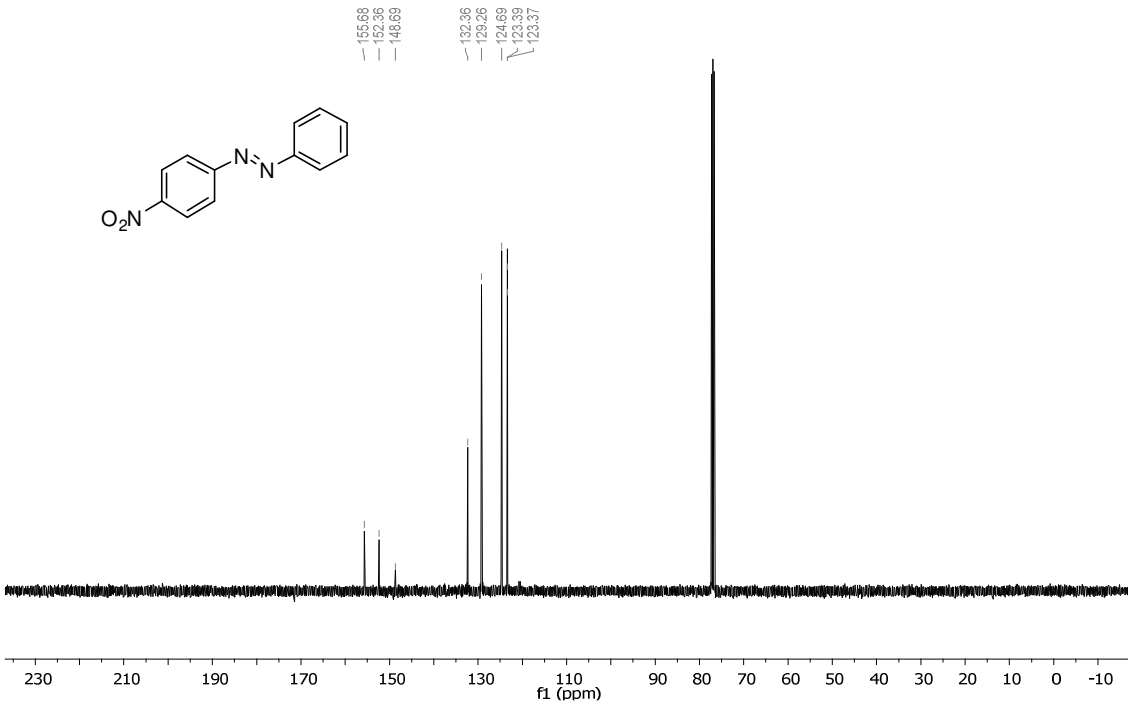

[6] NMR spectra of *trans*-azobenzenes may include minor signals from their *cis*-isomers. For clarity, these are not included in the integration or peak list.

^{1}H-NMR, **9**

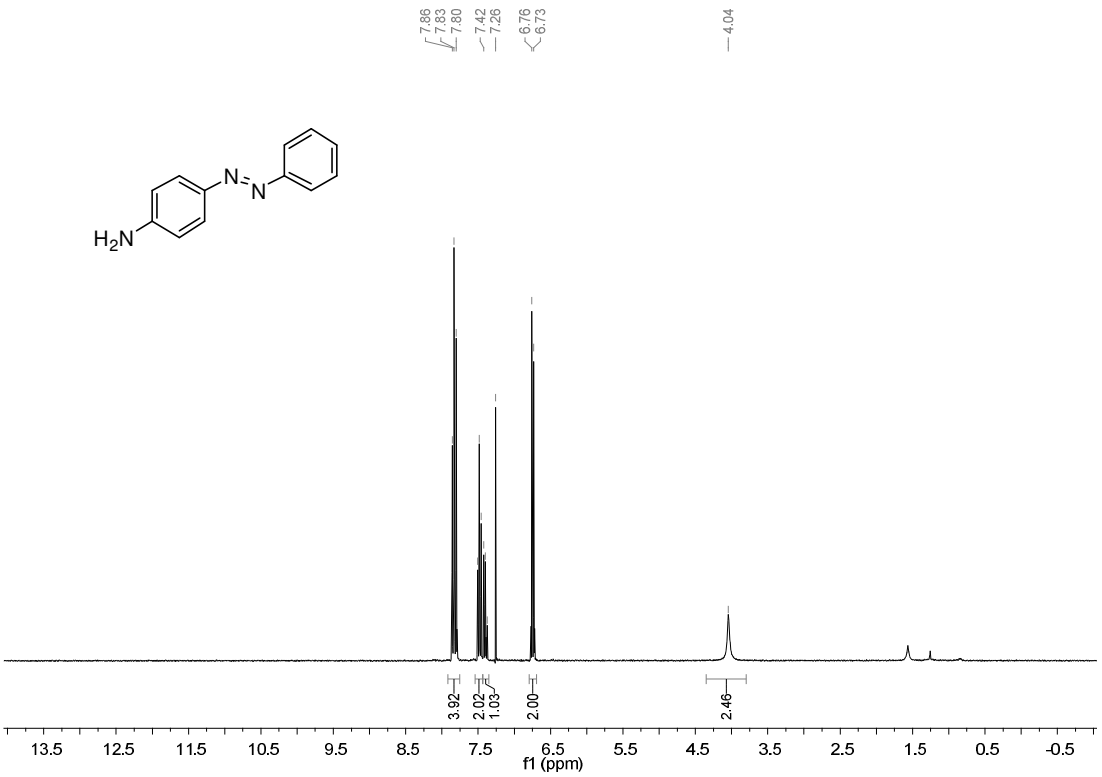

^{13}C-NMR, **9**

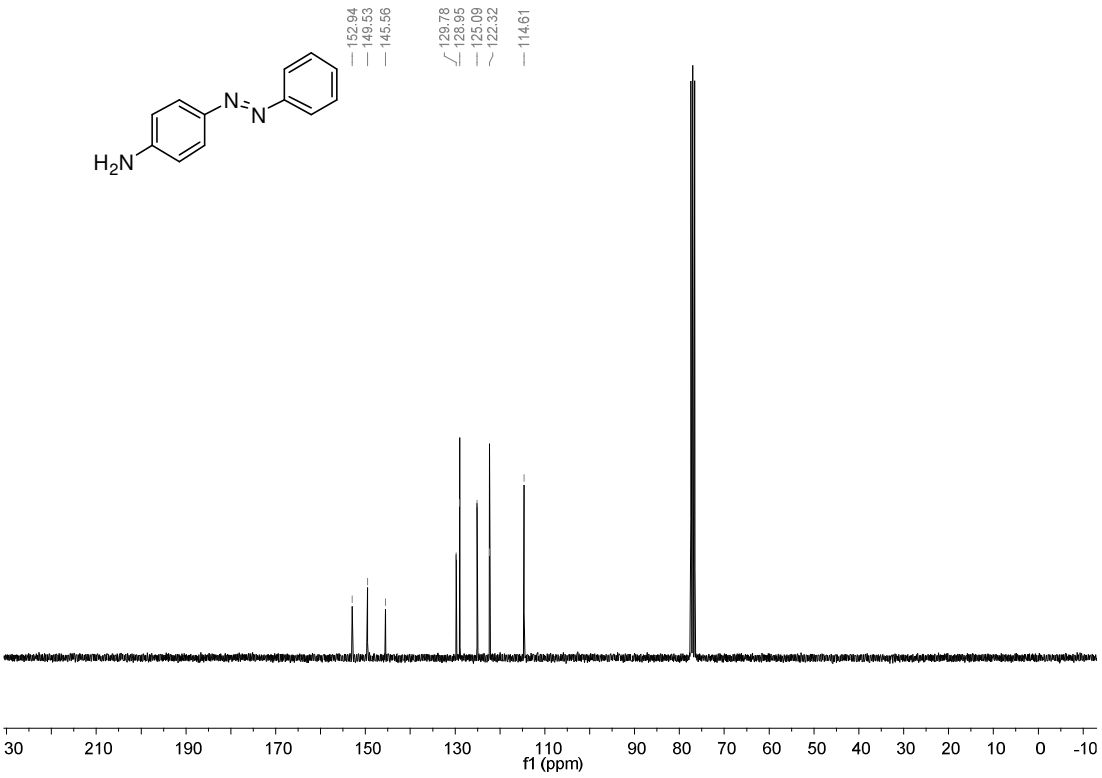

^{1}H-NMR, **11**

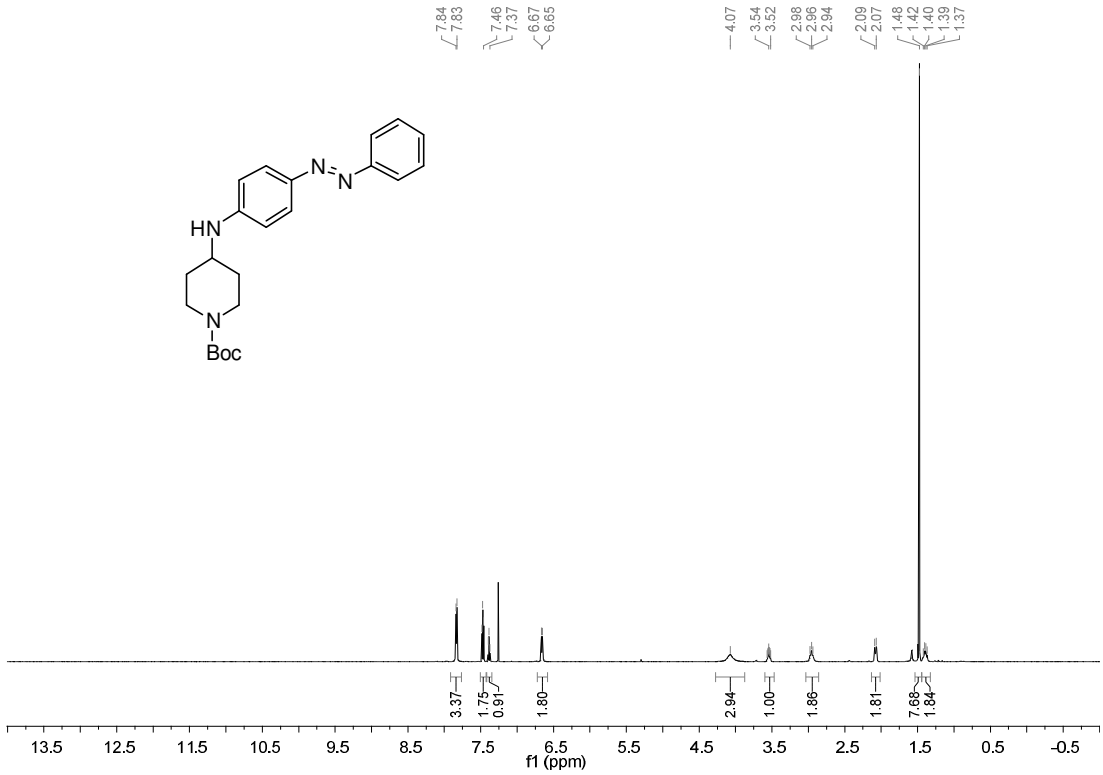

^{13}C-NMR, **11**

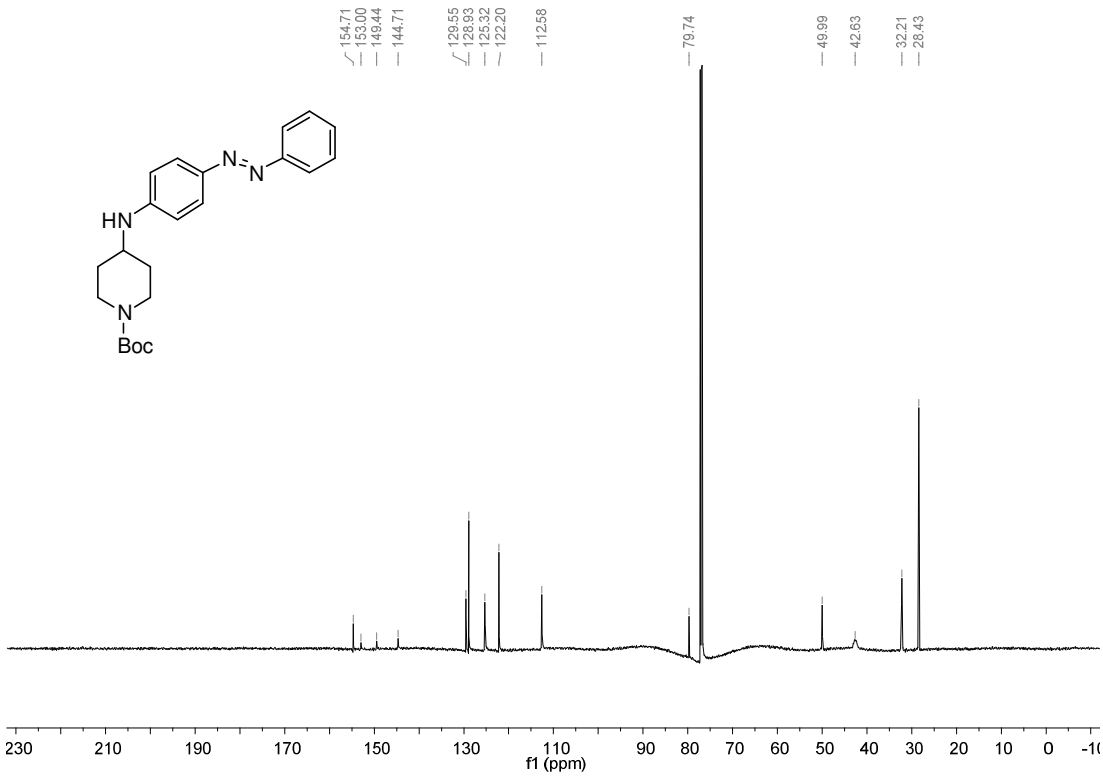

^{1}H-NMR, **12**

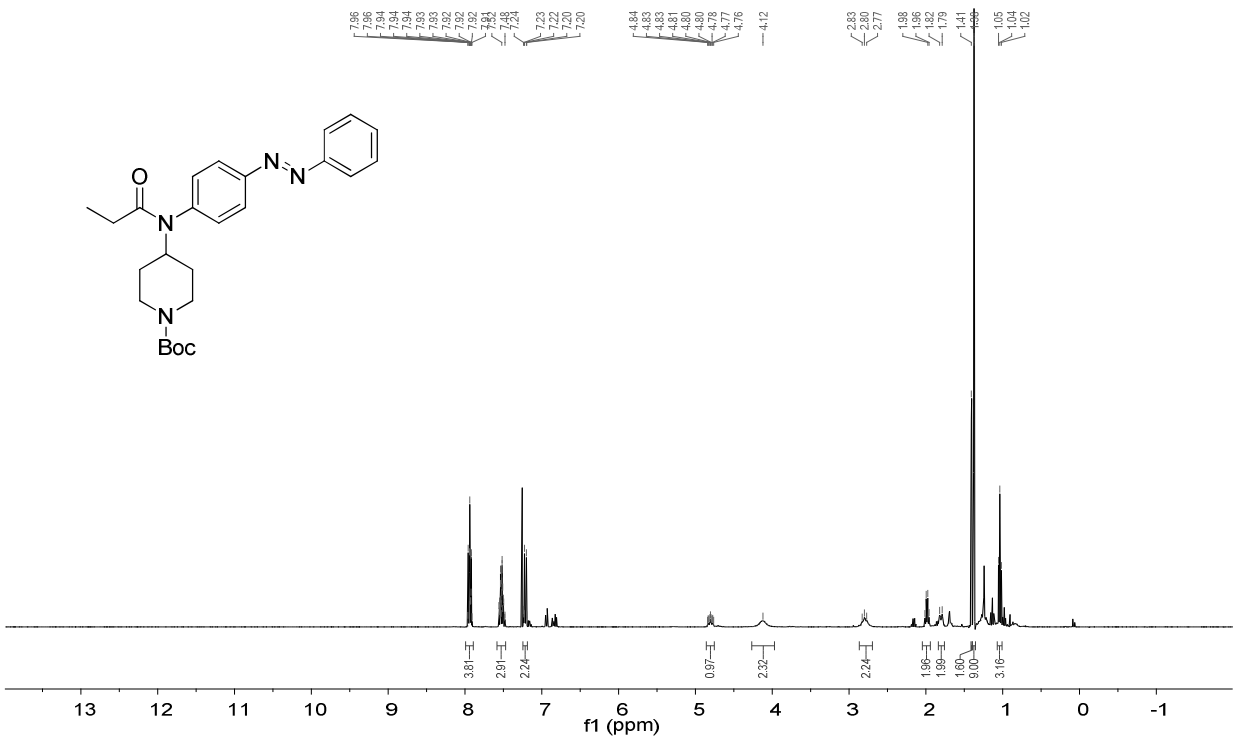

^{13}C-NMR, **12**

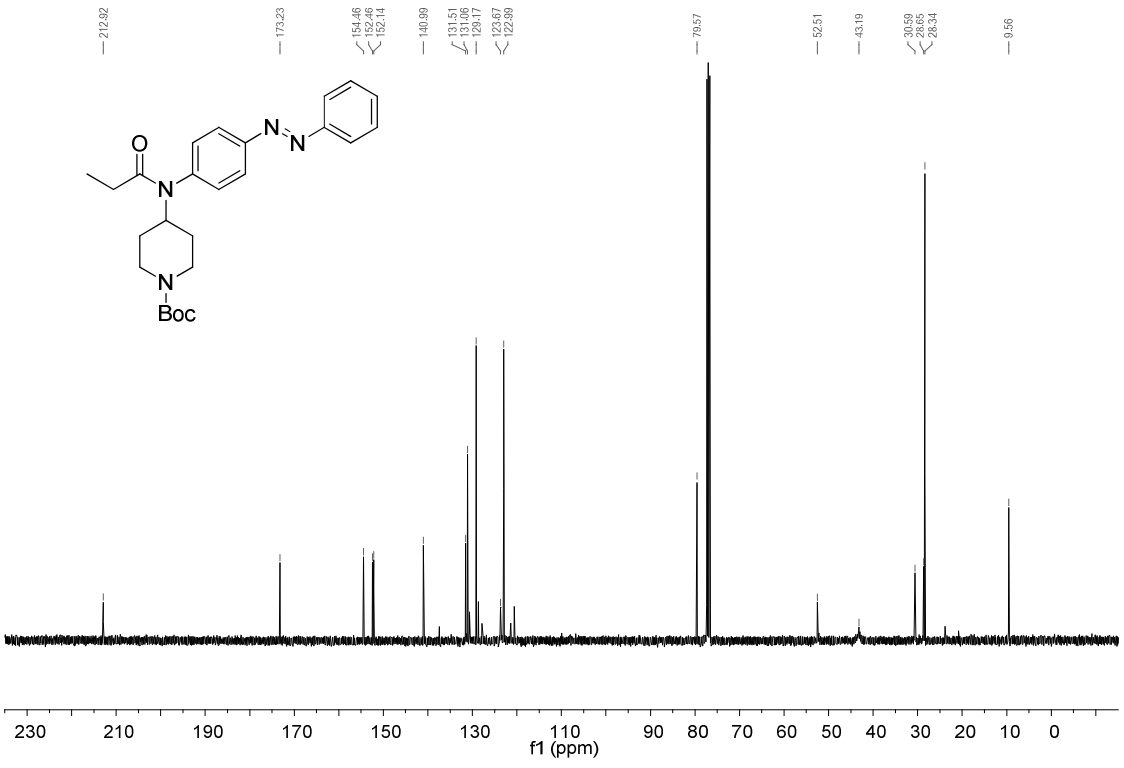

^{1}H-NMR, **13**

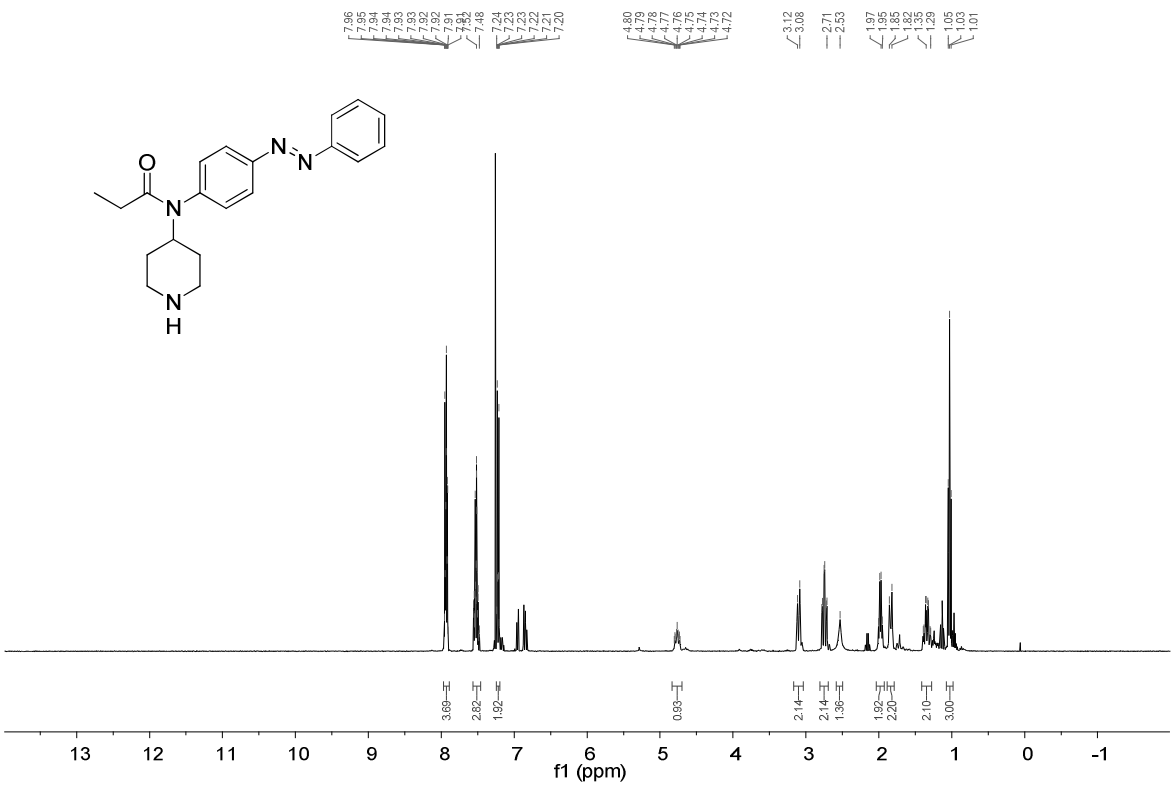

^{13}C-NMR, **13**

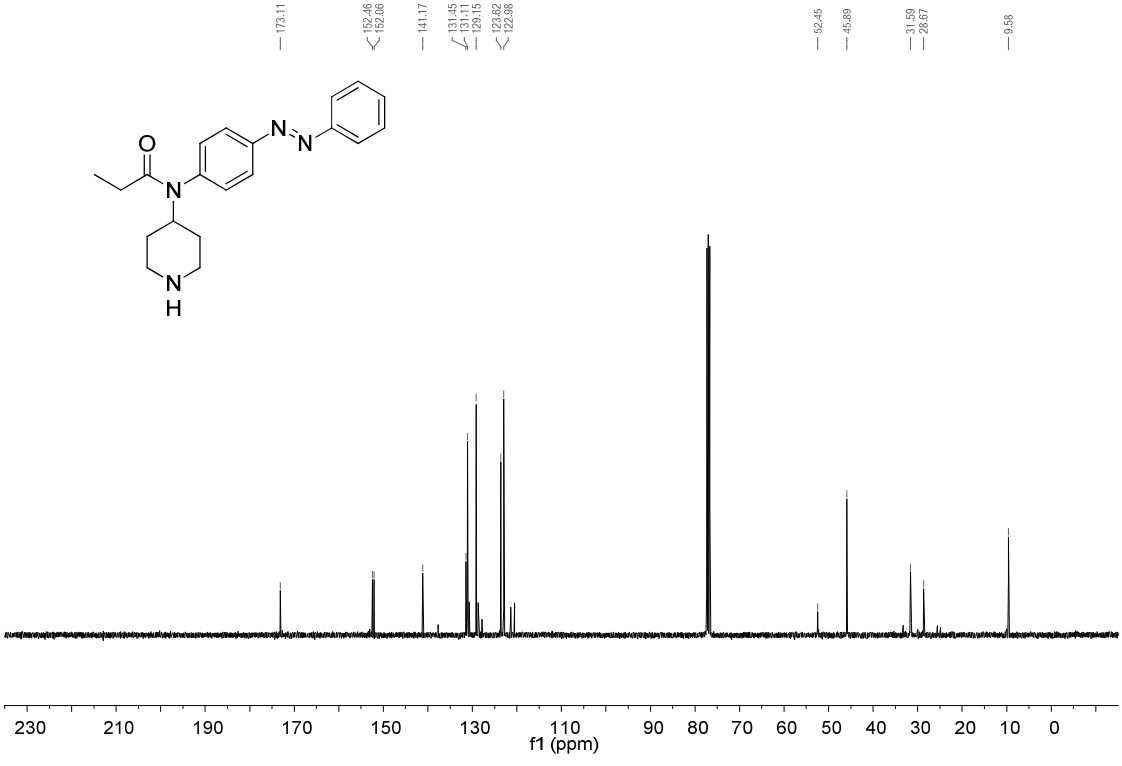

^{1}H-NMR, **PF II**

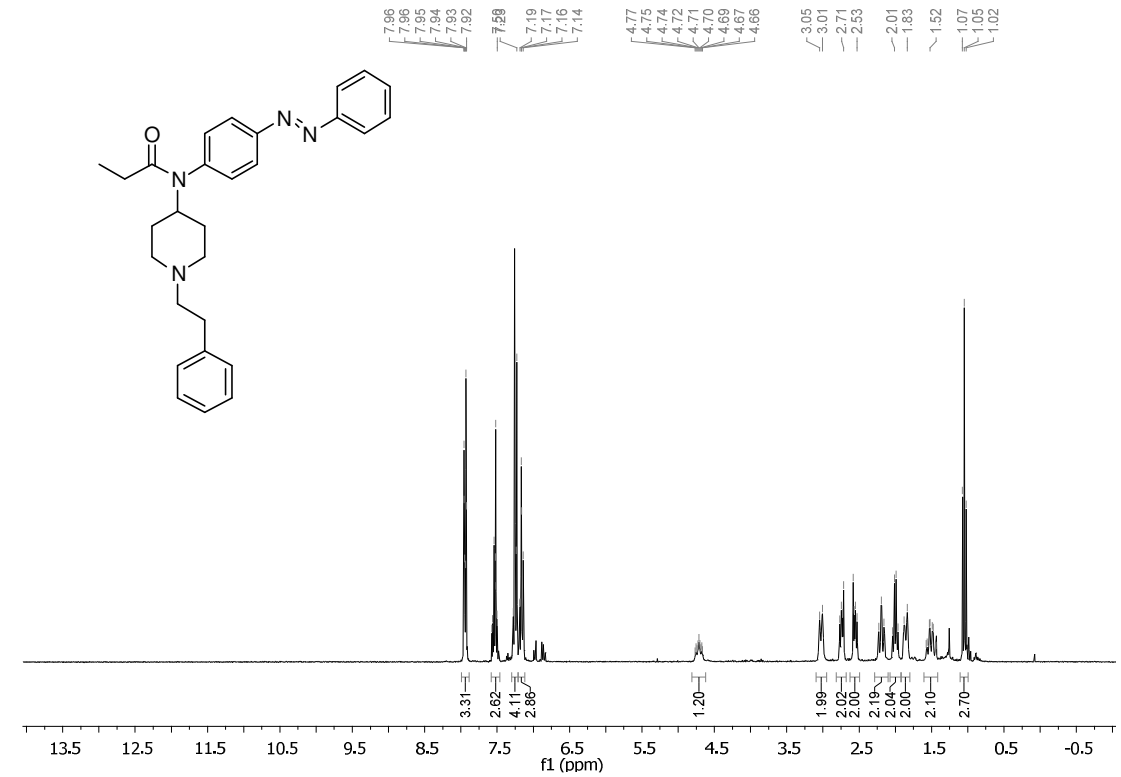

^{13}C-NMR, **PF II**

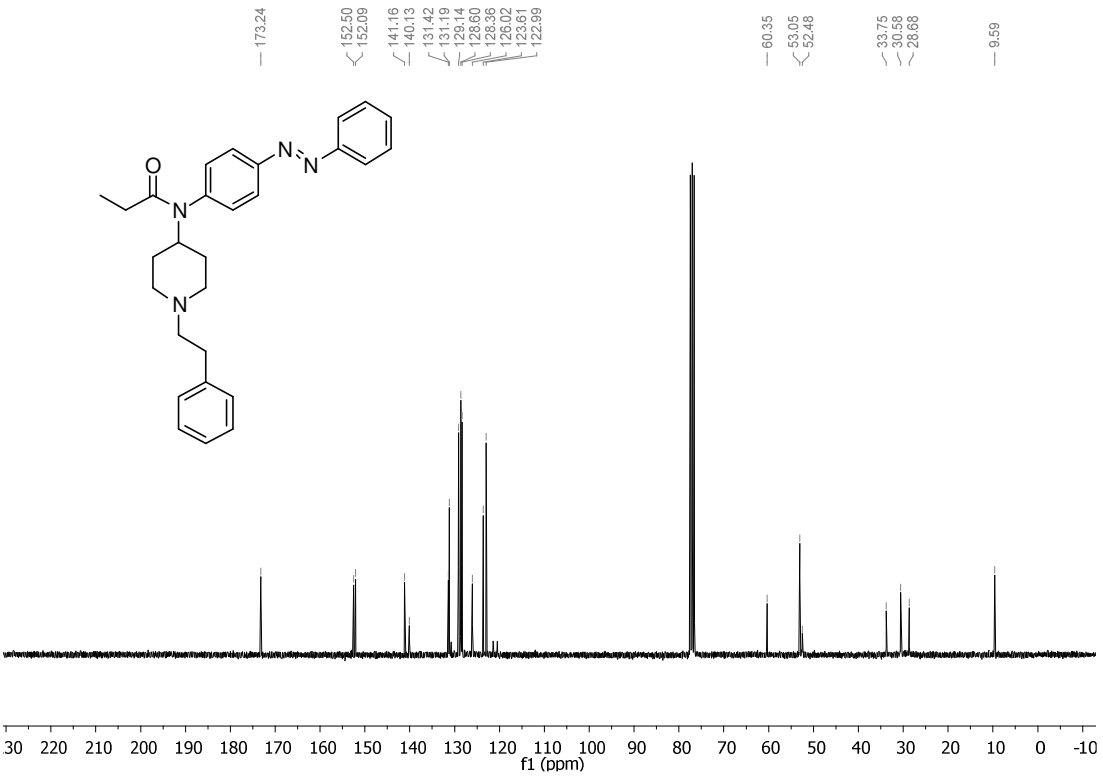

VI

Photochromic Agonists for Dopamine Receptors

Matthias Schönberger[1], Prashant Donthamsetti[2], Jonathan Javitch[2] & Dirk Trauner[1]

[1]Ludwig-Maximilians University, Chemistry Department and Center for Intergrated Protein Science Munich (CIPSM), Munich, Germany.

[2]Center for Molecular Recognition and Departments of Psychiatry and Pharmacology, Columbia University College of Physicians and Surgeons, New York, New York, United States

Dopamine receptors (DRs) play a major role in human health and disease, being involved in learning, motivation and addiction. All DRs belong to the family A of G-protein coupled receptors that also includes rhodopsin, which is operated by light through the action of a photoswitchable terpene. We now show how DRs can be operated by light using a photoswitchable azobenzene version of the known DR-agonist PPHT. Racemic and enantiomerically pure photochromic ligands have been synthesized and tested on both D2 and D3 receptors using a bioluminescence assay. One candidate showed pronounced light dependent changes in potency as well as efficacy at the D3R.

Content

Introduction

Dopamine Receptors and GPCRs. Dopamine receptors (DRs) belong to the family A of G-protein coupled receptors (GPCRs) that also includes rhodopsin, serotonin receptors, muscarinic AChRs, opioid receptors among others.[1] GPCRs assemble the largest family of transmembrane signaling proteins in the human genome and are a prominent drug target.[2-4] Their name has been coined based on their function as guanidine nucleotide exchange factors on heterotrimeric G-proteins. When activated by an agonist, GPCRs catalyze the exchange of GDP to GTP at the alpha subunit of heterotrimeric G-proteins. As a consequence, the Gα subunit dissociates from the Gβγ complex. Both remnants stay attached to the membrane and trigger individual signaling cascades. For instance, the Gβγ complex activates G-protein coupled inwardly rectifying potassium (GIRK) channels leading to hyperpolarization of the cell.[5,6] The Gα subunit can in turn activate ($G\alpha_s$) or inhibit ($G\alpha_i$) the adenylyl cyclase, or activate phospholipase C ($G\alpha_q$). Generally, heterotrimeric G-proteins are named after the action of their Gα subunit. For example, Gs would be a G-protein consisting of $G\alpha_s\beta\gamma$.

In addition, GPCRs can trigger G-protein independent signaling. For instance, after phosphorylation, GPCRs attract arrestins, which prevent further G-protein signaling, lead to receptor internalization and prompt individual signaling cascades.[7-9]

Many GPCRs display basal activity that can be modulated by different types of ligands. An agonist would amplify the basal activity, an inverse agonist would reduce it and an antagonist would leave it unchanged while impeding agonists and inverse agonists to come to action. Noteworthy, since GPCRs are incredibly versatile signaling machines, different agonists can bias certain signaling pathways.[10-12]

In the nervous system, DRs are expressed in both presynaptic and postsynaptic membranes. They can be divided into activating D_1-like receptors (D_1 and D_5), which couple predominantly to Gs G-proteins, and deactivating D_2-like receptors (D_2, D_3 and D_4), which couple to Gi G-proteins (Figure 1A).[13]

Upon synaptic activity, **dopamine** (**DA**) (Figure 1A) is released into the synaptic cleft by calcium induced vesicle release. DA-signaling is terminated by two major mechanisms. First, **DA** binds to D_2-like autoreceptors at the presynaptic cell, leading to

hyperpolarization and therefore inhibition of further vesicle release. Second, **DA**-transporters guide the catecholamine back into the presyanptic cell, where it is metabolized by monoamine oxidases.

DRs at the postsynaptic side can be activating or deactivating. In general, **DA** has an inhibitory effect on the nervous system due to a predominance of D_2-like receptors.[14] Due to the high sequence similarity in the ligand binding pocket, D_2 and D_3 receptors are difficult to differentiate pharmacologically and are often referred to as $D_{2/3}$ receptors (D2/3Rs).[15] In 2010, the first X-ray structure of a dopamine receptor, *viz* D3R with its antagonist **eticlopride**, was disclosed (Figure 1A).[16]

Dopamine Receptor Ligands. Given the tremendous impact of DRs in human health and disease, as well as their role in addiction and drug abuse,[17] many synthetic DR-ligands have been developed (Figure 1A)[13,18]. Racemic *N*-alkylated aminotetraline **7-OH-DPAT** is a D2/3R-agonist with slight preference towards D3R.[19] The indolinone **ropinirol** has a similar pharmacological profile as the native ligand **DA** and is used for the treatment of Parkinson´s disease.[20] **Apomorphine** is non-selective DR-agonist that is derived from the opioid morphine, but lacks opioid activity.[21] **PPHT** structurally resembles **7-OH-DPAT** and is also used as a racemate.[22] Even though being based on different molecular platforms, all of the listed agonists display features of **DA**, in particular a phenethylamine moiety.

A

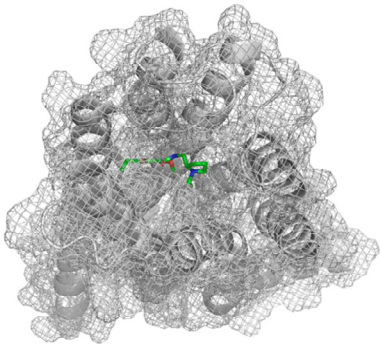

receptor	G-protein	classification
D1	$G_{s/olf}$	D1-like
D2	$G_{i/o}$	D2-like
D3	$G_{i/o}$	
D4	$G_{i/o}$	
D5	$G_{s/olf}$	D1-like

B

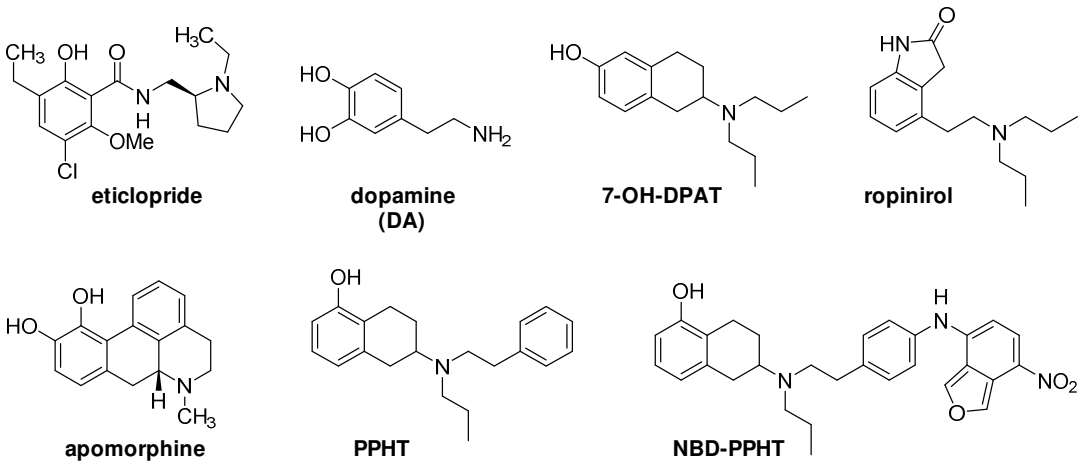

C

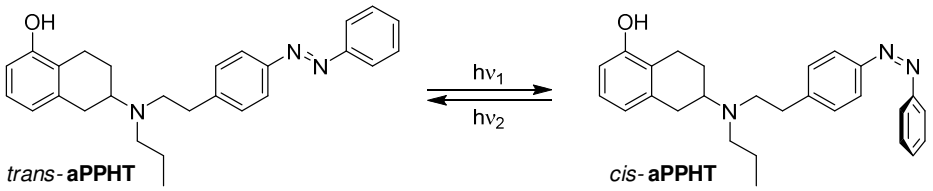

Figure 1. Dopamine receptor, ligands and design of a photochromic ligand (PCL). A) X-ray structure of a D3 dopamine receptor co-crystallized with **eticlopride** (D3R, pdb 3PBL) from top view and table of DR-subtypes and their primary G-protein coupling partners. D_1 and D_5 have an activating effect and are referred to as D_1-like. $D_{2\text{-}4}$ have an inhibitory effect and are referred to as D_2-like.[23] B) D2/3R agonists. **DPAT** = dipropyl-aminotetraline, **PPHT** = phenethyl-propyl-hydroxytetraline. C) Isomerization of a photoswitchable version of **PPHT** called **aPPHT**.

Results and discussion

PCL design and synthesis. To broaden the reach of photopharmacology and develop novel optical tools for investigating DRs with high spatiotemporal precision,[24] **PPHT** was chosen as a platform for photochromic DR agonists. Derivatives such as **NBD-PPHT** demonstrate tolerance for aromatic substitution at the 4′-position of the pendent phenethyl moiety.[25] We therefore designed azobenzene versions of **PPHT** called **aPPHT** as depicted in Figure 1C.

To furnish photoswitchable **PPHT** derivatives as photochromic ligands (PCLs) for DRs, different synthetic strategies were established, each having individual advantages. The first synthesis led to racemic **aPPHT**. Commercial tetralone **1** underwent reductive amination with building block **2** that was known from our previous syntheses.(chapter III) The resulting secondary amine was obtained after aqueous work-up and applied to another reductive amination with propanal.

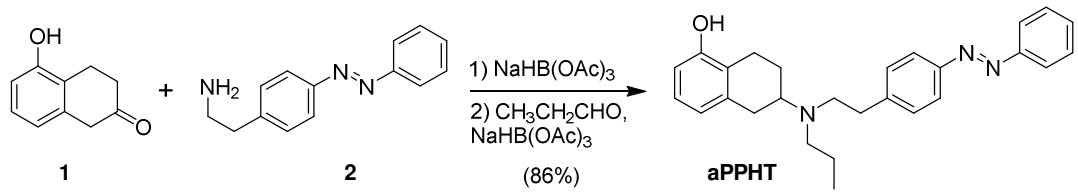

Scheme 1. Synthesis of racemic **aPPHT**.

Even though the parent compound **PPHT** is used as a racemate, it is known from similar DR-agonists such as 5-OH-DPAT that enantiomers can drastically differ in pharmacodynamics.[26] Accordingly, alternative routes with enantiomerically pure aminotetralins were developed. Bakthavachalam *et al.* developed a synthesis for *(R)* and *(S)*-**PPHT** derivatives in 1991 that served as a platform for our approach (Scheme 2A).[25] Permethylation of dihydroxy naphthalene **3** was followed by reduction using sodium in ethanol. The resulting methyl enol ether was cleaved during acidic work-up and tautomerized to the corresponding tetralone. Reductive amination with benzylamine gave rise to amino tetraline **4**.

Benzylamine delivers the nitrogen for future **aPPHT** molecules and furthermore enables crucial π–π-interactions in the subsequent chiral resolution using toluoyl tartaric acid derivatives. A crystal structure of the diastereomeric salt **I** is shown in Scheme 2B, demonstrating a strong complex of two π–π-interactions and a hydrogen bond network that is orchestrated by an additional water molecule.

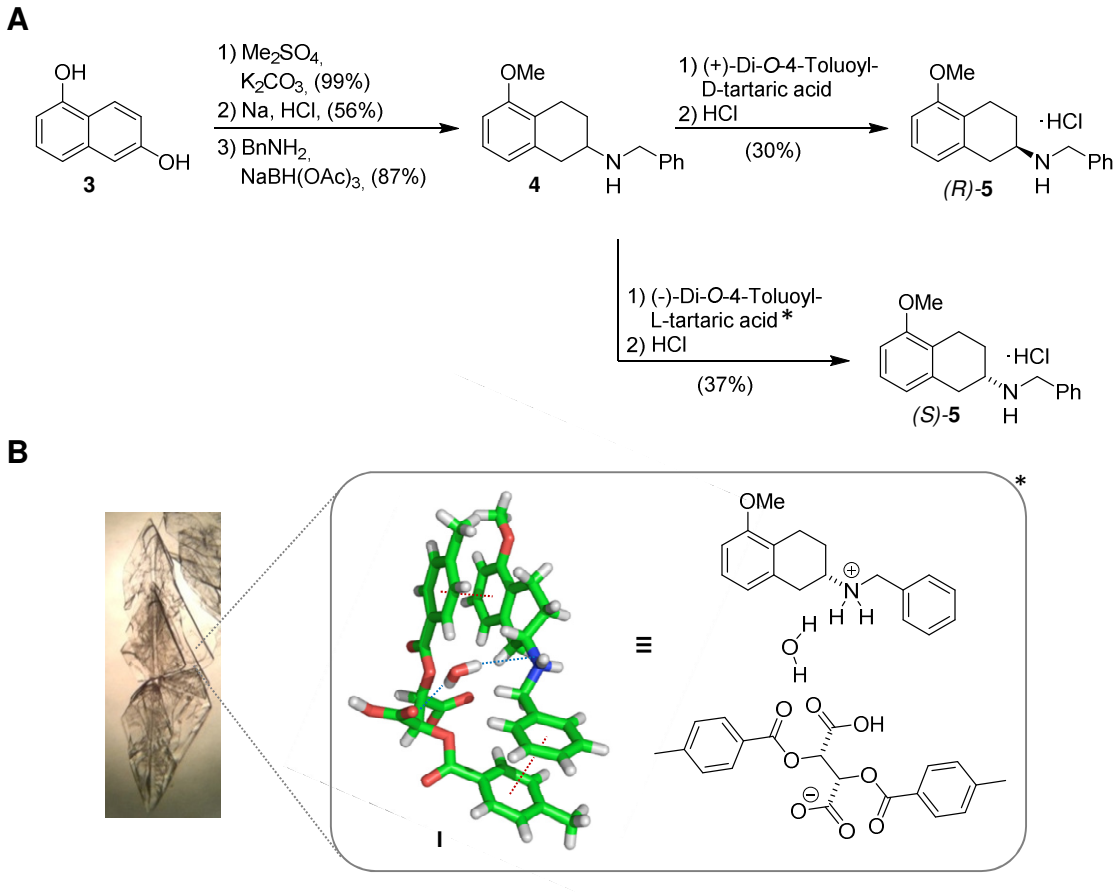

Scheme 2. Enantiomerically pure aminotetraline building blocks. A) Synthesis started from dihydroxy naphtaline **3** that was functionalized to racemic **4** in three steps. Precipitation with tartaric acid derivatives was used for resolution of the enantiomers. B) Crystal and X-ray structure of the tartaric acid/aminotetraline complex **I** demonstrates the desired stereochemistry. Dotted red lines indicate π-stacking, dotted blue lines indicates hydrogen bonding.

To furnish the target molecules *(R)*-**aPPHT** and *(S)*-**aPPHT**, two approaches were followed (Scheme 3). First, *(R)*-**5** was propylated and deprotected yielding amino tetraline *(R)*-**6** (Scheme 3A). Amide coupling with **7** followed by reduction and demethylation gave rise to known aniline *(R)*-**8**[25,27] that served as a nucleophile for a consecutive Mills reaction with nitrosobenzene yielding *(R)*-**aPPHT**. Employing aniline

(R)-**8** as an azobenzene precursor allows preparing many differently substituted **aPPHT**-derivatives in just one step.

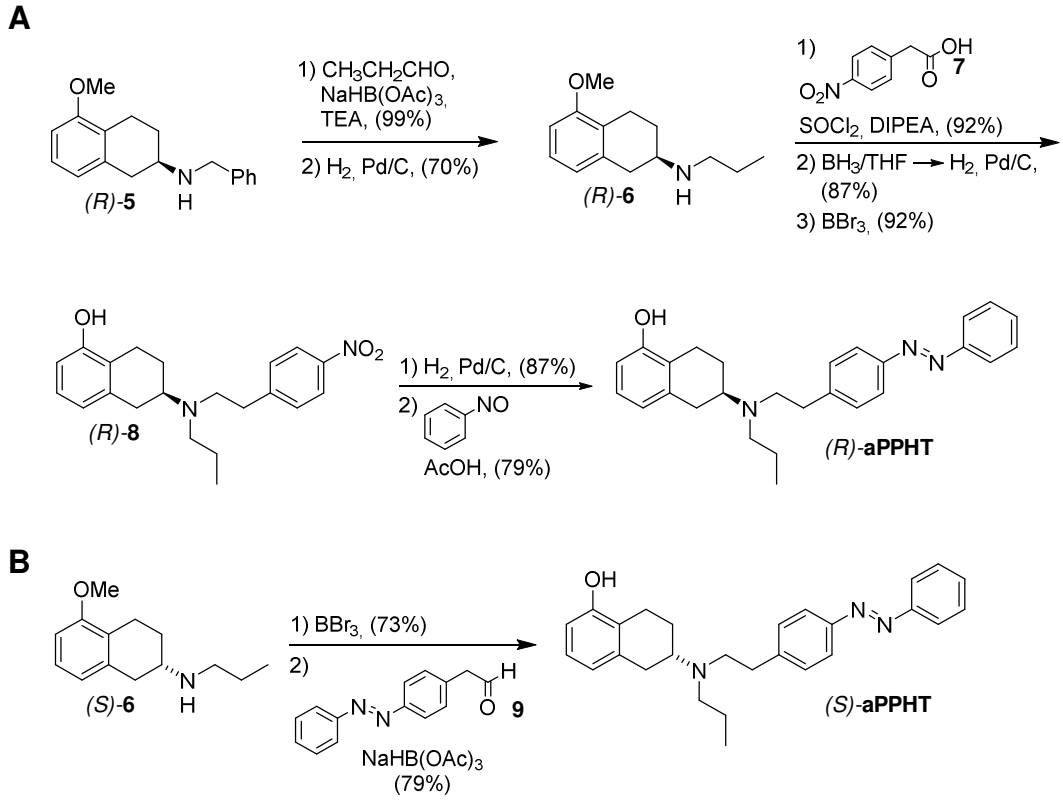

Scheme 3. Synthesis of chiral **aPPHTs**.

To offer an alternative, more modular synthesis, the order of functional group modification after chiral resolution was changed employing an azobenzene building block was (Scheme 3B). Starting from secondary amine *(S)*-**6** (Scheme 3B), *O*-demethylation was followed by reductive amination with freshly prepared aldehyde **9**[28] giving *(S)*-**aPPHT**.

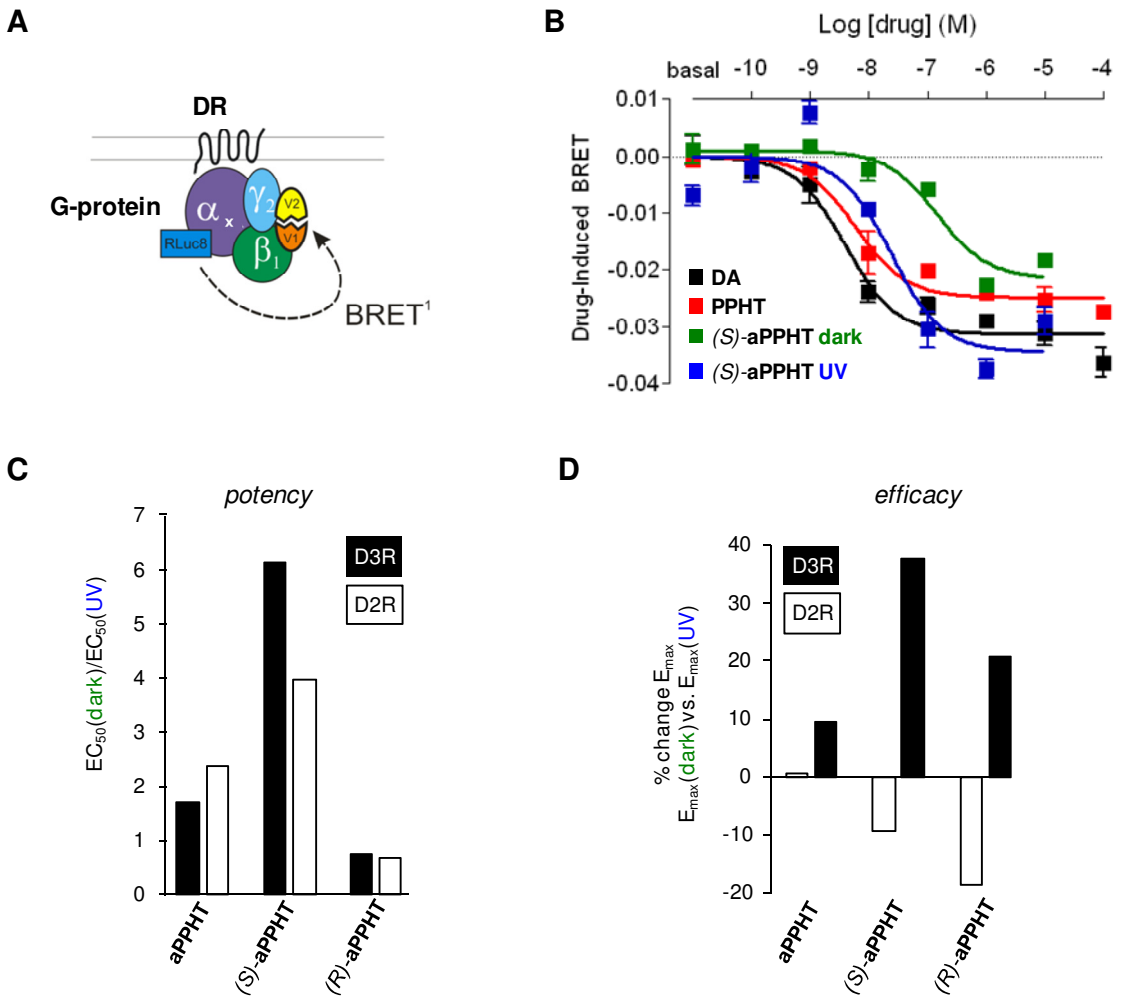

Figure 2. BRET-Assay of **aPPHTs**.[7] A) DR read-out via bioluminescence resonance energy transfer (BRET). B) Representative dose-response curves on D3R. **DA** (black line), **PPHT** (red line), and *(S)*-**aPPHT** with (blue line) and without (green line) UV-pre-illumination. C) Comparison of potency change after pre-illumination. Black bars indicate the EC_{50}-ratio using D3R, white bars using D2R. Potency of *(S)*-**aPPHT** changes most drastically after pre-illumination, especially on D3R. D) Comparison of maximal efficacy after pre-illumination. *(S)*-**aPPHT** activates D3R 40% more when pre-illuminated with UV-light. (Error bars indicate SEM, n = 3).

With racemic **aPPHT** and its single enantiomers in hand, it was next tested if the novel PCLs trigger the guanine nucleotide exchange factor activity of DRs. Therefore, an assay that is based on a bioluminescence resonance energy transfer (BRET)[1] between the Gα and Gβγ-subunit of heterotrimeric G-proteins was employed (Figure 2A).[15] Binding of a DR-agonist stabilizes a receptor conformation that catalyzes the exchange of GDP for GTP at G-proteins. The consequential dissociation of the heterotrimeric

[7] All BRET-data were acquired and analyzed by Prashant Donthamsetti from Columbia University (Javitch research group)

protein complex leads to an increased distance between Gα and Gβγ-subunits and therefore a reduced BRET signal. Corresponding dose-response curves of **DA** and **PPHT** are depicted in Figure 2B (black and red line respectively. D3R and *(S)*-**aPPHT** are chosen as an example). In comparison to these known agonists, dark adapted, i.e. *trans*-enriched, *(S)*-**aPPHT** showed both lower potency and efficacy (Fig 2B, green line).

Addressing the photoswitching properties of **aPPHTs** in-time was not compatible with the BRET-assay. However, we relied on the thermal stability of alkylated *cis*-azobenzenes and performed the identical experiment with a solution of the photoswitch that was pre-illuminated with UV-light, i.e. *cis*-enriched (Figure 2B, blue line, *(S)*-**aPPHT** as an example). Compared to the dark adapted compound, *cis-(S)*-**aPPHT** has not only improved potency, but also efficacy.

While the experimental setup did not allow in-time investigation of reversible photoswitching, it was capable of outlining important trends and allows comparing different PCLs and receptors. All molecules – **aPPHT**, *(R)*-**aPPHT** and *(S)*-**aPPHT** – were compared for their ability to change their potentcy and efficacy on both D2R and D3R after UV-pre-illumination. *(S)*-**aPPHT** provides the most pronounced change in potency with a 4-fold lower EC_{50} at D2R and 6-fold lower at D3R after UV-pre-illumination (Figure 2C). Advantageously, the combination of *(S)*-**aPPHT** and D3R also leads to the highest change in efficacy with a 40% higher receptor activation after *cis*-enrichment (related to full **DA**-activation, Figure 2D). Interestingly, both enantiomers change their efficacies in the opposite direction when comparing D2R and D3R. For the former, the maximal effect is reduced after pre-illumination, while for the latter it is enhanced. These valuable insights demonstrated that there is a significant difference between the **aPPHT** enantiomers. *(S)*-**aPPHT** provides the biggest change in both potency and efficacy when comparing *trans* and *cis*-enriched solutions, in particular at the D3R.

Summary and Outlook

We have developed photochromic ligands for dopamine receptors. Racemic and enantiomerically pure azobenzene derivatives of **PPHT** (**aPPHTs**) have been synthesized. Preliminary testing using a BRET assay has identified *(S)*-**aPPHT** as a promising candidate for switching the dopamine D3 receptor with light. Future electrophysiological testing will reveal the full potential of *(S)*-**aPPHT**.

Acknowledgements

We thank Prashant Domthansetti and Jonathan Javitch from Columbia University for being open-minded and enthusiastic collaborators.

Abbreviations

DR	Dopamine receptor
AChR	Acetylcholine receptor
GPCR	G-Protein coupled receptor
GDP	Guanosine diphosphate
GTP	Guanosine triphosphate
GIRK	G-Protein coupled inwardly rectifying potassium
DA	Dopamine
DPAT	Dipropyl aminotetraline
PPHT	Propyl phenethyl aminotetraline
PCL	Photochromic ligand
NBD	Nitrobenzoxadiazole
aPPHT	Azo-PPHT
TEA	Triethylamine
DIPEA	Diisopropyl ethyl amine
BRET	Bioluminescence resonance energy transfer
DCM	Dichloromethane
DCE	1,2-Dichloroethane

REFERENCES

1. Katritch, V., Cherezov, V. & Stevens, R.C. Diversity and modularity of G protein-coupled receptor structures. *Trends Pharmacol Sci* **33**, 17-27 (2012).

2. Ma, P. & Zemmel, R. Value of novelty? *Nat Rev Drug Discov* **1**, 571-572 (2002).

3. Lagerstrom, M.C. & Schioth, H.B. Structural diversity of G protein-coupled receptors and significance for drug discovery. *Nat Rev Drug Discov* **7**, 339-57 (2008).

4. Stevens, R.C. et al. The GPCR Network: a large-scale collaboration to determine human GPCR structure and function. *Nat Rev Drug Discov* **12**, 25-34 (2013).

5. Lüscher, C. & Slesinger, P.A. Emerging roles for G protein-gated inwardly rectifying potassium (GIRK) channels in health and disease. *Nat Rev Neurosci* **11**, 301-315 (2010).

6. Lacey, M.G., Mercuri, N.B. & North, R.A. Dopamine acts on D2 receptors to increase potassium conductance in neurones of the rat substantia nigra zona compacta. *J Physiol* **392**, 397-416 (1987).

7. Chen, X. et al. Structure-Functional Selectivity Relationship Studies of Î²-Arrestin-Biased Dopamine D2 Receptor Agonists. *Journal of Medicinal Chemistry* **55**, 7141-7153 (2012).

8. Zhang, J. et al. Cellular trafficking of G protein-coupled receptor/beta-arrestin endocytic complexes. *J Biol Chem* **274**, 10999-1006 (1999).

9. Kim, K.M. et al. Differential regulation of the dopamine D2 and D3 receptors by G protein-coupled receptor kinases and beta-arrestins. *J Biol Chem* **276**, 37409-14 (2001).

10. Urizar, E. et al. CODA-RET reveals functional selectivity as a result of GPCR heteromerization. *Nat Chem Biol* **7**, 624-30 (2011).

11. Shonberg, J. et al. A Structure-Activity Analysis of Biased Agonism at the Dopamine D2 Receptor. *Journal of Medicinal Chemistry* **56**, 9199-9221 (2013).

12. Hiller, C. et al. Functionally Selective Dopamine D2/D3 Receptor Agonists Comprising an Enyne Moiety. *Journal of Medicinal Chemistry* **56**, 5130-5141 (2013).

13. Beaulieu, J.M. & Gainetdinov, R.R. The physiology, signaling, and pharmacology of dopamine receptors. *Pharmacol Rev* **63**, 182-217 (2011).

14. Volkow, N.D. et al. Predominance of D2 receptors in mediating dopamine's effects in brain metabolism: effects of alcoholism. *J Neurosci* **33**, 4527-35 (2013).

15. Newman, A.H. et al. Molecular determinants of selectivity and efficacy at the dopamine D3 receptor. *J Med Chem* **55**, 6689-99 (2012).

16. Chien, E.Y. et al. Structure of the human dopamine D3 receptor in complex with a D2/D3 selective antagonist. *Science* **330**, 1091-5 (2010).

17. Volkow, N.D., Wang, G.-J., Fowler, J.S. & Tomasi, D. Addiction Circuitry in the Human Brain. *Annual Review of Pharmacology and Toxicology* **52**, 321-336 (2012).

18. Mottola, D.M. et al. Functional Selectivity of Dopamine Receptor Agonists. I. Selective Activation of Postsynaptic Dopamine D2 Receptors Linked to Adenylate Cyclase. *Journal of Pharmacology and Experimental Therapeutics* **301**, 1166-1178 (2002).

19. Pritchard, L.M. et al. 7-OH-DPAT and PD 128907 Selectively Activate the D3 Dopamine Receptor in a Novel Environment. *Neuropsychopharmacology* **28**, 100-107 (2002).

20. Tulloch, I.F. Pharmacologic profile of ropinirole: a nonergoline dopamine agonist. *Neurology* **49**, S58-62 (1997).

21. Millan, M.J. et al. Differential Actions of Antiparkinson Agents at Multiple Classes of Monoaminergic Receptor. I. A Multivariate Analysis of the Binding Profiles of 14 Drugs at 21 Native and Cloned Human Receptor Subtypes. *Journal of Pharmacology and Experimental Therapeutics* **303**, 791-804 (2002).

22. Seeman, P. et al. Dopamine D2 receptor binding sites for agonists. A tetrahedral model. *Molecular Pharmacology* **28**, 391-399 (1985).

23. Neve, K.A., Seamans, J.K. & Trantham-Davidson, H. Dopamine receptor signaling. *J Recept Signal Transduct Res* **24**, 165-205 (2004).

24. Fehrentz, T., Schonberger, M. & Trauner, D. Optochemical genetics. *Angew Chem Int Ed Engl* **50**, 12156-82 (2011).

25. Bakthavachalam, V., Baindur, N., Madras, B.K. & Neumeyer, J.L. Fluorescent probes for dopamine receptors: synthesis and characterization of fluorescein and 7-nitrobenz-2-oxa-1,3-diazol-4-yl conjugates of D-1 and D-2 receptor ligands. *J Med Chem* **34**, 3235-41 (1991).

26. Karlsson, A., Bjork, L., Pettersson, C., Anden, N.E. & Hacksell, U. (R)- and (S)-5-hydroxy-2-(dipropylamino)tetralin (5-OH DPAT): assessment of optical purities and dopaminergic activities. *Chirality* **2**, 90-5 (1990).

27. Soriano, A. et al. Adenosine A2A receptor-antagonist/dopamine D2 receptor-agonist bivalent ligands as pharmacological tools to detect A2A-D2 receptor heteromers. *J Med Chem* **52**, 5590-602 (2009).

28. Schönberger, M. & Trauner, D. A Photochromic Agonist for μ-Opioid Receptors. *Angewandte Chemie International Edition* **in press**(2014).

Experimental Procedures

aPPHT

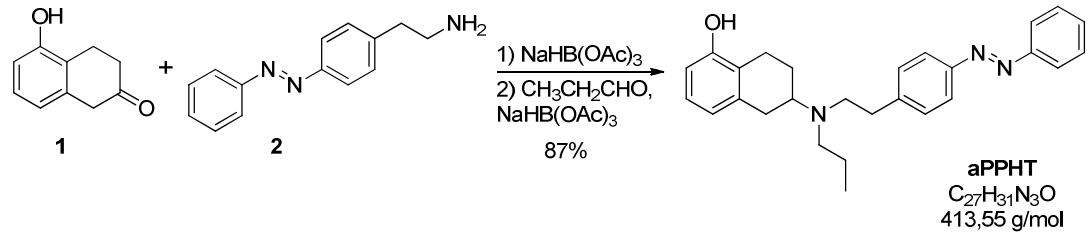

Amine **2** (73 mg, 0.32 mmol, 1.05 eq) and hydroxytetralone **1** (50 mg, 0.31 mmol, 1.0 eq) were dissolved in 2 mL DCE under N_2-atm. $NaHB(OAc)_3$ (103 mg, 0.46 mmol, 1.5 eq) was added and the resulting reaction suspension was stirred overnight. The reaction was quenched by partitioning between EtOAc and conc. $NaHCO_{3(aq)}$ and the organic phase was further washed with $NaHCO_{3(aq)}$, 10% $NaCl_{(aq)}$ and brine. The EtOAc layer was dried using Na_2SO_4 and concentrated in vacuo yielding the crude alkylation product as an orange oil, which was immediately transferred to the next step.

The freshly prepared secondary amine (described above) was redissolved in 1.5 mL DCE under N_2-atm and treated with propionaldehyde (25 µL, 0.34 mmol, 1.2 eq) followed by $NaHB(OAc)_3$ (103 mg, 0.46 mmol, 1.5 eq). After 5 h, the reaction was quenched and worked up as described above yielding the crude product tertiary amine. Medium pressure chromatography (Biotage, 25 g SiO_2 column, gradient 10 to 100% EtOAc in hexanes) afforded **aPPHT** as an orange oil (110 mg, 0.27 mmol, 87%).

TLC (SiO_2, 50% EtOAc, 50% hexanes) R_f = 0.6 (UV)

^{1}H NMR (599 MHz, $CDCl_3$) δ = 7.94 – 7.89 (m, 2H), 7.89 – 7.83 (m, 2H), 7.54 – 7.49 (m, 2H), 7.49 – 7.44 (m, 1H), 7.37 – 7.32 (m, 2H), 6.99 (t, *J*=7.8, 1H), 6.68 (d, *J*=7.7, 1H), 6.60 (d, *J*=7.9, 1H), 5.40 (s, 1H), 3.06 – 2.87 (m, 3H), 2.85 (s, 4H), 2.82 – 2.66 (m, *J*=28.9, 15.2, 9.4, 1H), 2.63 – 2.53 (m, 3H), 2.13 – 2.07 (m, 1H), 1.68 – 1.57 (m, 1H), 1.57 – 1.47 (m, 2H), 0.91 (t, *J*=7.3, 3H).

^{13}C NMR (151 MHz, $CDCl_3$) δ = 153.46, 152.72, 151.07, 144.48, 138.37, 130.72, 129.52, 129.04, 126.40, 122.94, 122.83, 122.73, 121.68, 111.97, 56.58, 52.62, 52.54, 35.81, 32.24, 25.70, 23.60, 22.08, 11.93.

HRMS (ESI, positive): calcd for $C_{27}H_{32}N_3O$ $[M+H]^+$: 414.2545; found: 414.2537.

Dimethoxy naphthalene s1[27]

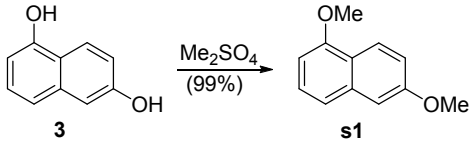

3 **s1**

$C_{12}H_{12}O_2$
188,22 g/mol

To a solution of K_2CO_3 (30.2 g, 219.0 mmol, 3.5 eq) in acetone (100 ml) were sequentially added 1,6-Dihydronapthalene **3** (10.0 g, 62.4 mmol, 1.0 eq) and Me_2SO_4 (23.6 g, 187.0 mmol, 3.5 eq) at room temperature under N_2-atmosphere. The solution was refluxed for 3.5 h, cooled to RT and filtered. The filtrate was concentrated *in vacuo*, dissolved in EtOAc (250 ml), washed with 1M $NaOH_{(aq)}$ (2x50 ml) and brine before drying over $MgSO_4$. The solution was concentrated *in vacuo* and the resulting crude product was purified by flash chromatography (SiO_2, gradient 0 to 20% EtOAc in hexanes). The product was obtained as a yellow solid (11.74 g, 62.4 mmol, 99 %).

TLC (SiO_2, 20 % EtOAc in hexane), R_f = 0.71 (UV)

^{1}H NMR (400 MHz, dmso-d_6) δ = 8.01 (d, *J*=9.2, 1H), 7.34 (d, *J*=4.8, 2H), 7.24 (d, *J*=2.6, 1H), 7.08 (dd, *J*=2.6, 9.2, 1H), 6.81 – 6.74 (m, 1H), 3.91 (s, 3H), 3.83 (s, 3H).

HRMS (EI): calc. for $C_{12}H_{12}O_2$ $(M)^-$: 188.0837; found: 188.0824.

Methoxytetralone s2[27]

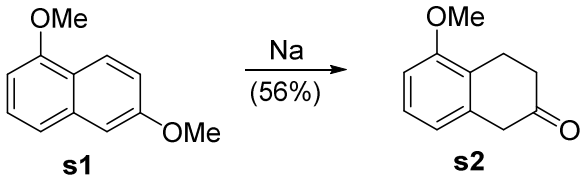

s1 **s2**

$C_{11}H_{12}O_2$
176,21 g/mol

A solution of 1,6-dimethoxynaphatalene **s1** (11.74 g, 62.4 mmol, 1.0 eq.) in EtOH (176 ml) was heated to 50 °C. To this solution, metallic Na (14.33 g, 624 mmol, 10.0 eq.) was added in small potions over a period of 30 min. After heat formation had slowed down, the solution was heated to reflux for 2.5 h. After the reaction mixture was cooled to room temperature and pH was adjusted to pH < 1 with 5 M $HCl_{(aq)}$. The resulting mixture was refluxed for 30 min and then stirred overnight at RT. After dilution with H_2O (100 ml), the aqueous solution was extracted with DCM (4 x 150 ml). Combined organic layers were washed with 10% $NaCl_{(aq)}$ (1 x 100 ml) and brine before beign dried over $MgSO_4$ and concentrated *in vacuo*. The resulting crude material was purified by flash chromatography (SiO_2, gradient 0 - 10% EtOAc in hexane). The product was obatained as a yellow oil (6.1342 g, 34.81 mmol, 56 %).

TLC (SiO2, 20% EtOAc, 80% hexanes) R_f = 0.42 (UV)

^{1}H NMR (400 MHz, dmso-d_6) δ = 7.14 (t, 1H), 6.84 (d, *J*=8.0, 1H), 6.73 (d, *J*=8.4, 1H), 3.77 (s, 3H), 3.53 (s, 2H), 2.96 (t, *J*=6.7, 2H), 2.41 – 2.35 (m, 2H).

HRMS (EI): calc. for $C_{11}H_{12}O_2$ $(M)^-$: 176.0837; found: 176.0831.

***N*-Benzyl-aminotetraline 4**[25]

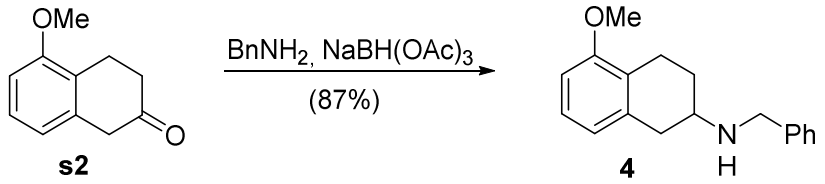

s2 **4**

$C_{18}H_{21}NO$
267,37 g/mol

To a solution of tetralone **s2** (6.13 g, 34.81 mmol, 1.0 eq) in DCE (90 ml) was added benzyl amine (4.95 ml, 4.85 g, 45.3 mmol, 1.3 eq) followed by $NaBH(OAc)_3$ (13.3 g, 62.7 mmol, 1.8 eq). The reaction mixture was stirred over night at room temperature and then partitioned between conc. $NaHCO_{3(aq)}$ (90 ml) and EtOAc (90 ml). The layers were separated and the aqueous layer was extracted with EtOAc (4 x 90 ml). The combined organic layers were washed with brine, dried over $MgSO_4$ and concentrated *in vacuo*. The resulting crude material was purified by flash chromatography (SiO_2, gradient 0 to 10 % MeOH in DCM + 1 % TEA). The product was obatained as a brown oil (8.082 g, 30.23 mmol, 87 %).

TLC (SiO_2, 4 % MeOH in DCM + 1 % TEA), R_f = 0.67 (UV, ninhydrin)

^{1}H NMR (400 MHz, dmso-d_6) δ = 7.34 (dd, *J*=3.2, 5.2, 2H), 7.30 – 7.24 (m, 2H), 7.21 – 7.15 (m, 1H), 7.02 (t, *J*=7.9, 1H), 6.68 (d, *J*=8.0, 1H), 6.62 (d, *J*=7.6, 1H), 3.77 (s, 2H), 3.71 (s, 3H), 2.91 (dd, *J*=4.2, 16.0, 1H), 2.79 – 2.69 (m, 2H), 2.52 – 2.34 (m, 2H), 2.03 – 1.92 (m, 1H), 1.44 (dtd, *J*=5.8, 10.2, 12.7, 1H).

^{13}C NMR (101 MHz, dmso-d_6) δ = 157.10, 141.70, 137.02, 128.48, 128.37, 126.84, 126.52, 124.77, 121.66, 107.59, 55.49, 52.12, 50.53, 36.52, 28.83, 22.12.

HRMS (EI): calc. for $C_{18}H_{21}NO$ $(M)^-$: 267.1623; found: 267.1625.

***N*-Benzyl-aminotetraline** *(R)*-**5**[25]

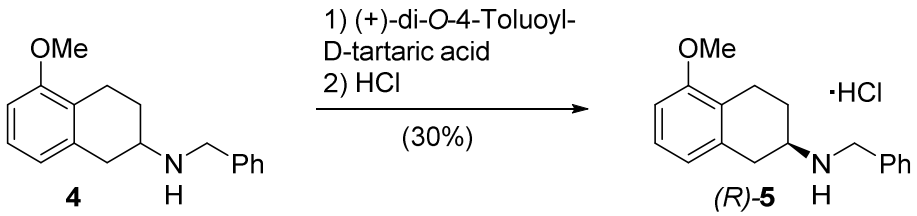

To a solution of *N*-benzyl-5-methoxy-1,2,3,4-tetrahydronaphthalen-2-amine **xx** (4.9 g, 18.3 mmol, 1.0 eq) in acetone (60 mL) was added (+)-Di-p-toluoyl-D-tartaric acid (7.8 g, 20.2 mmol, 1.1 eq). The solution was refluxed for 1 h and then stirred over night at RT. The resulting precipitate was removed by filtration and recrystallized 2 times from acetone. The pure tartrate salt (3.6 g, 5.5 mmol, 30 % yield) was converted to the HCl salt (1.650 g, 5.43 mmol, 99 % yield).

$[\alpha]_D$ (HCl salt) = + 58.2 ° (c = 2, MeOH).

***N*-Benzyl-aminotetraline** *(S)*-**8**[25]

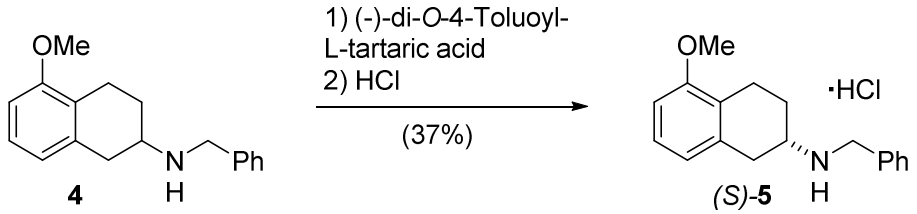

The partially enriched aminotetraline from the resolution above was free based and treated with 1 eq (-)-Di-p-toluoyl-L-tartaric acid. The precipitated tartrate salt was recrystallized until optical rotation was constant.

$[\alpha]_D$ (HCl salt) = - 58.4 ° (c = 2, MeOH).

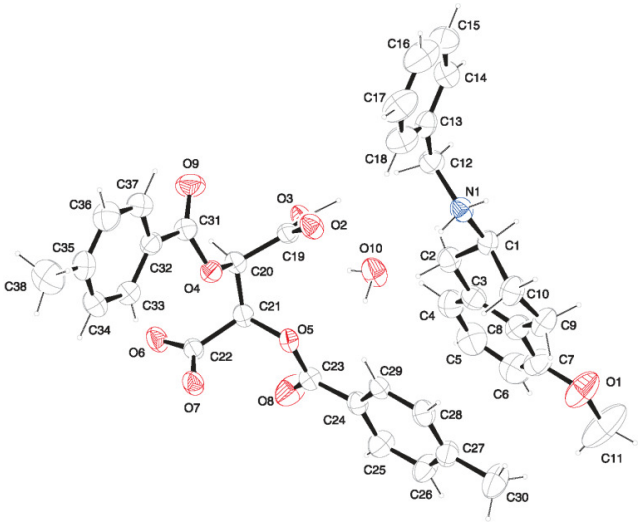

1. Crystallographic data. Diastereomeric salt intermeidate **I**

	I
net formula	$C_{38}H_{41}NO_{10}$
M_r/g mol^{-1}	671.733
crystal size/mm	0.35 × 0.23 × 0.09
T/K	173(2)
radiation	MoKα
diffractometer	'KappaCCD'
crystal system	monoclinic
space group	$P2_1$
a/Å	7.4782(2)
b/Å	29.0521(10)
c/Å	8.0823(2)
α/°	90
β/°	100.029(2)
γ/°	90
V/Å^3	1729.11(9)
Z	2
calc. density/g cm^{-3}	1.29021(7)
μ/mm^{-1}	0.093
absorption correction	none
refls. measured	9889
R_{int}	0.0374
mean σ(*I*)/*I*	0.0349
θ range	3.31–25.25
observed refls.	2678
x, y (weighting scheme)	0.0673, 0.4279
hydrogen refinement	mixed
Flack parameter	0.2(13)
refls in refinement	3115
parameters	460
restraints	1
$R(F_{obs})$	0.0435
$R_w(F^2)$	0.1179
S	1.059
shift/error$_{max}$	0.001
max electron density/e Å^{-3}	0.189
min electron density/e Å^{-3}	–0.167

***N*-Benzyl-*N*-propyl-aminotetraline** *(R)*-**s3**[25]

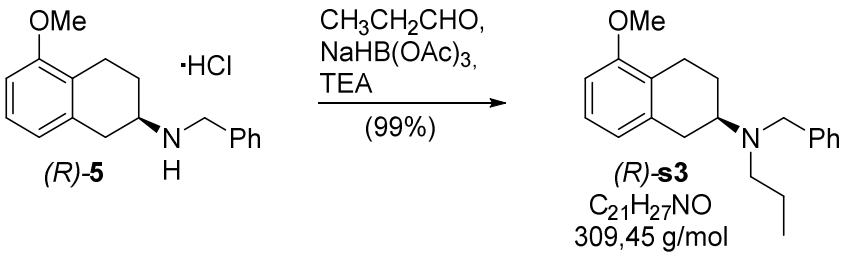

To a solution of *(R)*-**5** (800 mg, 2.6 mmol, 1.0 eq) and TEA (544 mg, 5.27 mmol, 2.0 eq) in DCE (25 mL) was added propionaldehyde (177 mg, 3.1 mmol, 1.1 eq) followed by $NaBH(OAc)_3$ (854 mg, 4.0 mmol, 1.5 eq). The reaction mixture was stirred for 3 h at RT and concentrated *in vacuo* before it was partitioned between conc. $NaHCO_{3(aq)}$ (60 mL) and EtOAc (60 mL). The layers were separated and the aqueous layer was extracted with EtOAc (3 x 60 mL). Combined organic layers were washed with brine, dried on Na_2SO_4 and concentrated *in vacuo*. The product was obtained as a white amorphous solid (810 mg, 2.62 mmol, 99 %).

^{1}H NMR (400 MHz, dmso-d_6) δ = 7.31 (s, 2H), 7.26 (s, 2H), 7.17 (s, 1H), 7.01 (t, *J*=7.8, 1H), 6.66 (d, *J*=8.3, 1H), 6.63 (d, *J*=7.8, 1H), 3.69 (s, 3H), 3.62 (s, 2H), 2.84 (d, *J*=17.6, 2H), 2.74 (s, 2H), 2.43 (s, 2H), 2.39 – 2.29 (m, 1H), 2.06 – 1.87 (m, 1H), 1.60 – 1.44 (m, 1H), 1.36 (s, 2H), 0.77 (t, *J*=7.3, 3H).

^{13}C NMR (101 MHz, dmso-d_6) δ = 157.16, 141.72, 137.98, 128.49, 126.90, 126.62, 124.64, 121.76, 107.60, 55.61, 55.49, 54.29, 51.82, 32.04, 25.01, 23.93, 21.64, 12.11.

HRMS (ESI, positive): calc. for $C_{21}H_{28}NO$ $(M+1)^+$: 310.2171; found: 310.2166.

$[\alpha]_D$ = + 24.5 ° (c = 1, MeOH).

***N*-Propyl-aminotetraline** *(R)*-**6**[25,27]

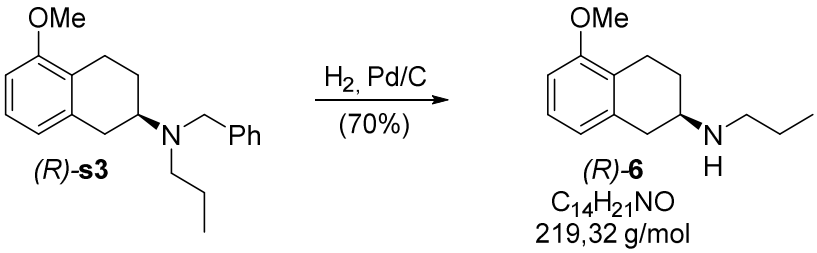

To a solution of (*R*)-**s3** (760 mg, 2.41 mmol, 1.0 eq) in MeOH (10 mL) was added Pd/C (256 mg (10% Pd), 0.24 mmol, 0.1 eq). The reaction mixture was then stirred vigorously over night under a H_2 atmosphere at RT. The reaction suspension was then filtrated and the filtrate concentrated *in vacuo*. The product was obtained as a brown oil (524 mg, 2.39 mmol, 70 %).

1H NMR (400 MHz, dmso-d_6) δ = 7.01 (t, *J*=7.9, 1H), 6.67 (d, *J*=8.0, 1H), 6.60 (d, *J*=7.6, 1H), 3.70 (s, 3H), 2.86 (dd, *J*=4.2, 15.9, 1H), 2.71 (ddd, *J*=4.1, 8.6, 9.9, 2H), 2.52 (t, *J*=7.3, 2H), 2.46 – 2.35 (m, 2H), 1.98 – 1.87 (m, 1H), 1.45 – 1.30 (m, 3H), 1.16 (s, 1H), 0.85 (t, *J*=7.4, 3H).

13C NMR (75 MHz, dmso-d_6) δ = 157.11, 137.11, 126.46, 124.85, 121.65, 107.55, 55.47, 53.08, 49.03, 36.78, 29.08, 23.59, 22.15, 12.35.

HRMS (ESI, positive): calc. for $C_{14}H_{22}NO$ $(M+1)^+$: 220.1701; found: 220.1697.

$[\alpha]_D$ = + 69.8 ° (c = 1, MeOH).

Amide *(R)*-**s4**[25,27]

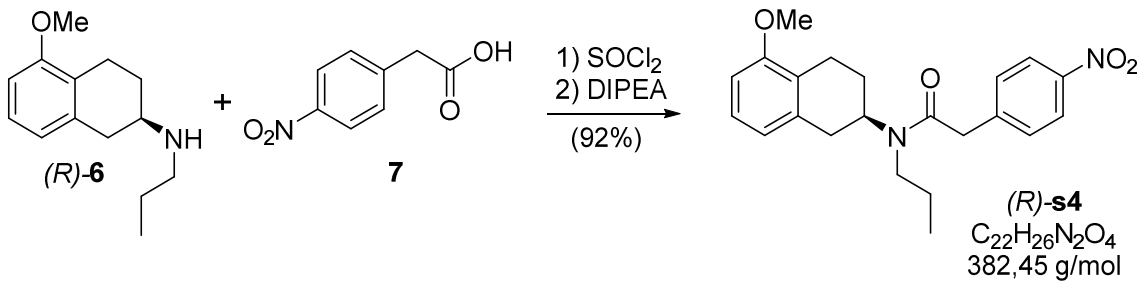

Preperation of acid chloride. A solution of 4-Nitrophenylacetic acid **7** (826 mg, 4.56 mmol, 2.0 eq) and $SOCl_2$ (2712 mg, 22.8 mmol, 10.0 eq) in dry THF (15 mL) was refluxed for 3 h. The solvent was removed *in vacuo* und the resulting acid chloride was stripped with chloroform (2 x 10 mL) followed by DCM (1 x 10 mL).

Amide coupling. The freshly prepared acid chloride was redissolved in 15 mL DCM and added to an ice-cooled solution of (*R*)-**6** (500 mg, 2.28 mmol, 1.0 eq) in 15 mL DCM under N_2-atmosphere. The solution was warmed to RT and stirred over night and DIPEA (1.18 g, 9.12 mmol, 4.0 eq) was added, which turned the orange reaction suspension to a dark red solution. This solution was concentrated *in vacuo*, redissolved in EtOAc (50 mL) and washed with conc. $NaHCO_{3(aq)}$ (2 x 20 mL) and brine. The EtOAc layer was separated, dried over Na_2SO_4 and concentrated *in vacuo*. The resulting crude amide was purified by automated flash column chromatography (Biotage, 100 g SiO_2, gradient 1 – 10 % MeOH in DCM). The product was obtained as a brown oil (798 mg, 2.09 mmol, 92 %).

TLC (SiO2, 40% EtOAc, 60% hexanes), R_f = 0.44 (UV)

^{1}H NMR (300 MHz, dmso) δ = 8.21 – 8.11 (m, 2H), 7.50 (dd, *J*=11.6, 8.8, 2H), 7.05 (td, *J*=7.9, 3.7, 1H), 6.72 (dd, *J*=8.1, 3.2, 1H), 6.64 (d, *J*=7.8, 1H), 4.37 – 4.23 (m, 1H), 4.11 – 4.00 (m, *J*=9.6, 1H), 3.88 (t, *J*=7.8, 1H), 3.73 (s, 3H), 3.17 – 3.08 (m, *J*=4.7, 1H), 2.99 – 2.77 (m, 3H), 2.75 – 2.60 (m, 2H), 1.88 – 1.68 (m, *J*=23.8, 11.8, 2H), 1.67 – 1.42 (m, *J*=30.8, 3H), 0.84 (dt, *J*=22.9, 7.4, 3H).

^{13}C NMR (75 MHz, dmso-d_6) δ = 169.68, 169.36, 157.21, 157.18, 146.60, 146.57, 145.17, 145.13, 137.10, 136.72, 131.22, 130.93, 126.81, 126.78, 124.02, 123.94, 123.64, 123.57, 121.57, 121.51, 107.89, 107.83, 55.60, 55.57, 55.34, 53.49, 51.62, 46.31, 43.39, 40.08, 33.89, 32.96, 27.93, 26.92, 24.59, 23.83, 23.64, 22.82, 11.92, 11.61.

HRMS (ESI, positive): calc. for $C_{22}H_{27}N_2O_4$ $(M+1)^+$: 383.1971; found: 383.1967.

HRMS (ESI, negative): calc. for $C_{22}H_{25}N_2O_4$ $(M-1)^-$: 381.1814; found: 381.1829.

Tertiary amine *(R)*-**s5**[25,27]

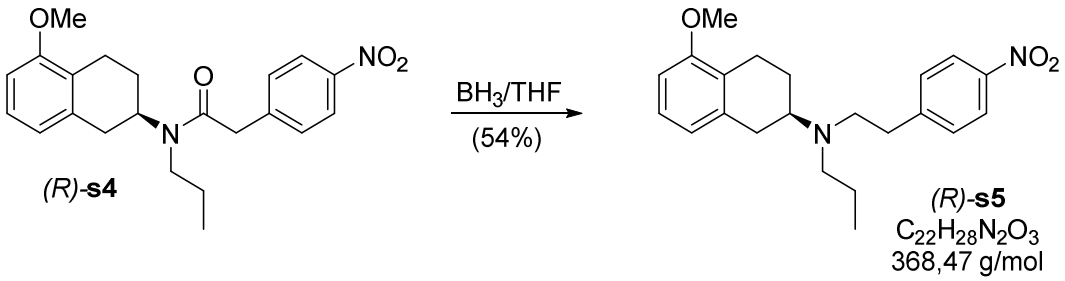

An ice-cooled solution of (*R*)-**s4** (500 mg, 1.13 mmol, 1.0 eq) in dry THF (20 mL) under N_2-atmosphere was slowly treated with a 1-M solution of BH_3·THF in THF (3.92 mL, 3.92 mmol, 3.0 eq). After stirring for 5 min at 0 °C, the solution was refluxed for 2 h. After cooling to RT, Na_2CO_3 (624 mg, 5.88 mmol, 5.2 eq) was added. The resulting solution was cooled to 0 °C and a 20 % solution of $(NH_4)_2S_{(aq)}$ (1.21 mL, 3.92 mmol, 3.0 eq) was added. The reaction mixture was then refluxed over night, cooled to RT and quenched with 6 M $HCl_{(aq)}$. It was then dissolved in H_2O, basified with conc. $NaOH_{(aq)}$ to pH = 14 and extracted with DCM (3 x 20 mL). The combined organic layers were washed with brine and dried over Na_2SO_4. The resulting solution was concentrated *in vacuo* and the crude material was purified by automated flash column chromatography (Biotage, 50 g SiO_2, gradient 2 – 55 % EtOAc in hexane). The product was obtained as a yellow oil (260 mg, 0.71 mmol, 54 %).

TLC (SiO2, 40% EtOAc, 60% hexanes), R_f = 0.61 (UV)

^{1}H NMR (400 MHz, dmso) δ = 8.12 – 8.05 (m, 2H), 7.51 – 7.43 (m, 2H), 7.00 (t, *J*=7.9, 1H), 6.64 (dd, *J*=21.2, 7.7, 2H), 3.70 (s, 3H), 2.86 – 2.70 (m, 5H), 2.62 (ddd, *J*=27.2, 16.4, 8.4, 2H), 2.47 (td, *J*=3.5, 1.6, 2H), 2.43 (d, *J*=7.3, 1H), 2.41 – 2.34 (m, 1H), 1.84 (dd, *J*=9.3, 2.6, 1H), 1.51 – 1.35 (m, 1H), 1.30 (dq, *J*=14.3, 7.2, 2H), 0.75 (t, *J*=7.3, 3H).

^{13}C NMR (101 MHz, dmso-d_6) δ = 157.13, 150.03, 146.18, 137.93, 130.58, 126.55, 124.76, 123.52, 121.80, 107.55, 55.87, 55.49, 51.89, 51.79, 35.25, 32.25, 25.47, 23.81, 21.96, 12.12.

HRMS (ESI, positive): calc. for $C_{22}H_{29}N_2O_3$ $(M+1)^+$: 369.2178; found: 369.2173.

HRMS (ESI, negative): calc. for $C_{22}H_{27}N_2O_3$ $(M-1)^-$: 367.2022; found: 367.2031.

$[\alpha]_D$ = + 14.5 ° (c = 1, MeOH).

Hydroxytetraline *(R)*-**s6**

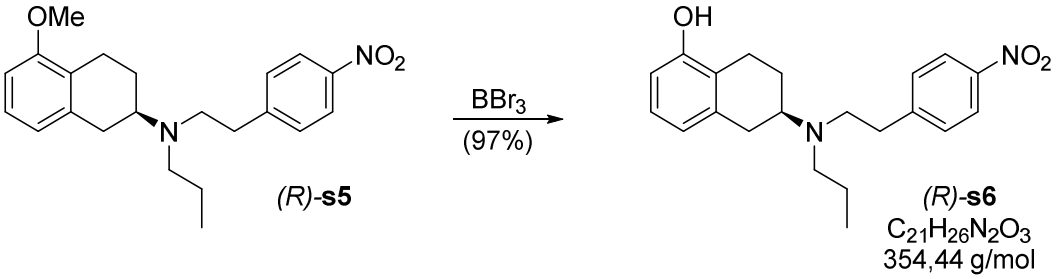

(R)-**s5**

(R)-**s6**
$C_{21}H_{26}N_2O_3$
354,44 g/mol

A solution of (*R*)-**s5** (225 mg, 0.665 mmol, 1.0 eq) in 1 mL DCM was cooled to - 78 °C under N_2-atmosphere and treated with a 1-M solution of BBr_3 in DCM (1462 µL, 1.46 mmol, 2.2 eq) was added and the reaction mixture was stirred for 30 min at – 78 °C. The reaction mixture was allowed to warm to room temperature and stirred for another 1.5 h before it was quenched with MeOH (2 mL). This solution was partitioned between conc. $NaHCO_{3(aq)}$ (20 mL) and DCM (20 mL). The layers were separated and the aqueous layer was extracted with DCM (3 x 10 mL). Combined organic layers were washed with brine, dried over Na_2SO_4 and concentrated *in vacuo*. The residue was purified using flash column chromatography (SiO_2, gradient 10 – 40 % EtOAc in hexane). The product was obtained as an orange oil (210 mg, 0.59 mmol, 97 %).

TLC (SiO2, 40% EtOAc, 60% hexanes), R_f = 0.42 (UV)

^{1}H NMR (400 MHz, dmso-d_6) δ = 9.11 (s, 1H), 8.14 – 8.09 (m, 2H), 7.52 – 7.47 (m, 2H), 6.83 (t, *J*=7.7, 1H), 6.53 (d, *J*=7.9, 1H), 6.46 (d, *J*=7.2, 1H), 2.84 – 2.71 (m, 5H), 2.67 – 2.51 (m, 2H), 2.44 (t, *J*=7.2, 2H), 2.42 – 2.32 (m, 1H), 1.90 – 1.80 (m, 1H), 1.43 (ddd, *J*=5.6, 12.0, 23.9, 1H), 1.31 (tt, *J*=7.2, 14.5, 2H), 1.23 – 1.18 (m, 1H), 0.75 (t, *J*=7.3, 3H).

^{13}C NMR (101 MHz, dmso-d_6) δ = 155.16, 150.07, 146.19, 138.06, 130.61, 126.28, 123.53, 123.35, 120.23, 111.87, 56.09, 51.91, 51.81, 35.28, 32.32, 25.62, 23.94, 21.99, 12.13.

HRMS (ESI, positive): calc. for $C_{21}H_{27}N_2O_3$ $(M+1)^+$: 355.2022; found: 355.2017.

HRMS (ESI, negative): calc. for $C_{21}H_{25}N_2O_3$ $(M-1)^-$: 353.1865; found: 353.1875.

$[\alpha]_D$ = + 13.4 ° (c = 1, MeOH).

Aniline *(R)*-**8**[25,27]

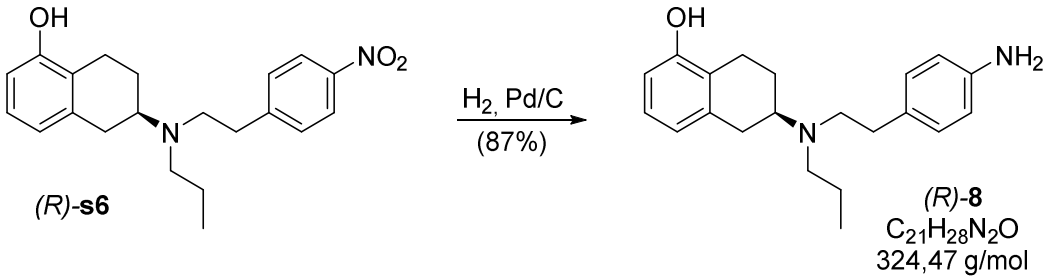

(R)-**s6**

(R)-**8**
$C_{21}H_{28}N_2O$
324,47 g/mol

A solution of (*R*)-**s6** (180 mg, 0.508 mmol, 1.0 eq) was dissolved in 10 mL MeOH at room temperature. A small amount of palladium on charcoal (10% Pd) was added and the atmosphere was exchanged with H_2. After vigorous stirring over night, the reaction mixture was filtered through celite and the filtrate was concentrated under reduced pressure. Filtration through a small plug of silica (first hexane, then ethyl acetate) afforded the product as a white amorphous solid (144 mg, 0.444mmol, 87%).

TLC (SiO2, 10% MeOH, 90% DCM), R_f = 0.31 (UV + ninhydrin)

HRMS (ESI, positive): calc. for $C_{21}H_{29}N_2O$ $(M+1)^+$: 325.2274; found: 325.2272.

HRMS (ESI, negative): calc. for $C_{21}H_{27}N_2O$ $(M-1)^-$: 323.2129; found: 325.2130.

(R)-**aPPHT**

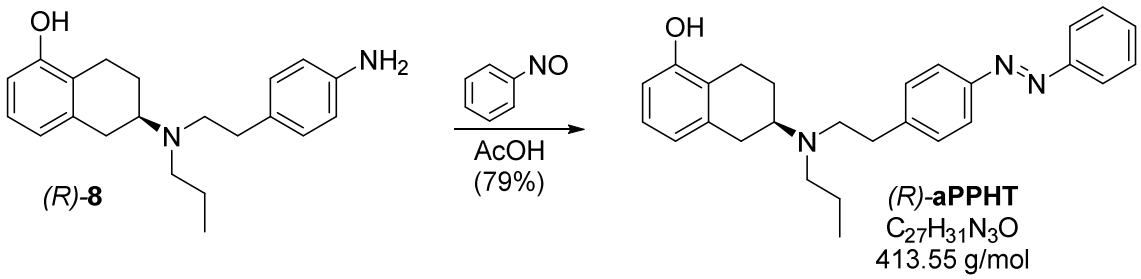

(R)-**8** (21 mg, 0.065 mmol, 1 eq) was dissolved in 2 mL DCM and treated with nitrosobenzene (10 mg, 0.097 mmol, 1.5 eq) and acetic acid (37 µL, 0.65 mmol, 10 eq). After stirring for 12 hours, the reaction was diluted with ethylacetate and extracted with $NaHCO_{3(aq)}$, water and brine. The organic layer was seperated, dried over Na_2SO_4 and concentrated under reduced pressure. Purification of the crude using silica gel chromatography (gradient 0% to 5% MeOH in DCM) afforded *(R)*-**aPPHT** as an orange oil (21 mg, 0.051 mmol, 79%).

TLC (SiO_2, 10% MeOH, 90% DCM), R_f = 0.48 (UV).

^{1}H NMR (400 MHz, $CDCl_3$) δ = 7.92 – 7.81 (m, 3H), 7.55 – 7.41 (m, 3H), 7.33 (d, *J*=8.3, 2H), 6.97 (t, *J*=7.8, 1H), 6.66 (d, *J*=7.7, 1H), 6.58 (d, *J*=7.9, 1H), 3.06 – 2.62 (m, 8H), 2.57 (s, 3H), 2.14 – 2.02 (m, 1H), 1.48 (s, 4H), 0.89 (t, *J*=7.4, 3H).

HRMS (ESI) calcd for $C_{27}H_{32}N_3O$ $[M+H]^+$: 414.2545; found: 414.2542.

HRMS (ESI) calcd for $C_{27}H_{30}N_3O$ $[M-H]^-$: 412.2389; found: 412.2398.

IR ν_{max}: 2952, 2925, 2849, 2358, 2332, 1658, 1585, 1465, 1276, 1261, 1084, 1020, 796, 768, 687.

***N*-Benzyl-*N*-propyl-aminotetraline** *(S)*-**s3**[25]

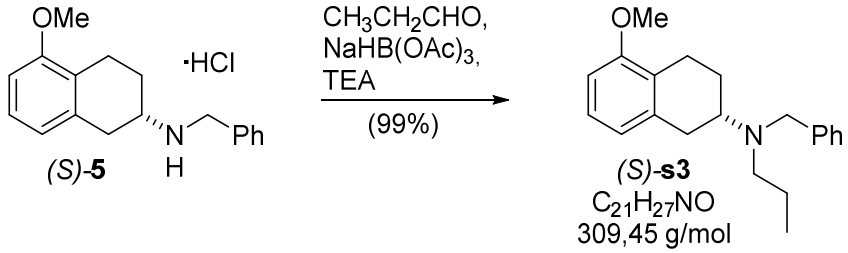

To a solution of (*S*)-**5** (300 mg, 0.987 mmol, 1.0 eq) and TEA (0.27 ml, 200 mg, 1.97 mmol, 2.0 eq) in DCE (10.5 ml) was added propionaldehyde (86.2 µl, 68.8 mg, 1.18 mmol, 1.2 eq) followed by $NaBH(OAc)_3$ (314 mg, 1.48 mmol, 1.5 eq). The reaction mixture was stirred for 4.5 h at RT and concentrated *in vacuo* before it was partitioned between conc. $NH_4Cl_{(aq)}$ (20 ml) and EtOAc (20 ml). The layers were separated and the organic layer was washed with conc. $NaHCO_{3(aq)}$ (20 ml) and brine, dried over $MgSO_4$ and concentrated *in vacuo*. The product was obtained as a yellow oil (305 mg, 0.98 mmol, 99 %).

TLC (SiO_2, 2 % EtOH in DCM), R_f = 0.36 (UV, ninhydrin)

^{1}H NMR (400 MHz, $CDCl_3$) δ 7.39 (d, *J* = 7.2 Hz, 2H), 7.29 (t, *J* = 7.3 Hz, 2H), 7.21 (t, *J* = 7.2 Hz, 1H), 7.08 (t, *J* = 7.9 Hz, 1H), 6.71 (d, *J* = 7.6 Hz, 1H), 6.64 (d, *J* = 8.1 Hz, 1H), 3.80 (s, 3H), 3.71 (d, *J* = 6.4 Hz, 2H), 2.99 (dt, *J* = 21.5, 10.8 Hz, 2H), 2.89 – 2.77 (m, 2H), 2.52 (t, 2H), 2.49 – 2.43 (m, 1H), 2.17 – 2.05 (m, 1H), 1.66 – 1.54 (m, 1H), 1.46 (h, *J* = 7.3 Hz, 2H), 0.87 (t, *J* = 7.4 Hz, 3H).

^{13}C NMR (101 MHz, $CDCl_3$) δ 157.18, 141.48, 138.29, 128.35, 128.06, 126.45, 126.06, 125.36, 121.63, 106.79, 55.43, 55.20, 54.40, 51.97, 32.13, 25.04, 23.92, 21.70, 11.85.

HRMS (ESI, positive): calc. for $C_{21}H_{28}NO$ $(M+H)^+$: 310.2165; found 310.2169.

$[\alpha]_D^{21}$ = - 48.8 ^{o} (c=1, MeOH)

_N_-Propyl-aminotetraline *(S)*-**6**[25,27]

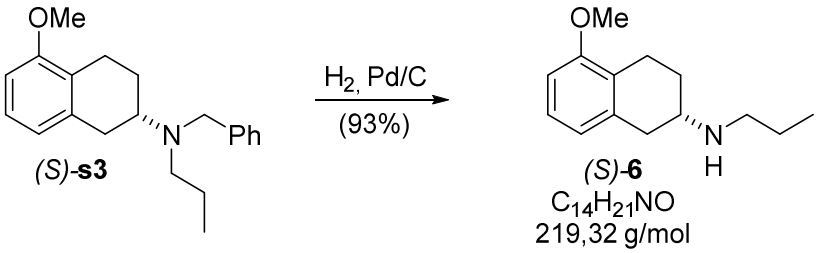

A solution of (*S*)-s**3** (344 mg, 1.11 mmol, 1.0 eq.) in MeOH (5 ml) was added to Pd/C (10% Pd) under nitrogen atmosphere. The reaction was stirred vigorously over night under H_2 atmosphere at RT. The resulting suspension was then filtered over celite and the filtrate concentrate *in vacuo*. The product was obtained as a white solid (227 mg, 1.03 mmol, 93 %).

TLC (SiO_2, 5 % MeOH in DCM), R_f = 0.28 (UV, ninhydrin)

^{1}H NMR (599 MHz, $CDCl_3$) δ 7.09 (t, *J* = 7.9 Hz, 1H), 6.69 (d, *J* = 7.7 Hz, 1H), 6.67 (d, *J* = 8.1 Hz, 1H), 3.81 (s, 3H), 3.11 (t, 2H), 2.96 (d, *J* = 20.4 Hz, 1H), 2.91 – 2.76 (m, 3H), 2.62 – 2.51 (m, 1H), 2.28 (s, 1H), 1.74 (s, 3H), 0.99 (t, *J* = 7.4 Hz, 3H).

^{13}C NMR (151 MHz, $CDCl_3$) δ 157.11, 135.53, 126.39, 124.55, 121.39, 107.25, 55.22, 53.74, 48.18, 35.15, 27.89, 22.20, 22.09, 11.72.

HRMS (ESI, positive): calc. for $C_{14}H_{22}NO$ $(M+H)^+$: 220.1696; found 220.1699.

$[\alpha]_D^{22}$ = - 74.2 ° (c=1, MeOH)

Hydroxytetraline *(S)*-***s*7**

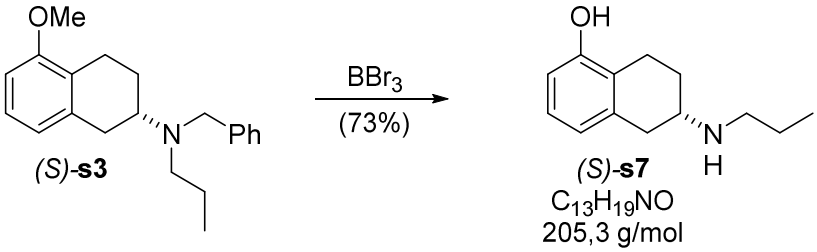

A solution of (*S*)-**s3** (63 mg, 0.25 mmol, 1.0 eq) in 1 mL DCM was cooled to - 78 °C under N_2-atmosphere and treated with a 1-M solution of BBr_3 in DCM (790 µL, 0.54 mmol, 2.2 eq). The reaction mixture was stirred for 30 min at –78 °C before being allowed to warm to room temperature and stirred for another 1.5 h. Then, the reaction was quenched with MeOH (2 mL). This solution was partitioned between water (20 mL) and ethyl acetate (20 mL). The organic layer was washed with 1-M-NaOH and brine, dried over Na_2SO_4 and concentrated under reduced pressuer affording the product as a colorless oil (37 mg, 0.18 mmol, 73 %).

^{1}H NMR (300 MHz, $CDCl_3$) δ = 6.98 (t, *J*=7.8, 1H), 6.65 (d, *J*=7.5, 1H), 6.57 (d, *J*=7.9, 1H), 4.14 – 3.75 (m, 1H), 2.92 (ddd, *J*=23.5, 19.6, 9.8, 3H), 2.64 (ddd, *J*=37.7, 23.2, 11.2, 4H), 2.11 (s, 1H), 1.57 (dq, *J*=14.6, 7.3, 3H), 1.01 – 0.92 (m, 3H). (phenol not detected)

^{13}C NMR (75 MHz, $CDCl_3$) δ = 153.81, 136.90, 126.32, 123.06, 121.22, 112.04, 53.19, 48.91, 36.53, 28.93, 23.28, 22.00, 11.84.

HRMS (EI): calc. for $C_{13}H_{19}NO$ (M): 205.1467; found 205.1462.

(S)-**aPPHT**

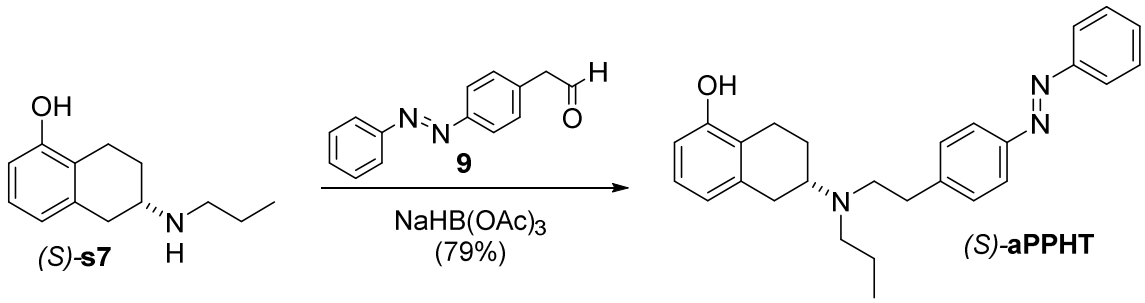

(S)-***s7*** (12 mg, 0.059 mmol, 1.0 eq) was dissolved in 3 mL DCE and freshly prepared aldehyde **9** was added (from 1.5 eq of the corresponding alcolohl), followed by $NaHB(OAc)_3$ (19 mg, 0.09 mmol, 1.5 eq). The reaction suspension was stirred over night, diluted with ethyl acetate and extracted with conc. $NaHCO_{3(aq)}$ and brine. The organic layer was dried over Na_2SO_4 and concentrated under *vacuo*. Flash column chromatography (SiO_2, gradient 0 to 5% MeOH in DCM) afforded *(S)*-**aPPHT** as an orange amorphous solid (19 mg, 0.046 mmol, 79%).

Analytical data matched those of its enantiomere and the racemate.

Additional Azobenzene Building Blocks

Phenethyl alcohol 13 & **14**

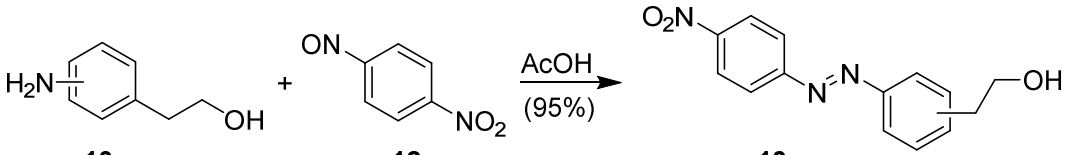

10: *para*
11: *meta*

12

13: *para*
14: *meta*

$C_{14}H_{13}N_3O_3$
271,3 g/mol

4-Aminophenethyl alcohol **10** or 3-aminophenethyl alcohol **11** (0.5 g, 3.64 mmol, 1 equiv.) were dissolved in 10 mL DCM. Then, **12** (0.832 g, 5.47 mmol, 1.5 equiv.**)** was added, followed by AcOH (2.1 mL, 36.4 mmol, 10 equiv.) and the reaction was stirred at rt under N_2 atmosphere for 1.5 hours. The orange-colored mixture was diluted in 60 mL EtOAc and then washed sequentially with 1M HCl (2 x 30 mL), 1M NaOH (2 x 30 mL), and brine (1 x 30 mL). Organic phase was collected and dried with Na_2SO_4 before concentrating to dryness using rotary evaporation. Crude material was purified by flash column chromatography (silica gel, wet loading, gradient 20% → 30% → 40% → 60% EtOAc in Hexanes). The final product **13** and **14** was an orange-red crystalline solid (932 mg, 3.44 mmol, 95 %).

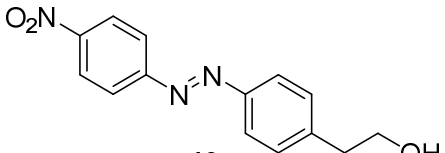

13

TLC (SiO_2, 50% EtOAc, 50% hexanes) R_f = 0.4 (UV + Ninhydrin)

HRMS (EI**)** calc'd for $C_{14}H_{13}N_3O_3$ $[M+H]^+$ = 271.0957; found = 271.0952

^{1}H NMR (200 MHz, $CDCl_3$) δ = 8.36 (d, *J*=8.8, 2H), 8.00 (d, *J*=8.8, 2H), 7.92 (d, *J*=8.3, 2H), 7.42 (d, *J*=8.2, 2H), 3.94 (t, *J*=6.5, 2H), 2.97 (t, *J*=6.5, 2H).

IR ν_{max}: 3518, 3398, 3063, 2945, 2884, 1605, 1590, 1514, 1496, 1454, 1415, 1376, 1325, 1220, 1200, 1142, 1105, 1041, 944, 860, 828, 793, 755, 729, 686

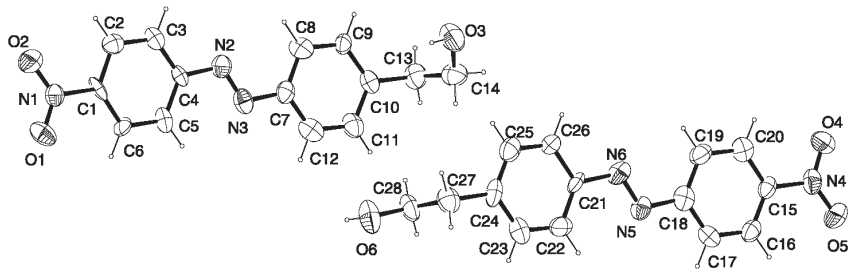

Crystallographic data. **13**

	13
net formula	$C_{14}H_{13}N_3O_3$
M_r/g mol^{-1}	271.271
crystal size/mm	0.30 × 0.12 × 0.03
T/K	173(2)
radiation	MoKα
diffractometer	'KappaCCD'
crystal system	triclinic
space group	*P*1bar
a/Å	7.0940(15)
b/Å	7.4039(16)
c/Å	25.182(6)
α/°	95.475(11)
β/°	90.719(9)
γ/°	99.206(11)
V/Å^3	1299.1(5)
Z	4
calc. density/g cm^{-3}	1.3870(5)
μ/mm^{-1}	0.100
absorption correction	none
refls. measured	4271
R_{int}	0.0612
mean σ(*I*)/*I*	0.0999
θ range	3.25–25.29
observed refls.	1582
x, y (weighting scheme)	0, 7.5736
hydrogen refinement	constr
refls in refinement	3330
parameters	363
restraints	0
$R(F_{obs})$	0.1329
$R_w(F^2)$	0.2548
S	1.150
shift/error$_{max}$	0.001
max electron density/e Å^{-3}	0.229
min electron density/e Å^{-3}	−0.234

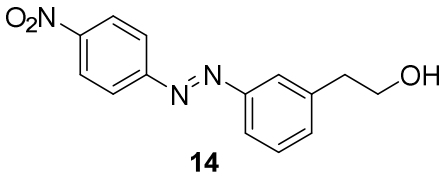

14

^{1}H NMR (599 MHz, $CDCl_3$) δ = 8.42 – 8.35 (m, 2H), 8.06 – 8.00 (m, 2H), 7.88 – 7.83 (m, *J*=2.1, 1.7, 2H), 7.54 – 7.48 (m, 1H), 7.44 (d, *J*=7.3, 1H), 3.96 (t, *J*=6.5, 2H), 3.00 (t, *J*=6.5, 2H), 1.59 (s, 1H).

^{13}C NMR (151 MHz, $CDCl_3$) δ = 155.68, 152.61, 148.70, 140.12, 133.11, 129.44, 124.73, 123.54, 123.40, 121.95, 63.48, 63.38, 39.03, 38.93.

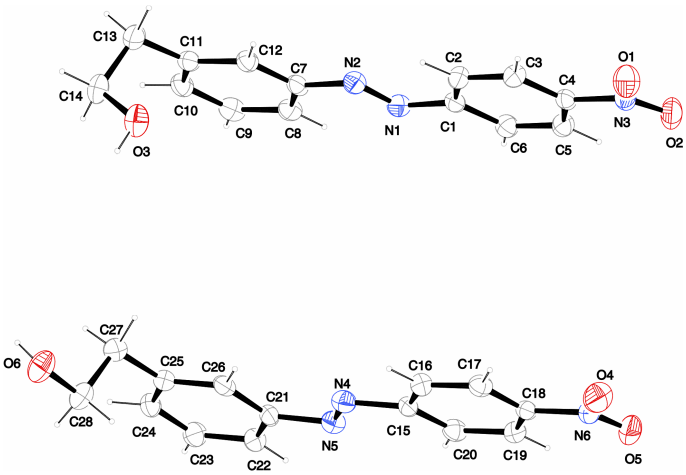

Crystallographic data. **14**

	14
net formula	$C_{14}H_{13}N_3O_3$
M_r/g mol^{-1}	271.271
crystal size/mm	0.28 × 0.12 × 0.02
T/K	200(2)
radiation	MoKα
diffractometer	'KappaCCD'
crystal system	triclinic
space group	$P\bar{1}$
a/Å	6.4286(2)
b/Å	14.1216(6)
c/Å	16.0098(6)
α/°	112.830(2)
β/°	94.583(2)
γ/°	100.381(2)
V/Å^3	1299.50(8)
Z	4
calc. density/g cm^{-3}	1.38657(9)
μ/mm^{-1}	0.100
absorption correction	none
refls. measured	8779
R_{int}	0.0339
mean σ(I)/I	0.0534
θ range	3.22–25.39
observed refls.	2915
x, y (weighting scheme)	0.1054, 0.1286
hydrogen refinement	constr
refls in refinement	4743
parameters	363
restraints	0
$R(F_{obs})$	0.0620
$R_w(F^2)$	0.1879
S	1.032
shift/error$_{max}$	0.001
max electron density/e Å^{-3}	0.435
min electron density/e Å^{-3}	−0.208

Phenethyl alcohol 15

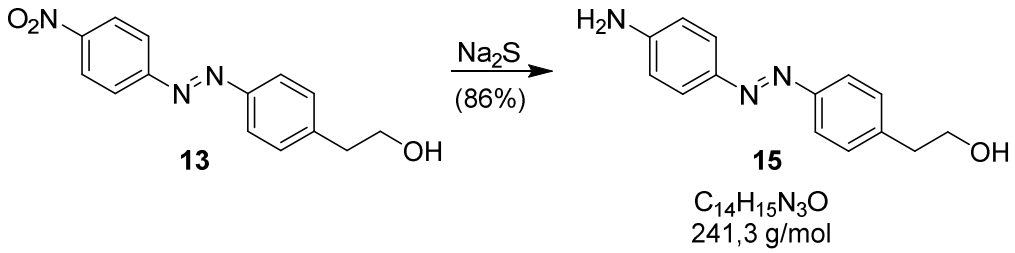

$C_{14}H_{15}N_3O$
241,3 g/mol

13 (800 mg, 2.95 mmol, 1 equiv.) and Na_2S (460 mg, 5.9 mmol, 2 equiv.) were added to 30 mL of a 2:1 mixture of dioxane:H_2O and heated to 80 °C. After allowing the reaction to proceed for 1.5 hours, the cloudy, orange reaction mixture was diluted with 80 mL EtOAc and washed in a separatory funnel with 1M NaOH (2 x 40 mL). The combined aqueous layers were extracted using EtOAc (2 x 20 mL). All organic phases were pooled and dried with Na_2SO_4. Removal of solvent via rotary evaporation yielded the yellow-orange crystalline product **15** (604.1 mg, 2.54 mmol, 86%).

TLC (SiO_2, 10% MeOH in DCM) - R_f = 0.6 (UV + Ninhydrin)

HRMS (EI**)** calc'd for $C_{14}H_{15}N_3O$ $[M+H]^+$ = 241.1215; found = 241.1205

^{1}H NMR (599 MHz, $CDCl_3$) δ = 7.84 – 7.74 (m, 4H), 7.33 (d, *J*=8.2, 2H), 6.77 – 6.69 (m, 2H), 4.01 (s, 2H), 3.90 (t, *J*=6.6, 2H), 2.93 (t, *J*=6.6, 2H).

^{13}C NMR (151 MHz, $CDCl_3$) δ = 151.75, 149.42, 145.56, 140.48, 129.59, 125.00, 122.54, 114.61, 63.53, 39.02.

IR ν_{max}: 3336, 3213, 3029, 2928, 2877, 1636, 1597, 1502, 1470, 1454, 1428, 1403, 1364, 1306, 1277, 1232, 1190, 1153, 1141, 1104, 1054, 1023, 1010, 952, 872, 838, 789

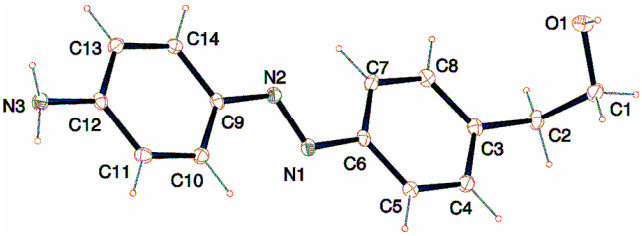

Crystallographic data. **15**

	15
net formula	$C_{14}H_{15}N_3O$
M_r/g mol^{-1}	241.289
crystal size/mm	0.178 × 0.056 × 0.022
T/K	100(2)
radiation	'Mo Kα
diffractometer	'Bruker D8Venture'
crystal system	orthorhombic
space group	*Pna*2$_1$
a/Å	11.1035(6)
b/Å	13.9708(7)
c/Å	7.8951(5)
α/°	90
β/°	90
γ/°	90
V/Å^3	1224.73(12)
Z	4
calc. density/g cm^{-3}	1.30861(13)
μ/mm^{-1}	0.085
absorption correction	multi-scan
transmission factor range	0.8230–0.9143
refls. measured	16779
R_{int}	0.0684
mean σ(*I*)/*I*	0.0399
θ range	3.45–25.11
observed refls.	1792
x, y (weighting scheme)	0.0461, 0.2715
hydrogen refinement	mixed
Flack parameter	–0.5(19)
refls in refinement	2128
parameters	175
restraints	1
$R(F_{obs})$	0.0382
$R_w(F^2)$	0.0910
S	1.069
shift/error$_{max}$	0.001
max electron density/e Å^{-3}	0.154
min electron density/e Å^{-3}	–0.177

C-bound H: constr, N- and O-bound H: refall.

Flack parameter meaningless, no anomalous scatterer (Mo readiation).

Phenethyl alcohol 16

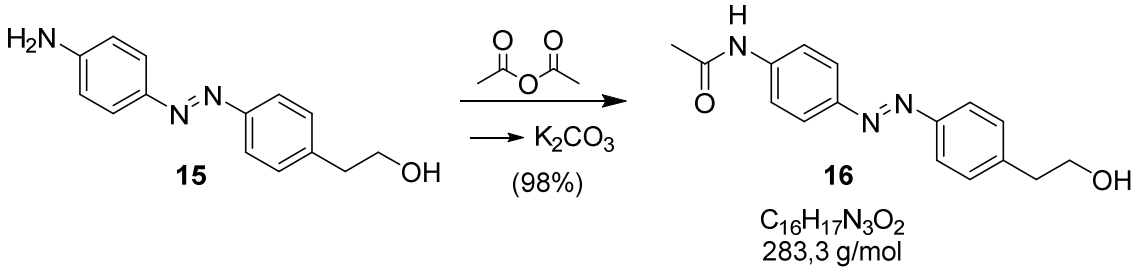

15 (533 mg, 2.21 mmol, 1 equiv.) was dissolved in 20 mL DCM and cooled on an ice bath. Both acetic anhydride (622 µL, 6.63 mmol, 3 equiv.) and triethylamine (675 µL, 4.86 mmol, 2.2 equiv.) were added under N_2 atmosphere. After 15 minutes of stirring at 0-5℃, the flask was then warmed to rt and left to stir overnight under N_2 atmosphere. 60 mL of EtOAc was added to the reaction mixture, which was then washed sequentially with $NaHCO_3$ (40 mL), NH_4Cl, (40 mL) and brine (40 mL). The organic phase was dried with Na_2SO_4 and the solvent was removed via rotary evaporation, yielding a yellow-orange powder (705 mg, 2.17 mmol, 98%).The *N*- and *O*-protected intermediate was used in the following reaction.

Intermediate:

TLC (SiO_2, 1:1 EtOAc:Hexanes) - R_f = 0.6 (UV + Ninhydrin)

HRMS (EI**)** calc'd for $C_{18}H_{19}N_3O_3$ $[M+H]^+$ = 325.1426; found = 325.1428

The intermediate (600 mg, 1.84 mmol, 1 equiv.) was mixed with K_2CO_3 (255 mg, 1.84 mmol, 1 eq) in 30 mL MeOH and stirred at rt for two hours. The reaction mixture was partitioned between 50 mL 10% NaCl and 100 mL EtOAc. The organic layer was washed with brine (50 mL) and the combined aqueous phases were extracted with chloroform (50 mL) and EtOAc (20 mL). The pooled organic phases was dried over Na_2SO_4 and concentrated *via* rotary evaporation, yielding the yellow-orange product **16** in quantitative yield (520 mg, 1.84 mmol).

TLC (SiO_2, 10% MeOH in DCM) - R_f = 0.5 (UV)

HRMS (EI**)** calc'd for $C_{16}H_{17}N_3O_2$ $[M+H]^+$ = 283.1321; found = 283.1314

^{1}H NMR (400 MHz, cd_3od) δ = 7.89 – 7.82 (m, 2H), 7.82 – 7.77 (m, 2H), 7.76 – 7.68 (m, 2H), 7.42 – 7.34 (m, 2H), 3.79 (t, *J*=6.9, 2H), 2.88 (t, *J*=6.9, 2H), 2.14 (s, 3H).

^{13}C NMR (101 MHz, cd_3od) δ = 170.36, 151.19, 148.67, 142.56, 141.28, 129.39, 123.13, 122.25, 119.58, 62.41, 38.61, 22.53.

IR ν_{max}: 3296, 3126, 3057, 2935, 2892, 2361, 1661, 1599, 1543, 1502, 1437, 1393, 1372, 1333, 1302, 1270, 1230, 1194, 1156, 1109, 1053, 1020, 962, 950, 898, 846, 827, 809, 726, 704, 662

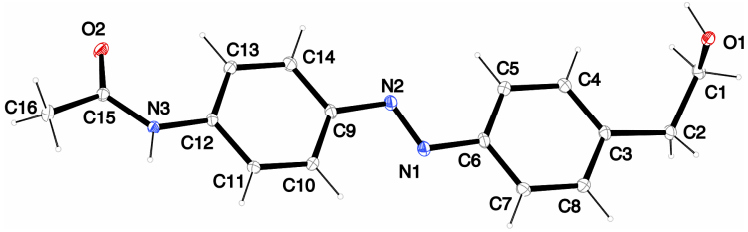

Crystallographic data. **16**

	16
net formula	$C_{16}H_{17}N_3O_2$
M_r/g mol^{-1}	283.325
crystal size/mm	0.194 × 0.051 × 0.051
T/K	100(2)
radiation	'Mo Kα
diffractometer	'Bruker D8Venture'
crystal system	monoclinic
space group	$P2_1/n$
a/Å	4.67990(10)
b/Å	13.5414(4)
c/Å	22.3063(6)
α/°	90
β/°	94.1120(10)
γ/°	90
V/Å^3	1409.96(6)
Z	4
calc. density/g cm^{-3}	1.33473(6)
μ/mm^{-1}	0.090
absorption correction	multi-scan
transmission factor range	0.8941–0.9143
refls. measured	22974
R_{int}	0.0340
mean σ(I)/I	0.0212
θ range	3.01–27.56
observed refls.	2797
x, y (weighting scheme)	0.0479, 1.0071
hydrogen refinement	mixed
refls in refinement	3226
parameters	199
restraints	0
$R(F_{obs})$	0.0442
$R_w(F^2)$	0.1202
S	1.094
shift/error$_{max}$	0.001
max electron density/e Å^{-3}	0.399
min electron density/e Å^{-3}	–0.222

C-bound H: constr, O- and N-bound H: refall.

Phenethyl alcohol 17

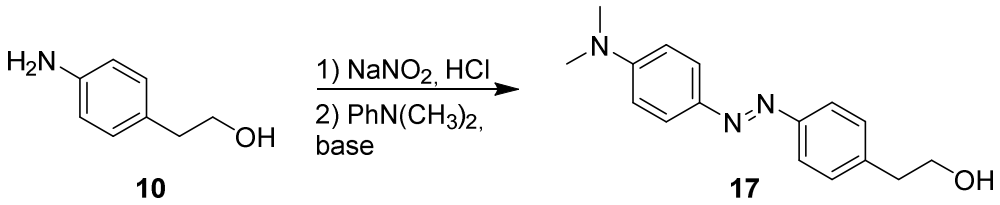

10 **17**

$C_{16}H_{19}N_3O$
269,3 g/mol

base	isol. yield
NaOH	0%
NaAc	87%
pyr.	90%

Diazonium salt formation

4-aminophenethyl alcohol **10** (3.5 g, 25.5 mmol, 1 equiv.) was added to 69 mL H_20 and cooled in an ice bath and concentrated aqueous HCl (8 mL, 76.5 mmol, 3 equiv.) was added. A solution of $NaNO_2$ (1.9 g, 28.1 mmol, 1.1 eq) in 22 mL H_20 were added slowly, keeping the reaction temperature between 0 - 5°C. After stirring at 0 °C for 30 min the yellow diazonium salt solution was carried to the next step immediately.

Base 1: NaOH

NaOH (2.04 g, 51 mmol, 6 equiv.) was dissolved in 30 mL 1:1 H_20:MeOH with stirring at 0-5°C. N,N-dimethylanilin (1.08 mL, 8.5 mmol, 1 equiv.) was added to this solution. Next, one third of the above described diazonium salt solution (1 equiv.) was added dropwise. The solution was stirred on an ice bath for 30 min and was then allowed to warm to rt overnight. No conversion was observed by TLC.

Base 2: NaOAc

Experimental procedure was identical to Base 1 with NaOH being substituted with NaOAc (4.18 g, 51 mmol, 6 equiv.). After the overnight reaction, TLC confirmed desired product formation. The cloudy, yellow-green reaction mixture was diluted with 200 mL EtOAc in a separatory funnel and washed sequentially with H_20 (1 x 100 mL), 1M NaOH (1 x 100 mL), and brine (1 x 100 mL). The pooled organic phases were dried with Na_2SO_4 and concentrated *via* rotary evaporation. Crude material was purified by flash column chromatography (silica gel, wet loading in DCM, gradient 10% → 50% EtOAc in hexanes), yielding the yellow-brown product **17** (1.99 g, 7.4 mmol, 87%).

Base 3: pyridine

Experimental procedure was identical to Base 1 with NaOH being substituted with pyridine (4.12 mL, 51 mmol, 6 equiv.) dissolved in 30 mL pure MeOH. After reacting overnight, TLC confirmed desired product formation and an aqueous workup was performed. The reaction mixture was diluted with 100 mL EtOAc and the resulting solution was washed sequentially with NH_4Cl (200 mL), NaOH (100 mL), 1M NaOH (100 mL), H_20 (100 mL), and brine (100 mL). After back extraction using EtOAc (2 x 50 mL), the pooled organic phases were dried with Na_2SO_4 and the solvent was removed *via* rotary evaporation. The crude material was purified by flash column chromatography (silica gel, wet loading in $CHCl_3$, gradient 10% → 50% → 60% → 70% → 80% EtOAc in hexanes) yielding the product as a bright orange powder **17** (2.06 g, 7.66 mmol, 90%).

TLC (SiO_2, 1:1 EtOAc:Hexanes) - R_f = 0.4 (UV + Ninhydrin)

HRMS (ESI**)** calc'd for $C_{16}H_{17}N_3O_2$ $[M+H]^+$ = 270.1601, found = 270.1598

^{1}H NMR (599 MHz, cdcl$_3$) δ = 7.89 – 7.83 (m, 2H), 7.80 – 7.76 (m, 2H), 7.34 – 7.30 (m, 2H), 6.78 – 6.72 (m, 2H), 3.89 (t, *J*=6.6, 2H), 3.16 (s, 1H), 2.92 (t, *J*=6.6, 2H).

^{13}C NMR (151 MHz, cdcl$_3$) δ = 152.33, 151.99, 143.63, 139.98, 129.56, 124.85, 122.39, 111.49, 63.56, 40.30, 39.02.

IR ν_{max}: 3216, 2856, 1599, 1561, 1513, 1472, 1443, 1423, 1403, 1360, 1310, 1227, 1154, 1138, 1040, 1011, 941, 835, 725, 674, 660

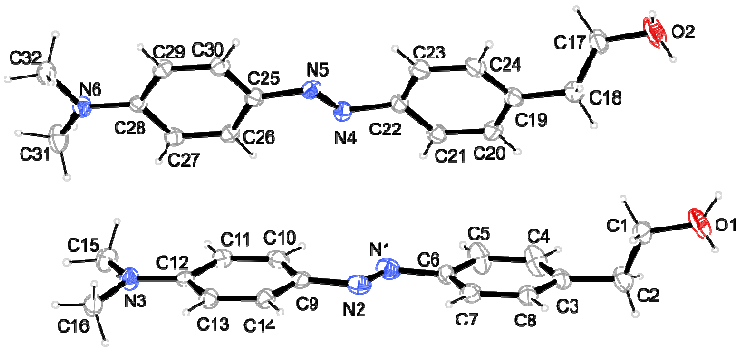

Crystallographic data. **17**

	17
net formula	$C_{16}H_{19}N_3O$
M_r/g mol^{-1}	269.342
crystal size/mm	0.161 × 0.125 × 0.026
T/K	100(2)
radiation	'Mo Kα
diffractometer	'Bruker D8Venture'
crystal system	triclinic
space group	*P*1bar
a/Å	8.1881(8)
b/Å	9.6270(8)
c/Å	18.7815(16)
α/°	90.979(3)
β/°	100.522(3)
γ/°	101.182(3)
V/Å^3	1425.8(2)
Z	4
calc. density/g cm^{-3}	1.25476(18)
μ/mm^{-1}	0.081
absorption correction	multi-scan
transmission factor range	0.8718–0.9281
refls. measured	12957
R_{int}	0.0329
mean σ(*I*)/*I*	0.0444
θ range	2.48–25.39
observed refls.	3456
x, y (weighting scheme)	0.0572, 0.5451
hydrogen refinement	mixed
refls in refinement	5203
parameters	374
restraints	4
$R(F_{obs})$	0.0497
$R_w(F^2)$	0.1332
S	1.034
shift/error$_{max}$	0.001
max electron density/e Å^{-3}	0.383
min electron density/e Å^{-3}	–0.272

C-bound H: constr, O-bound H: refxyz (3), noref (1).

VII

Developing Photoswitchable Adenosines for Optical Control of Adenosine Receptors

Matthias Schönberger, Dirk Trauner

Ludwig-Maximilians University, Chemistry Department and Center for Integrated Protein Science Munich (CIPSM), Munich, Germany

Extracellular adenosine is an important signaling molecule as a neuromodulator and a cell protecting agent. It binds to adenosine receptors (ARs) of the family A of G-protein coupled receptors. Caffeine, the most widely used psychoactive drug, antagonizes the action of adenosine on ARs. ARs are prime pharmaceutical targets for treatment of Parkinson´s disease and anti-inflammatory agents. We have now developed a photoswitchable version of adenosine as a potential photopharmacological tool for these all-important receptors.

Content

Introduction

Extracellular adenosine is an important signaling molecule in the central nervous system.[1,2] It binds to A_1, A_{2A} and A_3 adenosine receptors, which are members of the family A of G-Protein coupled receptors GPCRs.

Caffeine is an adenosine receptor (AR) antagonist and probably the most widely used psychoactive drug in the world, even though withdrawal leads to unpleasant symptoms such as headache, depressed mood, and muscle pain.[3] ARs in the striatum orchestrate the psychomotor stimulant effect of caffeine.[4] AR receptors in the shell of the nucleus accumbens are involved in the arousal effect of caffeine.[5]

Some modulatory effects of adenosine are mediated by other transmembrane receptors such as the $\alpha_3\beta_4$ nicotinic acetyl choline receptor that is transactivated through intracellular signaling cascaeds.[6] Activation of the adenosine A_{2A} receptor (A2AR) by agonists contributes to motoneuron survival through activation of tyrosine kinase receptor TrkB.[7] In addition, ARs are involved receptor-receptor-interactions. For instance, in the striatum, ARs interact with other metabotropic receptors such as the cannabinoid CB_1 receptor,[8] dopamine D2 receptors,[9,10] and mGluR5.[11,12]

Being that ARs in the central nervous system modulate a number of physiological functions, they are targeted therapeutically in many diseases.[13] AR ligands are currently intensely investigated in academic and industrial research.[14,15] Extensive structure activity relationships (SARs) data have been accumulated and many drugs are currently investigated in clinical trials.[16-18] Especially, potent A2AR antagonists are of interest for treatment of Parkinson's disease.[19,20]

Crystal structure analysis by Ray Stevens and coworkers has provided structural data for both the activated and inactivated (A2AR).[21,22] As is the case for all G-protein coupled receptors (GPCRs), A_{2A} receptors have seven membrane spanning helices and mainly communicate via eponymous G-protein activation.[23-26] The crystal structure of A2AR has facilitated the discovery of novel chemotypes for antagonists.[22,27-29]

A

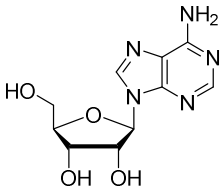

adenosine

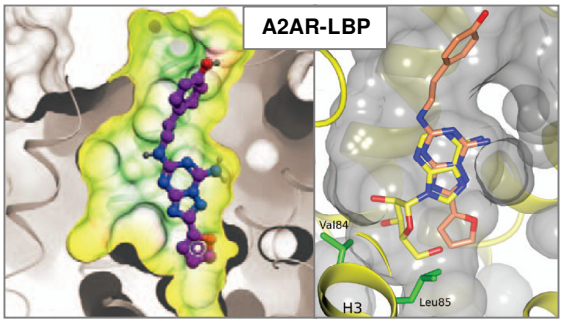

co ZM241385 **co adenosine**

B

	antagonists	agonists
seletive	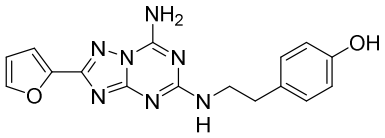 **ZM241385**	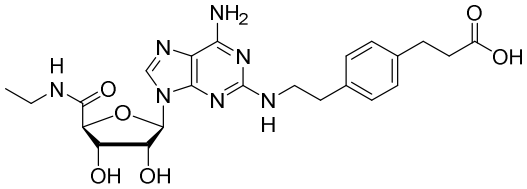 **CGS216805**
non-seletive	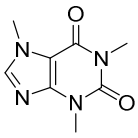 **caffeine**	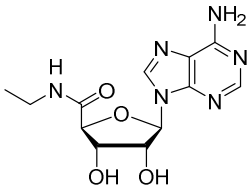 **NECA** (5′-(*N*-Ethylcarboxamido)adenosine)

Figure 1. Adenosine receptor and ligands. A) Structure of the native agonist **adenosine**; ligand binding pocket (LBP) from crystal structures of the A2AR with **ZM241385** (left, adapted from Stevens 2013[30]) and **adenosine** (right, adapted from Lebon *et al.* 2011[31]). **Adenosine** is shown in yellow. Structural data of **ZM241385** have been added highlighting the overlay of the heterocyclic core and the different side chain interaction made by the ribose functional group. B) AR antagonists **ZM241385** and **caffeine**, and AR agonists **CGS216805** and **NECA**. 2-Substituted ligands **ZM241385** and **CGS216805** are more selective for A2AR.

Figure 1 depicts selected natural and synthetic ligands that, in combination with an A2AR crystal structures, guided the design of a photoswitchable AR agonist.[32] The native agonist **adenosine** (Figre 1A) is a 6-amino purine with a ribose attached to N^9. Synthetic agonists **NECA** and **CGS21680** (figure 1B, right) share the hetero aromatic purine core. The ribose moiety attached to N^9 is slightly modified with an *N*-ethyl carboxamid at $C^{5'}$. In comparison to adenosine and the non-subtype-specific synthetic agonist **NECA**, **CGS21680** carries a comparatively large phenethylamine derivative in 2-position. The crystal structure of an A2AR with adenosine showed that the ribose functional group makes important interactions with amino acids at the bottom of the ligand binding pocket (LBP).[31]

AR antagonists are devoid of the ribose moiety. **Caffeine** is a per-*N*-methylated xanthine (Figure 1B) that is not selective for one particular AR. The triazolo-triazine **ZM241385** is substituted in 8-position with a furan ring. Similar **CGS21680**, it also features a comparatively large phenethylamine substituent in 2-position. The crystal structure of A2AR with the synthetic antagonist **ZM241385** revealed a narrow LBP perpendicular to the membrane and helped explaining SARs.[28] The heterocyclic core is positioned in the same way as **adenosine**, however, amino acid residues important for receptor activation cannot be reached (Figure 1A, right panel).

Results and Discussion

Based on these findings, 1st generation photoswitchable AR agonists as shown in Scheme 1A were synthesized. **Azoadenosines** are equipped with a 2-amino functional group that is further substituted with a phenethyl azobenzene building block resembling the substitution pattern of **ZM241385** and **CGS21680**. Ribose was chosen as the agonistic pharmacophore resembling the native agonist **adenosine**. Ribose was deliberately chosen over the *N*-ethyl carboxamido derivative as present in **NECA** and **CGS21680** in order to facilitate dissociation from the LBP upon photoswitching.

Synthesis started from commercial 2-iodo-adenosine **1** that underwent chemoselective reaction with neat unprotected 4-amino-phenethylamine **2** (Scheme 1B). The resulting aniline could be readily reacted with commercial nitrosobenzene **3** yielding **azo-adenosine-1**.

To provide a photochromic ligand (PCL) with a more pronounced sterical change after isomerization, the biphenyl derivative **azo-adenosine-2** was synthesized. The required nitroso-biphenyl **3** was obtained by oxidation of amino-biphenyl using oxone. Due to the poor solubility of biphenyl derivatives in aqueous solvents, the oxidation did not proceed as fast and complete as for anilines.[33-35] However, using a five-fold excess of the amine and prolonged reaction times allowed preparing **azo-adenosine-2**.

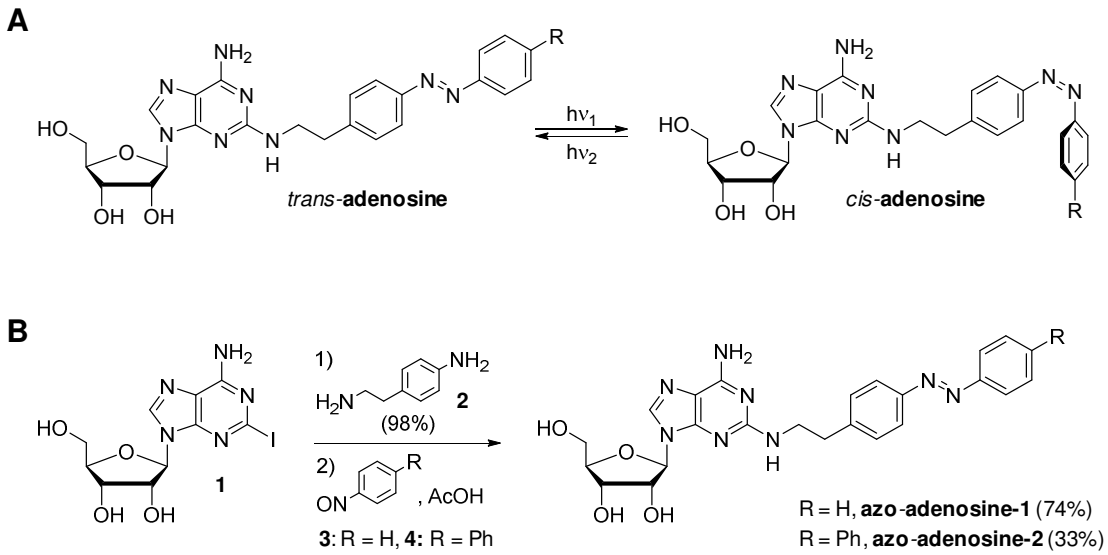

Scheme 1. Design and synthesis of **azoadenosines**.

Summary and Outlook

Photoswitchable versions of the neuromodulator adenosine have been designed and synthesized. Future biological testing in will show whether these molecules are efficient photochromic ligands for ARs.

A_1 and A_3 adenosine receptor subtypes typically couple to G_i G-proteins, leading to inhibition of the adenylyl cyclase and activation of G-protein coupled inwardly rectifying potassium (GIRK) channels.[36,37] Therefore, photopharmacological testing could be carried out in analogy to previous work using GIRK channel electrophysiologiy.[38]

By contrast, A_{2A} adenosine receptor subtypes typically couple to G_s G-proteins, leading to activation of the adenylyl cyclase.[39] The lack of in-time read-out methods for cAMP levels complicates quantitative and qualitative assessment of photoswitching associated to A2AR. Redirecting A2AR signaling to phospholipase C using a chimeric G_{qs} G-protein would allow Ca2+ imaging as an alternative.[40,41]

GPCRs are famous for their multifunctional activity, which is believed to originate from structural flexibility between distinct receptor conformations.[19,24] In the case of adenosine receptors, this intrinsic versatility is paired with interesting heteromerization events.[42] Therefore, tools for selective and reversible receptor activation will be of great value for GPCR-research.

General Considerations

All reagents were purchased from commercial suppliers and used without further puri_cation. All reactions were carried out under magnetic stirring. The glassware was dried at 120 _C prior to usage. Analytical thin layer chromatography (TLC) was carried out on Merck silica gel 60 F254 TLC plates and visualized under UV light.

Flash chromatography was performed on Dynamic Adsorbents Silica Gel (40-63 _m particle size).

Proton (^{1}H) and carbon (^{13}C) spectra were measured on a Varian Mercury instruments at 300 or 400 MHz. Chemical shifts are reported in ppm with the solvent resonance employed as the internal standard ($CDCl_3$ at 7.26 and 77.0 ppm respectively). The following abbreviations are used to explain the multiplicities: s = singlet, d = doublet, t = triplet, q = quartet, m = multiplet, br = broad.

IR spectra were recorded on a Perkin Elmer Spectrometer BY FT-IR System with a Smith Dura sample IR II ATR-unit. The absorption bands are reported in wave numbers (cm□1). High resolution mass spectra

(HRMS) were recorded on a Varian MAT CH 7A for electron impact ionization (EI) and on a Varian MAT 711 spectrometer for electron spray ionization (ESI).

Aniline s1

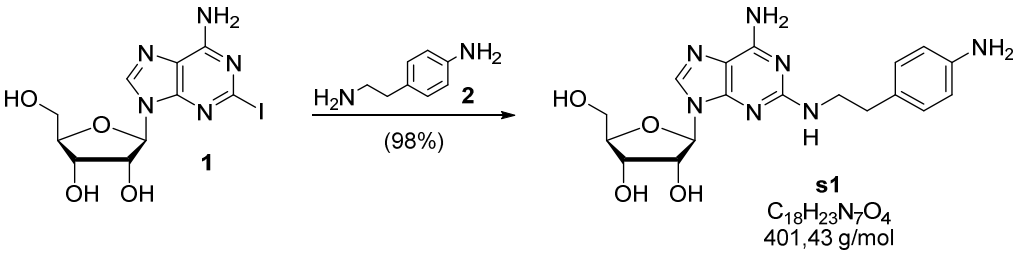

2-Iodoadenosine **1** (150 mg, 0.38 mmol, 1.0 eq) was suspended in neat amino phenethylamine **2 (**251 µL, 1.91 mmol, 5.0 eq) and heated to 110 °C under Ar-gas atm. At approximately 70 °C, the mixture turned into a homogeneous solution. TLC monitoring (SiO_2, 20% MeOH, 80% DCM) indicated complete turnover after 3 h. The reaction mixture was allowed to cool to rt (solid gum), diluted with MeOH and purified using reverse phase flash column chromatography (C-18, isogratic 30% MeOH, 70% H2O). The clean product **s1** was obtained as an off-white foam after lyophilization (150 mg, 0.37 mmol, 98%).

TLC (SiO_2, 20% MeOH, 80% DCM) Rf = 0.47 (UV + ninhydrine)

^{1}H-NMR (400 MHz, DMSO-d_6) δ = 7.90 (s, 1H), 6.90 (d, *J*=8.4, 2H), 6.71 (s, 2H), 6.56 - 6.44 (m, 2H), 6.02 (t, *J*=5.7, 1H), 5.73 (d, *J*=6.1, 1H), 5.38 (d, *J*=6.2, 1H), 5.12 (d, *J*=4.7, 2H), 4.82 (s, 2H), 4.60 (s, 1H), 4.19 - 4.05 (m, 2H), 3.90 (q, *J*=4.0, 1H), 3.70 - 3.45 (m, 2H), 3.16 (d, *J*=5.2, 1H), 2.63 (dd, *J*=6.6, 8.6, 2H).

^{13}C NMR (101 MHz, dmso) δ = 159.67, 156.46, 151.91, 147.03, 136.81, 129.48, 127.33, 114.43, 114.07, 87.62, 85.73, 73.34, 71.13, 62.26, 43.80, 35.08.

HRMS (ESI) calcd for $C_{18}H_{24}N_7O_4$ $[M+H]^+$: 402.1884; found: 402.1881

Azo-adenosines

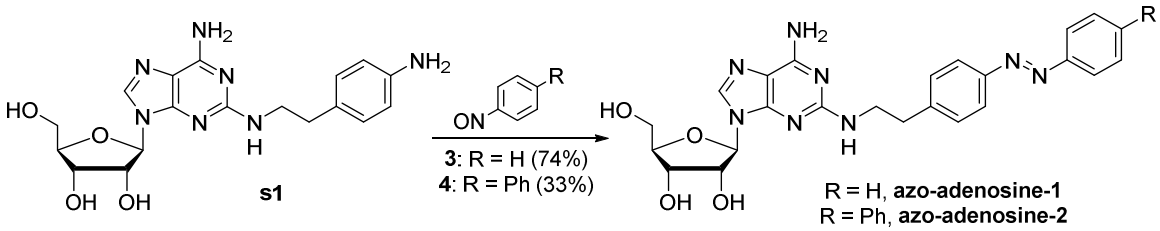

Formation of nitrosobenzenes

Nitrosobenzene **3** was commerzially available. 4-Phenyl-nitrosobenzene **4** was prepared freshly. Aminobiphenyl (189 mg, 1.12 mmol, 4.5 eq.) was dissolved in DCM (5 mL) and H2O (10 mL). Oxone (689 mg, 1.12 mmol, 4.5 eq.) in 5 mL H2O was slowly added to the solution under nitrogen atmosphere. After vigorous stirring for 17 hours, the reaction mixture was diluted with EtOAc. The organic layer was washed with 1-M-HCl, 1-M-NaOH and brine, and dried over Na_2SO_4. After removal of the solvent *in vacuo*, the crude nitroso arene was submitted to the next step as a DCM solution.

Mills coupling

Aniline **s1** (1.0 eq., 10 to 150 mg scale) and the corresponding nitrosobenzene (1.5 eq. **3** and 4.5 eq **4**) were dissolved in 2 mL DCM and acetic acid was added (10 eq.). After 2-23 hours, the reaction mixture was concentrated *in vacuo*. The reaction mixture was dissolved in 20 mL chloroform and washed with 20 mL $NaHCO_3$(conc.). The aqueous phase was extracted 3 times with 30 mL ethyl acetate. Combined organic layers were dried over Na_2SO_4 and concentrated *in vacuo*. Purification using flash column chromatography (SiO_2, isocratic 10% MeOH, 90% DCM) yielded azo-adenosines as orange amorphous solids.

Azo-adenosine-1

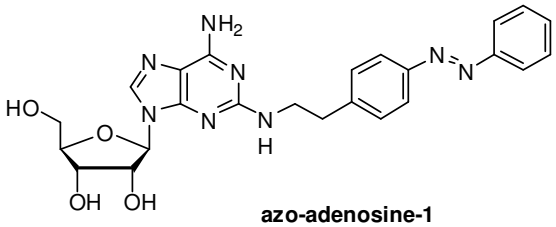

azo-adenosine-1
$C_{24}H_{26}N_8O_4$
490,52 g/mol

TLC (SiO_2, 20% MeOH, 80% DCM) R_f = 0.72 (UV)

^{1}H-NMR(400 MHz, CD_3OD) δ = 7.96 - 7.79 (m, 6H), 7.59 - 7.38 (m, 5H), 7.31 - 7.09 (m, 1H), 6.88 - 6.74 (m, 1H), 5.84 (dd, *J*=6.2, 10.7, 1H), 4.83 - 4.72 (m, 2H), 4.39 - 4.26 (m, 1H), 4.18 - 4.07 (m, 1H), 3.90 - 3.80 (m, 1H), 3.78 - 3.43 (m, 5H), 2.99 (t, *J*=7.2, 2H).

^{13}C NMR (101 MHz, CD_3OD) δ = 159.41, 156.13, 152.60, 151.08, 143.75, 140.00, 137.35, 130.62, 129.42, 128.79, 127.12, 122.49, 122.26, 113.43, 89.27, 86.08, 73.40, 71.20, 62.09, 42.58, 35.43.

HRMS (ESI) calcd for $C_{24}H_{26}N_8O_4$ $[M+H]^+$: 491.2150; found: 491.2147

IR ν_{max}: 3477, 3362, 3206, 2924, 2855, 2362, 1639, 1599, 1538, 1491, 1417, 1123, 1056, 903, 686.

Azo-adenosine-2

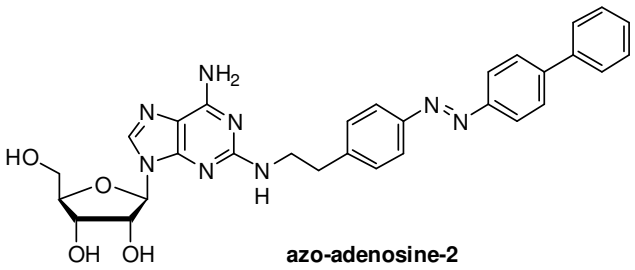

azo-adenosine-2
$C_{30}H_{30}N_8O_4$
566,62 g/mol

TLC (SiO2, 10% MeOH, 90% DCM) R_f = 0.38 (UV)

^{1}H-NMR (400 MHz, DMSO-d_6) δ = 8.19 (s, 1H), 8.06 - 7.75 (m, 9H), 7.51 (m, 6H), 6.81 (s, 2H), 6.35 (s, 1H), 5.81 (d, *J*=6.0, 1H), 4.69 (s, 1H), 4.20 (s, 1H), 3.96 (d, *J*=3.5, 1H), 3.65 (m, 5H), 3.00 (t, *J*=7.1, 2H).

^{13}C NMR (101 MHz, DMSO-d_6) δ = 163.63, 159.64, 156.52, 151.93, 151.55, 150.91, 144.85, 143.19, 139.42, 136.88, 130.29, 129.53, 128.62, 128.09, 127.21, 123.58, 123.14, 114.14, 87.61, 85.70, 73.39, 71.13, 62.23, 43.08, 35.73.

HRMS (ESI) calcd. for $C_{30}H_{30}N_8O_4$ [M+H]+: 567.2463; found: 567.2459.

IR ν_{max}: 3357, 3175, 2923, 1697, 1633, 1595, 1538, 1483, 1405, 1354, 1321, 1262, 1223, 1109, 1085, 1051, 901, 848, 788, 765, 725, 693.

REFERENCES

1. Ferre, S. et al. Role of adenosine in the control of homosynaptic plasticity in striatal excitatory synapses. *J Integr Neurosci* **4**, 445-64 (2005).

2. Cunha, R.A. Different cellular sources and different roles of adenosine: A1 receptor-mediated inhibition through astrocytic-driven volume transmission and synapse-restricted A2A receptor-mediated facilitation of plasticity. *Neurochem Int* **52**, 65-72 (2008).

3. Juliano, L.M. & Griffiths, R.R. A critical review of caffeine withdrawal: empirical validation of symptoms and signs, incidence, severity, and associated features. *Psychopharmacology (Berl)* **176**, 1-29 (2004).

4. Fisone, G., Borgkvist, A. & Usiello, A. Caffeine as a psychomotor stimulant: mechanism of action. *Cell Mol Life Sci* **61**, 857-72 (2004).

5. Lazarus, M. et al. Arousal effect of caffeine depends on adenosine A2A receptors in the shell of the nucleus accumbens. *J Neurosci* **31**, 10067-75 (2011).

6. Di Angelantonio, S. et al. Adenosine A2A receptor induces protein kinase A-dependent functional modulation of human (alpha)3(beta)4 nicotinic receptor. *J Physiol* **589**, 2755-66 (2011).

7. Wiese, S. et al. Adenosine receptor A2A-R contributes to motoneuron survival by transactivating the tyrosine kinase receptor TrkB. *Proc Natl Acad Sci U S A* **104**, 17210-5 (2007).

8. Carriba, P. et al. Striatal adenosine A2A and cannabinoid CB1 receptors form functional heteromeric complexes that mediate the motor effects of cannabinoids. *Neuropsychopharmacology* **32**, 2249-59 (2007).

9. Marcellino, D. et al. Cocaine produces D2R-mediated conformational changes in the adenosine A(2A)R-dopamine D2R heteromer. *Biochem Biophys Res Commun* **394**, 988-92 (2010).

10. Ferre, S. et al. Adenosine receptor heteromers and their integrative role in striatal function. *ScientificWorldJournal* **7**, 74-85 (2007).

11. Brown, R.M., Duncan, J.R., Stagnitti, M.R., Ledent, C. & Lawrence, A.J. mGlu5 and adenosine A2A receptor interactions regulate the conditioned effects of cocaine. *Int J Neuropsychopharmacol* **15**, 995-1001 (2011).

12. Ferre, S., Ciruela, F., Woods, A.S., Lluis, C. & Franco, R. Functional relevance of neurotransmitter receptor heteromers in the central nervous system. *Trends Neurosci* **30**, 440-6 (2007).

13. Fredholm, B.B., Chen, J.F., Masino, S.A. & Vaugeois, J.M. Actions of adenosine at its receptors in the CNS: insights from knockouts and drugs. *Annu Rev Pharmacol Toxicol* **45**, 385-412 (2005).

14. Wei, J., Wang, S., Gao, S., Dai, X. & Gao, Q. 3D-pharmacophore models for selective A2A and A2B adenosine receptor antagonists. *J Chem Inf Model* **47**, 613-25 (2007).

15. Wilson, C.N. & Mustafa, S.J. Adenosine receptors in health and disease. Preface. *Handb Exp Pharmacol*, v-vi (2009).

16. Barodia, S.K. et al. Novel 8-(furan-2-yl)-3-benzyl thiazolo [5,4-e][1,2,4] triazolo [1,5-c] pyrimidine-2(3H)-thione as selective adenosine A(2A) receptor antagonist. *Neurosci Lett* (2010).

17. Jacobson, K.A. & Gao, Z.G. Adenosine receptors as therapeutic targets. *Nat Rev Drug Discov* **5**, 247-64 (2006).

18. Carlsson, J. et al. Structure-based discovery of A2A adenosine receptor ligands. *J Med Chem* **53**, 3748-55 (2010).

19. Schwarzschild, M.A., Agnati, L., Fuxe, K., Chen, J.-F. & Morelli, M. Targeting adenosine A2A receptors in Parkinson's disease. *Trends in neurosciences* **29**, 647-654 (2006).

20. Sams, A.G. et al. Hit-to-lead optimization of a series of carboxamides of ethyl 2-amino-4-phenylthiazole-5-carboxylates as novel adenosine A2A receptor antagonists. *Bioorg Med Chem Lett* **20**, 5241-4 (2010).

21. Xu, F. et al. Structure of an agonist-bound human A2A adenosine receptor. *Science* **332**, 322-7 (2011).

22. Jaakola, V.P. et al. The 2.6 angstrom crystal structure of a human A2A adenosine receptor bound to an antagonist. *Science* **322**, 1211-7 (2008).

23. Katritch, V., Cherezov, V. & Stevens, R.C. Diversity and modularity of G protein-coupled receptor structures. *Trends Pharmacol Sci* **33**, 17-27 (2012).

24. Rosenbaum, D.M., Rasmussen, S.G. & Kobilka, B.K. The structure and function of G-protein-coupled receptors. *Nature* **459**, 356-63 (2009).

25. Oldham, W.M. & Hamm, H.E. Heterotrimeric G protein activation by G-protein-coupled receptors. *Nat Rev Mol Cell Biol* **9**, 60-71 (2008).

26. Lebon, G. et al. Agonist-bound adenosine A2A receptor structures reveal common features of GPCR activation. *Nature* **474**, 521-525 (2011).

27. Katritch, V. et al. Structure-based discovery of novel chemotypes for adenosine A(2A) receptor antagonists. *J Med Chem* **53**, 1799-809 (2010).

28. Jaakola, V.P. et al. Ligand binding and subtype selectivity of the human A(2A) adenosine receptor: identification and characterization of essential amino acid residues. *J Biol Chem* **285**, 13032-44 (2010).

29. Piirainen, H., Ashok, Y., Nanekar, R.T. & Jaakola, V.P. Structural features of adenosine receptors: from crystal to function. *Biochim Biophys Acta* **1808**, 1233-44 (2010).

30. Stevens, R.C. et al. The GPCR Network: a large-scale collaboration to determine human GPCR structure and function. *Nat Rev Drug Discov* **12**, 25-34 (2013).

31. Lebon, G. et al. Agonist-bound adenosine A2A receptor structures reveal common features of GPCR activation. *Nature* **474**, 521-5 (2011).

32. Cherezov, V. et al. High-resolution crystal structure of an engineered human beta2-adrenergic G protein-coupled receptor. *Science* **318**, 1258-65 (2007).

33. Yu, B.-C., Shirai, Y. & Tour, J.M. Syntheses of new functionalized azobenzenes for potential molecular electronic devices. *Tetrahedron* **62**, 10303-10310 (2006).

34. Ueno, K. & Akiyoshi, S. Kinetic Study on the Condensation Reaction of Aniline and Nitrosobenzenes. *Journal of the American Chemical Society* **76**, 3670-3672 (1954).

35. Priewisch, B. & RÃ¼ck-Braun, K. Efficient Preparation of Nitrosoarenes for the Synthesis of Azobenzenesâ€ *The Journal of Organic Chemistry* **70**, 2350-2352 (2005).

36. Cordeaux, Y., Ijzerman, A.P. & Hill, S.J. Coupling of the human A1 adenosine receptor to different heterotrimeric G proteins: evidence for agonist-specific G protein activation. *British Journal of Pharmacology* **143**, 705-714 (2004).

37. Jockers, R. et al. Species difference in the G protein selectivity of the human and bovine A1-adenosine receptor. *J Biol Chem* **269**, 32077-84 (1994).

38. Levitz, J. et al. Optical control of metabotropic glutamate receptors. *Nat Neurosci* **16**, 507-16 (2013).

39. Olah, M.E. Identification of A2a adenosine receptor domains involved in selective coupling to Gs. Analysis of chimeric A1/A2a adenosine receptors. *J Biol Chem* **272**, 337-44 (1997).

40. Conklin, B.R., Farfel, Z., Lustig, K.D., Julius, D. & Bourne, H.R. Substitution of three amino acids switches receptor specificity of Gq[alpha] to that of Gi[alpha]. *Nature* **363**, 274-276 (1993).

41. Conklin, B.R. et al. Carboxyl-terminal mutations of Gq alpha and Gs alpha that alter the fidelity of receptor activation. *Molecular Pharmacology* **50**, 885-890 (1996).

42. Agnati, L.F., Ferre, S., Lluis, C., Franco, R. & Fuxe, K. Molecular mechanisms and therapeutical implications of intramembrane receptor/receptor interactions

among heptahelical receptors with examples from the striatopallidal GABA neurons. *Pharmacol Rev* **55**, 509-50 (2003).

43. Banghart, M., Borges, K., Isacoff, E., Trauner, D. & Kramer, R.H. Light-activated ion channels for remote control of neuronal firing. *Nat Neurosci* **7**, 1381-6 (2004).

44. Janovjak, H., Szobota, S., Wyart, C., Trauner, D. & Isacoff, E.Y. A light-gated, potassium-selective glutamate receptor for the optical inhibition of neuronal firing. *Nat Neurosci* **13**, 1027-32 (2010).

45. Volgraf, M. et al. Allosteric control of an ionotropic glutamate receptor with an optical switch. *Nat Chem Biol* **2**, 47-52 (2006).

VIII

Synthesis of Photoswitchable Benzodiazepines

Matthias Schönberger & Dirk Trauner

Department of Chemistry, Ludwig-Maximilians-Universität, and Center for Integrated Protein Science, 81377 Munich, Germany.

Benzodiazepines (BZDs) are positive allosteric modulators (PAMs) of $GABA_A$ receptors. They are used as powerful sedative, anticonvulsive and anxiolytic drugs. However, BZD use leads to drug addiction and further research is needed to reduce side effects. We have developed azobenzene derivatives of the potent BZD clonazepam. These photochromic ligands may act as photoswitchable PAMs of $GABA_A$ receptors.

Content

Introduction

$GABA_A$ receptors. $GABA_A$ receptors are chloride selective ion channels of the pentameric ligand gated ion channel (pLGIC) super-family that also includes nicotinic acetylcholine receptors (nAChR), glycine receptors (GlyR), *Erwinia chrysanthemi* ligand gated ion channels (ELIC), *Gloeobacter violaceus* ligand gated ion channels (GLIC) and 5-hydroxytrytamine-type-3-receptors (5HT3).[1] Even though $GABA_A$ receptors themselves have not been crystallized to date, recent crystal structure elucidation of ELIC and GLIC has provided detailed structural insights to the general pentameric channel architecture.[2] All of the abovementioned receptors share a prominent cysteine loop in their amino-terminal domain. Therefore, they are also referred to as the "cys-loop" family.[3,4] In addition, they share a pentameric architecture with five individual subunits assembling a central ion conductive pore. Each subunit consists of a large hydrophilic amino-terminal extracellular domain and four membrane spanning domains (TM1-4).[5-7]

There are eight different classes of subunits making a total of 19 different subunits that can form heteropentameric $GABA_A$ receptors: α (1-6), β (1-3), γ (1-3), δ, ε, ρ (1-3), θ and π.[6] $GABA_A$ receptors consisting of two α_1, two β_2 and one γ_2 subunit are the major isoform in brain. The arrangement of these subunits has been determined to be γ_2-β_2-α_1-β_2-α_1 (Figure 1).[8,9] Each receptor has individual functional and pharmacological properties based on its subunit composition.[10,11]

$GABA_A$ receptors allow influx of chloride ions when two molecules of the native agonist γ-amino-butyric acid (GABA) bind to the channel at the interface of the α and β subunit. This results in membrane hyperpolarization (inhibitory postsynaptic potential).[12,13] Therefore, GABA is the most prime inhibitory neurotransmitter in the vertebrate brain.[14]

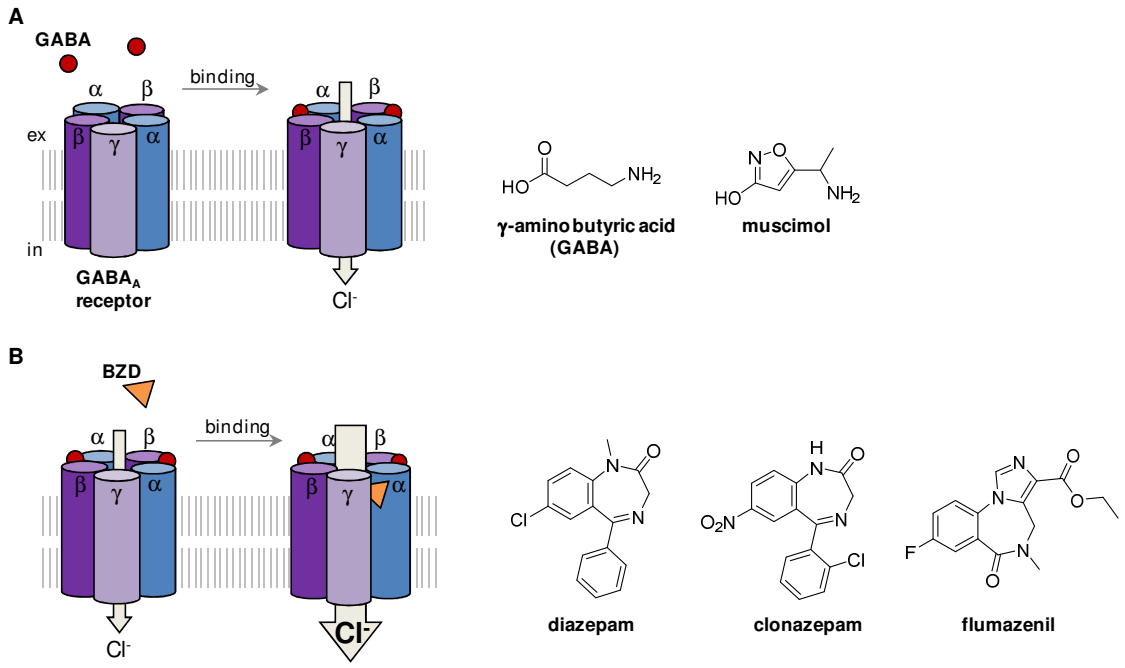

Figure 1. $GABA_A$ receptors. A) Schematic drawing of a $GABA_A$ receptor (left) and chemical structure of its agonists **GABA** and **muscimol** (right). B) Mechanism of action of benzodiazepines (BZDs) and chemical structures of the classical BZDs **diazepam** and **clonazepam**. **Flumazenil** is a competitive BZD antagonist.

Benzodiazepines. Benzodiazepines (BZDs) are positive allosteric modulators of $GABA_A$ receptors, binding at the extracellular interface of the α and γ subunit (Figure 1B).[15] BZDs are highly effective anxiolytics and are further used for treatment of insomnia, convulsive disorders, muscle relaxation and sedation. Due to undesired side effects including drowsiness, confusion and most importantly drug addiction,[16,17] their use is, however, limited.[12,13]

BZDs are positive allosteric modulators of $GABA_A$ receptors, enhancing the effect of GABA by increasing the channel open frequency.[13,18] $GABA_A$ receptors with $\alpha_{1\text{-}3}$ or α_5 subunits are involved in phasic inhibition and are BZD sensitive. By contrast, α_4 or α_6 containing isoforms lead to tonic inhibition and are BZD insensitive.[5] The different α-subunit isoforms also contribute to different effects by BZDs.[19] For instance, receptors containing α_1 subunits appear to be responsible for the sedative properties of classic BZDs and those containing α_2 or α_3 subunits cause anxiolytic effects.[20]

Diazepam was one of the first BZDs that was synthesized and marketed (valium®), followed by many other derivates including the more potent **clonazepam**.[21] The imidazole **flumazenil** is a competitive antagonist of BZDs.[22]

Results and Discussion

Design of photochromic ligands. Given the important role of $GABA_A$ receptors in human health and disease, and the associated pharmacological impact of BZDs, we decided to develop photoswitchable azobenzene derivatives of **clonazepam** as photochromic ligands (PCLs), *viz* photo-benzodiazepines (pBZs, Figure 2).[23] Since PCLs are permanently modified with the comparatively large azobenzene moiety, they have to be designed carefully. Ideally, one of the photoisomers provides high pharmacological activity, while the other isomer does not.[24]

Since there is no X-ray structure of a $GABA_A$ receptor with a BZD, we developed two molecular platforms for combining an azobenzene functional group with **clonazepam** (Figure 2B). pBZs of the first generation carried the azobenzene as an extention of the annulated benzo ring (**pBZ1.1**). Recently published azobenzene-BZD-derivatives with this substitution pattern showed only micromolar IC_{50} values in an antihelmintic test against *Schistosoma mansoni*.[25] However, the reported synthetic route of Mahajan *et al.* relied on a diazotization reactions with phenolates. Resulting 4′-hydroxy derivatives, which are uncommon for BZDs were not tested for $GABA_A$ receptor activity. [25] To avoid hydrogen bond donors in 4′-position, we turned to Mills reaction for azobenzene formation.[26]

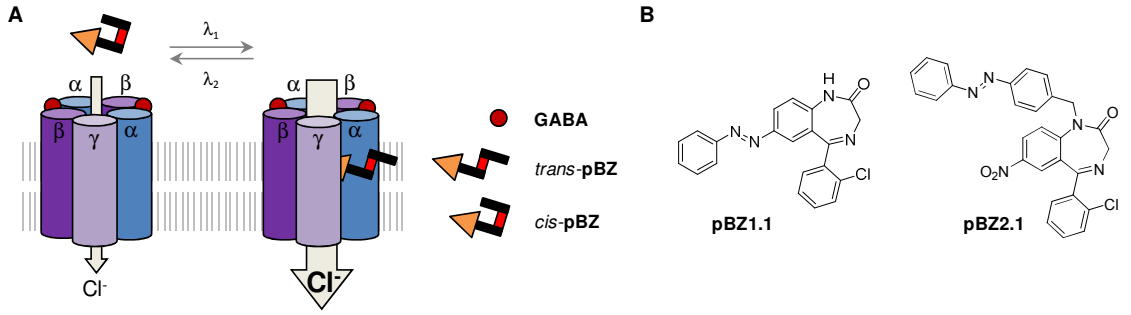

Figure 2. Photo-benzodiazepines (pBZs). A) Proposed mechanism of action of pBZs. B) Two representative pBZs with different chemical design.

pBZs of second generation were alkylated with a benzyl azobenzene at the anilide nitrogen of the seven-membered BZD ring (**pBZ2.1**, Figure 2B).

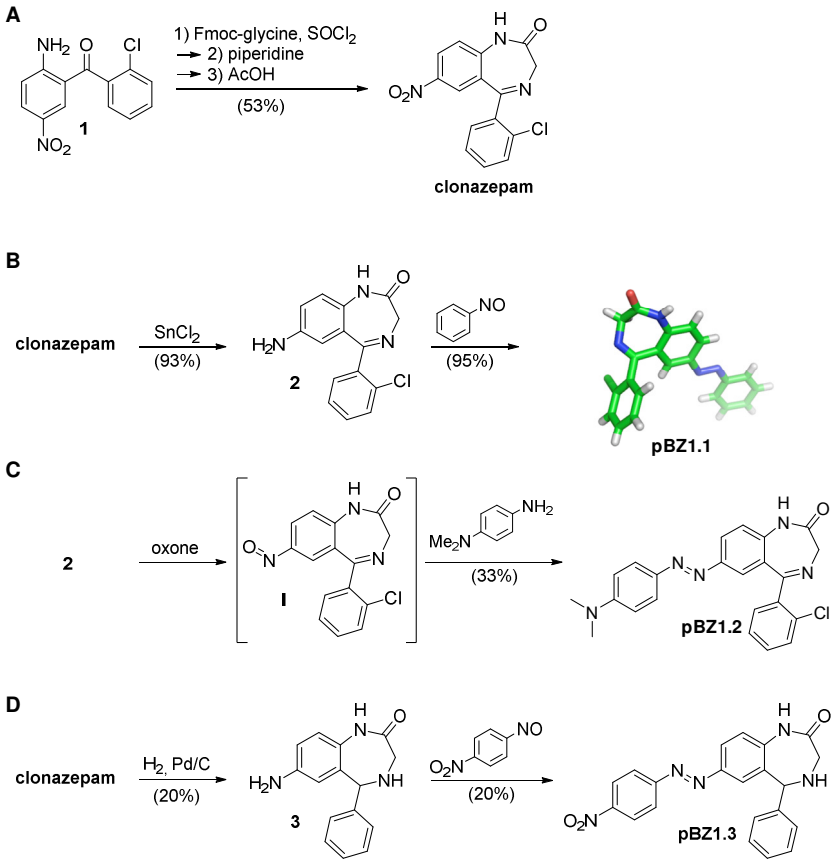

Scheme 1. Chemical synthesis of **clonazepam** (A) and photoswitchable derivatives **pBZ1.1** (B), **pBZ1.2** (C) and **pBZ1.3** (D).

Synthesis of photochromic ligands. First, **clonazepam** was ssynthesized from commercial benzophenone **1**. To set up a Sternbach cyclization, Fmoc-glycine was coupled to **1** using acid chloride activation (Scheme 1A). After deprotection, cyclodehydration was achieved by boiling in toluene and acetic acid.

C**lonazepam** was then used as a basis for all pBZs. For first generation molecules, clonazepam had to be set up for a Mills reaction. To install the required aniline functional group, it was reduced using $SnCl_2$ in HCl/MeOH affording **2**. Condensation with commercial nitrosobenzene in a mixture of acetic acid and DCM yielded **pBZ1.1** (Scheme 1B). Crystal structure analysis demonstrated the planar annulated azobenzene and the 2-chloro benzene ring that is oriented perpendicular to the seven-membered ring.

For electron rich 4′-substitution, **2** could also be oxidized to the corresponding nitroso intermediate **I** that was subsequently condensed with commercial *N,N*-dimethyl-4-amino-aniline giving **pBZ1.2** (Scheme 1C). Hydrogen gas and palladium on charcoal reduced not only clonazepam′s nitro group, but also the Schiff base and the

chlorobenzene, yielding the dihydro BZD **3** (Scheme 1D). Coupling with freshly prepared 4-nitro nitrosobenzene gave access to **pBZ1.3**.

Table 1. Synthesis of 2nd generation **pBZs** and list of molecules.

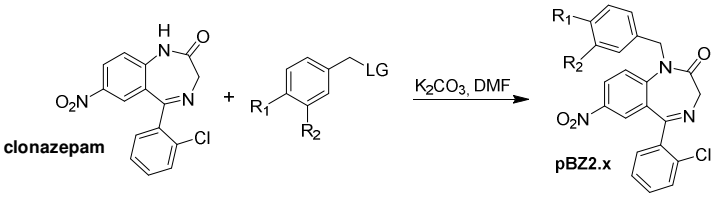

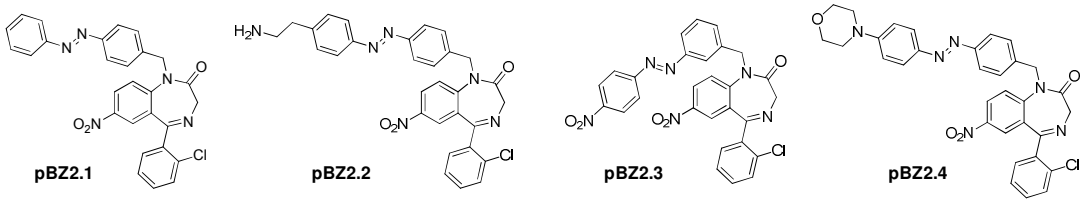

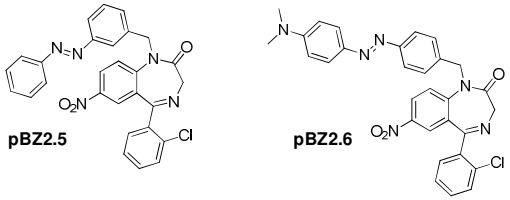

For second generation pBZs, benzyl azobenzene building blocks were prepared and equipped with a leaving group. Either corresponding benzyl alcohols were converted to mesylates using mesyl chloride or to benzyl bromides *via* Appel reaction (see Experimental section). Best alkylation reactions were obtained when **clonazepam** was deprotonated with K_2CO_3 in DMF at 0 °C and subsequently treated with the desired building block (Table 1). Table 1 shows the resulting **pBZ2.1-6** molecules that vary in the substitution and of the azobenzene. In addition, the isothiocyanate derivative **north-NCS** was prepared for cystein labeling reactions.

Biological testing was performed by our collaborators Simon Middendorp and Erwin Sigel from Bern University. It was found that all pBZ1 molecules were inactive as PAMs on $\alpha_1\beta_2\gamma_2$GABA$_A$ receptors at all concentrations regardless of the illumination wavelength. The relatively large substituent in 7-position was not tolerated. Wether these molecules may act as BZD antagonists has yet to be determined.

By contrast, all pBZ2 molecules were active. However, photoeffects were small and the maximally activating effect could in many cases not be determined due to solubility issues. Nevertheless, PAM activity was maintained after substitution and the observed photoeffects affirm that the substitution pattern of pBZ2s may be a promising platform for future PCLs.

Summary and Outlook

In conclusion, a small series of photoswitchable **clonazepam** derivatives (pBZs) have been synthesized. First generation pBZ1 molecules, substituted in 7-position, were inactive as PAMs on $\alpha_1\beta_2\gamma_2$GABA$_A$ receptors. Second generation pBZ2 molecules, substituted at N^1, were PAMs, however, lacked pronounced photoswitching and had only poor solubility.

To improve both photoswitching and solubility, differently substituted azobenzenes may be installed in future. In particular ortho- and meta-benzyl derivatives might be interesting candidates. Hydrophilic 4′-substitution might also increase both photoswitching and solubility.

Wether existing pBZs have distinct effects on different GABA$_A$ receptor isoforms remains to be determined. Subtype selective photopharmacology might be very helpful for developing novel therapeutics.

Abbreviations

ATR	attenuated total reflectance
Boc	*tert*-butyloxycarbonyl
BPh	benzophenone
BZD	benzodiazepine
calc.	calculated
cat.	catalytic
Cbz	benzyloxycarbonyl
CDI	1,1'-carbonyldiimidazole
δ	chemical shift (NMR)
DCM	dichloromethane
DIPEA	*N*,*N*-diisopropylethylamine
DMSO	dimethylsulfoxide
DMF	dimethylformamide
eq.	equivalent(s)
ESI	electron spray ionization
Et	ethyl
Fmoc	fluorenylmethoxycarbonyl
FT	fourier transform
GABA	γ-aminobutyric acid
gly.	glycine
HBTU	2-(1H-benzotriazole-1-yl)-1,1,3,3-tetramethylaminium hexafluorophosphate
HMPA	hexamethylphosphoramide
HPLC	high-performance liquid chromatography
HRMS	high resolution mass spectrometry
IC_{50}	half maximal inhibitory concentration
IR	infrared spectroscopy

isohex	*iso*-hexanes
λ_{max}	absorption maximum
Me	methyl
MPLC	medium pressure liquid chromatography
NMM	*N*-methylmorpholine
NMR	nuclear magnetic resonance
PCL	photochromic ligand
PG	protecting group
ppm	parts per million
PTL	photoswitched tethered ligands
R_f	retention factor (TLC)
rt	room temperature
Rt	retention time (HPLC)
sat.	saturated
sm	starting material
TEA	triethylamine
TLC	thin layer chromatography
THF	tetrahydrofuran
Ts	tosyl
UV	ultra-violet
VIS	visible light

Experimentals

General Methods

All reactions were conducted in oven-dried glassware equipped with a magnetic stir bar using freshly distilled solvents. Tetrahydrofuran was distilled from sodium benzophenone. All other commercially available reagents were used as received.

All salt solutions used in aqueous work ups were aqueous and saturated if not otherwise noted.

Thin layer chromatography was performed on E. Merck 0.25 mm silica gel 60 F_{254} precoated glass plates and the compounds were detected on thin-layer chromatography plates using UV light at 254 nm and/or ninhydrine stain.

Flash column chromatography was carried out with silica gel 60 (40-63 μm).

HPLC was performed on a VARIAN PrepStar Model SD-1 system equipped with UV/VIS detector VARIAN 380-LC on Microsorb 60 C_{18} silica (particle size: 8 μm) reverse-phase column. Composition of the products was assessed by analytical reverse phase HPLC using a column (250 x 4.6 mm) employing following methods:

Method A: 20% MeOH with 0.1% formic acid in H_2O over the first 3 min, 20 to 90% MeOH in H_2O linear gradient over 52 min; flow rate: 0.75 mL/min.

Method B: 10% MeOH with 0.1% formic acid in H_2O over the first 5 min, 10 to 90% MeOH in H_2O linear gradient over 52 min; flow rate: 0.75 mL/min.

Methods for preparative reverse phase HPLC (250 x 21.4 mm):

Method A: 40% MeOH with 0.1% formic acid in H_2O over the first 3 min, 40 to 90% MeOH in H_2O linear gradient over 52 min; flow rate: 15.75 mL/min.

Method B: 30% MeOH with 0.1% formic acid in H_2O over the first 3 min, 30 to 70% MeOH in H_2O linear gradient over 52 min; flow rate: 15.75 mL/min.

NMR spectra (^{1}H-NMR, ^{13}C-NMR) were recorded on VARIAN VNMRS 300, VNMRS 400, INOVA 400 or VNMRS 600 spectrometers with deuterated chloroform ($CDCl_3$) or dimethylsulfoxide (*d6*-DMSO) as solvents. Chemical shifts δ are reported in ppm relative to the known value of residual solvent signal and coupling constants are in Hz. The following abbreviations are used to describe peak patterns: s (singlet), d (doublet), t (triplet), and m (multiplet).

IR spectra were recorded as ATR (attenuated total reflectance) on a PERKIN ELMER Spectrum BX II (FTIR System) and are reported as wave numbers (cm^{-1}). As detector a SMITHS DETEVTION DuraSampl*IR* II Diamond ATR senor was used.

Mass spectrometry: Molecular weights were assessed by electronspray ionization mass spectrometry in high resolution (ESI/HRMS) performed on a THERMO FINNIGAN LTQ FT spectrometer at the Department of Chemistry and Pharmaceutical Science of Ludwig-Maximilians-Universität Munich.

Melting points were taken on a Büchi apparatus using open capillary tubes and remain uncorrected.

UV/VIS spectra were recorded on a VARIAN 50 Scan 50 spectrophotometer in precision cells made of quartz SUPRASIL®.

List of Molecules

Table 2. Building blocks.

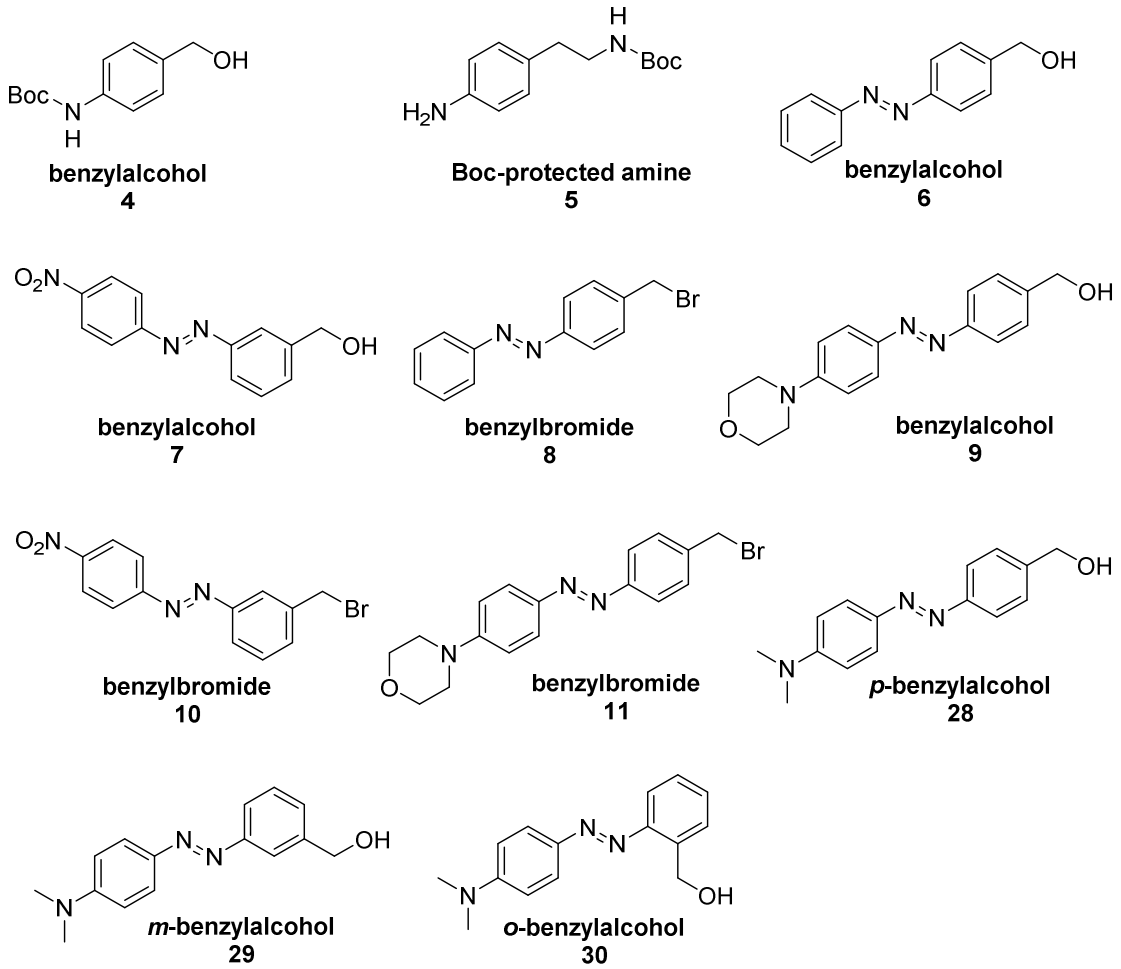

Table 3. Benzodiazepines.

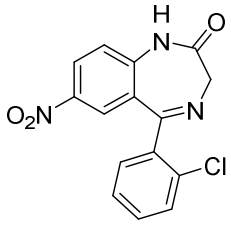

clonazepam

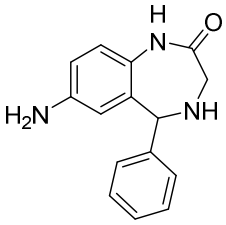

benzodiazepine 2

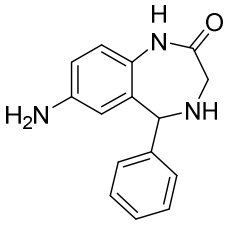

dihydro benzodiazepine 3

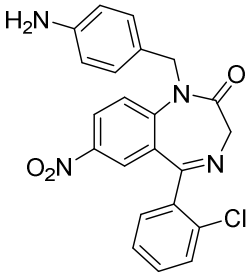

benzodiazepine 12

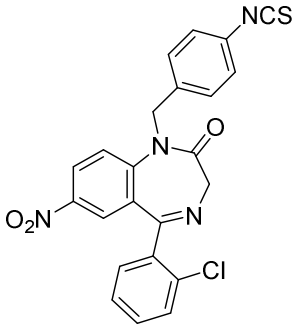

North-benzyl-NCS

Table 4. 1st Generation Photo-Benzodiazepines (pBZs).

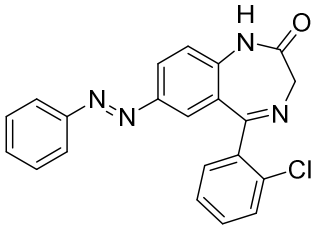

pBZ1.1

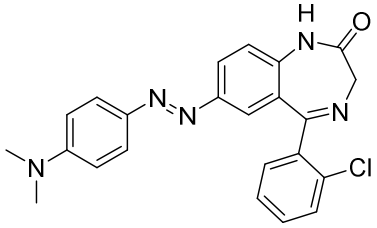

pBZ1.2

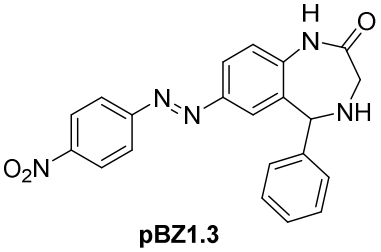

pBZ1.3

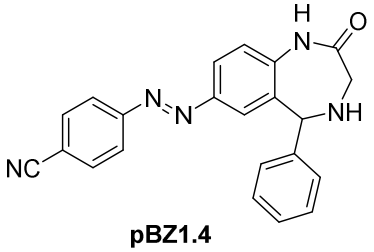

pBZ1.4

Table 5. 2nd Generation Photo-Benzodiazepines (pBZs).

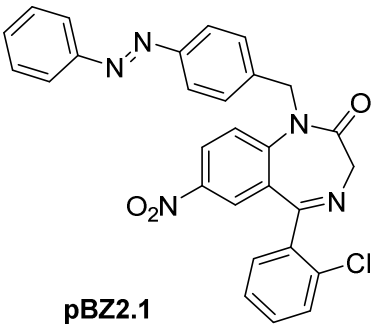

pBZ2.1

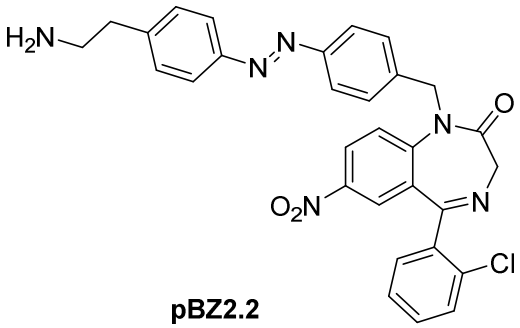

pBZ2.2

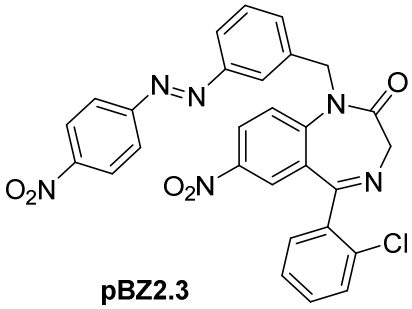

pBZ2.3

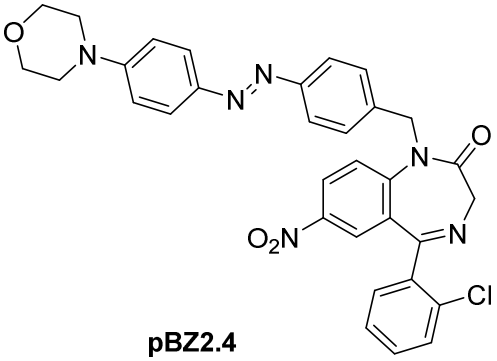

pBZ2.4

Table 6. Isolated intermediates and side products.

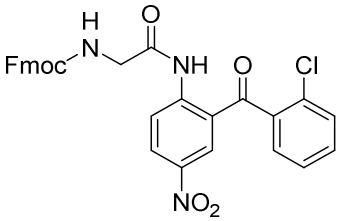

Fmoc-protected benzophenone
13

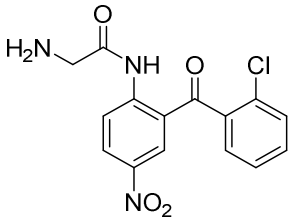

primary amine
14

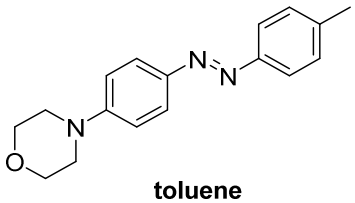

toluene
15

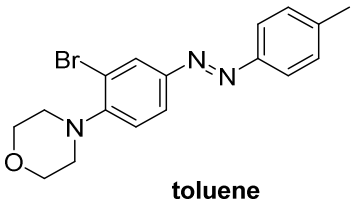

toluene
16

Experimental Procedures Clonazepam & 1st Generation pBZs

Clonazepam

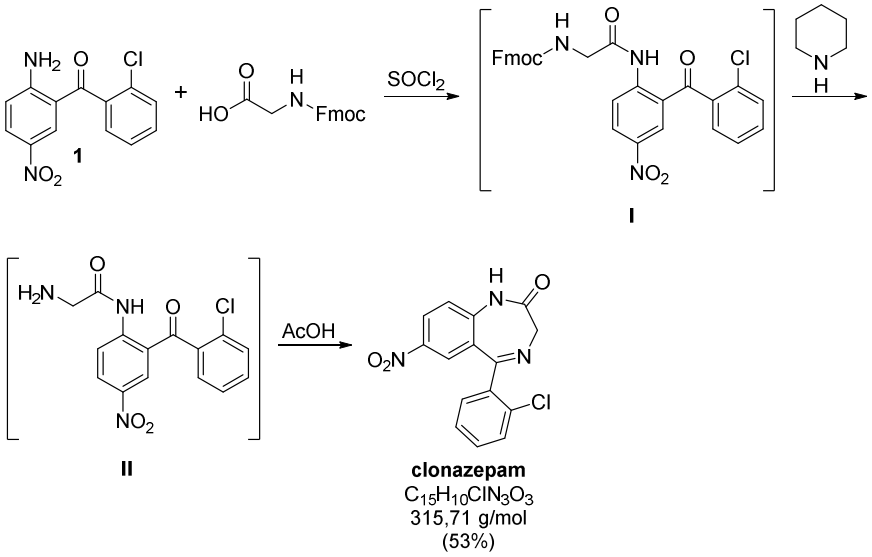

To *N*-Fmoc-glycine (8.60 g, 28.9 mmol, 2 eq.) in 70 mL freshly distilled tetrahydrofuran, 10.5 mL thionyl chloride (145 mmol, 10 eq.) were added under argon atmosphere and the solution was heated to 60 °C for 1 h. The solvent was removed *in vacuo* and the oily residue was co-evaporated with chloroform twice. The crude material was dissolved in 70 mL chloroform benzophenone **1** (4.00 g, 13.4 mmol, 1 eq.) was added. The reaction mixture was stirred at 68 °C overnight. After cooling to room temperature, the solution was washed with aqueous solution of $NaHCO_3$ (2 x 50 mL). The organic layer was dried over Na_2SO_4, filtered and the solvent was removed *in vacuo*. The solid residue was purified by recrystallization. The product was washed with cold methanol yielding 7.82 g (97%) of carbamate intermediate **I** as a white solid.

I (4.99 g, 8.97 mmol, 1.0 eq.) was dissolved in 160 mL freshly distilled tetrahydrofuran and 4.42 mL piperidine (44.8 mmol, 5.0 eq.) were added. The progress of the reaction was monitored using TLC (silica; 10% MeOH/DCM). Over the course of 1.5 h, white precipitation occurred. Additional 2.5 eq. of piperidine and 20 mL tetrahydrofuran were added. The reaction was terminated after a total reaction time of 16.5 h and the solvent was removed under reduced pressure yielding intermediate **II**. Without further purification, the crude was suspended in 200 mL toluene and 2.76 mL (48.3 mmol, 5.0 eq.) acetic acid were added. The resulting reaction mixture was refluxed for 4 h at 123 °C. After removal of the solvent using rotary evaporation, the residue was taken up in 200 mL ethyl acetate. The solution was washed with sat. $NaHCO_3$ (3 x 80 mL) and brine (80 mL). After drying over Na_2SO_4 the extract was filtered and the solvent was removed under reduced pressure. Purification using flash column chromatography (silica, gradient: 0-20% MeOH/DCM) yielded **clonazepam** (1.47 g, 53%) as a pale yellow solid.

TLC (silica; 10% MeOH, 90% DCM) R_f = 0.56 (UV)

mp = 237-238 °C

IR (FT, ATR): 3103, 3057, 2972, 2898, 2843, 1691, 1614, 1538, 1334, 1313, 1300, 1256, 1100, 1014, 843, 771, 764, 750, 740, 730 cm^{-1}.

^{1}H NMR (400 MHz, dmso-d_6) δ = 11.27 (s, 1H), 8.36 (dd, *J*=9.0, 2.7, 1H), 7.72 (d, *J*=2.5, 1H), 7.66 – 7.62 (m, 1H), 7.56 – 7.47 (m, 3H), 7.41 (d, *J*=9.0, 1H), 4.29 (s, 2H).

^{13}C NMR (101 MHz, dmso-d_6) δ = 169.74, 168.32, 144.81, 142.02, 138.44, 132.22, 132.01, 131.92, 130.27, 128.01, 127.38, 126.92, 125.36, 122.62, 57.55.

HRMS (ESI, positive): calc. for $C_{15}H_{11}ClN_3O_3$ $(M+H)^+$: 316.0489; found: 316.0484.

HRMS (ESI, negative): calc. for $C_{15}H_9ClN_3O_3$ $(M)^-$: 314.0338; found: 314.0337.

Amino Benzodiazepine 2

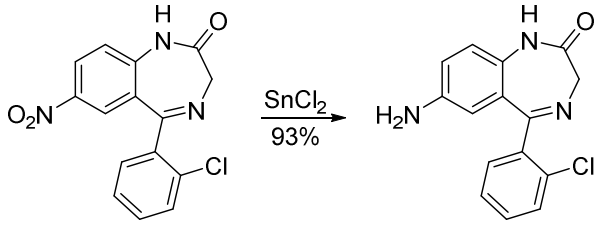

clonazepam **2**

$C_{15}H_{12}ClN_3O$
285,73 g/mol

Clonazepam (200 mg, 0.633 mmol, 1.0 eq.) was treated with 1.2 mL 6M HCl and tin(II) chloride dihydrate dissolved in 1.2 mL 6M HCl was added. To the yellow suspension, 8 mL methanol were added and the suspension turned gradually into a red solution. After 5 h stirring at room temperature methanol was removed under reduced pressure and the reaction mixture was basified with 1M NaOH. The aqueous solution was extracted with dichloromethane (3 x 15 mL) and combined organic layers were dried over $NaSO_4$, filtered and concentrated under reduced pressure. The crude product was purified using flash column chromatography (silica pretreated with 1% TEA/DCM, gradient: 0-5% MeOH/DCM) yielding **2** (168 mg, 93%) as a pale brown solid.

TLC (silica; 10% MeOH, 90% DCM) R_f = 0.50 (UV)

mp = 125-126 °C

IR (FT, ATR): 3339, 3207, 3051, 2886, 1668, 1610, 1500, 1341, 1307, 1231, 1058, 1010, 823, 765, 752, 736 cm^{-1}.

^{1}H NMR (400 MHz, dmso-d_6) δ = 10.09 (s, 1H), 7.49 – 7.36 (m, 4H), 6.87 (d, *J*=8.6, 1H), 6.70 (dd, *J*=8.6, 2.6, 1H), 6.11 (d, *J*=2.6, 1H), 5.07 (s, 2H), 4.05 (s, 2H).

^{13}C NMR (101 MHz, dmso-d_6) δ = 169.69, 169.58, 144.73, 139.87, 132.30, 131.53, 130.99, 130.02, 128.99, 128.48, 127.56, 122.40, 118.56, 112.43, 57.35.

HRMS (ESI, positive): calc. for $C_{15}H_{13}ClN_3O$ $(M+H)^+$: 286.0747; found: 286.0741.

Amino Dihydobenzodiazepine 3

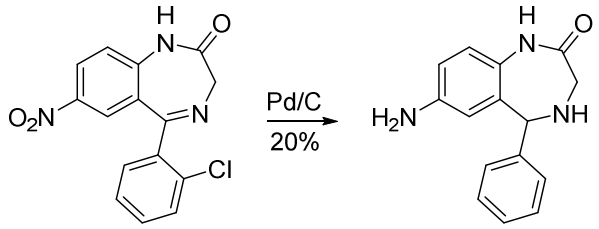

clonazepam

3
$C_{15}H_{15}N_3O$
253,30 g/mol

To a solution **clonazepam** (43 mg, 0.14 mmol, 1 eq.) in 40 mL methanol and 63 µL (1.1 mmol, 8 eq.) acetic acid, 10% palladium on carbon (15 mg, 0.014 mmol, 0.1 eq.) were added. The reaction mixture was stirred under a hydrogen atmosphere for 8 h at room temperature. After filtration, the solvent was removed under reduced pressure and the residue was partitioned between 30 mL ethyl acetate and aqueous solution of $NaHCO_3$ (15 mL). The organic phase was washed with aqueous solution of $NaHCO_3$ (2 x 15 mL) and aqueous solution of NaCl (15 mL). After drying over $NaSO_4$, filtration and removal of the solvent using rotary evaporation, the residue was purified using flash column chromatography (silica; gradient: 0-10% MeOH/DCM) yielding **3** (7 mg, 20%).

TLC (silica; 10% MeOH, 90% DCM) R_f = 0.50 (UV)

^{1}H-NMR (400 MHz, dmso-d_6): δ 9.33 (s, 1H), 7.31 (d, ^3J = 4.4 Hz, 4H), 7.27-7.21 (m, 1H), 6.70 (d, ^3J = 8.4 Hz, 1H), 6.39 (dd, ^3J = 8.4, ^4J = 2.6 Hz, 1H), 5.86 (d, ^4J = 2.4 Hz, 1H), 5.04 (s, 1H), 4.79 (s, 2H), 3.44 (s, 1H), 3.16 (s, 2H) ppm.

^{13}C-NMR (100 MHz, dmso-d_6): δ 172.3, 145.7, 143.0, 134.6, 128.6, 128.5, 127.8, 127.4, 122.2, 114.6, 113.6, 61.4, 50.4 ppm.

HRMS (ESI, positive): calc. for $C_{15}H_{16}N_3O$ $(M+H)^+$: 254.1293; found: 254.1287.

pBZ1.1

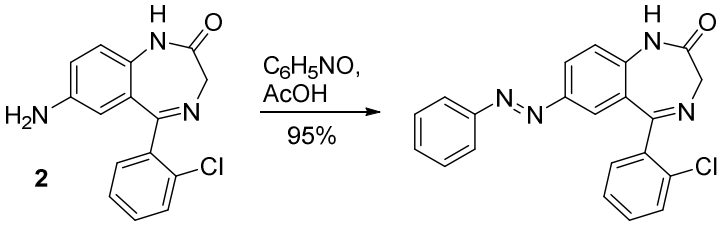

2 (50 mg, 0.16 mmol, 1 eq.) was dissolved in 2 mL acetic acid, followed by addition of nitrosobenzene **17** (17 mg, 0.16 mmol, 1 eq.) and the reaction mixture was stirred for 12 h at room temperature. The mixture was treated with aqueous solution of $NaHCO_3$ and was basified with Na_2CO_3. The aqueous layer was extracted with dichloromethane (3 x 15 mL) and the combined organic layers were dried over Na_2SO_4. After filtration, the solvent was removed under reduced pressure and the crude product was purified using flash column chromatography (silica; gradient: 0-2% MeOH/DCM) yielding 56 mg (94.6%) of **pBZ1.1** as an orange solid.

TLC (silica; 10% MeOH, 90% DCM) R_f = 0.53 (UV)

mp = 255-257 °C

λ_{max} = 340 nm

IR (FT, ATR): 3056, 2959, 1682, 1611, 1488, 1360, 1235, 1060, 1016, 843, 742 cm^{-1}.

^{1}H-NMR ($CDCl_3$, 400 MHz): δ 8.72 (s, 1H), 8.04 (dd, ^3J = 8.6, ^4J = 2.2 Hz, 1H), 7.83 (ddd, ^3J =4.4, ^3J = 3.7, ^4J = 1.6 Hz, 2H), 7.67 (d, ^4J = 2.2 Hz, 1H), 7.63-7.59 (m, 1H), 7.50-7.45 (m, 3H), 7.42-7.36 (m, 3H), 7.23 (d, ^3J = 8.7 Hz, 1H), 4.46 (s, 2H) ppm.

^{13}C NMR (101 MHz, $CDCl_3$) δ = 170.68, 170.24, 152.33, 148.27, 139.55, 138.63, 133.27, 131.39, 131.11, 130.94, 130.17, 129.10, 128.96, 128.35, 127.72, 127.01, 126.96, 124.23, 123.89, 122.87, 122.56, 121.65, 121.33, 56.62.

HRMS (ESI, positive): calc. for $C_{21}H_{16}ClN_4O$ $(M+H)^+$: 375.8309; found: 375.1011.

HRMS (ESI, negative): calc. for $C_{21}H_{14}ClN_4O$ $(M)^-$: 373.0862; found: 373.0857.

General procedure I: Oxone oxidation and subsequent Mills reaction yielding diazobenzenes 18, 19 and 20 [8]

A solution of an aniline (1 eq.) in dichloromethane was treated with an aqueous solution of Oxone® (3-4.5 eq.). The biphasic reaction mixture was stirred vigorously at room temperature until TLC monitoring showed no further consumption of the starting material (17-24 h). Phases were separated and the aqueous layer was extracted with dichloromethane three times. The combined organic layers were washed with 1M HCl, aqueous solution of $NaHCO_3$, water and aqueous solution of NaCl. After drying over Na_2SO_4, extracts were filtered and the solvent was removed under reduced pressure yielding crude nitrosoarenes.

Without further purification, nitosoarenes were dissolved in acetic acid, followed by addition of corresponding aniline. The reaction mixture was stirred at room temperature until TLC monitoring indicates complete reaction (17-21 h). The mixture was treated with aqueous solution of $NaHCO_3$ and was basified with Na_2CO_3. The aqueous layer was extracted with dichloromethane three times and the combined organic layers were dried over Na_2SO_4. After filtration, the solvent was removed under reduced pressure and the crude product was purified from major impurities using quick flash column chromatography (silica; gradient: 0-5% MeOH/DCM). Purification of the isolated crude product using HPLC yielded the desired azobenzenes **18**, **19** and **20**.

[8] Priewisch, B. & Rück-Braun, K. Efficient Preparation of Nitrosoarenes for the Synthesis of Azobenzenesâ€ *The Journal of Organic Chemistry* **70**, 2350-2352 (2005).

pBZ1.2

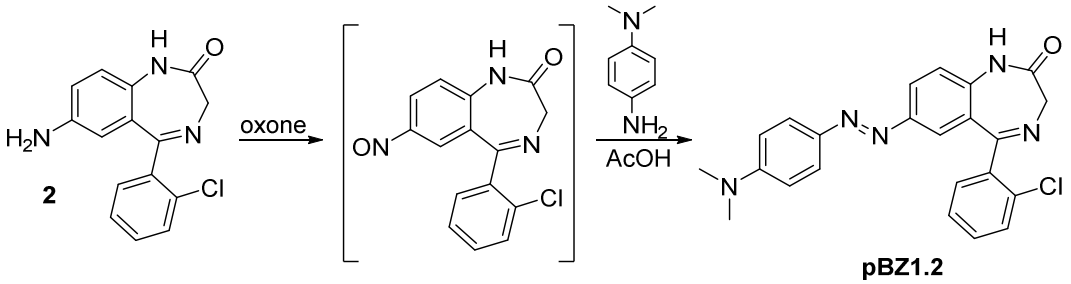

Following general procedure I, **clonazepam** (50 mg, 0.088 mmol, 1 eq.) in 2 mL chloroform was treated with Oxone® (242 mg, 0.394 mmol, 4.5 eq.) dissolved in 4 mL water. For aqueous work up, the organic layer was washed with aqueous solution of $NaHCO_3$, water and aqueous solution of NaCl.

The resulting crude nitroso compound was dissolved in 2 mL acetic acid and *N,N*-dimethyl-*p*-phenylenediamine (18 mg, 0.13 mmol, 1.5 eq.) was added. Aqueous work up und purification (HPLC: method A) yielded 10 mg (33%) of **pBZ1.2** as a brown solid.

HPLC (C-18, analytical HPLC, method A) Rt = 32.4 min

TLC (silica; 10% MeOH, 90% DCM) R_f = 0.55 (UV)

mp = 250-253 °C

λ_{max} = 433 nm

IR (FT, ATR): 2920, 2853, 1682, 1598, 1517, 1361, 1230, 1141, 1058, 1011, 944, 821, 750 cm^{-1}.

^{1}H-NMR ($CDCl_3$, 600 MHz): 8.81 (s, 1H), 7.96 (dd, ^3J = 8.6, ^4J = 2.2 Hz, 1H), 7.80-7.76 (m, 2H), 7.61-7.57 (m, 1H), 7.55 (d, ^4J = 2.2 Hz, 1H), 7.41-7.34 (m, 3H), 7.19 (d, ^3J = 8.7 Hz, 1H), 6.74-6.66 (m, 2H), 4.44 (s, 2H), 3.07 (s, 6H) ppm.

^{13}C-NMR ($CDCl_3$, 150 MHz): δ 170.9, 170.5, 152.6, 149.1, 143.3, 138.9, 138.2, 133.3, 131.1, 130.8, 130.1, 128.3, 126.9, 125.5, 125.1, 123.7, 121.6, 111.5, 56.6, 40.3 ppm.

HRMS (ESI, positive): calc. for $C_{23}H_{21}ClN_5O$ $(M+H)^+$: 418.1435; found: 418.1428.

HRMS (ESI, negative): calc. for $C_{23}H_{19}ClN_5O$ $(M)^-$: 416.1284; found: 416.1282.

pBZ1.3

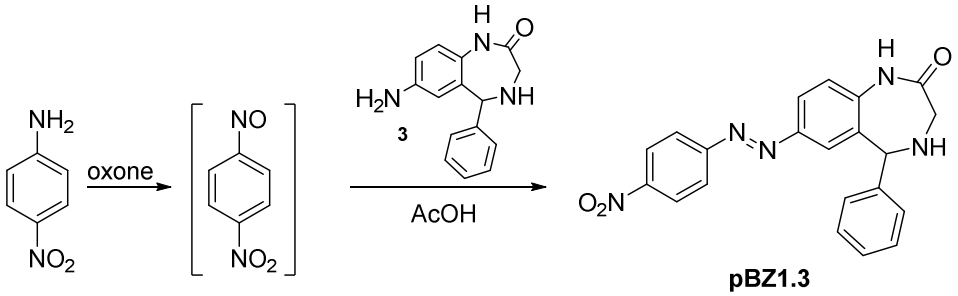

Following general procedure I. 4-Nitroaniline (29 mg, 0.21 mmol, 1.5 eq.) in 1 mL dichloromethane was treated with Oxone® (128 mg, 0.42 mmol, 3 eq.) dissolved in 4 mL water. The biphasic mixture was stirred for 9 h at room temperature and another eq. Oxone® and 1 mL dichloromethane was added.

Resulting crude nitroso compound was dissolved in 1 mL acetic acid and **3** (40 mg, 0.14 mmol, 1 eq.) in 2.5 mL acetic acid was added. Aqueous work up und purification (HPLC: method B) yielded 10 mg (20%) **pBZ1.3** as an orange solid.

HPLC (C-18, analytical HPLC, method B) Rt = 45.9 min

TLC (silica; 10% MeOH, 90% DCM) R_f = 0.63 (UV)

mp = 273-276 °C (decomp.)

λ_{max} = 375 nm

IR (FT, ATR):3188, 3060, 1648, 1587, 1516, 1485, 1375, 1339, 1095, 857, 731, 699, 687 cm^{-1}.

^{1}H NMR (400 MHz, dmso-d_6) δ = 10.29 (s, 1H), 8.34 (d, *J*=9.2, 2H), 7.91 (d, *J*=9.2, 2H), 7.80 (dd, *J*=8.6, 2.3, 1H), 7.42 – 7.24 (m, 7H), 5.36 (s, 1H), 3.72 (s, 1H), 3.50 (d, *J*=16.4, 1H), 3.34 (d, *J*=16.6, 1H).

^{13}C NMR (101 MHz, dmso-d_6) δ = 174.50, 155.65, 148.53, 147.68, 142.53, 141.99, 134.64, 128.83, 128.68, 127.77, 126.54, 125.45, 123.65, 122.30, 121.70, 62.47, 51.21.

HRMS (ESI, negative): calc. for $C_{21}H_{16}N_5O_3$ $(M)^-$: 386.1259; found: 386.1256.

pBZ1.4

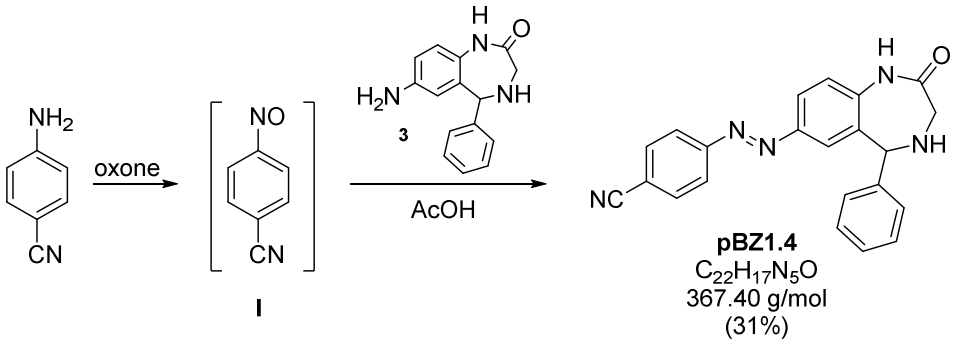

Following general procedure I. 4-Aminobenzonitrile (25 mg, 0.21 mmol, 1.5 eq.) in 1 mL dichloromethane was treated with Oxone® (128 mg, 0.42 mmol, 3 eq.) in 4 mL water. The biphasic mixture was stirred for 9 h at room temperature and another eq. Oxone® and 1 mL dichloromethane was added.

Resulting crude nitroso compound was dissolved in 1 mL acetic acid and **3** (40 mg, 0.14 mmol, 1 eq.) in 2.5 mL acetic acid was added. Aqueous work up und purification (HPLC: method B) yielded 15 mg (31%) of **pBZ1.4** as an orange solid.

HPLC (C-18, analytical HPLC, method A) Rt = 28.2 min

TLC (silica; 10% MeOH, 90% DCM) R_f = 0.63 (UV)

mp = 250-253 °C

λ_{max} = 362 nm

IR (FT, ATR): 3194, 3061, 2922, 2224, 1652, 1588, 1486, 1404, 1376, 1321, 1178, 1095, 844, 737, 670 cm^{-1}.

^{1}H NMR (400 MHz, dmso-d_6) δ = 10.27 (s, 1H), 7.97 (d, *J*=8.8, 2H), 7.84 (d, *J*=8.8, 2H), 7.78 (dd, *J*=8.6, 2.3, 1H), 7.39 – 7.24 (m, 7H), 5.35 (s, 1H), 3.71 (s, 1H), 3.41 (dd, *J*=59.9, 11.6, 2H).

^{13}C NMR (101 MHz, dmso-d_6) δ = 174.46, 154.46, 147.61, 142.32, 141.99, 134.58, 134.16, 128.82, 128.67, 127.75, 126.39, 123.37, 122.18, 121.67, 118.86, 113.17, 62.47, 51.15.

HRMS (ESI, negative): calc. for $C_{22}H_{16}N_5O$ $(M)^-$: 366.1360; found: 366.1359.

Fmoc-protected Benzophenone 13 (isolated intermediate)

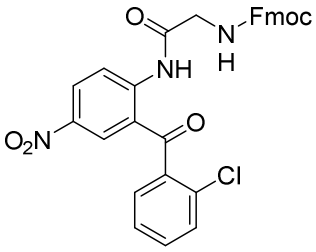

13
$C_{30}H_{22}ClN_3O_6$
555,97 g/mol

^{1}H NMR (400 MHz, $CDCl_3$) δ = 12.26 (s, 1H), 9.02 (d, *J*=9.3, 1H), 8.42 (dd, *J*=9.4, 2.4, 1H), 8.25 (d, *J*=2.6, 1H), 7.74 (d, *J*=7.5, 2H), 7.61 (d, *J*=7.3, 2H), 7.50 (t, *J*=7.5, 2H), 7.36 (ddd, *J*=31.6, 16.3, 7.5, 4H), 7.22 (t, *J*=7.4, 2H), 5.60 (s, 1H), 4.48 (d, *J*=6.9, 2H), 4.26 (t, *J*=6.9, 1H), 4.18 (d, *J*=5.7, 2H).

^{13}C NMR (101 MHz, $CDCl_3$) δ = 197.89, 169.24, 156.67, 145.78, 143.69, 141.93, 141.24, 137.06, 132.28, 130.98, 130.50, 130.27, 129.65, 128.89, 127.68, 127.22, 127.00, 125.08, 121.28, 121.03, 119.93, 67.73, 47.06, 45.92.

Primary Amine 14 (isolated intermediate)

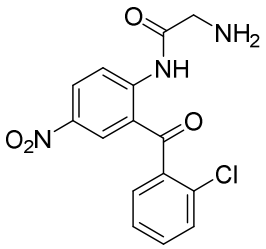

14
$C_{15}H_{12}ClN_3O_4$
333,73 g/mol

TLC (silica; 10% MeOH, 90% DCM) R_f = 0.67 (UV, ninhydrin)

mp = 191-193 °C

IR (FT, ATR): 3450, 3318, 3193, 1676, 1624, 1609, 1576, 1502, 1331, 1287, 1267, 1251, 1228, 1158, 1116, 765, 751 cm^{-1}.

^{1}H-NMR (400 MHz, dmso-d_6): *δ* 9.87 (t, ^3J = 4.9 Hz, 1H), 8.24 (dd, ^3J = 9.5, ^4J = 2.7 Hz, 1H), 7.93 (d, ^4J = 2.7 Hz, 1H), 7.66 (s, 1H), 7.63 (dt, ^3J = 8.0, ^4J = 1.1 Hz, 1H), 7.62-7.55 (m, 1H), 7.53-7.51 (m, 2H), 7.37 (s, 1H), 6.80 (d, ^3J = 9.6 Hz, 1H), 4.10 (d, ^3J = 5.0 Hz, 2H).

^{13}C-NMR (100 MHz, dmso-d_6): *δ* 196.0, 169.6, 154.5, 138.4, 135.3, 132.2, 131.8, 130.8, 130.3, 129.8, 129.3, 128.0, 115.4, 114.0, 45.7 ppm.

HRMS (ESI, negative): calc. for $C_{15}H_{12}Cl_2N_3O_4$ $(M+Cl)^-$: 368.0205; found: 368.0210.

Experimental Procedures 2nd Generation pBZs

Benzylalcohol 4

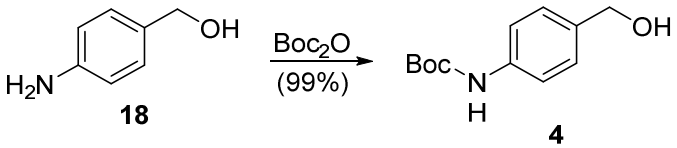

18 **4**

$C_{12}H_{17}NO_3$
223,27 g/mol

The title compound was synthesized as described in the patent literature.[9]

^{1}H NMR (400 MHz, dmso-d_6) δ = 9.25 (s, 1H), 7.36 (d, *J*=8.5, 2H), 7.15 (d, *J*=8.7, 2H), 5.03 (t, *J*=5.7, 1H), 4.38 (d, *J*=5.7, 2H), 1.45 (s, 9H).

^{13}C NMR (75 MHz, $CDCl_3$) δ = 158.00, 143.31, 141.29, 132.10, 84.06, 67.84, 33.36.

TLC (SiO_2, 50% EtOAc, 50% hexanes), *Rf* = 0.54 (UV).

HRMS (EI) calcd for $C_{12}H_{17}NO_3$ $[M]^+$: 223.1208; found: 223.1196.

Boc-protected amine 5[10]

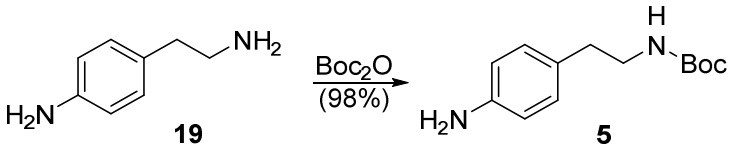

19 **5**

$C_{13}H_{20}N_2O_2$
236,31

[9] WO2008034124 (A2) — 2008-03-20 "Targeted polymeric prodrugs containing multifunctional linkers".

[10] US2003220372 (A1) — 2003-11-27. „Imidazole compounds as anti-inflammatory and analgesic agents".

Benzylalcohol 6

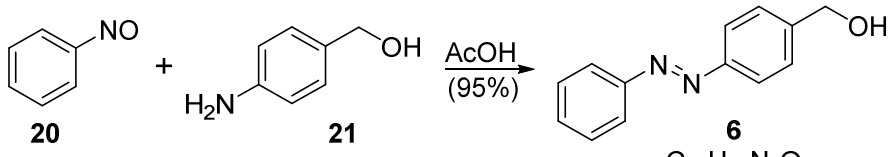

20 **21** **6**

$C_{13}H_{12}N_2O$
212,25 g/mol

Nitrosobenzene **20** (478 mg, 4.47 mmol, 1.1 eq), aniline **21** (500 mg, 4.06 mmol, 1.0 eq) and acetic acid (1.16 mL, 20.3 mmol, 5 eq) were mixed in 50 mL DCM and stirred under N_2-atm over night. The orange reaction solution was concentrated to approximately 10 mL under reduced pressure, diluted with 50 mL EtOAc and extracted with 30 mL aliquots of 1-M-NaOH(aq), 1-M-HCl(aq) and brine. The EtOAc layer was separated, dried over Na_2SO_4 and concentrated using rotary evaporation. The resulting crude orange solid was purified using silica gel chromatography (gradient, 0 to 50% EtOAc in hexanes) affording **6** as an amorphous orange solid (817 mg, 3.85 mmol, 95% yield, corresponding *m*-compound from 3-amino benzyl alcohol).

Analytics matched those reported in the literature.[11]

^{1}H NMR (599 MHz, $CDCl_3$) δ = 7.95 – 7.90 (m, 4H), 7.56 – 7.46 (m, 5H), 4.79 (s, 2H).

^{13}C NMR (151 MHz, $CDCl_3$) δ = 152.62, 152.10, 143.79, 130.98, 129.07, 127.41, 123.06, 122.82, 64.88.

TLC (SiO_2, 50% EtOAc, 50% hexanes), *Rf* = 0.57 (UV).

HRMS (EI) calcd for $C_{13}H_{12}N_2O$ $[M]^+$: 212.0950; found: 212.0946.

[11] Fatás, P., E. Longo, et al. "Bis(azobenzene)-Based Photoswitchable, Prochiral, Cα-Tetrasubstituted α-Amino Acids for Nanomaterials Applications." Chemistry – A European Journal **17**(45): 12606-12611.

Benzylalcohol 7

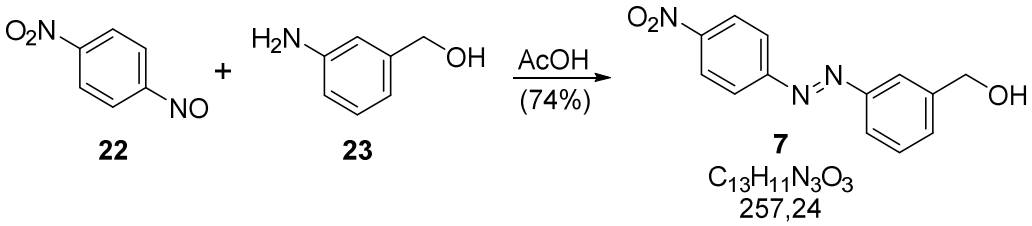

22 **23** **7**

$C_{13}H_{11}N_3O_3$
257,24

Nitrosobenzene **22** (1.85 g, 12.2 mmol, 1.5 eq)[12] was dissolved in 10 mL DCM and treated with AcOH (4.65 mL, 81.2 mmol, 10.0 eq), followed by 3-aminobenzyl alcohol **23** (1.0 g, 8.1 mmol, 1.0 eq). The reaction mixture was allowed to stir at rt under N_2-atm over night and purified using silica gel flash chromatography (gradient, 1 to 5% MeOH in DCM) yielding **7** as a red powder (1.54 g, 6.0 mmol, 74% yield).

TLC (SiO_2, 10% MeOH, 90% DCM), *Rf* = 0.69 (UV).

HRMS (EI) calcd for $C_{13}H_{11}N_3O_3$ $[M]^+$: 257.0800; found: 257.0796.

^{1}H NMR (300 MHz, $CDCl_3$) δ = 8.38 (d, *J*=8.9, 2H), 8.03 (d, *J*=8.9, 2H), 7.97 (s, 1H), 7.95 – 7.84 (m, 1H), 7.55 (d, *J*=5.4, 2H), 4.83 (s, 2H), 1.90 (s, 1H).

^{13}C NMR (75 MHz, $CDCl_3$) δ = 155.62, 152.58, 148.74, 142.31, 130.63, 129.47, 124.72, 123.42, 123.14, 121.05, 64.71.

[12] Prepared as described before in this report.

Benzylalcohol 9

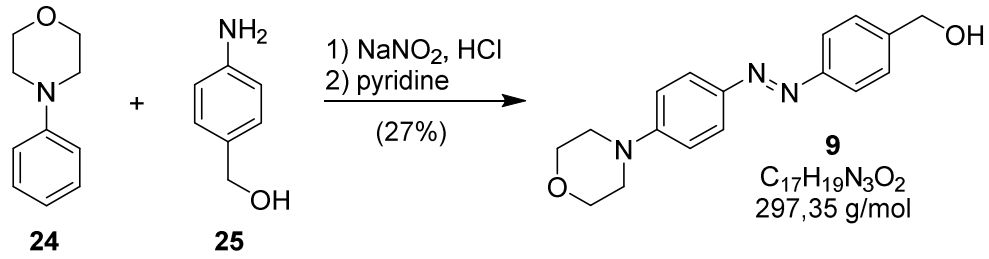

24 25

4-Aminobenzyl alcohol **25** (1000 mg, 8.12 mmol, 1.2 eq) was dissolved in water (15 ml) and HCl conc. (2 ml, 24.00 mmol, 3.6 eq) was added. The solution was cooled to 0 °C and after 10 min, sodium nitrate (630 mg, 9.14 mmol, 1.4 eq) was added carefully as a solution in water (5 ml). After stirring for 45 min at 0 °C, the diazonium salt solution was added slowly to a solution of 4-phenylmorpholine **24** (1000 mg, 8.12 mmol, 1.2 eq) in methanol (125 ml) and pyridine (2.74 ml, 33.80 mmol, 5 eq). The resulting reaction solution was stirred for 5 h at 0 °C and allowed to heated to room temperature over night. The solvent was removed using rotary evaporation. Purification using flash column chromatography (silica, gradient 1-3% MeOH in $CHCl_3$) yielded **9** as a red amorphous solid (540 mg, 1.82 mmol, 27%).

TLC (SiO_2, 50% EtOAc in hexanes), R_f = 0.46 (UV).

^{1}H NMR (599 MHz, $CDCl_3$) δ = 7.88 (d, *J = 9.1*, 2H), 7.85 (d, *J = 8.4*, 2H), 7.47 (d, *J = 8.6*, 2H), 6.97 (d, *J = 9.1*, 2H), 4.76 (s, 2H), 3.89 – 3.86 (m, 4H), 3.33 – 3.29 (m, 4H).

^{13}C NMR (151 MHz, $CDCl_3$) δ = 153.1, 152.4, 145.7, 142.7, 127.4, 124.6, 122.6, 114.4, 66.6, 65.0, 48.1.

IR (FT, ATR) : 3462, 2966, 2871, 2844, 1599, 1504, 1444, 1378, 1343, 1303, 1267, 1230, 1156, 1114, 1048, 1024, 924, 829 cm^{-1}.

HRMS (ESI, positiv): calcd. for $C_{17}H_{20}N_3O_2$ $(M+H)^+$:298.1556; found: 298.1548.

Benzylbromide 8

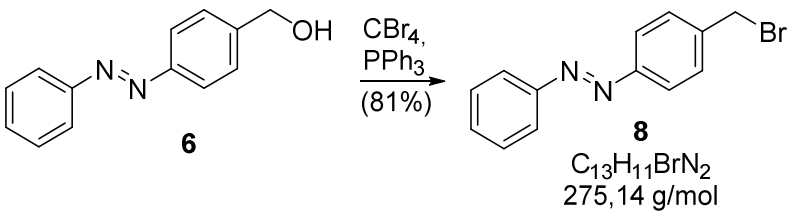

Carbontetrabromide (1.56 g, 4.71 mmol, 2.0 eq) and triphenylphosphin (1.24 mg, 4.71 mmol, 2.0 eq) were dissolved in 10 mL DCM before benzylalcohol **6** (500 mg, 2.36 mmol, 1.0 eq) was added. After stirring for 2 h under N2-atm, the reaction was diluted with 50 mL EtOAc and and extracted with 30 mL aliquots of 1-M-$HCl_{(aq)}$, 1-M-$NaOH_{(aq)}$ and brine. The EtOAc layer was separated, dried over Na_2SO_4 and concentrated using rotary evaporation. The resulting crude orange solid was purified using automated medium pressure chromatography (Biotage, 10 g SiO_2-column, gradient 0 to 10% EtOAc in hexanes) affording **8** as an amorphous orange solid (512 mg, 3.85 mmol, 81% yield, *m*-compound analogously).

Analytical data match those reported in the literature.[13]

^{1}H NMR (599 MHz, $CDCl_3$) δ = 7.96 – 7.87 (m, 4H), 7.57 – 7.46 (m, 5H), 4.56 (s, 2H).

TLC (SiO_2, 10% EtOAc, 90% hexanes), *Rf* = 0.55 (UV).

HRMS (EI) calcd for $C_{13}H_{11Br}N_2$ $[M]^+$: 274.0106; found: 274.0106.

[13] Yu, G., C. Han, et al. "Pillar[6]arene-Based Photoresponsive Hostâ€“Guest Complexation." Journal of the American Chemical Society **134**(20): 8711-8717.

Benzylbromide 10

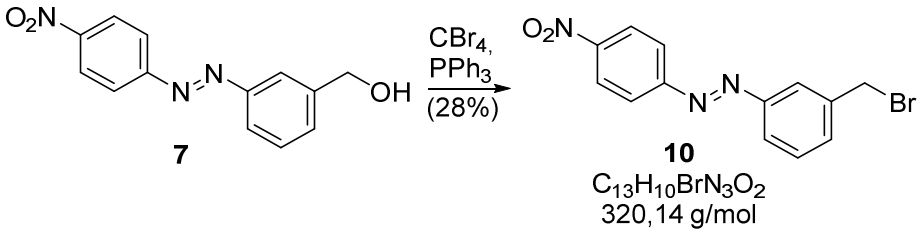

7 **10**

$C_{13}H_{10}BrN_3O_2$

320,14 g/mol

Benzylbromide **10** was prepared analogously to benzylbromide **8** *via* Appel reaction.

^{1}H NMR (599 MHz, $CDCl_3$) δ = 8.39 (d, *J*=8.6, 2H), 8.04 (d, *J*=8.6, 2H), 8.00 (s, 1H), 7.97 – 7.89 (m, 1H), 7.62 – 7.50 (m, 2H), 4.70 (s, 0H), 4.59 (s, 2H).

^{13}C NMR (151 MHz, $CDCl_3$) δ = 155.51, 152.54, 148.85, 139.21, 132.71, 129.79, 124.75, 123.84, 123.50, 123.35, 32.42.

TLC (SiO_2, 20% EtOAc, 80% hexanes), *Rf* = 0.59 (UV).

Benzylbromide 11

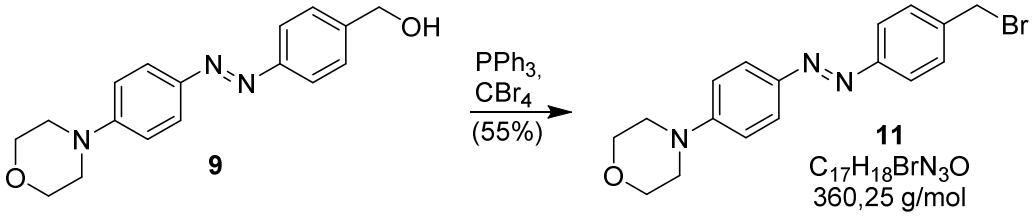

9 **11**

$C_{17}H_{18}BrN_3O$

360,25 g/mol

9 (200 mg, 0.61 mmol, 1.0 eq) was dissolved in THF (8 ml) and treated with carbon tetrabromide (401 mg, 1.21 mmol, 2.0 eq) and triphenylphosphine (318 mg, 1.21 mmol, 2.0 eq) was added. The Solution was stirred over night and the solvent was removed under reduced pressure. Purification using flash column chromatography (silica, gradient 30-40% EtOAc in hexanes) yielded **11** as dark powder (120 mg, 0.33 mmol, 55%).

TLC (SiO_2, 30% EtOAc in hexanes), R_f = 0.38 (UV).

^{1}H NMR (200 MHz, $CDCl_3$) δ = 7.90 (d, *J = 9.1*, 2H), 7.83 (d, *J = 8.4*, 2H), 7.50 (d, *J = 8.3*, 2H), 6.98 (d, *J = 9.2*, 2H), 4.55 (s, 2H), 3.97 – 3.80 (m, 4H), 3.39 – 3.26 (m, 4H).

^{13}C NMR (101 MHz, $CDCl_3$) δ 153.0, 152.5, 145.7, 139.4, 129.8, 124.9, 122.8, 114.6, 66.5, 48.2, 33.1.

IR (FT, ATR) : 2955, 2855, 2834, 1599, 1568, 1507, 1446, 1404, 1378, 1346, 1304, 1264, 1233, 1159, 1143, 1119, 1069, 1050, 924, 848, 827, 731 cm^{-1}.

HRMS (ESI, positiv): calcd. for $C_{17}H_{19}BrN_3O$ $(M+H)^+$: 360.0711; found: 360.0706.

Toluene 15

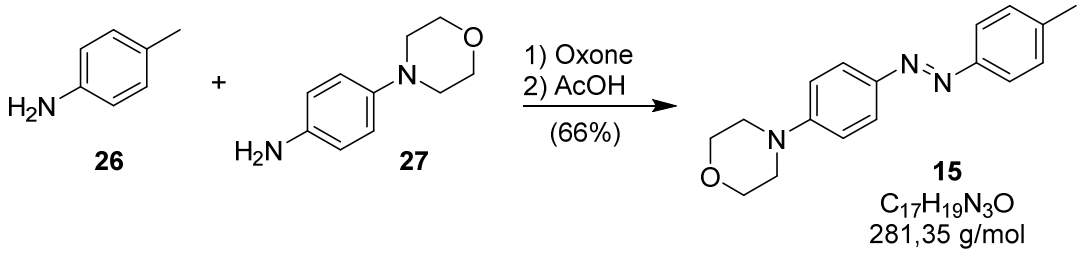

p-Aminotoluene **26** (1000 mg, 9.33 mmol, 1.5 eq) was dissolved in DCM (25 ml) and Oxone® (6120 mg, 9.95 mmol, 1.6 eq) was slowly added as an aqueous solution (100 ml) under N_2-atmosphere. The dispersion was stirred vigorously for 3 h before layers were separated. The aqueous layer was washed two more times with DCM (12 ml). Combined organic layers were washed with 1-M-$HCl_{(aq)}$ (2×15 ml), saturated $NaHCO_{3(aq)}$ (2×15 ml) and brine (2×25 ml). The organic phase was dried over Na_2SO_4 and concentrated to approximately 10 mL under reduced pressure and 4-morpholinoaniline **27** (1100 mg, 6.22 mmol, 1.0 eq) was added followed by acetic acid (1.8 ml, 31.10 mmol, 5.0 eq). After stirring over night, the red reaction solution was washed with 5-M-$NaOH_{(aq)}$ (5 ml), saturated-$NaHCO_{3(aq)}$ (2×20 ml), brine (2×20 ml) and dried over Na_2SO_4. The solvent was removed under reduced pressure. Purification using flash column chromatography (silica, gradient 30-50% EtOAc in hexanes) yielded **15** as a red powder (1160 mg, 4.1 mmol, 66%).

TLC (SiO_2, 50% EtOAc, 50% Hexanes), R_f = 0.5 (UV).

^{1}H NMR (300 MHz, $CDCl_3$) δ = 7.88 (d, *J=9.2*, 1H), 7.78 (d, *J=8.3*, 1H), 7.29 (d, *J=8.0*, 1H), 6.97 (d, *J=9.2*, 1H), 3.92 – 3.82 (m, *J=5.7*, *4.1*, 2H), 3.36 – 3.24 (m, 2H), 2.42 (s, 2H).

^{13}C NMR (75 MHz, $CDCl_3$) δ = 152.9, 151.0, 145.8, 140.4, 129.6, 124.4, 122.4, 114.5, 66.7, 48.2, 21.4.

IR (FT, ATR) : 3040, 2966, 2897, 2855, 2834, 1597, 1568, 1504, 1449, 1415, 1375, 1346, 1307, 1267, 1233, 1156, 1124, 1069, 1053, 927, 827, 731, 708 cm^{-1}.

HRMS (ESI, positiv): calcd. for $C_{17}H_{20}N_3O$ $(M+H)^+$: 282.1606; found: 282.1597.

Toluene 16

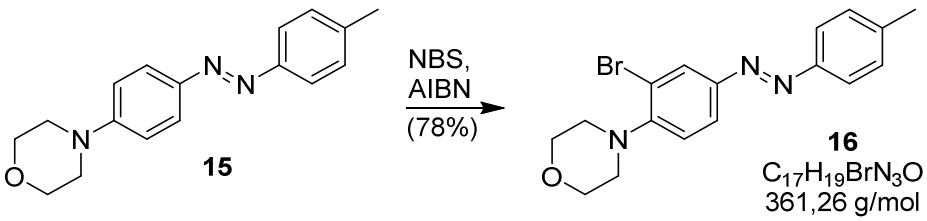

15 (50 mg, 0.178 mmol, 1.0 eq), NBS (35 mg, 0.195 mmol, 1.1 eq) and AIBN (3 mg, 0.018 mmol, 0.1 eq) were dissolved in CCl_4 (6.5 ml) and heated to reflux over night. EtOAc (30 ml) was added and the organic resulting solution was washed with 1-M-NaOH (8 ml), saturated $NaHCO_{3(aq)}$ (2 × 7 ml) and brine (2 × 7 ml). The organic phase was seperated, dried over Na_2SO_4 and concentrated under reduced pressure. Quick flash column chromatography (silica, gradient 10-50% EtOAc in hexanes) followed by a second purification using flash column chromatography (silica, gradient 5-15% EtOAc in hexanes) yielded **16** as a dark powder (50 mg, 0.139 mmol, 78%).

TLC (SiO_2, 30% EtOAc, 70% hexanes), R_f = 0.6 (UV)

^{1}H NMR (300 MHz, $CDCl_3$) δ = 8.16 (d, *J = 2.2*, 1H), 7.87 (dd, *J = 8.5, 2.3*, 1H), 7.80 (d, *J = 8.2*, 2H), 7.35 – 7.25 (m, 2H), 7.13 (d, *J = 8.5*, 1H), 3.95 – 3.87 (m, 4H), 3.20 – 3.10 (m, 4H), 2.43 (s, 3H).

^{13}C NMR (75 MHz, $CDCl_3$) δ = 152.2, 150.6, 148.8, 141.6, 129.7, 127.1, 124.5, 122.8, 120.3, 119.7, 67.0, 51.9, 21.5.

IR (FT, ATR) : 3040, 2950, 2913, 2844, 2823, 1602, 1583, 1557, 1475, 1446, 1391, 1370, 1333, 1296, 1230, 1206, 1114, 1067, 1027, 937, 919, 890, 824, 876 cm^{-1}.

HRMS (ESI, positiv): calcd. for $C_{17}H_{20}BrN_3O$ $(M+H)^+$: 360.0711; found: 360.0684.

General Procedure II: N-alkylation of Clonazepam using benzyl bromides

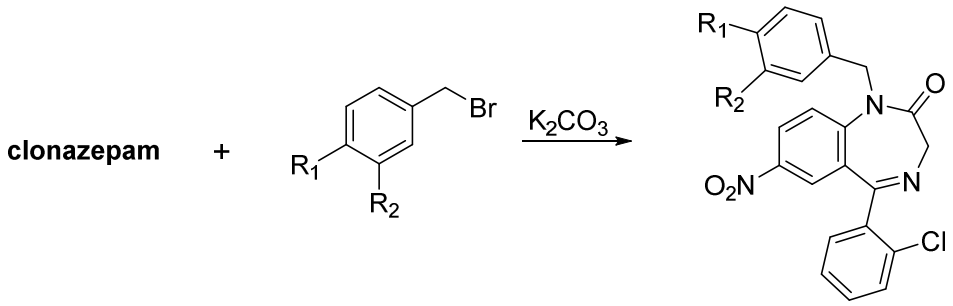

Clonazepam (50.0 mg, 0.16 mmol, 1.0 eq) was dissolved in 1 mL dry DMF, treated with K_2CO_3 (43.8 mg, 0.32 mmol, 2.0 eq) and cooled to 0 °C under N_2-atm. The corresponding benzylbromide (0.19 mmol, 1.2 eq) dissolved in 0.6 mL dry DMF was added and the reaction mixture was allowed to stir for 45 min. The reaction solution was diluted with 10 mL EA and extracted with 10% $NaCl_{(aq)}$, saturated $NH_4Cl_{(aq)}$, saturated $NaHCO_{3(aq)}$ and brine. The organic layer was dried using Na_2SO_4, concentrated *in vacuo* and purified using MPLC (Biotage,10 g SiO_2-column, gradient 35% to 100% EtOAc in hexanes)[14] yielding the *N*-alkylated product in 95 – 98% yield.

Table 1. N-Benzylated **clonazepam** derivatives derived from benzyl chlorides.

R_1	R_2	product	yield
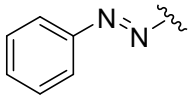	H	**pBZ2.1**	98%
H	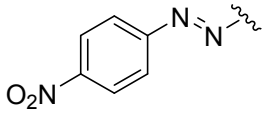	**pBZ2.3**	96%
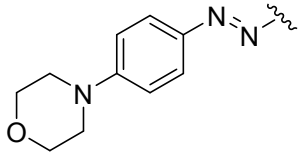	H	**pBZ2.4**	96%
H	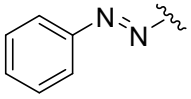	**pBZ2.5**	86%
SCN-	H	**North-NCS**	95%

[14] A mixture of MeOH/DCM, EA/DCM can also be used as a mobile phase for silica gel chromatography with equal success. Additionally, reverse phase MPLC (4g C-18, gradient 30% to 90% MeCN in H2O) is possible.

pBZ2.1

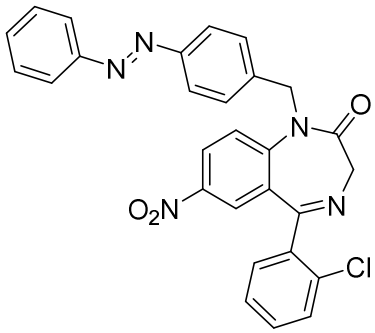

pBZ2.1
$C_{28}H_{20}ClN_5O_3$
509,94 g/mol

^{1}H NMR (400 MHz, dmso-d_6) δ = 8.35 (ddd, *J*=29.5, 9.2, 2.8, 1H), 7.96 – 7.73 (m, 4H), 7.66 (dd, *J*=8.2, 2.7, 1H), 7.63 – 7.40 (m, 8H), 7.27 – 7.03 (m, 1H), 6.76 (ddd, *J*=8.5, 5.2, 3.6, 1H), 5.27 (dt, *J*=77.3, 16.0, 2H), 4.77 (dd, *J*=23.2, 11.1, 1H), 4.05 (dd, *J*=27.8, 10.9, 1H).

^{13}C NMR (101 MHz, dmso-d_6) δ = 168.35, 168.33, 168.30, 154.01, 153.18, 152.30, 151.63, 146.93, 146.82, 143.14, 143.03, 140.66, 137.54, 137.51, 135.93, 132.31, 132.24, 132.17, 132.05, 130.56, 130.52, 130.34, 129.93, 129.25, 128.69, 127.98, 127.53, 126.70, 124.29, 124.23, 123.17, 122.99, 120.60, 120.18, 57.23, 49.58.

TLC (SiO_2, 60% EtOAc, 40% hexanes), *Rf* = 0.54 (UV).

HRMS (ESI) calcd for $C_{12}H_{17}NO_3$ $[M]^+$: 510.1333; found:510.1330.

pBZ2.3

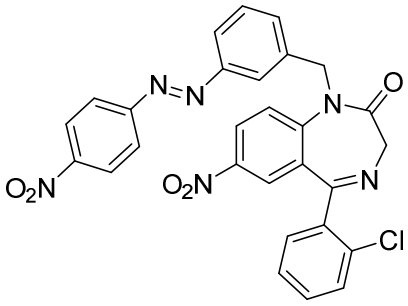

pBZ2.3
$C_{28}H_{19}ClN_6O_5$
554,94

^{1}H NMR (599 MHz, $CDCl_3$) δ = 8.35 (d, *J*=8.9, 2H), 8.30 (dd, *J*=9.1, 2.7, 1H), 7.96 (d, *J*=8.9, 2H), 7.90 (d, *J*=2.7, 1H), 7.89 – 7.86 (m, 1H), 7.84 (s, 1H), 7.63 – 7.27 (m, 7H), 5.51 (d, *J*=15.6, 1H), 5.23 (d, *J*=15.6, 1H), 5.10 (d, *J*=10.7, 1H), 3.97 (d, *J*=10.7, 1H).

^{13}C NMR (151 MHz, $CDCl_3$) δ = 168.71, 168.23, 155.43, 152.58, 148.81, 146.65, 143.57, 137.54, 136.91, 132.93, 131.79, 131.69, 131.47, 131.08, 130.34, 129.91, 127.35, 126.08, 124.78, 124.68, 123.51, 122.98, 122.59, 122.44, 56.89, 50.43.

TLC (SiO_2, 60% EtOAc, 40% Hex), *Rf* = 0.42 (UV).

HRMS (ESI) calcd for $[M+H]^+$: 555.1184; found: 555.1177.

pBZ2.4

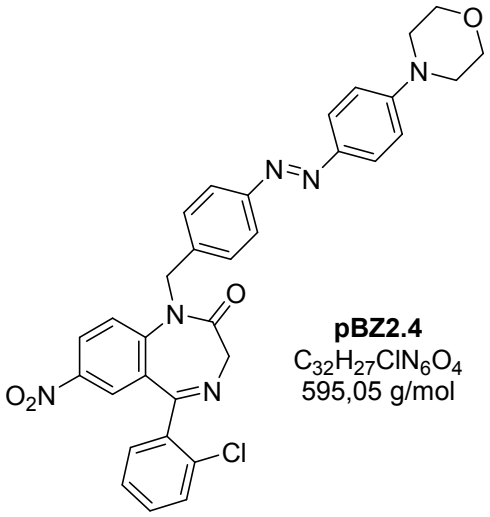

pBZ2.4
$C_{32}H_{27}ClN_6O_4$
595,05 g/mol

TLC (SiO_2,10% MeOH, 90% DCM), R_f = 0.64 (UV).

^{1}H NMR (599 MHz, $CDCl_3$) δ = 8.22 (dd, *J = 9.1, 2.7*, 1H), 7.88 – 7.82 (m, 3H), 7.77 (d, *J = 8.4*, 2H), 7.51 (d, *J = 9.2*, 2H), 7.42 – 7.27 (m, 5H), 6.96 – 6.92 (m, 2H), 5.33 (d, *J = 15.8*, 1H), 5.25 – 5.15 (m, 1H), 5.06 (d, *J = 10.8*, 1H), 3.93 (d, *J = 11.0*, 1H), 3.87 – 3.83 (m, 4H), 3.32 – 3.28 (m, 4H).

^{13}C NMR (151 MHz, $CDCl_3$) δ = 168.7, 168.1, 153.2, 152.5, 146.8, 145.5, 143.4, 137.8, 137.0, 132.9, 131.7, 131.6, 130.9, 130.3, 128.3, 127.3, 126.0, 124.7, 124.7, 124.6, 122.9, 122.6, 114.3, 66.6, 56.9, 50.6, 48.0.

IR (FT, ATR) : 3040, 2960, 2844, 1684, 1597, 1573, 1517, 1504, 1481, 1449, 1417, 1378, 1338, 1262, 1227, 1156, 1140, 1109, 1067, 1046, 1019, 985, 924, 885, 827, 732, 700 cm^{-1}.

HRMS (ESI, positiv): calcd. for $C_{32}H_{28}ClN_6O_4$ $(M+H)^+$: 595.1861; found: 595.1849.

pBZ2.5

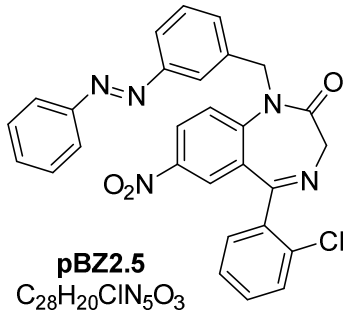

pBZ2.5
$C_{28}H_{20}ClN_5O_3$
510,0 g/mol

^{1}H NMR (400 MHz, $CDCl_3$) δ = 8.28 (dd, *J*=9.1, 2.7, 1H), 7.91 (d, *J*=2.6, 1H), 7.89 (dd, *J*=8.0, 1.7, 2H), 7.87 – 7.79 (m, *J*=15.2, 7.3, 2H), 7.60 (d, *J*=9.1, 1H), 7.58 – 7.45 (m, 5H), 7.43 – 7.31 (m, 4H), 5.46 (d, *J*=15.6, 1H), 5.27 (d, *J*=15.6, 1H), 5.11 (d, *J*=10.6, 1H), 3.99 (d, *J*=10.7, 1H).

^{13}C NMR (101 MHz, $CDCl_3$) δ = 168.74, 168.17, 152.87, 152.45, 146.78, 143.48, 137.28, 136.99, 132.97, 131.72, 131.62, 131.29, 130.97, 130.36, 130.12, 129.78, 129.11, 127.32, 126.10, 124.77, 122.95, 122.67, 122.23, 122.10, 56.93, 50.56.

HRMS (ESI, positiv): calcd. for $C_{28}H_{21}ClN_5O_3$ $(M+H)^+$: 510.1327; found: 510.1326.

North-NCS

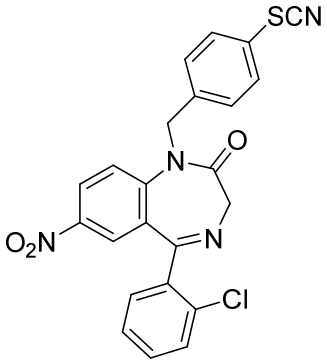

North-NCS
$C_{23}H_{15}ClN_4O_3S$
462,91 g/mol

TLC (SiO_2, 10% MeOH, 90% DCM), R_f = 0.46 (UV).

^{1}H NMR (400 MHz, $CDCl_3$) δ = 8.25 (d, *J = 2.7*, 1H), 7.87 (d, *J = 2.4*, 1H), 7.55 (dd, *J = 7.2*, *1.9*, 1H), 7.50 (d, *J = 9.1*, 1H), 7.46 – 7.38 (m, 2H), 7.33 (dd, *J = 7.5, 1.4*, 1H), 7.23 (d*, J = 8.7*, 2H), 7.13 (d, *J = 8.7*, 2H), 5.35 (d, *J = 15.6*, 1H), 5.07 (d, *J = 15.8*, 1H), 5.02 (d, *J = 10.8*, 1H), 3.91 (d*, J = 10.8*, 1H).

^{13}C NMR (101 MHz, $CDCl_3$) δ = 168.7, 168.1, 146.5, 143.5, 136.9, 135.4, 132.9, 131.9, 131.7, 131.0, 130.9, 130.4, 129.0, 127.4, 126.2, 126.1, 124.7, 122.5, 56.8, 50.2.

IR (FT, ATR) : 3060, 2971, 2850, 2179, 2079, 1678, 1604, 1575, 1520, 1501, 1480, 1433, 1417, 1338, 1311, 1282, 1259, 1217, 1180, 1162, 1098, 1072, 1053, 1017, 982, 929, 908, 882, 837, 779, 729 cm^{-1}.

HRMS (ESI, positiv): calcd. for $C_{23}H_{16}ClN_4O_3S$ $(M+H)^+$: 463.0632; found: 463.0621.

Benzodiazepine 12

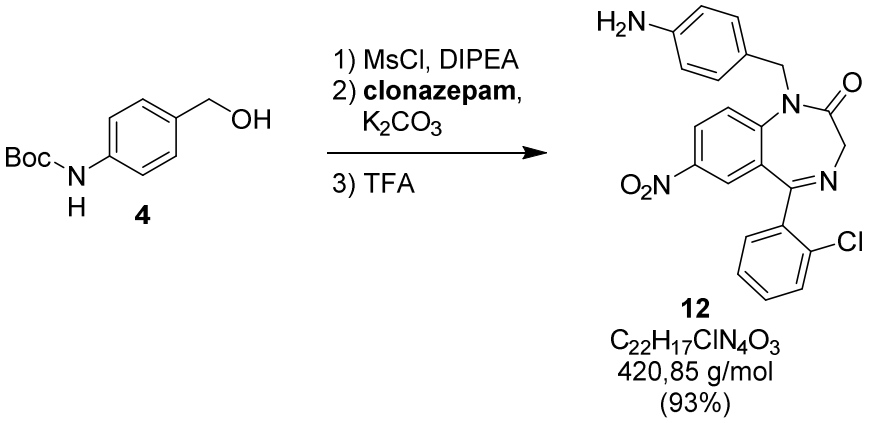

Alcohol **4** (46 mg, 0.21 mmol, 1.3 eq) was dissolved in 1 mL DCM, treated with DIPEA (72 µL, 0.41 mmol, 2.6 eq) and cooled to 0 °C under N_2-atm before MsCl (25 µL, 0.32 mmol, 2.0 eq) was added. After 15 min, the reaction mixture was allowed to warm to rt over the course of two hours. 5 mL EtOAc were added and the organic phase was extracted with 2 mL portions of saturated $NH_4Cl_{(aq)}$, $NaHCO_{3(aq)}$ and brine. The organic layer was separated, dried over Na_2SO_4 and concentrated *under vacuo*.

Clonazepam (50 mg, 0.16 mmol, 1.0 eq) was dissolved in 1 mL anhydrous DMF, treated with K_2CO_3 (57 mg, 0.41 mmol, 2.6 eq) and cooled to 0 °C under N_2-atm before the above described mesylate was added as a solution in 0.5 mL anhydrous DMF. After reacting for 1 h at 0 °C, the reaction suspension was diluted with 20 mL EtOAc and extracted with 5 mL portions of saturated NH_4Cl(aq), $NaHCO_{3(aq)}$, 10% $NaCl_{(aq)}$ and brine. The organic layer was separated, dried over Na_2SO_4 and concentrated *under vacuo*. The crude Boc-protected material was redissolved in 1 mL anhydrous DCM and treated with 1 mL TFA for 10 min at rt. The red solution was diluted with EtOAc and extracted with conc. $NaHCO_{3(aq)}$. The organic layer was dried over Na_2SO_4 and concentrated *under vacuo*. The resulting orange crude was purified using MPLC (Biotage, 10 g SiO_2-column, gradient 20 to 100% EtOAc in hexanes) affording the title compound as an orange amorphous solid (62 mg, 0.147 mmol, 93% yield).

^{1}H NMR (400 MHz, dmso-d_6) δ = 8.33 (dd, *J*=9.2, 2.8, 1H), 7.93 (d, *J*=9.2, 1H), 7.61 (d, *J*=2.7, 1H), 7.53 – 7.35 (m, 4H), 6.84 (d, *J*=8.4, 2H), 6.39 (d, *J*=8.5, 2H), 5.32 (d, *J*=15.2, 1H), 4.87 (d, *J*=15.3, 1H), 4.73 (d, *J*=10.7, 1H), 3.94 (d, *J*=10.8, 1H).

^{13}C NMR (101 MHz, dmso-d_6) δ = 168.14, 167.96, 148.55, 147.00, 142.91, 137.60, 132.27, 132.11, 130.79, 130.24, 129.43, 127.77, 126.27, 124.70, 124.05, 123.67, 114.10, 57.30, 49.15.

TLC (SiO_2, 70% EtOAc, 30% hexanes), *Rf* = 0.50 (UV).

HRMS (EI) calcd for $C_{22}H_{17}ClN_4O_3$ $[M]^+$: 420.0989; found: 420.0982.

IR ν_{max}: 3448, 3360, 3218, 2856, 1678, 1608, 1517, 1342, 909, 730.

pBZ2.2

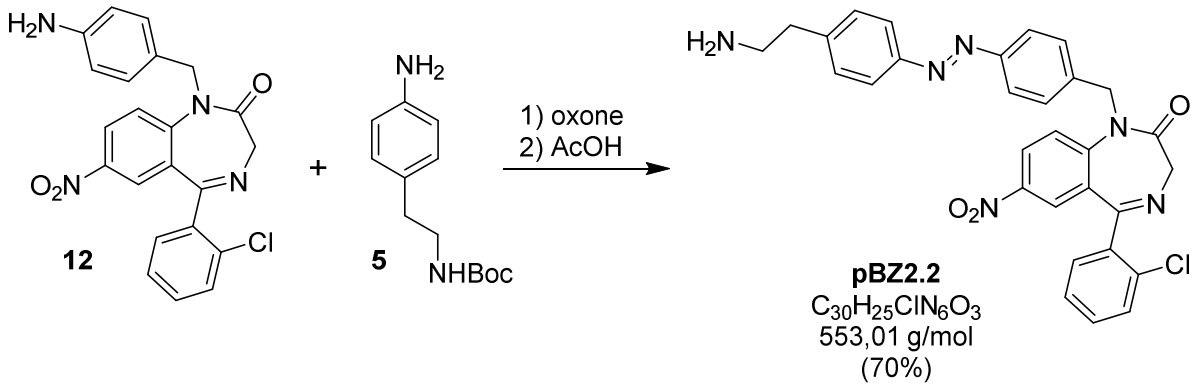

Step 1: Formation of nitrosobenzene

5 (500 mg, 2.1 mmol, 1.0 eq) was dissolved in 400 mL of a 1:1 H2O/DCM mixture and treated with oxone (2.6 g, 4.2 mmol, 2 eq). After stirring intensely for 5h, the green organic layer was filtered through a small plug of silica. The filtrate was concentrated (260 mg, 50% yield, crude) and immediately used for the next step.

Step 2: Mills coupling

12 (25 mg, 0.06 mmol, 1.0 eq) was dissolved in 1 mL DCM and freshly prepared nitroso species described above (30 mg, 0.12 mmol, 2.0 eq) was added, followed by AcOH. After reacting over night, the orange reaction solution was filtered through a small plug of silica and concentrated under reduced pressure. The resulting crude Boc-protected material was redissolved in 2 mL of 1:1 TFA/DCM and stirred for 15 min at rt. After dilution with EtOAc, TFA was removed by basic extraction with $NaHCO_{3(aq)}$. The EtOAc-layer was separated, dried using Na_2SO_4 and concentrated using rotary evaporation. The resulting crude material was purified using silica gel chromatography (gradient 2 to 10% MeOH in DCM, 1% TEA as additive) yielding **pBZ2.2** as an orange amorphous solid (23 mg, 0.04 mmol, 70% yield, 90% yield b.r.s.m.).

^{1}H NMR (599 MHz, $CDCl_3$) δ = 8.25 (ddd, *J*=15.3, 9.1, 2.7, 1H), 7.89 (dd, *J*=4.8, 2.6, 1H), 7.87 – 7.80 (m, 4H), 7.53 (t, *J*=6.2, 2H), 7.47 – 7.30 (m, 6H), 7.16 – 6.73 (m, 1H), 5.36 (d, *J*=15.6, 1H), 5.23 (d, *J*=15.8, 1H), 5.08 (d, *J*=10.7, 1H), 3.95 (d, *J*=10.6, 1H), 2.95 (dt, *J*=71.4, 7.0, 2H), 2.74 (dt, *J*=102.8, 6.9, 2H).

^{13}C NMR (151 MHz, $CDCl_3$) δ = 168.70, 168.09, 152.27, 151.18, 146.76, 143.66, 143.50, 138.69, 136.98, 132.94, 131.73, 131.59, 130.98, 130.36, 129.54, 128.36, 127.31, 125.99, 124.72, 123.28, 123.05, 122.56, 56.89, 50.59, 43.38, 40.04.

TLC (SiO2, 10% MeOH, 90% DCM + 1% TEA), *Rf* = 0.43 (UV, ninhydrine).

IR ν_{max}: 3368, 3057, 2961, 2926, 2856, 2226, 1685, 1608, 1522, 1342, 1261, 1102, 1020, 798, 730.

pBZ2.6

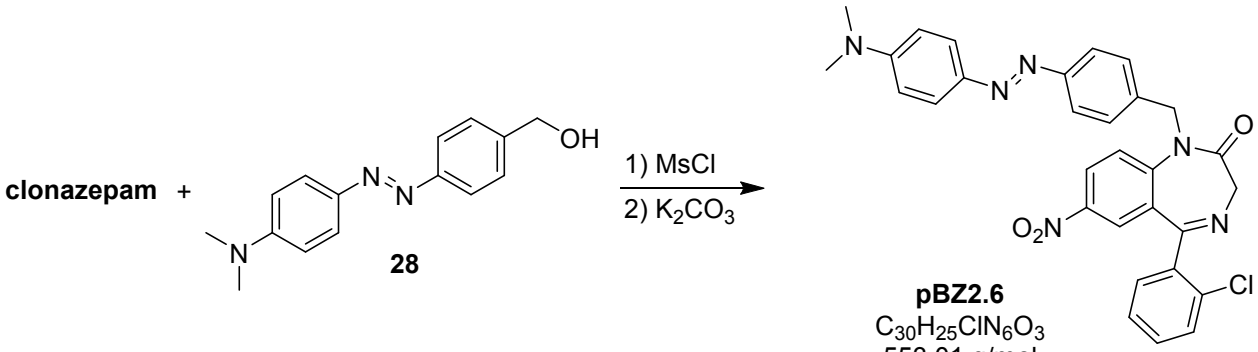

28 was synthesized from 4-amino-benzyl alcohol and *N,N*-dimethylaniline by standard diazotization conditions (see below). Consecutive mesylation and alkylation was performed in analogy to the synthesis of **12**. (0.24 mmol scale).

^{1}H NMR (599 MHz, $CDCl_3$) δ = 8.23 (dd, *J*=9.1, 2.7, 1H), 7.87 (d, *J*=2.7, 1H), 7.84 (dd, *J*=9.7, 2.5, 2H), 7.77 – 7.73 (m, 2H), 7.53 (t, *J*=6.2, 1H), 7.42 – 7.34 (m, 2H), 7.34 – 7.31 (m, 3H), 6.73 (d, *J*=9.3, 2H), 5.32 (d, *J*=15.6, 1H), 5.21 (d, *J*=15.5, 1H), 5.06 (d, *J*=10.6, 1H), 3.94 (d, *J*=10.6, 1H), 3.07 (s, 6H).

^{13}C NMR (151 MHz, $CDCl_3$) δ = 168.68, 168.07, 152.80, 152.53, 146.83, 143.51, 143.42, 137.04, 137.02, 132.96, 131.66, 131.55, 130.92, 130.34, 128.30, 127.26, 125.94, 125.07, 124.66, 122.68, 122.66, 111.46, 56.93, 50.59, 40.28.

HRMS (ESI, positiv): calcd. for $C_{30}H_{26}ClN_6O_3$ $(M+H)^+$: 553.1749; found: 553.1754.

Benzyl alcohol building blocks by diazotization

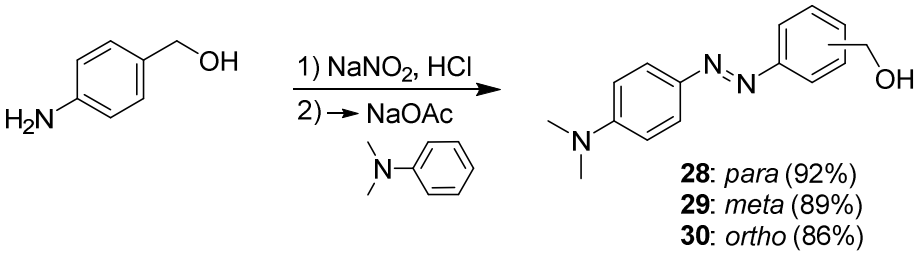

3-aminobenzyl aclohol (1 g, 8.1 mmol, 1 equiv.) was dissolved in 40 mL H_20 at 0 °C and concentrated aqueous HCl (2.4 mL, 24.4 mmol, 3 equiv.) was added. A solution of $NaNO_2$ (616 mg, 8.9 mmol, 1.1 eq) in 15 mL H_20 were added slowly (T < 5°C). After stirring at 0 °C for 30 min the yellow diazonium salt solution was added to a 0 °C solution of *N,N*-dimethyl aniline (1 mL, 8.1 mmol, 1 equiv.) and NaOAc (4 g, 48.7 mmol, 6 equiv.). After allowing tp warm to rt for 3 hours, the reaction mixture was diluted with 100 mL EtOAcl and washed sequentially with H_20 (1 x 50 mL), 1M NaOH (1 x 50 mL), and brine (1 x 50 mL). The combined organic phases were dried with Na_2SO_4 and concentrated *via* rotary evaporation.

Crude material was purified by flash column chromatography (silica gel, gradient 10% → 50% EtOAc in hexanes).

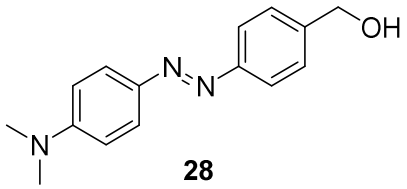

28

^{1}H NMR (300 MHz, $CDCl_3$) δ = 7.87 (dd, *J*=13.2, 8.8, 4H), 7.56 – 7.39 (m, 2H), 6.77 (d, *J*=9.2, 2H), 4.76 (s, 2H), 3.10 (s, 6H).

^{13}C NMR (75 MHz, $CDCl_3$) δ = 152.69, 152.44, 143.64, 142.02, 127.46, 124.97, 122.39, 111.52, 65.08, 40.31.

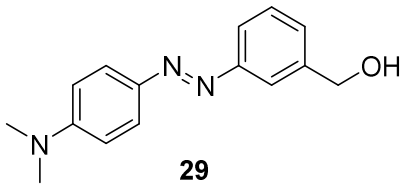

29

^{1}H NMR (400 MHz, $CDCl_3$) δ = 7.91 – 7.84 (m, 2H), 7.84 – 7.80 (m, 1H), 7.78 – 7.73 (m, 1H), 7.45 (dd, *J*=9.6, 5.8, 1H), 7.39 – 7.35 (m, 1H), 6.82 – 6.68 (m, 2H), 4.76 (s, 2H), 3.07 (s, 6H).

^{13}C NMR (101 MHz, $CDCl_3$) δ = 153.37, 152.47, 143.56, 141.82, 129.13, 127.74, 125.00, 122.00, 119.97, 111.50, 65.16, 40.28.

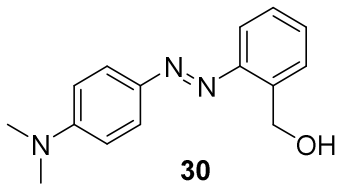

30

^{1}H NMR (300 MHz, $CDCl_3$) δ = 7.95 – 7.74 (m, 3H), 7.55 – 7.30 (m, 3H), 6.81 – 6.65 (m, 2H), 4.99 (s, 2H), 3.16 – 2.97 (m, 6H).

^{13}C NMR (75 MHz, $CDCl_3$) δ = 152.72, 151.10, 143.46, 137.18, 129.54, 128.99, 128.32, 125.22, 118.22, 111.54, 63.85, 40.26.

X-ray Crystallography

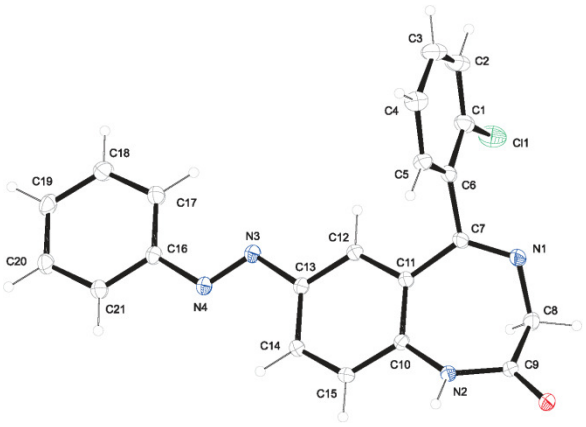

Crystallographic data. **pBZ1.1**

	pBZ1.1
net formula	$C_{21}H_{15}ClN_4O$
M_r/g mol^{-1}	374.823
crystal size/mm	0.21 × 0.20 × 0.11
T/K	173(2)
radiation	MoKα
diffractometer	'KappaCCD'
crystal system	monoclinic
space group	$P2_1/c$
a/Å	14.8963(3)
b/Å	14.8445(3)
c/Å	8.0924(2)
α/°	90
β/°	101.6300(10)
γ/°	90
V/Å^3	1752.72(7)
Z	4
calc. density/g cm^{-3}	1.42046(6)
μ/mm^{-1}	0.237
absorption correction	none
refls. measured	13417
R_{int}	0.0287
mean σ(I)/I	0.0240
θ range	3.45–27.47
observed refls.	3276
x, y (weighting scheme)	0.0536, 0.8023
hydrogen refinement	mixed
refls in refinement	4001
parameters	248
restraints	0
$R(F_{obs})$	0.0425
$R_w(F^2)$	0.1174
S	1.049
shift/error$_{max}$	0.001
max electron density/e Å^{-3}	0.285
min electron density/e Å^{-3}	–0.372

C-bound H: constr., N-bound H: refall.

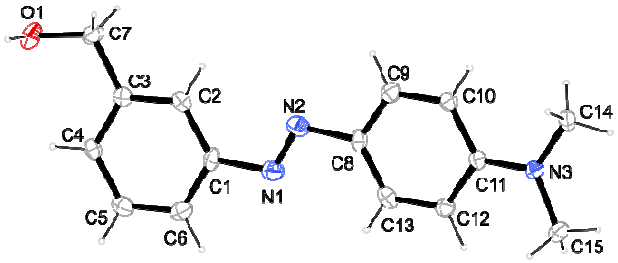

Crystallographic data. **29**

	29
net formula	$C_{15}H_{17}N_3O$
M_r/g mol^{-1}	255.315
crystal size/mm	0.125 × 0.068 × 0.035
T/K	100(2)
radiation	'Mo Kα
diffractometer	'Bruker D8Venture'
crystal system	orthorhombic
space group	$P2_12_12_1$
a/Å	5.8740(3)
b/Å	7.5687(4)
c/Å	28.9814(17)
α/°	90
β/°	90
γ/°	90
V/Å^3	1288.47(12)
Z	4
calc. density/g cm^{-3}	1.31619(12)
μ/mm^{-1}	0.085
absorption correction	multi-scan
transmission factor range	0.9359–0.9580
refls. measured	22213
R_{int}	0.0339
mean σ(I)/I	0.0183
θ range	3.42–25.34
observed refls.	2160
x, y (weighting scheme)	0.0430, 0.3886
hydrogen refinement	constr
Flack parameter	–0.7(15)
refls in refinement	2341
parameters	175
restraints	0
$R(F_{obs})$	0.0329
$R_w(F^2)$	0.0854
S	1.072
shift/error$_{max}$	0.001
max electron density/e Å^{-3}	0.327
min electron density/e Å^{-3}	–0.160

Flack test meaningless, Mo radiation, no anomalous scatterer.

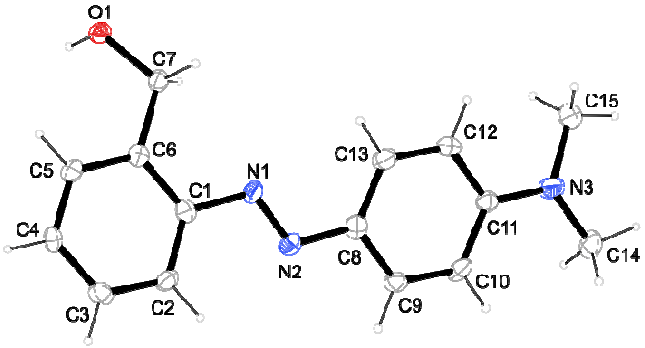

Crystallographic data. **30**

	30
net formula	$C_{15}H_{17}N_3O$
M_r/g mol^{-1}	255.315
crystal size/mm	0.119 × 0.047 × 0.026
T/K	100(2)
radiation	'Mo Kα
diffractometer	'Bruker D8Venture'
crystal system	monoclinic
space group	*Cc*
a/Å	20.2378(19)
b/Å	18.5558(16)
c/Å	27.772(3)
α/°	90
β/°	98.287(3)
γ/°	90
V/Å^3	10320.4(17)
Z	32
calc. density/g cm^{-3}	1.3146(2)
μ/mm^{-1}	0.085
absorption correction	multi-scan
transmission factor range	0.9298–0.9580
refls. measured	91227
R_{int}	0.0519
mean σ(*I*)/*I*	0.0483
θ range	2.19–25.47
observed refls.	13609
x, y (weighting scheme)	0.0599, 0.9816
hydrogen refinement	constr
Flack parameter	–0.2(11)
refls in refinement	18758
parameters	1393
restraints	2
$R(F_{obs})$	0.0427
$R_w(F^2)$	0.1111
S	1.012
shift/error$_{max}$	0.001
max electron density/e Å^{-3}	0.295
min electron density/e Å^{-3}	–0.219

References

1. Schofield, P.R. et al. Sequence anf functional expression of the GABA-A receptor shows a ligand-gated receptor super-family. *Nature* **328**, 221-227 (1987).

2. Absalom, N.L., Schofield, P.R. & Lewis, T.M. Pore Structure of the Cys-loop Ligand-gated Ion Channels. *Neurochemical Research* **34**, 1805-1815 (2009).

3. Bartos, M., Corradi, J. & Bouzat, C. Structural basis of activation of cys-loop receptors: the extracellular-transmembrane interface as a coupling region. *Mol Neurobiol* **40**, 236-52 (2009).

4. Barnard, E.A. The transmitter-gated channels: A range of receptor types and structures. *Trends in Pharmacological Sciences* **17**, 305-309 (1996).

5. Jacob, T.C., Moss, S.J. & Jurd, R. GABA(A) receptor trafficking and its role in the dynamic modulation of neuronal inhibition. *Nature Reviews Neuroscience* **9**, 331-343 (2008).

6. Olsen, R.W. & Sieghart, W. International union of pharmacology. LXX. Subtypes of gamma-aminobutyric Acid(A) receptors: Classification on the basis of subunit composition, pharmacology, and function. Update. *Pharmacological Reviews* **60**, 243-260 (2008).

7. Smith, G.B. & Olsen, R.W. FUNCTIONAL DOMAINS OF GABA(A) RECEPTORS. *Trends in Pharmacological Sciences* **16**, 162-168 (1995).

8. Baumann, S.W., Baur, R. & Sigel, E. Forced subunit assembly in alpha(1)beta(2)gamma(2) GABA(A) receptors - Insight into the absolute arrangement. *Journal of Biological Chemistry* **277**, 46020-46025 (2002).

9. Baumann, S.W., Baur, R. & Sigel, E. Subunit arrangement of gamma-aminobutyric acid type a receptors. *Journal of Biological Chemistry* **276**, 36275-36280 (2001).

10. Sigel, E., Baur, R., Boulineau, N. & Minier, F. Impact of subunit positioning on GABA(A) receptor function. *Biochemical Society Transactions* **34**, 868-871 (2006).

11. Rudolph, U. et al. Benzodiazepine actions mediated by specific [gamma]-aminobutyric acidA receptor subtypes. *Nature* **401**, 796-800 (1999).

12. Wafford, K.A. GABA(A) receptor subtypes: any clues to the mechanism of benzodiazepine dependence? *Current Opinion in Pharmacology* **5**, 47-52 (2005).

13. Atack, J.R. The benzodiazepine binding site of GABA(A) receptors as a target for the development of novel anxiolytics. *Expert Opinion on Investigational Drugs* **14**, 601-618 (2005).

14. Bormann, J. The 'ABC' of GABA receptors. *Trends in Pharmacological Sciences* **21**, 16-19 (2000).

15. Sieghart, W. STRUCTURE AND PHARMACOLOGY OF GAMMA-AMINOBUTYRIC ACID(A) RECEPTOR SUBTYPES. *Pharmacological Reviews* **47**, 181-234 (1995).

16. Tan, K.R. et al. Neural bases for addictive properties of benzodiazepines. *Nature* **463**, 769-774 (2010).

17. Tan, K.R., Rudolph, U. & Lüscher, C. Hooked on benzodiazepines: $GABA_A$ receptor subtypes and addiction. *Trends in Neurosciences* **34**, 188-197 (2011).

18. D'Hulst, C., Atack, J.R. & Kooy, R.F. The complexity of the GABA(A) receptor shapes unique pharmacological profiles. *Drug Discovery Today* **14**, 866-875 (2009).

19. Mohler, H., Fritschy, J.M. & Rudolph, U. A new benzodiazepine pharmacology. *Journal of Pharmacology and Experimental Therapeutics* **300**, 2-8 (2002).

20. Atack, J.R. GABA(A) receptor subtype-selective efficacy: TPA023, an alpha 2/alpha 3 selective non-sedating anxiolytic and alpha 5IA, an alpha 5 selective cognition enhancer. *Cns Neuroscience & Therapeutics* **14**, 25-35 (2008).

21. Sternbach, L.H. et al. Quinazolines and 1,4-Benzodiazepines. X. Nitro-Substituted 5-Phenyl-1,4-Benzodiazepine Derivatives. *J Med Chem* **6**, 261-5 (1963).

22. Hunkeler, W. et al. Selective antagonists of benzodiazepines. *Nature* **290**, 514-516 (1981).

23. Fehrentz, T., Schönberger, M. & Trauner, D. Optochemical Genetics. *Angewandte Chemie International Edition* **50**, 12156-12182 (2011).

24. Kramer, R.H., Fortin, D.L. & Trauner, D. New photochemical tools for controlling neuronal activity. *Current Opinion in Neurobiology* **19**, 544-552 (2009).

25. Mahajan, A., Kumar, V., Mansour, N.R., Bickle, Q. & Chibale, K. Meclonazepam analogues as potential new antihelmintic agents. *Bioorg Med Chem Lett* **18**, 2333-6 (2008).

26. Yu, B.C., Shirai, Y. & Tour, J.M. Syntheses of new functionalized azobenzenes for potential molecular electronic devices. *Tetrahedron* **62**, 10303-10310 (2006).

Acknowledgements

I want to thank my thesis advisor Dirk Trauner for providing a special working environment. I truly enjoyed the scientific freedom and access to seemingly unlimited resources that will be hard to find in other places.

None of my projects would have been possible without collaborators. I am particularly thankful to Mike Althaus, Martin Fronius and Wolfgang Clauss from Gießen University. Working with you was a great learning experience. I enjoyed every time I spent in your lab, thank you for being so open minded, welcoming and supportive.

Jonathan Javitch and Prashant Domthansetti from Columbia University were great collaborators. Thank you guys for showing me your lab and sharing your thoughts on GPCRs. It will be great to continuing this work.

Overlapping with Harald Janovjak and doing research in his lab at IST Austria was a great pleasure. Thank you for all scientific and unscientific advice.

I have had the pleasure to work with many talented students over the years and I am grateful to each and every one of them: Regina Scharf, Tina Weller, Christian Maier, Florian Steinmann, Katharina Hüll, Denis Höfler, Vincent Grenier, Renee Marie Bogdanovic, Antonio Rizzo.

The intellectual development that was necessary to meet the scientific challenges during my PhD research was enabled by inspiring and talented group members as well as fellows from the IMPRS and Studienstiftung.

Needless to say, I am very grateful to my family, in particular my parents and siblings.

Forschungszusammenfassung

”DEVELOPING PHOTOPHARMACOLOGY FOR TRANSMEMBRANE RECEPTORS“

“DIE ENTWICKLING VON PHOTOPHARMAKOLOGIE FÜR TRANSMEMBRANREZEPTOREN”

Dissertation von

Matthias Schönberger

aus Trier

an der

Ludwigs-Maximilian Universität

2014

IMPRS-LS, AG Prof. Dr. Dirk Trauner

Photopharmakologie

Das Konzept der Photopharmakologie ist eine Erweiterung der Pharmakologie und verfolgt das Ziel physiologische Prozesse durch die Wirkung kleiner Moleküle mit Licht zu steuern. Die Lichtsensitivität wird hierbei durch Azobenzenphotoschalter installiert, die mit pharmakologisch aktiven Molekülen verbunden werden. Die lichtinduzierte *cis/trans*-Isomerisierung des Azobenzens führt dann zu Veränderungen der pharmakologischen Wirksamkeit und erlaubt somit eine räumlich und zeitlich präzise Kontrolle biologischer Prozesse. Demzufolge stellt die Photopharmakologie ein interdisziplinäres Forschungsfeld dar, welches das Entwerfen neuer Wirkstoffe, deren Synthese und funktionelle Charakterisierung umschließt. In dieser Arbeit wurde diese Herangehensweise auf eine Vielzahl von Transmembranproteinen angewendet, die eine Schlüsselstelle in zellulärer Kommunikation und wichtige Stellschrauben in physiologischen Prozessen sind.

1) *Ein photoschaltbarer epithelialer Natriumkanal* (ENaC). Der ENaC ist ein heterotrimerer Komplex aus Transmembranproteinen, die einen Ionenkanal mit hoher Leitfähigkeit für Natriumionen bilden. αβγENaCs sind in Niere und Lunge gut untersucht, wo sie den transepithelialen Wassertransport kontrollieren. Die Rolle von δβγENaCs ist hingegen weniger gut verstanden und wirft vor allem in Gehirn von Primaten nach wie vor Fragen auf.

Anhand des gut erforschten kaliumsparenden Diuretikums Amilorid wurden lichtschaltbare Azobenzenderivate, die Photoamiloride, entworfen, synthetisiert und funktionell mittel UV/Vis-Spektroskopie, Zweielektroden Spannungsklemme (TEVC), Membranfleckenklemme (patch clamp) und transepithelialer Voltohmmetrie untersucht. Im Zuge dessen wurden hochwirksame neue ENaC-Blocker entdeckt, wovon ein Kandidat (**PA1**) hervorragende Eigenschaften als lichtschaltbarer ENaC-Blocker an der δβγ-Isoform zeigte (Abb. 1). Mit Elektrophysiologie an *Xenopus* oocyten und HEK-Zellen, die den menschlichen δβγENaC exprimierten, konnte demonstriert werden, dass *cis*-**PA1** ein wesentlich stärkerer δβγENaC-Blocker ist als *trans*-**PA1** und somit eine Kontrolle der Kanalaktivität durch einen Wechseln zwischen 400 und 500 nm Bestrahlung erlaubt. Da die Effekte an der αβγ-Isoform wesentlich geringer waren, konnte dieses neuartige Werkzeug dazu verwendet werden die funktionelle Rolle von δβγENaC in einer gemischten Population der beiden Isoformen nachzuweisen.

Die Entwicklung des ersten lichtschaltbaren ENaC-Blockers stellt eine große Erungenschaft dar und erweitert die Möglichkeiten diesen interessanten Ionenkanal weiter zu erforschen. Die Selektivität für die wenig verstandene δβγ-Isoform ist eine weitere Bereicherung, ebenso wie das Potential der δβγENaC/**PA1**-Kombination als optogenetisches Werkzeug.

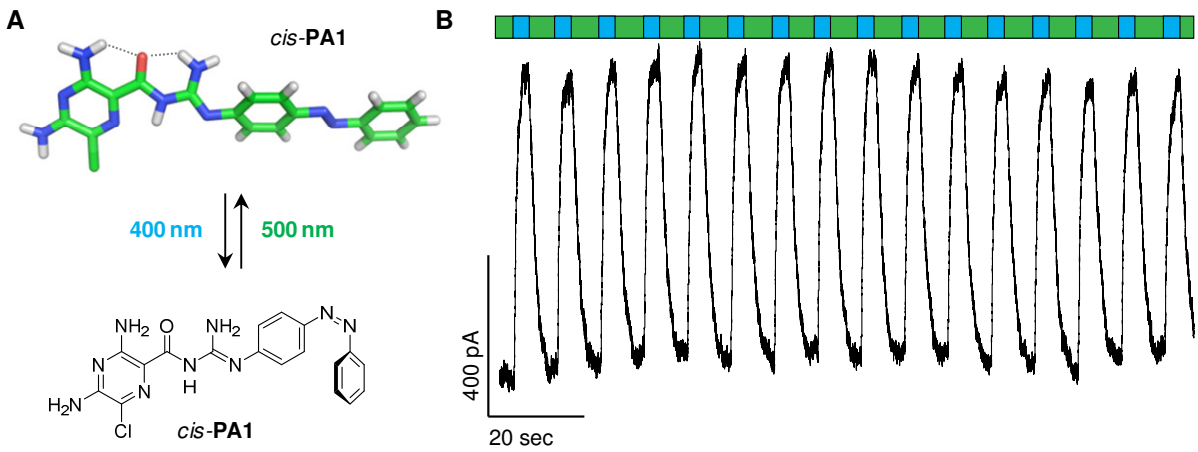

Abb. 1. **PA1** – Ein photoschaltbarer ENaC-Blocker. A) Die (Kristall)Struktur von **PA1** und dessen Isomerisierung mit 400 und 500 nm. B) Die Isomerisierung von **PA1** (10 μM) erlaubt die robuste, reversible Kontrolle von δβγENaC-Strömen in HEK293t Zellen mit Licht (grün = 500 nm, blau = 400 nm, Ganzzellableitung Membranfleckenklemme).

2) *Ein photoschaltbarer Blocker für Spannungsgesteuerte Ionenkanäle*. Neuronale Kommunikation fußt in der Weiterleitung elektischer Signale. Spannungsgesteuerte Ionenkanäle sind fundamentale Glieder in der neuronalen Kommunikationskette und sind in die Generierung und Progagierung von Aktionspotentialen (APs) involviert.

Um das neuronale Feuern von APs mit Licht zu kontrollieren, wurde ein Azobenzenderivat des langwirkdenden Oberflächenanästhetikums Fomocain entworfen und hergestellt – das **Fotocain** (Abb. 2). Elektrophysiologische Untersuchungen an dissoziierten Neuronen und akuten Hirnschnitten der Maus zeigten, dass **Fotocain** in seiner *cis*-Form unter 350 nm Bestrahlung APs zulässt, diese in seiner *trans*-Form unter 450 nm Bestrahlung jedoch inibiert. Diese gewünschte Funktionalität in Verbindung mit interessanten pharmakokinetischen Eigenschaften, die auf die milde Basizität der Morpholingruppe zurückzuführen sind, machen **Fotocain** zu einem äußerst nützlichen neuen Werkzeug, das die Reichweite der neuronalen Photopharmakologie erweitert.

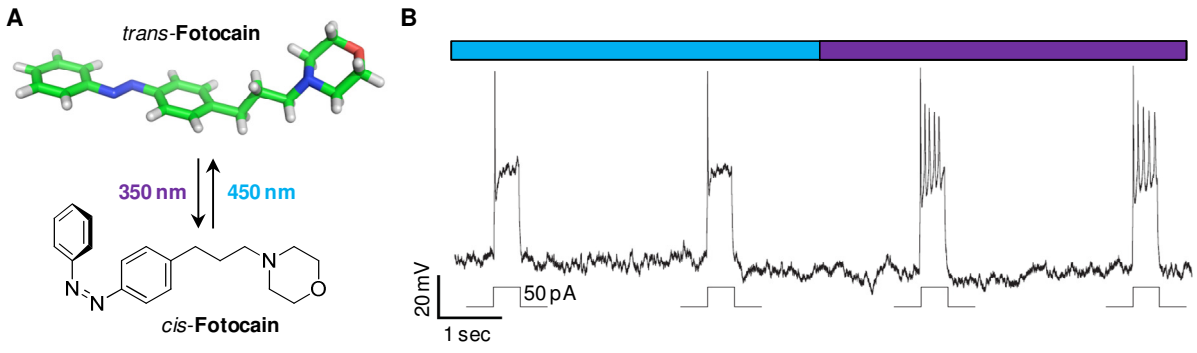

Abb. 2. **Fotocain** – Ein photoschaltbarer Blocker spannungsgesteuertert Ionenkanäle. A) Die (Kristall)Struktur von **Fotocain** und dessen Isomerisierung mit 350, bzw. 450 nm. B) Das Feuern von Aktionspotentialen dissoziierter Neurone kann mit **Fotocain** (50 µM) kontrolliert werden (blau = 450 nm, violett = 350 nm, Ganzzellableitung Membranfleckenklemme)

3) *Ein photoschaltbarer Agonist des µ-Opioid Rezeptors* (MOR). Opioidrezeptoren (ORs) gehören zu der Gruppe der G-Protein gekoppelten Rezeptoren (GPCRs) der Klasse A und werden im zentralen Nervensystem (ZNS), im Rückenmark und im Verdauungstrackt von Säugern exprimiert. Sie sind die Rezeptoren der nativen Endorphine und Dynorphine, des natürlich vorkommenden Morphins und der synthetischen Opioide, wie beispielsweise Fentanyl. Obwohl Opioide seit Jahrtausenden als Anesthetika pharmakologisch geschätzt und genutzt werden, stellt deren Einsatz wegen ihres Suchtpotentials und zahlreicher Nebenwirkungen nach wie vor eine große Herausforderung dar.

Auf Basis des Fentanyls wurden photoschaltbare Azobenzenderivate entworfen, hergestellt und funktionell untersucht (Abb. 3). Dazu wurde der MOR in HEK-Zellen mit einem G-Protein aktivierten einwärtsgleichrichtenden Kaliumkanal (GIRK-Kanal) co-exprimiert. Diese Kombination greift zum einen die native Signalkaskade des MOR im ZNS auf und ermöglicht es zum anderen die reversible Rezeptoraktivierung direkt mit Membranfleckenklemme auszulesen. Im Zuge dieser Experimente wurde ein Photofentanylderivat entdeckt, das einen ausgezeichneten photoschaltbaren Agonisten des MORs darstellt. In seiner *trans*-Form aktiviert das Molekül den Rezeptor sehr stark, in seiner *cis*-Form hingegen sehr schwach. Somit ist **Photofentanyl** der erste photoschaltbare Agonist für den MOR. Darüberhinaus ist dies die erste Demonstration von Photopharmakologie an einem GPCR der Familie A, zu der auch Rhodopsin gehört, und eröffnet möglicherweise die Möglichkeit weitere Mitglieder dieser Wichtigen Proteinfamilie lichtschaltbar zu machen.

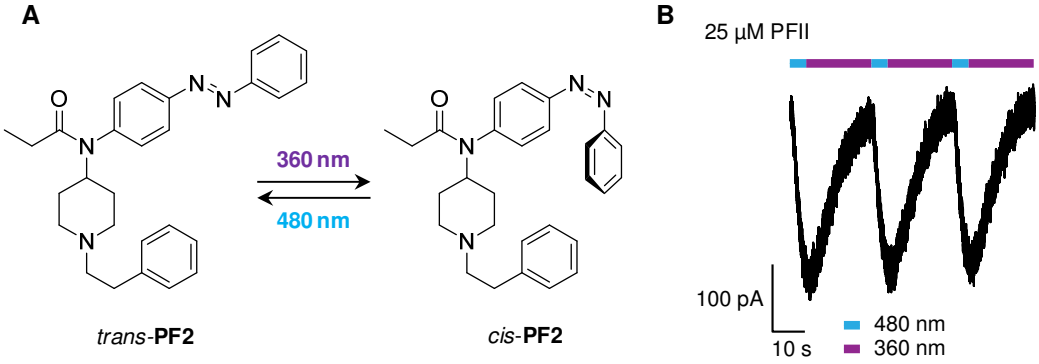

Abb. 3. **Photofentanyl** – Ein photoschaltbarer Agonist des μ-Opioid Rezeptors (MOR). A) Die Struktur des Photofentanyls-2 (**PF2**) und dessen lichtinduzierte Isomerisierung. B) Die Wirkung von **PF2** an HEK293t Zellen, die den MOR und GIRK-Kanäle exprimieren (Ganzzellableitung Membranfleckenklemme).

4) *Photoschaltbare Agonisten für den Dopaminrezeptor* (DR). Der DR gehört ebenso wie der MOR zu der Familie A G-protein gekoppelter Rezeptoren. Die fünf bekannten Subtypen D_1-D_5 sind sowhol prä- als auch postsynaptisch in dopaminergen Neuronen anzufinden und werden von dem endogenen Neurotransmitter Dopamin (DA) aktiviert. Das Dopaminsystem wird auch als Belohnungssystem bezeichnet und spielt eine elementarere Rolle in der Entwicklung von Sucht.

Anhand des bekannten DR-Agonisten **PPHT** wurde eine Serie von Azobenzenderivaten entworfen und synthetisiert (**aPPHT**, Abb. 4). Obwohl **PPHT** racemisch eingesetzt wird, wurden verschiedene synthetische Routen ausgearbeitet um enantiomerenreine Verbindungen herzustellen. Dabei wurde der Komplex aus einem Weinsäurederivat und einem *N*-Benzylaminotetralin mit Röntgenstrukturanalyse untersucht, womit die wichtige Interaktion zwischen den Toloylsäureresten der Weinsäure und der Benzyleinheit des Tetralins demonstriert werden konnte. Die letztlich etablierte modulare Syntheseroute mit Azobenzenbausteinen und dem chiralen Aminotetralin bieten eine vielseitige Plattform, um viele verschiedene photoschaltbare PPHT-Derivate mit robuster Chemie herzustellen. Vorläufige Tests der bereits hergestellten Photoschalter durch Kollaborationspartner an der Columbia Universität identifizierten bereits einen vielversprechenden Kandidaten für einen photoschaltbaren Agonisten des D3R.

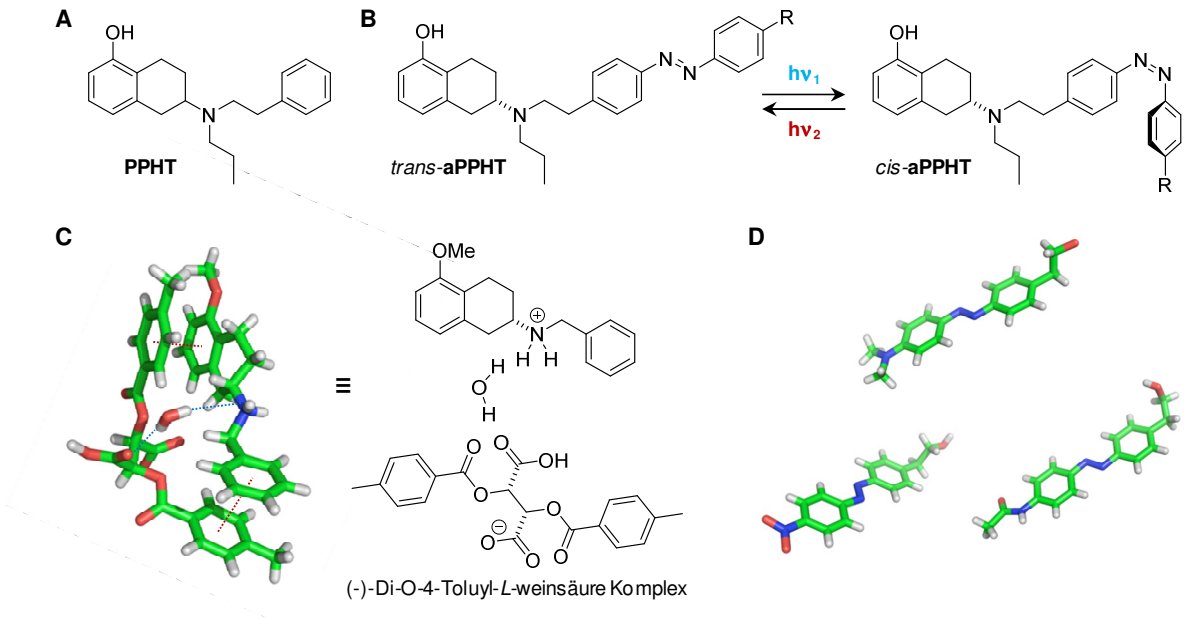

Abb. 4. **aPPHT** – Ein photoschaltbarer Agonist des Dopaminrezeptors (DR). A) **PPHT** ist ein bekannter DR-Agonist, der racemisch eingesetzt wird. B) Struktur eines representativen chiralen photoschaltbaren PPHTs (**aPPHT**) und dessen Isomerisierung. C) Kristallstruktur eines Komplexes aus einem Weinsäurederivat und und einem Aminotetralin, das eine Zwischenstufe in der Synthese chiraler aPPHT-Moleküle ist. D) Kristallstrukturen verschiedener Azobenzenbausteine, die durch eine reduktive Amminierung mit einem Aminotetralinbaustein verknüpft werden können.

5) *Photoschaltbare Agonisten für den Adenosinrezeptor* (AR). Der AR gehört ebenso wie der MOR und DR zur Familie A der G-protein gekoppelten Rezeptoren. ARs werden im ZNS exprimiert und sind vor allem als das Ziel der weltweit meist gebrauchten psychoaktiven Substanz, nämlich Koffein, bekannt. Es wird derzeit spekuliert ob ARs in der Zellmembran mit DRs wechselwirken und ihre Aktivität gegenseitig in Form von Rezeptorheteromultimeren modulieren.

Anhand des endogenen Liganden Adenosin und abgeleitet von synthetischen AR-Agonisten wurden photoschaltbare Azobenzenderivate entworfen und synthetisiert, die wahrscheinlich als photoschaltzbare Agonisten am A1- und A2A-AR wirken (Abb. 5).

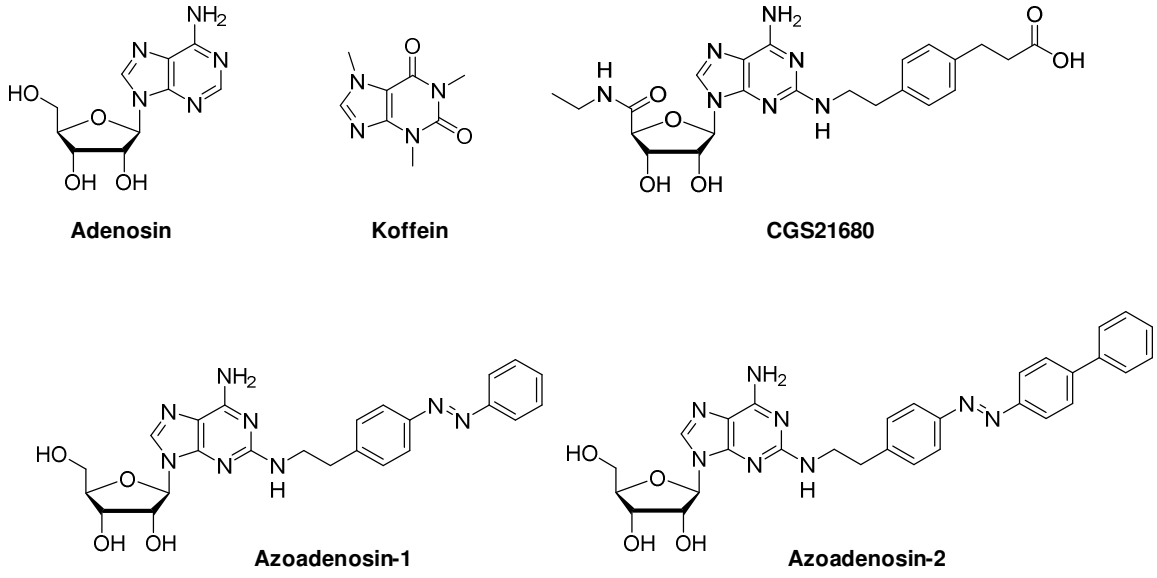

Abb. 5. **Azoadenosin** – Ein photoschaltbarer Agonist des Adenosinrezeptors (AR). Adenosin ist der native **Agonist** der ARs. **Koffein** antagonisiert dessen Effekt. Der synthetische Agonist **CGS21680** unterstreicht die Toleranz für ausladende Substitutionen am C-2. Anhand dessen wurden die photoschaltbaren **Azoadenosine 1** und **2** entworfen und synthetisiert.

6) *Photoschaltbare Benzodiazepine* (BZ). Benzodiazepine sind weitverbreitete sedierende, krampflösende und angstlösende Wirkstoffe, die als allosterische Aktivatoren an $GABA_A$-Rezeptoren wirken. Diese Rezeptoren, die nach ihrem endogenen Liganden γ-Aminobuttersäure (GABA) benannt sind, sind die hauptsächlichen Vermittler inhibitorischer Signale in der neuronalen Kommunikation.

Aufgrund des diversen, hoch interessanten, aber nicht gänzlich unproblematischen Wirkungsprofils der Benzodiazepine, wurden zahlreiche Azobenzenderivate hergestellt, die möglicherweise die Türen für eine neuartige Erforschung der $GABA_A$-Rezeptor-BZ-Interaktion öffnen (Abb. 6).

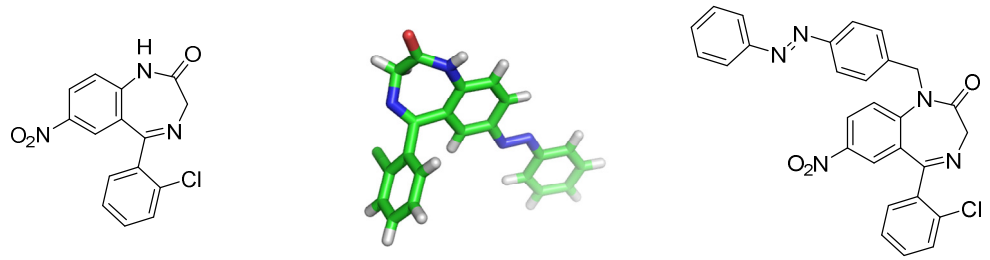

Clonazepam **pBZ1.1** **pBZ2.1**

Abb. 6. **Photo-Benzodiazepine** (pBZs) – Photoschaltbare Aktivatoren für den $GABA_A$-Rezeptor. **Clonazepam** ist ein bekanntes, nicht photoschaltbares BZ. **pBZ1.1** (Kristallstruktur) ist ein Repräsentant einer Serie von pBZs, die eine Azobenzengruppe als Verlängerung des anelierten Benzenring. pBZ2.1 ist Repräsentant einer Serie von pBZs, die mit benzylischen Azobenzenen am Anilidstickstoff des Diazepinrings verknüpft sind.